City Research Online

City, University of London Institutional Repository

FINITE-AMPLITUDE PATTERNS OF

CONVECTION NEAR A LATERAL

BOUNDARY

by

VALERIE SIVAPRAGASAM

Thesis submitted for the degree of

Doctor of Philosophy

Department of Mathematics

City University

London

July 1995

Acknowledgements

I am very grateful to my supervisor, Professor P.G. Daniels, without whose patience, encouragement and thoughtful and constructive advice I could not have completed this research.

I have received a lot of help in writing this thesis from a number of people and I would like to take this opportunity to show how much I appreciate it. I am particularly indebted to my mother for her constant support over the last three years and for giving up a lot of her valuable time to motivate and help me write this thesis as well as reading the chapters for any errors. I wish to thank Roshan for typing up the majority of the thesis for me without any complaints in such a short time. Finally, I would like to express my gratitude to my father for printing various chapters for me when I asked him even though he was very busy at work.

All the combined help has assured the completion of this thesis and I will never forget their kindness to me. Thank you very much.

Dedicated to my Mother who gave me

encouragement and assistance throughout my life.

Thank you

Abstract

The formation of convective patterns in Rayleigh-Bénard and related systems, in particular the interaction between orthogonal roll patterns in the neighbourhood of a lateral boundary, is studied analytically and numerically. The effects on the patterns of convection of forcing at the boundary, the Prandtl number of the fluid, the wavelength perpendicular to the boundary and the wavelength parallel to the boundary are also included. Numerical solutions are found using an explicit finite difference scheme and appear to be in good agreement with theoretical predictions. The evolution of the roll pattern with time is illustrated by contour plots.

Weakly nonlinear theory is used to determine finite-amplitude patterns of convection near a lateral boundary $x=0$, leading to a coupled pair of equations for the amplitudes of x-rolls and y-rolls parallel and perpendicular to the boundary respectively. The solution for real amplitude functions independent of y is described in detail in chapter 2. This identifies a steady-state structure consisting of two main regions, one containing a combination of x-rolls and y-rolls and the other containing x-rolls only. The transition zone which occurs between the two regions is considered in chapter 3. Complex amplitude functions are then considered, allowing variations in the wavelength of the x-roll pattern to be considered in chapter 4 and of the y-roll pattern in chapter 5. Finally, phase-winding effects associated with variations in the wavelength of the x-roll pattern when there is no lateral forcing are investigated in chapter 6.

Contents

Chapter 1

Introduction

Convective patterns in thin fluid layers uniformly heated from below and uniformly cooled above have been the subject of many theoretical, numerical and experimental studies over the last 100 years since the attempt by Rayleigh (1916) to describe the experimental observations of Bénard (1900). Many of these investigations have concerned unbounded layers (ie. those which extend to infinity in horizontal directions) although more recently the desire to make realistic comparisons with experimental work has led to studies of the role played by the lateral walls of a finite container. A further impetus is provided by the knowledge from experimental observations that, however distant, the walls do exert a significant influence on the geometric properties of the cellular motions which develop when the state of pure conduction becomes unstable. For an infinite layer, linear theory predicts that the conductive state of no motion becomes unstable when the applied temperature difference is sufficiently great for buoyancy to overcome the frictional resistance of the fluid, as measured by the size of the Rayleigh number, R. The main results of this linear theory are summarised by Chandrasekhar (1963).

Davis (1967) studied the influence of lateral walls on the convective process in a rigid, perfectly conducting, three-dimensional rectangular box of fluid heated from below using a linear analysis combined with a Galerkin method. Finite rolls (cells with two non-zero velocity components dependent on all three spatial variables) with axes parallel to the shorter sides were predicted to occur at the onset of convection. Davies-Jones (1970) studied convective motions in a fluid contained in an infinite rectangular channel heated from below. The results show that the preferred mode at the onset of convection is that of transverse rolls with axes perpendicular to the channel walls, consistent with the predictions of Davis (1967) for convection in a box. The cells which appear at the onset of convection resemble finite rolls very closely for channel

3

aspect ratios (height to width) outside the range 0.1 to 1. Inside this range they show noticeable departures from roll form, and in fact 'exact' finite rolls are only obtained if the sidewalls are infinitely far apart.

Schluter, Lortz and Busse (1965) studied weakly nonlinear motions in an infinite horizontal layer of fluid heated from below for both rigid and free upper and lower boundaries. The mathematical difficulties which arise in solving the Navier-Stokes equations imply that nonlinear steady-state solutions are not known exactly, but the flows have relatively small amplitude if R is close to its critical value R_0, enabling the use of successive approximations. A multimodal discrete analysis method was used and a relationship was obtained between the Rayleigh number and the amplitudes of the nonlinear terms for rolls of arbitrary orientation. The nonlinear theory of Bénard convection in an infinite fluid layer confined between horizontal boundaries predicts that the amplitude of the motion undergoes a bifurcation as the Rayleigh number passes through the critical value for instability predicted by linear theory. Nonlinear aspects of the problem were described in the papers of Newell and Whitehead (1969) and Segel (1969). Near the critical Rayleigh number for an unbounded fluid, $R=R_0$, the solution may be expanded in powers of the small parameter R-R_0 and consists of convection cells of horizontal width comparable to the height of the layer, modulated in strength by an amplitude function, A, varying on large horizontal length scales proportional to $(R-R_0)^{-1/2}$ and $(R-R_0)^{-1/4}$ and a large time scale proportional to $(R-R_0)^{-1}$. The solution was developed by using the method of multiple scales, rather than a multimodal discrete analysis, and the nonlinear terms incorporated in a consistent manner, resulting in a nonlinear equation for A. Segel (1969) considered boundary conditions which the amplitude function must satisfy when the flow is confined laterally by rigid, perfectly insulating sidewalls although his results were later corrected by Brown and Stewartson (1977).

4

Daniels (1977) considered the presence of imperfectly insulating rigid lateral walls and showed that this alters the onset of Bénard convection in a confined fluid layer from a bifurcation to a continuous smooth transition as the Rayleigh number increases through the critical value. He obtained solutions for a simplified two-dimensional model with rigid distant sidewalls and free upper and lower surfaces and derived boundary conditions for the amplitude equation. Similar results were obtained for finite aspect ratios by Hall and Walton (1977). Later, Daniels (1978) examined different sizes of the sidewall forcing, λ, and its effect on the bifurcation structure and the method was extended by Stewartson and Weinstein (1979) to incorporate more realistic conditions corresponding to rigid horizontal and vertical boundaries. Sidewall forcing effects are also important in other related problems. The onset of Bénard convection in a shallow sloping rectangular container of large aspect ratio was considered by Daniels (1982). The major effect of the inclination is a combination of the large scale circulation driven by the temperature variation in the horizontal direction, and the small scale convective motions driven by the gravitational instability. The sidewalls of the container are important in the generation of the convective motion, equivalent to a non-zero value of λ, and it was found that the amplitude of the rolls increases smoothly with increasing Rayleigh number. An amplitude equation for the convective motion near onset was determined using the method of multiple scales and various solutions were obtained. Other examples of where sidewall forcing is important are found in cases where the geometry of the container is imperfect (Daniels 1982) or where rotation introduces centrifugal effects (Daniels 1980). Geometrical imperfections in a shallow two-dimensional layer uniformly heated from below result in two major effects on the pattern of cellular convection that evolves near the critical Rayleigh number. Sidewalls which are not quite vertical result in the initial development of rolls near the sidewalls and the rolls subsequently spread smoothly inwards as the Rayleigh number increases. If the horizontal surfaces are not quite parallel it can be shown that there is a lateral modulation of the rolls due to a combination of the misalignment of the horizontal

5

surfaces and the presence of the sidewalls.

Another important aspect of Rayleigh-Bénard convection is the manner in which the wavelength of the roll pattern changes as the Rayleigh number increases beyond its critical value and, in particular, the influence of lateral walls on the wavelength selection mechanism. Cross, Daniels, Hohenberg and Sigga (1981, 1983) determined the steady-state solutions of two-dimensional convection for Rayleigh numbers R slightly above threshold in a laterally finite container. They found that the allowed wavevectors which can occur as perturbations q to the critical wavenumber in the bulk of the container are reduced from a size $|q| \sim [(R-R_0)/R_0]^{1/2}$ in the laterally infinite system to the range $|q| \sim (R-R_0)/R_0$ in a system with rigid lateral walls. Therefore the presence of rigid sidewalls, no matter how far apart, severely restricts the band of possible wavenumbers which can occur in the bulk of the system. The hydrodynamic equations were expanded in terms of the small parameter $[(R-R_0)/R_0]^{1/2}$ to obtain amplitude equations and boundary conditions to a higher order than obtained by Newell and Whitehead (1969) and Segel (1969). It was also noted that the range of allowed wavevectors depends on the Prandtl number of the fluid and the thermal properties of the sidewalls. Daniels (1981) investigated how the steady-state solutions obtained by Cross et al evolved over time and examined the stability of the solutions. The complete evolution of the flow pattern from a static state takes place on various long time scales of which the most important are $t = O[(R-R_0)^{-1}]$ and $t = O[(R-R_0)^{-2}]$. The amplitude of convection (ie. the strength of the rolls) rises from zero to its final steady-state value on the time scale $t = O[(R-R_0)^{-1}]$, but the final lateral positioning of the rolls (which consists of a gradual change in the complex argument of the core-amplitude function, the modulus of which remains constant and uniform across the container) is only completed on the much longer time scale $t = O[(R-R_0)^{-2}]$. The results showed that as the Rayleigh number increases beyond its critical value for free horizontal boundaries, the wavelength of the rolls depends on the value of the Prandtl number. If the Prandtl number is

6

sufficiently high there is a smooth evolution with little change in the wavelength of convection, whereas if the Prandtl number is sufficiently small there is a discontinuous evolution in which, to preserve stability, the solution must continually jump from one solution branch to another, resulting in a decrease in the number of rolls, and the wavelength of convection then steadily increases with Rayleigh number.

The question of wavelength selection was also studied by Pomeau and Zaleski (1981) who obtained similar results for a one-dimensional model equation. They also discussed the likelihood of instability of the one-dimensional solution to cross-rolls near the sidewalls. An amplitude equation previously used to calculate steady states of convection in a finite container was studied numerically for the case of lateral forcing at the boundaries by Cross, Hohenberg and Safran (1982) to observe the evolution of the roll pattern, and in particular the wavenumber, with time. It was found that if q is not an allowed wavenumber initially it either increases or decreases in value with time to become an allowed wavenumber. The evolution of the roll pattern resulting from a change in the Rayleigh number for the case where there is no lateral forcing was considered by Daniels (1984), the steady-state solutions being those obtained by Cross et al (1983). The main evolution of the roll pattern occurs on the long time scale $t = O[(R-R_0)^2]$ where the phase of the solution is governed by a one-dimensional heat conduction equation which was solved subject to nonlinear boundary conditions imposed by the interaction with the sidewalls.

Daniels and Chana (1989) considered the onset of convection in an infinite rigid horizontal channel uniformly heated from below. A linearised solution of the three-dimensional Oberbeck-Boussinesq equations was obtained using a two-dimensional Galerkin representation of the cross-channel dependence, but allowing an analytical description in terms of the third coordinate x measured along the length of the channel, which identifies any adjustment in the

7

wavelength of the roll pattern. Neutral stability curves and the dependence of the critical Rayleigh number on the channel aspect ratio were determined and asymptotic results were found for narrow and wide channels which correspond to the limits of small and large aspect ratios respectively. These results were extended by Daniels and Ong (1990) to higher levels of truncation and to include modes of convection not previously examined, leading to more accurate results. This type of linear theory had earlier formed the basis of a model of convection in a long box with free boundaries at slightly supercritical Rayleigh numbers proposed by Daniels and Chana (1987) in which the wavelength adjustment was predicted theoretically in terms of transitions between different multiple-cell solutions of the kind previously identified for the two-dimensional model with stress-free boundaries by Cross et al (1983). Although in the long box the solutions are fully three-dimensional, a similar structure is relevant in the x direction, allowing multiple-scale techniques and matched asymptotic expansions to be used to take account of both nonlinear effects and the presence of the ends of the box. The results showed that for large Prandtl numbers the number of rolls will remain constant in the box as the Rayleigh number is gradually raised, but for smaller Prandtl numbers and most aspect ratios the number of rolls must decrease as the Rayleigh number is raised above its critical value. The weakly nonlinear theory for convection in an infinite channel uniformly heated from below was extended to the case of rigid horizontal boundaries and rigid thermally conducting sidewalls by Daniels and Ong (1990a). The overall description of the flow consisted of a combination of analytical and numerical techniques along and in the cross-section of the channel. They derived an amplitude equation governing the spatial and temporal evolution of the flow above the critical Rayleigh number and results were obtained for general Prandtl numbers and a wide range of aspect ratios. The linear theory for the corresponding system with thermally insulated sidewalls had earlier been investigated by Luijkx and Platten (1981).

Amplitude equations and boundary conditions provide an economical method for studying the effect of lateral boundaries on convection close to onset. Boundary conditions for the amplitude functions for rolls parallel and perpendicular to a sidewall have been determined for convection in large rectangular cells by Segel (1969) and Brown and Stewartson (1977) respectively. These results were generalized by Cross (1982) who derived boundary conditions for the amplitude function of convective rolls approaching a rigid sidewall at an arbitrary orientation. Pomeau and Zaleski (1981) argued that in large rectangular containers the cross-roll instability originally identified by Newell and Whitehead (1969) would be relevant near the lateral boundaries, so that theories based on purely two-dimensional roll patterns would be inadequate. This was confirmed by Greenside and Coughran (1984) who used a two-dimensional relaxational model equation introduced by Pomeau and Manneville (1980) to study numerically the effect of lateral boundaries on pattern formation near the onset of convection in rectangular planform containers. The model equation is an immense simplification of the Boussinesq equations and it was solved by a repeated solution of the linear constant-coefficient biharmonic problem. An implicit backward-Euler time integration scheme with a variable step-size and a variable-order time-step monitor was used as an accurate numerical integration method to solve the biharmonic problem. Their results clearly showed that in general whenever a roll comes into a sidewall it does so at right angles. They also studied the time scale required for the relaxational model to reach a stationary state and the results showed that for small planforms the fluid becomes stationary after about one horizontal diffusion time (ie. the time for a thermal perturbation to diffuse across a characteristic horizontal dimension of the cell). However for large planforms the time scale required for the fluid to become stationary is much larger than the horizontal diffusion time. The model equation introduced by Pomeau and Manneville (1980) was also studied by Daniels and Weinstein (1992) as a way of simulating patterns of convection in a fluid uniformly heated from below and included a description of the main features of the finite-amplitude motion near a lateral boundary taking into account the fact

9

that a roll pattern parallel to a sidewall is unstable to cross-rolls in the neighbourhood of the boundary. The amplitude equations for rolls parallel and perpendicular to the sidewall were derived and an analysis of the normal modes of the cross-roll instability was undertaken. The nonlinear evolution of a general disturbance was then studied theoretically and numerically and a stable finite-amplitude structure consisting of a mixture of rolls parallel and perpendicular to the boundary was found in the case when there is a small boundary imperfection, with a transition to rolls parallel to the boundary at a certain distance from the wall. It was also found that when the boundary imperfection is removed, a steady-state solution is not attained in a semi-infinite region extending from the wall and instead there is a continual logarithmically slow drift of the roll pattern with time as the region containing the cross-rolls increases in size. Investigations of the transition between transverse and longitudinal roll patterns in an infinite layer include those by Walton (1982, 1983) and Tesauro and Cross (1987).

There have been many experimental investigations of the Rayleigh-Bénard system. In order to determine accurate details about the convective properties of fluids heated from below, Dubois and Bergé (1978) measured the velocity in silicone oil by laser anemometry. The experimental velocity measurements were compared with the weakly nonlinear amplitude equations. Steady convection in a rectangular box heated from below and cooled from above was studied experimentally by Bühler, Kirchartz and Oertel (1979) and Oertel (1980). In addition, the steady linear Boussinesq equations were solved numerically using a Galerkin method and an explicit finite difference scheme to determine the onset of convection. The effect of the Prandtl number, P, on the steady flow pattern which develops at supercritical Rayleigh numbers was determined experimentally using the test fluids silicone oil ($P=1780$), water ($P=7$) and nitrogen ($P=0.71$). The flow configurations in nitrogen and silicone oil were observed experimentally using a differential interferometer and the density and velocity profiles were measured by means of a laser-differential interferometer and laser-anemo-interferometer.

The results were consistent with the subsequent theory of Chana and Daniels (1987) that for high Prandtl number fluids the number of convection rolls does not alter within the box whereas for low Prandtl number fluids the number of convection rolls decreases as the Rayleigh number increases. The results also agreed with the original prediction of Davis (1967) that at the onset of convection the preferred mode of convection consists of three-dimensional rolls (the rolls have a non-zero velocity component perpendicular to the sidewalls) with axes aligned perpendicular to the sidewalls of the channel. The experimental findings were also supported by finite element calculations of the nonlinear flow field (Oertel 1980). The wavelength of convective rolls was measured as a function of the aspect ratio in a long box near the onset of convection by Luijkx and Platten (1982). It was found that as the aspect ratio (width/height) of the cross-section of the box increases, the corresponding wavenumber decreases, reaches a minimum when the aspect ratio is about three and then increases consistent with the theoretical predictions by Davies-Jones (1970) and Luijkx and Platten (1981). In general, the flow in rectangular containers exhibits a sequence of transitions from steady, laminar to turbulent flow and this was studied at Rayleigh numbers ranging from the onset of convective flow to the onset of time dependence by Kolodner, Walden, Passner and Surko (1986) and Kessler (1987). They also measured the Nusselt number which describes the heat transfer from the bottom to the top of the box. A detailed account of much of the experimental work on Rayleigh-Bénard convection is contained in the book by Koschmieder (1993).

There have also been a number of theoretical studies of Rayleigh-Bénard convection in non-rectangular geometries. Joseph (1971) discussed convection in containers of fluid of arbitrary shape heated from below. The onset of finite-amplitude Bénard convection in a shallow cylindrical container of large radius with stress-free upper and lower surfaces and a rigid imperfectly insulated sidewall was investigated by Brown and Stewartson (1977, 1978), extending the linear theory developed by Zierep (1959). Amplitude equations for concentric roll

11

patterns were derived as a function of the radial coordinate. Boundary conditions for the amplitude equation were found at the centre and on the outer wall of the cylinder. The question of wavelength selection in cylindrical structures was investigated by Pomeau and Manneville (1981) and Daniels and Golbabai (1984).

There is a similarity between the convective cell pattern in Bénard convection and some of the most beautiful and familiar examples of spontaneous pattern formation in nature which can be found in the growth of crystals (eg. in snowflakes or the solidification of alloys, Langer 1980), phyllotaxis in plants (Rivier, Occelli, Pantaloni and Lissowski 1984) and liquid crystals (Guazzelli, Guyon and Wesfreid 1983, Dubois-Violette, Guazzelli and Prost 1983). Cellular convection is also thought to be important in plate tectonics and the motion of the Earth's mantle (McKenzie and Richter 1976). The present work aims to describe the formation of patterns of convection in Rayleigh-Bénard and related systems, in particular the interaction between orthogonal roll patterns in the vicinity of a lateral boundary. The effects of forcing at the boundary, the Prandtl number of the fluid, the wavelength in the x direction (perpendicular to the boundary) and the wavelength in the y direction (parallel to the boundary) on the patterns of convection are discussed in detail in the following chapters.

In chapter 2 amplitude equations and boundary conditions are derived for both the model system introduced by Pomeau and Manneville (1980) and the Rayleigh-Bénard system with rigid upper and lower boundaries. Normal modes of the cross-roll instability in the vicinity of a lateral boundary are then found and the nonlinear evolution of a general disturbance is examined theoretically and numerically using an explicit finite difference scheme for a range of different Prandtl numbers of the fluid and for different levels of forcing at the boundary. Attention is restricted to real amplitude functions independent of y.

12

The stable steady-state structure identified in chapter 2 involves a transition from a combination of rolls parallel and perpendicular to the boundary to a solution consisting entirely of rolls parallel to the boundary. The transition zone between these two main outer regions is studied in detail in chapter 3 and it emerges that the fourth order spatial derivative term in the amplitude equation plays a significant role. Steady-state solutions of the transition zone problem are obtained analytically and numerically using a fourth order Runge-Kutta method together with Newton iteration.

In chapter 4 the amplitudes of the x and y-rolls (parallel and perpendicular to the lateral boundary respectively) are allowed to be complex but still independent of y so that variations in the wavelength of the x-roll pattern can be studied. The relevant amplitude equations are determined and the range of allowed wavenumbers of steady-state solutions for the model system is examined when the amplitude of the y-rolls is both zero and non-zero. The complete steady-state solution structure for the case when the amplitude of the y-rolls is non-zero is found for the semi-infinite system when the lateral forcing is small, using the method of matched asymptotic expansions. The nonlinear evolution of a general disturbance is studied numerically using an explicit finite difference scheme for a variety of wavenumbers and different levels of forcing at the boundary. The results are also extended to include the effect of a second lateral boundary allowing predictions to be made of the possible range of wavenumbers in a finite container.

Spatial frequency modulation of the y-roll pattern, equivalent to a range of different wavelengths of the rolls perpendicular to the lateral boundary, is investigated in chapter 5. The amplitude equations and boundary conditions are obtained, followed by the determination of steady-state solutions. The effect of frequency modulation on the location of the transition zone is determined and the nonlinear evolution of an initial disturbance is studied theoretically and

13

numerically using an explicit finite difference scheme.

In chapter 6 phase-winding effects associated with variations of the wavelength of the x-roll pattern are investigated when there is frequency modulation of the y-roll pattern and no lateral forcing. Higher order amplitude equations are derived for the model system and the overall solution structure is established, consisting of two main outer regions separated by a transition zone (where the amplitude of the y-rolls falls to zero) and two wall regions near the lateral boundary. Solutions in the transition zone are found which lead to a number of continuity conditions for the outer solutions. The wall region solutions are then obtained and provide boundary conditions which complete the determination of the various constants which arise in the outer solutions. This allows the phase-winding properties of the system to be determined, showing how the lateral boundary restricts the range of wavelengths in the main x-roll pattern. Finally, the results are discussed with a view to possible future avenues of research.

Chapter 2

Finite-amplitude patterns of convection near a lateral boundary

2.1 Introduction

In this chapter, a pair of amplitude equations is studied as a means of simulating weakly nonlinear patterns of convection in a fluid uniformly heated from below. The aim is to describe the main features of the finite amplitude motion near a lateral boundary, incorporating the effect of an imperfection or forcing at the boundary measured by a parameter λ. In section 2.2 the analysis is based on a model equation introduced by Pomeau and Manneville (1980) and equations for the amplitudes of rolls parallel and perpendicular to the lateral boundary (x-rolls and y-rolls respectively) are derived. The boundary conditions for the amplitude functions are also determined. In section 2.3 the amplitude equations for the Rayleigh-Bénard system with rigid upper and lower boundaries are derived together with the boundary conditions for the amplitude functions. Here the coefficient μ of the nonlinear term representing the interaction between x-rolls and y-rolls is a function of the Prandtl number of the fluid. The range of possible values for μ in the amplitude equations is determined using the results of Schluter, Lortz and Busse (1965). The model equation of section 2.2 is then seen to be equivalent to the special case $\mu = 2$, which has been studied in the present context by Daniels and Weinstein (1992), who confirmed the importance of the cross-roll instability mechanism proposed by Pomeau and Zaleski (1981). Normal modes of the cross-roll instability are found for general μ in section 2.4 and aspects of the nonlinear evolution are studied theoretically in section 2.5. In section 2.6 the steady state to which the solution evolves for $\mu > 1$ is found theoretically. Section 2.7 examines the nonlinear evolution of a general disturbance numerically for general μ using an explicit finite difference scheme and section 2.8 describes an analysis of the case $\mu \leq 1$. In section 2.9 the results are discussed and a comparison is made between the analytical predictions of the behaviour for different values of μ and the results obtained numerically.

15

2.2 Amplitude equations and boundary conditions for a model system

In this section a non-dimensional model equation introduced by Pomeau and Manneville (1980) is considered. This equation for $\psi(x,y,t)$ has the form

$$\frac{\partial \psi}{\partial t} = \{\epsilon - (\nabla^2 + 1)^2\}\psi - \psi^3 \quad , \qquad (2.2.1)$$

where $\nabla^2 = \partial^2/\partial x^2 + \partial^2/\partial y^2$, x and y denote Cartesian coordinates and t denotes time. This simple model equation contains the essential ingredients of diffusion (time and spatial dependency) and cubic nonlinearity which characterise the Rayleigh-Bénard problem. The parameter ϵ is equivalent to the excess of the Rayleigh number above its critical value for an infinite layer. A semi-infinite domain $x \geq 0$ is examined and at the lateral boundary it is assumed that

$$\psi = 2\lambda\epsilon^{1/2} \quad , \quad \frac{\partial \psi}{\partial x} = 0 \quad \text{at} \quad x = 0 \quad . \qquad (2.2.2)$$

When $\lambda = 0$ these conditions imitate those associated with a rigid impermeable wall, while a non-zero value of λ corresponds to some kind of imperfection which could describe a finite porosity or thermal conductivity of the lateral boundary.

To study the stability of zero or near-zero solutions of the above system to non-zero disturbances in ψ, solutions of the linearised version of the model equation (2.2.1) may be sought in the form

$$\psi = e^{\sigma t} f(x,y) \quad , \qquad (2.2.3)$$

where the growth rate $\sigma = \sigma_r + i\sigma_i$ is to be determined. An arbitrary disturbance may be represented as a complete set of normal modes and the stability of each of these modes can be examined individually. Therefore a solution for ψ describing the perturbation is assumed in the form

$$\psi = ae^{\{\sigma t + i(k_x x + k_y y)\}} \quad (a \ll 1) \qquad (2.2.4)$$

where $k = (k_x^2 + k_y^2)^{1/2}$ is the wavenumber of the disturbance. Substitution of (2.2.4) into (2.2.1) leads to the result

$$\sigma = \epsilon - (-k^2 + 1)^2 \quad . \qquad (2.2.5)$$

In general, there are two states of marginal stability corresponding to the two ways in which the amplitude of a small disturbance can grow or be damped. It can grow (or be damped) aperiodically, which implies the transition from stability to instability takes place via a marginal state exhibiting a stationary pattern of motion and it is said that the *principle of the exchange of stabilities* is valid. Alternatively the amplitude can grow (or be damped) by oscillations of increasing (or decreasing) amplitude, which implies the transition takes place via a marginal state exhibiting oscillatory motions with a certain characteristic frequency, and then it is said to be a case of *overstability*. The difference between the two kinds of marginal states depends on whether or not the imaginary part σ_i of σ vanishes when the real part σ_r of σ vanishes. If $\sigma_r = 0$ implies $\sigma_i = 0$, then the principle of the exchange of stabilities is valid; otherwise it is a case of overstability.

In the Rayleigh-Bénard problem a certain critical adverse vertical temperature gradient must be exceeded before instability can set in and the motions which follow on exceeding this critical temperature gradient have a stationary cellular structure. The model equation (2.2.1) simulates the Rayleigh-Bénard problem, and it is seen that at the onset of instability $\sigma = 0$ and

$$\epsilon = (-k^2 + 1)^2 \quad . \qquad (2.2.6)$$

This relation between ϵ and k represents the neutral stability curve for the system, and the critical wavenumber is $k = 1$ at $\epsilon = 0$. When ϵ exceeds zero it can be expected that small disturbances with wavenumber k close to 1 will grow and that a nonlinear steady-state solution

17

for which ψ is non-zero will exist.

In an infinite system ψ may consist of a superposition of modes with arbitrary orientation (k_x, k_y) but in the present work the main interest is in the effect of a lateral boundary along the y-axis and modes which represent convection rolls parallel and perpendicular to this boundary will be considered, equivalent to x and y dependence of the form e^{ix} and e^{iy}, respectively. An amplitude-equation approach of the type introduced by Newell and Whitehead (1969) and Segel (1969) will be adopted, in order to incorporate the effects of spatial modulation, time-dependence and nonlinearity near the critical point.

A balance between terms in (2.2.1) suggests that motion develops with an amplitude ψ of order $\epsilon^{1/2}$. Therefore let

$$\psi = \epsilon^{1/2}\psi_0 + \epsilon\psi_1 + \epsilon^{3/2}\psi_2 + \ldots \quad , \quad \epsilon \to 0 \quad . \qquad (2.2.7)$$

In order to determine the most general form of the amplitude equations for the model system (2.2.1) and the boundary conditions (2.2.2), the semi-infinite domain $x \geq 0$ is allowed to contain x-rolls which have slow spatial modulation on length scales X and $\bar{Y}$ defined by

$$X = \epsilon^{1/2}x \quad , \quad \bar{Y} = \epsilon^{1/4}y \qquad (2.2.8)$$

and y-rolls which have slow spatial modulation on length scales $\bar{X}$ and Y defined by

$$\bar{X} = \epsilon^{1/4}x \quad , \quad Y = \epsilon^{1/2}y \quad . \qquad (2.2.9)$$

In addition, both sets of rolls are allowed to vary on a slow time scale τ defined by

$$\tau = \epsilon t \quad . \qquad (2.2.10)$$

These various scales are determined by the expectation of obtaining amplitude equations at order $\epsilon^{3/2}$ which contain all of the slow spatial and temporal variations of the amplitudes of both

18

x and y-rolls, following the analysis of Newell and Whitehead (1969) and Brown and Stewartson (1977).

At order $\epsilon^{1/2}$, substitution of (2.2.7) into (2.2.1) gives

$$(\nabla^2+1)^2\psi_0 = 0 \quad , \qquad\qquad (2.2.11)$$

where $\nabla^2 = \partial^2/\partial x^2 + \partial^2/\partial y^2$ and the solution for ψ_0 of interest here can be written in the form

$$\psi_0 = \psi_0^A(x,X,\bar{Y},\tau) + \psi_0^B(y,\bar{X},Y,\tau) \quad , \qquad\qquad (2.2.12)$$

where

$$\psi_0^A = A(X,\bar{Y},\tau)e^{ix} + c.c \qquad\qquad (2.2.13)$$

and

$$\psi_0^B = B(\bar{X},Y,\tau)e^{iy} + c.c \quad , \qquad\qquad (2.2.14)$$

where $c.c$ denotes the complex conjugate. Here A and B are the complex amplitude functions associated with x-rolls and y-rolls respectively. The method of multiple scales is used in the sense that in (2.2.1) and (2.2.2), an x-derivative $\partial/\partial x$ operating on ψ_0^A must be replaced by $\partial/\partial x + \epsilon^{1/2}\partial/\partial X$ and a y-derivative by $\epsilon^{1/4}\partial/\partial\bar{Y}$. Similarly a y-derivative $\partial/\partial y$ operating on ψ_0^B must be replaced by $\partial/\partial y + \epsilon^{1/2}\partial/\partial Y$ and an x-derivative by $\epsilon^{1/4}\partial/\partial\bar{X}$. At order ϵ it then follows that ψ_1 satisfies

$$(\nabla^2+1)^2\psi_1 = 0 \quad , \qquad\qquad (2.2.15)$$

giving

$$\psi_1 = \psi_1^A(x,X,\bar{Y},\tau) + \psi_1^B(y,\bar{X},Y,\tau) \quad , \qquad\qquad (2.2.16)$$

where

19

$$\psi_1{}^A = A_1(X,\overline{Y},\tau)e^{ix}+c.c \quad , \tag{2.2.17}$$

$$\psi_1{}^B = B_1(\overline{X},Y,\tau)e^{iy}+c.c \tag{2.2.18}$$

and A_1 and B_1 are further complex amplitude functions, to be considered in greater detail in chapter 6.

At order $\epsilon^{3/2}$, ψ_2 is found to satisfy

$$(\nabla^2+1)^2\psi_2 = \psi_0 - \frac{\partial\psi_0}{\partial\tau} - \left(\frac{\partial^4}{\partial\overline{Y}^4} + \frac{4\partial^4}{\partial x\partial X\partial\overline{Y}^2} + \frac{4\partial^4}{\partial x^2\partial X^2}\right)\psi_0{}^A$$
$$- \left(\frac{\partial^4}{\partial\overline{X}^4} + \frac{4\partial^4}{\partial y\partial Y\partial\overline{X}^2} + \frac{4\partial^4}{\partial y^2\partial Y^2}\right)\psi_0{}^B - \psi_0{}^3 \quad . \tag{2.2.19}$$

The right-hand side contains terms proportional to $e^{\pm ix}$, $e^{\pm 3ix}$, $e^{\pm iy}$, $e^{\pm 3iy}$, $e^{\pm i(x\pm 2y)}$ and $e^{\pm i(2x\pm y)}$. In order that the solution for ψ_2 does not grow with x or y, the secular terms proportional to $e^{\pm ix}$ and $e^{\pm iy}$ must be avoided, and after substitution for ψ_0 from (2.2.12) this requires that

$$\frac{\partial A}{\partial\tau} = A-3A(|A|^2+2|B|^2)+4\left(\frac{\partial}{\partial X}-\frac{i}{2}\frac{\partial^2}{\partial\overline{Y}^2}\right)^2 A \tag{2.2.20}$$

and that

$$\frac{\partial B}{\partial\tau} = B-3B(|B|^2+2|A|^2)+4\left(\frac{\partial}{\partial Y}-\frac{i}{2}\frac{\partial^2}{\partial\overline{X}^2}\right)^2 B \quad . \tag{2.2.21}$$

It is worth noting that to a leading approximation these amplitude equations may be restated in terms of the original spatial and temporal variables x, y and t by writing

$$\psi \sim \{\tilde{A}(x,y,t)e^{ix}+\tilde{B}(x,y,t)e^{iy}\}+c.c. \tag{2.2.22}$$

and then $\tilde{A}$ and $\tilde{B}$ satisfy

20

$$\frac{\partial \tilde{A}}{\partial t} = \epsilon\tilde{A} - 3\tilde{A}(|\tilde{A}|^2 + 2|\tilde{B}|^2) + 4\left(\frac{\partial}{\partial x} - \frac{i}{2}\frac{\partial^2}{\partial y^2}\right)^2 \tilde{A} \quad , \tag{2.2.23}$$

$$\frac{\partial \tilde{B}}{\partial t} = \epsilon\tilde{B} - 3\tilde{B}(|\tilde{B}|^2 + 2|\tilde{A}|^2) + 4\left(\frac{\partial}{\partial y} - \frac{i}{2}\frac{\partial^2}{\partial x^2}\right)^2 \tilde{B} \quad , \tag{2.2.24}$$

(Daniels & Weinstein 1992). It should be understood that the validity of (2.2.23) and (2.2.24) relies on the assumption that ϵ is small so that the amplitudes $\tilde{A}$ and $\tilde{B}$ are small, of order $\epsilon^{1/2}$, and develop on a long time scale t of order ϵ^{-1}. Scales of spatial modulation for $\tilde{A}$ and $\tilde{B}$ are more difficult to determine because of the coupling between the two modes implied by (2.2.23) and (2.2.24). Nevertheless the equations do contain all possible leading order variations with x and y and can therefore be used to describe the evolution of the system on appropriate length scales to be identified below.

Boundary conditions for the amplitude functions $\tilde{A}$ and $\tilde{B}$ are now determined. Near the lateral boundary $x=0$, the solutions of (2.2.23) and (2.2.24) must adjust to the conditions (2.2.2) on the ordinary length scale x and the equation valid in the boundary region is hence the steady linearised form of (2.2.1):

$$(\nabla^2 + 1)^2 \psi = 0 \quad , \tag{2.2.25}$$

which has a solution

$$\psi \sim \{e^{ix}(a_1 + b_1 x) + e^{iy}(a_2 + b_2 x + c_2 x^2 + d_2 x^3)\} + c.c \quad . \tag{2.2.26}$$

Matching of this form near the boundary with the outer solution for ψ given by (2.2.22) as $x \to 0$ gives

21

$$a_1 = \tilde{A}(0,y,t) \quad , \quad b_1 = \frac{\partial \tilde{A}}{\partial x}(0,y,t) \quad , \tag{2.2.27}$$

in which case $b_1 \ll a_1$ and therefore to a first approximation (2.2.2) gives

$$a_1 + a_1^\star = 2\lambda \epsilon^{1/2} \quad , \quad a_1 - a_1^\star = 0 \quad , \tag{2.2.28}$$

where $\star$ denotes complex conjugate. Thus $a_1 = \lambda \epsilon^{1/2}$ and (2.2.23) must be solved subject to

$$\tilde{A} = \lambda \epsilon^{1/2} \quad \text{at} \quad x = 0 \quad . \tag{2.2.29}$$

Similarly,

$$a_2 = \tilde{B}(0,y,t) \quad , \quad b_2 = \frac{\partial \tilde{B}}{\partial x}(0,y,t) \quad ,$$

$$2c_2 = \frac{\partial^2 \tilde{B}}{\partial x^2}(0,y,t) \quad , \quad 6d_2 = \frac{\partial^3 \tilde{B}}{\partial x^3}(0,y,t) \quad , \tag{2.2.30}$$

in which case $d_2 \ll c_2 \ll b_2 \ll a_2$ and therefore to a first approximation (2.2.2) gives $a_2 = b_2 = 0$. Thus (2.2.24) must be solved subject to

$$\tilde{B} = \frac{\partial \tilde{B}}{\partial x} = 0 \quad \text{at} \quad x = 0 \quad . \tag{2.2.31}$$

A similar result for the Oberbeck-Boussinesq system was first obtained by Brown and Stewartson (1977).

At large distances it will be supposed that a finite-amplitude roll pattern is established parallel to the lateral boundary and with no modulation in the y-direction such that

$$\tilde{A} \to \left(\frac{\epsilon}{3}\right)^{1/2} \quad , \quad \tilde{B} \to 0 \quad \text{as} \quad x \to \infty \quad . \tag{2.2.32}$$

It is anticipated that this situation will occur along the shorter lateral sides of a shallow box of rectangular planform.

To summarise this section, the leading order amplitude equations (2.2.23) and (2.2.24) have been obtained for solutions of the model equation corresponding to x-rolls and y-rolls, together with appropriate boundary conditions (2.2.29), (2.2.31) and (2.2.32). The amplitudes of the two sets of rolls are coupled through the nonlinear terms in the equations.

2.3 Amplitude equations for Rayleigh-Bénard convection with rigid surfaces

In this section it is shown that the amplitude equations (2.2.20) and (2.2.21) are in fact a special case of the equations governing weakly nonlinear convection in a real fluid layer bounded above and below by rigid horizontal surfaces. Here it is convenient to work in terms of Cartesian co-ordinates $\hat{x}$, $\hat{y}$, $\hat{z}$ non-dimensionalised with respect to the depth of the layer d, with $\hat{z}$ in the vertical direction. The temperature field in the fluid can be expressed in the form

$$\theta^* = \theta_0^* - \Delta\theta^*\hat{z} + \Delta\theta^*\theta(\hat{x},\hat{y},\hat{z},\hat{t}) \quad , \tag{2.3.1}$$

where $\theta_0^* \mp (\Delta\theta^*)/2$ are the constant temperatures of the upper and lower surfaces, $\hat{z} = \pm 1/2$, respectively and θ is a non-dimensional measure of the temperature relative to that of a state of pure conduction. The governing equations in the Boussinesq approximation then depend on two non-dimensional parameters, the Rayleigh number

$$R = \frac{\alpha g \Delta\theta^* d^3}{\kappa\nu} \quad , \tag{2.3.2}$$

where α is the coefficient of thermal expansion, g is the acceleration due to gravity, κ is the thermal diffusivity and ν is the kinematic viscosity, and the Prandtl number

$$P = \frac{\nu}{\kappa} \quad . \tag{2.3.3}$$

Linear theory (see Chandrasekhar 1963) predicts that instability first occurs when the Rayleigh number reaches a value $R_0 = 1707.76$ and the critical wavenumber for rolls is $q_0 = 3.117$. A weakly nonlinear theory can then be developed incorporating slow spatial and temporal

modulation, and nonlinear effects, for Rayleigh numbers R close to R_0. A significant amount of numerical work is involved in calculating the coefficients of the various terms which appear in the amplitude equations and contributions to this have been made by Schluter, Lortz and Busse (1965), Kelly and Pal (1978), Wesfried et al (1978), Cross (1980) and Chana and Daniels (1989).

Setting

$$R - R_0 = q^2 \epsilon \quad , \tag{2.3.4}$$

with q to be specified below, the solution is based on the assumption that ϵ is a small parameter, and for rolls with axes aligned perpendicular to the x-direction (x-rolls) the temperature field θ can be expressed in the form

$$\theta \sim \epsilon^{1/2} q \{ e^{iq_0 \hat{x}} \hat{A}(X, \bar{Y}, \hat{t}) + c.c \} g(\hat{z}) \quad , \tag{2.3.5}$$

where

$$\hat{x} = \epsilon^{-1/2} q_0^{-1} X \quad , \quad \hat{y} = \epsilon^{-1/4} q_0^{-1} \bar{Y} \quad , \quad \hat{t} = \epsilon^{-1} q^{-2} \hat{t} \quad . \tag{2.3.6}$$

The function $g(\hat{z})$ is determined from linear theory (see Chandrasekhar 1963) and if a normalization is assumed such that $g(0) = 1$, the equation for the complex amplitude function $\hat{A}$ has the form

$$\left(\hat{\mu}_1 + \frac{\hat{\mu}_2}{P} \right) \frac{\partial \hat{A}}{\partial \hat{t}} = \hat{A} + 4 \left(\frac{\partial}{\partial X} - \frac{i}{2} \frac{\partial^2}{\partial \bar{Y}^2} \right)^2 \hat{A} - \left(\hat{\mu}_4 + \frac{\hat{\mu}_5}{P} + \frac{\hat{\mu}_6}{P^2} \right) \hat{A} |\hat{A}|^2 \quad , \tag{2.3.7}$$

where it is convenient to choose $q = q_0 \hat{\mu}_3^{1/2}/2$ and

$$
\begin{aligned}
\hat{\mu}_1 &= 86.91 \quad , \quad \hat{\mu}_2 = \quad 44.47 \quad , \quad \hat{\mu}_3 = 252.20 \quad , \\
\hat{\mu}_4 &= 22281 \quad , \quad \hat{\mu}_5 = -150.37 \quad , \quad \hat{\mu}_6 = 265.05 \quad ,
\end{aligned}
\tag{2.3.8}
$$

are coefficients given by Daniels and Ong (1990a).

24

In the present study it is intended to investigate the interaction of x-rolls and y-rolls, and for this purpose the amplitude equation (2.3.7) must be extended to incorporate the resulting nonlinear interaction. This was first studied by Schluter at al (1965) and is equivalent to the addition of an extra term

$$-\left(\hat{\mu}_7+\frac{\hat{\mu}_8}{P}+\frac{\hat{\mu}_9}{P^2}\right)\hat{A}\,|\hat{B}|^2 \qquad (2.3.9)$$

on the right-hand side of (2.3.7), the temperature field now being given by

$$\hat{\theta} \sim \epsilon^{1/2}q\{\ e^{iq_0\hat{x}}\hat{A}\ +\ e^{iq_0\hat{y}}\hat{B}\ +\ c.c\ \}g(\hat{z})\quad , \qquad (2.3.10)$$

where $\hat{B}$ represents the amplitude of the y-rolls. The ratio of the two nonlinear terms, in $\hat{A}\,|\hat{A}|^2$ and $\hat{A}\,|\hat{B}|^2$, can be inferred from the calculations of Schluter et al (1965) as follows. Their existence conditions for the third order solution (without spatial or temporal modulation) are

$$-KR^{(2)}+\frac{1}{2}\sum T_{nm}C^{\star}{}_m C_m = 0\quad ,\quad m,\,n\,=\,(-2,\,-1,\,1,\,2)\quad , \qquad (2.3.11)$$

where $KR^{(2)}$ is a constant. These conditions are equivalent to amplitude equations for $\hat{A}$ (where $n=\pm 1$) and $\hat{B}$ (where $n=\pm 2$), with $C_1=\hat{A}$ and $C_2=\hat{B}$, giving respectively for $\hat{A}$:

$$-KR^{(2)}+T_{12}|\hat{B}|^2+T_{11}|\hat{A}|^2 \,=\, 0 \qquad (2.3.12)$$

and for $\hat{B}$:

$$-KR^{(2)}+T_{12}|\hat{A}|^2+T_{11}|\hat{B}|^2 \,=\, 0\quad . \qquad (2.3.13)$$

The nonlinear terms in $\hat{A}$ and $\hat{B}$ are seen to appear in the combinations

$$|\hat{A}|^2 \,+\, \frac{T_{12}}{T_{11}}|\hat{B}|^2 \quad , \qquad (2.3.14)$$

25

$$|\hat{B}|^2 + \frac{T_{12}}{T_{11}}|\hat{A}|^2 \quad , \tag{2.3.15}$$

in the equations for $\hat{A}$ and $\hat{B}$ respectively. These terms correspond to the nonlinear terms found in the amplitude equations (2.2.20) and (2.2.21), and so to determine the equivalent Rayleigh-Bénard system it is necessary to find the ratio $\mu = T_{12}/T_{11}$. The matrix elements T_{11} and T_{12} are defined by

$$T_{11} = 2L(-1,+1) + L(+1,-1) \quad , \tag{2.3.16}$$

$$T_{12} = 2[2L(0,0) + L(-1,+1)] \quad , \tag{2.3.17}$$

where for rigid upper and lower boundaries

$$L(\phi,-\phi) = q_0^4[L_{-1}(\phi)P^{-1} + L_0(\phi)P^0 + L_1(\phi)P^1] \quad . \tag{2.3.18}$$

Substitution of the appropriate values of the functions L_{-1}, L_0 and L_1 determined by Schluter et al (1965) then gives

$$T_{11} = \frac{q_0^4}{P}\left[125014P^2 - 843.9P + 1487.8\right] \tag{2.3.19}$$

and

$$T_{12} = \frac{2q_0^4}{P}\left[76712P^2 + 7564.4P + 10629.2\right] \tag{2.3.20}$$

so that

$$\frac{T_{12}}{T_{11}} = 2\left(\frac{76712P^2 + 7564.4P + 10629.2}{125014P^2 - 843.9P + 1487.8}\right) \quad , \quad 0 < P < \infty \quad . \tag{2.3.21}$$

It follows that the amplitude equation for $\hat{A}$ is

$$\left(\hat{\mu}_1 + \frac{\hat{\mu}_2}{P}\right)\frac{\partial \hat{A}}{\partial \hat{\tau}} = \hat{A} + 4\left(\frac{\partial}{\partial X} - \frac{i}{2}\frac{\partial^2}{\partial \overline{Y}^2}\right)^2 \hat{A} - \left(\hat{\mu}_4 + \frac{\hat{\mu}_5}{P} + \frac{\hat{\mu}_6}{P^2}\right)\hat{A}|\hat{A}|^2 - \left(\hat{\mu}_7 + \frac{\hat{\mu}_8}{P} + \frac{\hat{\mu}_9}{P^2}\right)\hat{A}|\hat{B}|^2$$

$$(2.3.22)$$

where

$$\hat{\mu}_7 = 27338.19 \quad , \quad \hat{\mu}_8 = 2695.76 \quad , \quad \hat{\mu}_9 = 3787.97 \quad . \qquad (2.3.23)$$

This can be simplified by applying the scale transformations

$$\hat{A} = \left(\frac{3}{\hat{\mu}_4 + \frac{\hat{\mu}_5}{P} + \frac{\hat{\mu}_6}{P^2}}\right)^{1/2} A \quad , \quad \hat{B} = \left(\frac{3}{\hat{\mu}_4 + \frac{\hat{\mu}_5}{P} + \frac{\hat{\mu}_6}{P^2}}\right)^{1/2} B \quad , \quad \hat{\tau} = \left(\hat{\mu}_1 + \frac{\hat{\mu}_2}{P}\right)\tau \quad ,$$

$$(2.3.24)$$

to give

$$\frac{\partial A}{\partial \tau} = A + 4\left(\frac{\partial}{\partial X} - \frac{i}{2}\frac{\partial^2}{\partial \overline{Y}^2}\right)^2 A - 3A(|A|^2 + \mu|B|^2) \quad , \qquad (2.3.25)$$

where

$$\mu = \frac{\hat{\mu}_7 P^2 + \hat{\mu}_8 P + \hat{\mu}_9}{\hat{\mu}_4 P^2 + \hat{\mu}_5 P + \hat{\mu}_6} \qquad (2.3.26)$$

and of course a similar argument implies that B must satisfy

$$\frac{\partial B}{\partial \tau} = B + 4\left(\frac{\partial}{\partial Y} - \frac{i}{2}\frac{\partial^2}{\partial \overline{X}^2}\right)^2 B - 3B(|B|^2 + \mu|A|^2) \quad , \qquad (2.3.27)$$

where

$$\hat{x} = \epsilon^{-1/4} q_0^{-1} \overline{X} \quad , \quad \hat{y} = \epsilon^{-1/2} q_0^{-1} Y \quad . \qquad (2.3.28)$$

From (2.3.26),

27

$$\mu \rightarrow 1.227 \quad \text{as} \quad P \rightarrow \infty \qquad\qquad (2.3.29)$$

and

$$\mu \rightarrow 14.288 \quad \text{as} \quad P \rightarrow 0 \qquad\qquad (2.3.30)$$

(see Figure 2.1) and the range of values of the parameter μ in the amplitude equations (2.3.25) and (2.3.27) is

$$1.227 < \mu < 14.288 \quad . \qquad\qquad (2.3.31)$$

The pair of equations (2.2.20) and (2.2.21) obtained for the model problem is seen to be precisely equivalent to the pair (2.3.25) and (2.3.27) for the Rayleigh-Bénard problem with rigid horizontal surfaces when the parameter μ takes the value 2.

It should be added that in the Rayleigh-Bénard system the boundary conditions at a lateral wall for the amplitude functions A and B are also similar to those derived for the model problem in section 2.2. In practice these must be derived by considering the region immediately adjacent to the wall. Stewartson and Weinstein (1979) considered the condition on A corresponding to lateral forcing at the wall, equivalent, for example, to a non-zero heat transfer there, and showed that the physical boundary condition translates into a condition of the form (2.2.29) on the amplitude function, $\lambda \epsilon^{1/2}$ representing the magnitude of the lateral forcing. Similarly, Chana and Daniels (1989) considered the relevant boundary conditions for B and argued that the conditions first derived for the stress-free case by Brown and Stewartson (1977) and derived for the model problem in (2.2.31) must also apply in the case of rigid horizontal surfaces. Thus the set of equations and boundary conditions of the model problem are directly relevant to the physical Rayleigh-Bénard problem, providing a strong motivation for studying this particular system in depth.

The overall system for the Rayleigh-Bénard problem derived in this section can be summarised in terms of variables not scaled with ϵ by writing

$$\tilde{A} = \epsilon^{1/2}A \quad , \quad \tilde{B} = \epsilon^{1/2}B \quad , \quad x = \epsilon^{-1/2}X \quad , \quad y = \epsilon^{-1/2}Y \quad , \quad t = \epsilon^{-1}\tau \quad , \quad (2.3.32)$$

to obtain

$$\frac{\partial \tilde{A}}{\partial t} = \epsilon\tilde{A} - 3\tilde{A}(|\tilde{A}|^2 + \mu|\tilde{B}|^2) + 4\left(\frac{\partial}{\partial x} - \frac{i}{2}\frac{\partial^2}{\partial y^2}\right)^2 \tilde{A} \quad , \qquad (2.3.33)$$

$$\frac{\partial \tilde{B}}{\partial t} = \epsilon\tilde{B} - 3\tilde{B}(|\tilde{B}|^2 + \mu|\tilde{A}|^2) + 4\left(\frac{\partial}{\partial y} - \frac{i}{2}\frac{\partial^2}{\partial x^2}\right)^2 \tilde{B} \quad , \qquad (2.3.34)$$

$$\tilde{A} = \lambda\epsilon^{1/2} \quad \text{at} \quad x = 0 \quad , \qquad (2.3.35)$$

$$\tilde{B} = \frac{\partial \tilde{B}}{\partial x} = 0 \quad \text{at} \quad x = 0 \quad , \qquad (2.3.36)$$

$$\tilde{A} \to \left(\frac{\epsilon}{3}\right)^{1/2} \quad , \quad \tilde{B} \to 0 \quad \text{as} \quad x \to \infty \quad , \qquad (2.3.37)$$

and this is seen to be equivalent to the system (2.2.23), (2.2.24), (2.2.29), (2.2.31) and (2.2.32) of the model problem when $\mu = 2$. An investigation of the effect of μ on the solution of the system is the main aim of this chapter.

2.4 Normal modes of the cross-roll instability for general μ

In this section the normal modes of the cross-roll instability are found for the system (2.3.33)-(2.3.37), restricting attention to solutions for which the amplitudes are real and independent of y. The roll pattern adjusts to its finite-amplitude form on a length scale x of order $\epsilon^{-1/2}$ and it is convenient to set

$$X = \epsilon^{1/2}x \quad , \quad \tau = \epsilon t \quad ,$$

$$\tilde{A}(x,y,t) = \epsilon^{1/2}A(X,\tau) \quad , \quad \tilde{B}(x,y,t) = \epsilon^{1/2}B(X,\tau) \tag{2.4.1}$$

giving the reduced system

$$\frac{\partial A}{\partial \tau} = 4\frac{\partial^2 A}{\partial X^2} + A - 3A^3 - 3\mu AB^2 \quad , \tag{2.4.2}$$

$$\frac{\partial B}{\partial \tau} = B - 3B^3 - 3\mu BA^2 - \epsilon\frac{\partial^4 B}{\partial X^4} \quad , \tag{2.4.3}$$

$$A = \lambda \quad \text{at} \quad X = 0 \quad , \tag{2.4.4}$$

$$B = \frac{\partial B}{\partial X} = 0 \quad \text{at} \quad X = 0 \quad , \tag{2.4.5}$$

$$A \to \frac{1}{\sqrt{3}} \quad , \quad B \to 0 \quad \text{as} \quad X \to \infty \quad . \tag{2.4.6}$$

One steady-state solution of the above system occurs when $B=0$ which means that only x-rolls parallel to the boundary are present. To simplify the problem the case of no imperfection is considered ($\lambda=0$) and the solution for A is found by substituting $B=0$ into the steady-state form of (2.4.2) producing

$$A = \frac{1}{\sqrt{3}}\tanh\left(\frac{X}{2\sqrt{2}}\right) \quad , \quad B = 0 \quad . \tag{2.4.7}$$

The stability of this steady-state solution is now considered. A cross-roll perturbation is introduced and it is assumed that these y-rolls have small amplitude so that the equation for B can be linearised, giving

$$\frac{\partial B}{\partial \tau} = B \left[1 - \mu \tanh^2\left(\frac{X}{2\sqrt{2}}\right) \right] - \epsilon \frac{\partial^4 B}{\partial X^4} \quad . \tag{2.4.8}$$

A study is made of normal modes of instability of the form

$$B(X,\tau) = F(X)\exp(\sigma\tau) \quad . \tag{2.4.9}$$

Upon substitution of (2.4.9) into (2.4.8) and the boundary conditions for B at $X=0$ and as $X \to \infty$ the following eigenvalue problem is obtained:

$$\epsilon \frac{\partial^4 F}{\partial X^4} - F \left[1 - \sigma - \mu \tanh^2\left(\frac{X}{2\sqrt{2}}\right) \right] = 0 \quad , \tag{2.4.10}$$

$$F = \frac{\partial F}{\partial X} = 0 \quad \text{at} \quad X = 0 \quad , \tag{2.4.11}$$

$$F \to 0 \quad \text{as} \quad X \to \infty \quad . \tag{2.4.12}$$

Pomeau and Zaleski (1981) used a Rayleigh-Ritz argument to illustrate the existence of positive eigenvalues σ in the above problem when $\mu=2$. As ϵ is a small parameter, the eigenvalue problem (2.4.10)-(2.4.12) is a singular perturbation problem and a WKB method can in fact be used to determine, analytically, the structure of the short-wave normal mode disturbances; the appropriate analysis for $\mu=2$ was carried out by Daniels and Weinstein (1992).

On the long length-scale X the solution can be written as

$$F \sim F_0(X)\sin\left[\epsilon^{-1/4} \int_0^X \omega(X')dX' + \theta \right] \quad , \quad \epsilon \to 0 \quad , \tag{2.4.13}$$

where θ is an arbitrary constant and

$$\omega(X) = \left[1 - \sigma - \mu \tanh^2\left(\frac{X}{2\sqrt{2}}\right) \right]^{1/4} \quad . \tag{2.4.14}$$

31

Further, terms of order $\epsilon^{1/4}$ yield

$$F_0(X) = a_0\omega^{-3/2} \qquad (2.4.15)$$

where a_0 is an arbitrary constant. This solution is valid for $X < X_0$ where X_0 is defined to be the value of X at which $\omega = 0$:

$$X_0 = 2\sqrt{2}\tanh^{-1}\left[\left(\frac{1-\sigma}{\mu}\right)^{1/2}\right] \quad , \quad 0 < \sigma < 1, \quad \mu > 0 \quad . \qquad (2.4.16)$$

In the region where $X < X_0$, ω is real and positive which implies that $F(X)$ is rapidly oscillating. It is assumed that $\mu > 0$ and then eigenfunctions of the type shown in (2.4.13) correspond to growth rates σ such that $1 - \mu < \sigma < 1$. As $X \rightarrow X_0$, $\omega \sim \hat{k}(X_0 - X)^{1/4}$, where

$$\hat{k} = 2^{-1/8}\left(\frac{1-\sigma}{\mu}\right)^{1/8}[\mu - 1 + \sigma]^{1/4} \qquad (2.4.17)$$

and it follows that

$$F \sim a_0\hat{k}^{-3/2}(X_0 - X)^{-3/8}\sin\left[\epsilon^{-1/4}\left(I(\sigma) - \frac{4\hat{k}(X_0 - X)^{5/4}}{5}\right) + \theta\right] \quad , \quad X \rightarrow X_0^- \quad , \qquad (2.4.18)$$

where

$$I(\sigma) = \int_0^{X_0}\omega(X')dX' \quad . \qquad (2.4.19)$$

It is now necessary to find the local solution near X_0, where the differential equation for F has the form

$$\epsilon\frac{\partial^4 F}{\partial X^4} - (X_0 - X)\hat{k}^4 F = 0 \quad , \qquad (2.4.20)$$

from which it can be seen that there is a variation on a local length scale ξ defined by

32

$$X = X_0 + \epsilon^{1/5} \hat{k}^{-4/5} \xi \quad , \tag{2.4.21}$$

where

$$F \sim a_0 \epsilon^{-3/40} f(\xi) \tag{2.4.22}$$

and

$$\frac{\partial^4 f}{\partial \xi^4} + \xi f = 0 \quad . \tag{2.4.23}$$

Just one of the four fundamental solutions of (2.4.23) avoids exponential growth both as $\xi \to \infty$ and $\xi \to -\infty$ and this solution, $f = f^{(1)}$, has the behaviour

$$f^{(1)} \sim (2\pi)^{-1/2} \xi^{-3/8} \exp\left(\frac{-2\sqrt{2} \xi^{5/4}}{5} \right) \cos\left(\frac{2\sqrt{2} \xi^{5/4}}{5} - \frac{\pi}{8} \right) \quad , \quad \xi \to \infty \quad ,$$

$$\tag{2.4.24}$$

$$f^{(1)} \sim (2\pi)^{-1/2} (-\xi)^{-3/8} \sin\left(\frac{-4(-\xi)^{5/4}}{5} + \frac{3\pi}{4} \right) \quad , \quad \xi \to -\infty \quad ,$$

(Ross 1966). The required solution of (2.4.23) is therefore

$$f = (2\pi)^{1/2} \hat{k}^{-6/5} f^{(1)} \quad , \tag{2.4.25}$$

and matching with (2.4.18) gives

$$I(\sigma) = \epsilon^{1/4} \left(\frac{3\pi}{4} - \theta \right) \quad . \tag{2.4.26}$$

The solution for F in the region $0 < X < X_0$ does not satisfy the boundary conditions at $X=0$ and thus a region exists near the lateral boundary in which the solution adjusts to these

33

boundary conditions. Near the lateral boundary, the differential equation for F is approximated by

$$\epsilon \frac{\partial^4 F}{\partial X^4} - (1-\sigma)F = 0 \quad , \tag{2.4.27}$$

from which it can be seen that near the wall there is a variation on a length scale $\bar{X}$ defined by $X = \epsilon^{1/4}\bar{X}$, and the local solution for F is

$$F \sim \bar{F}(\bar{X}) \quad , \tag{2.4.28}$$

where

$$\frac{\partial^4 \bar{F}}{\partial \bar{X}^4} - (1-\sigma)\bar{F} = 0 \tag{2.4.29}$$

and

$$\bar{F} = \frac{\partial \bar{F}}{\partial \bar{X}} = 0 \quad \text{at} \quad \bar{X} = 0 \quad . \tag{2.4.30}$$

The general solution avoiding exponential growth as $\bar{X} \to \infty$ is

$$\bar{F}(\bar{X}) = \bar{a} \, \sin[(1-\sigma)^{1/4}\bar{X} + \bar{\theta}] + \bar{b} \, e^{-(1-\sigma)^{1/4}\bar{X}} \tag{2.4.31}$$

and this satisfies the boundary conditions (2.4.30) provided

$$\bar{a} \, \sin\bar{\theta} + \bar{b} = 0 \quad , \quad \bar{a} \, \cos\bar{\theta} - \bar{b} = 0 \tag{2.4.32}$$

and as $\bar{X} \to \infty$ matches with the form of (2.4.13) as $X \to 0$ provided

$$\bar{a} = a_0(1-\sigma)^{-3/8} \quad , \quad \bar{\theta} = \theta \quad . \tag{2.4.33}$$

From (2.4.32),

34

$$\overline{\theta} = \frac{\pi}{4}(3-4n) \quad , \quad \overline{b} = \overline{a}\left((-1)^{n+1}\frac{1}{\sqrt{2}}\right) \tag{2.4.34}$$

for any integer n, and it now follows from (2.4.26) that

$$I(\sigma) = \epsilon^{1/4}n\pi \quad . \tag{2.4.35}$$

This implicit equation for the eigenvalue σ produces an infinite sequence of growth rates in the limit as $\epsilon \to 0$ and $n \to \infty$, with $\epsilon^{1/4}n$ of order unity.

In order to find a formula for the maximum growth rate, it is noted that this occurs when σ is near 1. Letting $\sigma = 1-\delta$ with δ taken to be small, it follows from (2.4.16) that

$$X_0 \sim 2^{3/2}\left(\frac{\delta}{\mu}\right)^{1/2} \tag{2.4.36}$$

and then

$$I \sim \int_0^{2^{3/2}\left(\frac{\delta}{\mu}\right)^{1/2}} \left[\delta - \frac{\mu X^2}{8}\right]^{1/4} dX \quad , \quad \sigma \to 1 \quad .$$

A substitution $Y = X\mu^{1/2}/2^{3/2}\delta^{1/2}$ gives

$$\begin{aligned} I &\sim \frac{2^{3/2}\delta^{3/4}}{\mu^{1/2}}\int_0^1 [1-Y^2]^{1/4}dY \\ &= \frac{2^{3/2}\delta^{3/4}}{\mu^{1/2}}\int_0^{\pi/2} \cos^{3/2}Z \, dZ \end{aligned} \tag{2.4.37}$$

and this integral can be determined in terms of Gamma functions to give

$$I \sim \frac{2^{1/2}\delta^{3/4}}{\mu^{1/2}}\frac{\Gamma\left(\frac{1}{2}\right)\Gamma\left(\frac{5}{4}\right)}{\Gamma\left(\frac{7}{4}\right)} = \frac{(1-\sigma)^{3/4}\,\Gamma^2\left(\frac{1}{4}\right)}{3\sqrt{\mu\pi}} \quad , \quad \sigma \to 1 \quad . \tag{2.4.38}$$

35

On combining this result with (2.4.35), the maximum growth rates are represented by

$$\sigma = 1 - 1.377\epsilon^{1/3} n^{4/3} \mu^{2/3} \quad , \quad \epsilon^{1/4} n \ll 1 \quad . \tag{2.4.39}$$

When the growth rate σ is close to 1, it can be readily seen from (2.4.36) that X_0 is close to zero and hence the disturbances are concentrated near the boundary. As the transition point X_0 increases in value, the growth rate decreases and is zero when

$$X_0 = 2\sqrt{2}\tanh^{-1}\left[\frac{1}{\sqrt{\mu}}\right] \quad , \tag{2.4.40}$$

for $\mu > 1$, so that growing modes are confined to a finite region in X. In general, $X_0 \rightarrow \infty$ as σ approaches the value $1-\mu$ and if $\mu < 1$ the solution would need to be reconsidered because growing modes (with $\sigma > 0$) would then exist for all values of X extending to infinity. Since $A = 1/\sqrt{(3\mu)}$ at $X = X_0$ the results of this section indicate that the x-roll pattern is unstable to cross-rolls in the locality of the wall where $0 \le A < 1/\sqrt{(3\mu)}$, a result equivalent to the cross-roll instability for an infinite fluid layer discussed by Newell and Whitehead (1969).

The theory described above does not actually include the maximum growth rates which occur for disturbances confined to the neighbourhood of the lateral boundary. As the growth rate increases to 1, X_0 decreases and the three regions of the WKB solution collapse into a single region near the wall. From (2.4.39) it is reasonable to assume that this unified structure is identified with growth rates

$$\sigma = 1 - \epsilon^{1/3}\Delta_n \tag{2.4.41}$$

where Δ_n, $n = 1, 2, \ldots$, are finite eigenvalues. The solution for F in this single region where X is small is now found. Locally the differential equation for F is approximated by

$$\epsilon \frac{\partial^4 F}{\partial X^4} - \left(1 - \sigma - \frac{\mu X^2}{8}\right) F = 0 \tag{2.4.42}$$

and a full balance of terms incorporating (2.4.41) suggests a local length scale $\tilde{X}$ defined by $X = \epsilon^{1/6} \tilde{X}$, with $F \sim \tilde{F}(\tilde{X})$. Then $\tilde{F}$ satisfies the system

$$\frac{\partial^4 \tilde{F}}{\partial \tilde{X}^4} - \left(\Delta - \frac{\mu \tilde{X}^2}{8}\right) \tilde{F} = 0 \quad,$$

$$\tilde{F} = \frac{\partial \tilde{F}}{\partial \tilde{X}} = 0 \quad \text{at} \quad \tilde{X} = 0 \quad, \tag{2.4.43}$$

$$\tilde{F} \to 0 \quad \text{as} \quad \tilde{X} \to \infty$$

and this needs to be solved numerically to find the eigenvalues $\Delta = \Delta_n$. The leading eigenvalue corresponding to the highest growth rate was found numerically to be

$$\Delta_1 = 2.29 \left(\frac{\mu}{2}\right)^{2/3} \quad . \tag{2.4.44}$$

Higher eigenvalues up to $n = 5$ were determined to be

$$\Delta_{2,3,4,5,\dots} = \left(\frac{\mu}{2}\right)^{2/3} (5.53, \ 9.47, \ 13.89, \ 18.69,\dots) \quad . \tag{2.4.45}$$

As $n \to \infty$,

$$\Delta_n \sim 1.377 n^{4/3} \mu^{2/3} \tag{2.4.46}$$

and the result (2.4.39) is recovered. It can be seen from the solutions (2.4.45) that the asymptotic formula (2.4.46) is rapidly approached as n increases.

2.5 Nonlinear evolution

The nonlinear evolution of the system (2.3.33)-(2.3.37) is now investigated for orthogonal roll solutions

$$\tilde{A}(x,y,t) = \epsilon^{1/2}A(X,\tau) \quad , \quad \tilde{B}(x,y,t) = \epsilon^{1/2}B(X,\tau) \quad , \tag{2.5.1}$$

where $x=\epsilon^{-1/2}X$ and $t=\epsilon^{-1}\tau$ and the amplitudes are assumed to be real and independent of y. Then A and B satisfy the reduced system

$$\frac{\partial A}{\partial \tau} = 4\frac{\partial^2 A}{\partial X^2} + A - 3A^3 - 3\mu AB^2 \quad , \tag{2.5.2}$$

$$\frac{\partial B}{\partial \tau} = B - 3B^3 - 3\mu A^2 B \quad , \tag{2.5.3}$$

to be solved subject to the boundary conditions

$$A = \lambda \quad \text{at} \quad X = 0 \quad ; \quad A \rightarrow \frac{1}{\sqrt{3}} \quad , \quad B \rightarrow 0 \quad \text{as} \quad X \rightarrow \infty \quad . \tag{2.5.4}$$

Solutions for positive initial profiles

$$A = A_0(X) \quad , \quad B = B_0(X) \quad \text{at} \quad \tau = 0 \tag{2.5.5}$$

and positive values of λ are examined although the results could easily be generalised to other cases.

It should be noted that in equation (2.4.3) the term $\partial^4 B/\partial X^4$ is formally of order ϵ and is therefore neglected relative to the other terms in the equation. Thus the equation for B no longer includes any spatial derivatives which means that the boundary conditions for B at $X=0$ cannot be satisfied. However, the necessary adjustment of the y-roll amplitude to the conditions (2.4.5) occurs within an inner region where $\tilde{X}=\epsilon^{-1/4}X=O(1)$ and the solution there is now briefly considered. Since $A=\lambda$ at $X=0$ it follows from (2.5.3) that

$$B(0,\tau) = B_+(\tau) = \left(\frac{B_0^2(0)[1-3\mu\lambda^2]e^{2(1-3\mu\lambda^2)\tau}}{1-3\mu\lambda^2-3B_0^2(0)[1-e^{2(1-3\mu\lambda^2)\tau}]} \right)^{1/2} \tag{2.5.6}$$

38

and in the inner region $A \approx \lambda$ and $B \sim \bar{B}(\bar{X}, \tau)$ where

$$\frac{\partial \bar{B}}{\partial \tau} = \bar{B}(1 - 3\mu\lambda^2) - 3\bar{B}^3 - \frac{\partial^4 \bar{B}}{\partial \bar{X}^4} \quad , \tag{2.5.7}$$

with

$$\bar{B} = \frac{\partial \bar{B}}{\partial \bar{X}} = 0 \quad \text{at} \quad \bar{X} = 0 \tag{2.5.8}$$

$$\bar{B} \rightarrow B_+(\tau) \quad \text{as} \quad \bar{X} \rightarrow \infty \quad . \tag{2.5.9}$$

An initial profile at $\tau = 0$ is needed to completely specify the problem for $\bar{B}$ and a full solution is not attempted here. However two limiting cases are considered.

First, if $\bar{B}$ is small the equation for $\bar{B}$ can be linearised ($\bar{B}^3$ is neglected) and there is a solution of the form

$$\bar{B} = B_0(0)\bar{f}(\eta)e^{(1-3\mu\lambda^2)\tau} \quad \text{where} \quad \eta = \frac{\bar{X}}{\tau^{1/4}} \quad , \tag{2.5.10}$$

assuming $B_0(0)e^{(1-3\mu\lambda^2)\tau} \ll 1$. The function $\bar{f}$ satisfies

$$\bar{f}^{IV} - \frac{\eta \bar{f}'}{4} = 0 \quad , \quad \bar{f} = \bar{f}' = 0 \quad (\eta = 0) \quad , \quad \bar{f} \rightarrow 1 \quad (\eta \rightarrow \infty) \tag{2.5.11}$$

and although a complete analytical solution is not possible it is seen that as $\eta \rightarrow \infty$ there are two exponentially damped oscillatory solutions for $\bar{f}$ in addition to the constant solution $\bar{f} = 1$. Thus

$$\bar{f} \sim 1 + \kappa(\eta)e^{-\frac{3}{2}\left(\frac{\eta}{4}\right)^{4/3}}\left(\bar{c}\cos\frac{3\sqrt{3}}{2}\left(\frac{\eta}{4}\right)^{4/3} + \bar{d}\sin\frac{3\sqrt{3}}{2}\left(\frac{\eta}{4}\right)^{4/3}\right) \tag{2.5.12}$$

where κ is an algebraic function of η and $\bar{c}$ and $\bar{d}$ are arbitrary constants which in principle are determined by satisfying the two boundary conditions at $\eta = 0$.

Second, it is possible to investigate the limiting form of the solution for large times. From (2.5.6) it can be deduced that when $\lambda^2 < 1/3\mu$,

$$B_+(\tau) \to \left(\frac{1-3\mu\lambda^2}{3}\right)^{1/2} \quad \text{as} \quad \tau \to \infty \tag{2.5.13}$$

and when $\lambda^2 > 1/3\mu$

$$B_+(\tau) \to 0 \quad \text{as} \quad \tau \to \infty \quad . \tag{2.5.14}$$

Therefore, as $\tau \to \infty$, $\bar{B}$ decays to zero provided $\lambda^2 > 1/3\mu$ which agrees with (2.5.10). However, when $\lambda^2 < 1/3\mu$, $\bar{B}$ moves towards a finite steady-state form as $\tau \to \infty$ in which

$$\bar{B} \sim \left(\frac{1-3\mu\lambda^2}{3}\right)^{1/2} - e^{-\left[\frac{1-3\mu\lambda^2}{2}\right]^{1/4}\bar{X}} \left(\bar{C}\cos\left[\frac{1-3\mu\lambda^2}{2}\right]^{1/4}\bar{X} + \bar{D}\sin\left[\frac{1-3\mu\lambda^2}{2}\right]^{1/4}\bar{X}\right) \quad \text{as} \quad \bar{X} \to \infty$$

$$\tag{2.5.15}$$

where $\bar{C}$ and $\bar{D}$ are constants. This shows that the nonlinear steady-state solution has a damped oscillatory character for large $\bar{X}$.

Generally, the results (2.5.12) and (2.5.15) give confidence that an inner solution exists of the required form to match with an outer solution of (2.5.2)-(2.5.5) and the main outer problem is now investigated. When $B=0$, steady-state solutions of the outer problem exist in the form

$$A = A_0(X) = \frac{1}{\sqrt{3}}\tanh\left[\frac{X+C_1}{2\sqrt{2}}\right] \quad \text{for} \quad \lambda < \frac{1}{\sqrt{3}} \quad , \tag{2.5.16}$$

and

$$A = A_0(X) = \frac{1}{\sqrt{3}}\coth\left[\frac{X+C_2}{2\sqrt{2}}\right] \quad \text{for} \quad \lambda > \frac{1}{\sqrt{3}} \quad , \tag{2.5.17}$$

where $C_1 = 2\sqrt{2}\tanh^{-1}(\sqrt{3}\lambda)$ and $C_2 = 2\sqrt{2}\coth^{-1}(\sqrt{3}\lambda)$. These solutions consist purely of x-rolls and the instability to cross-rolls is readily demonstrated by considering a small y-roll

40

disturbance of the form

$$B = B_0(X)e^{\sigma(X)\tau} \quad (B_0 \ll 1) \quad . \tag{2.5.18}$$

Substitution into (2.5.3) then shows that

$$\sigma(X) = 1 - 3\mu A_0^2(X) \quad , \tag{2.5.19}$$

so that y-rolls grow in any region where $A_0(X) < 1/\sqrt{(3\mu)}$. This agrees with the result obtained in the previous section for short-scale disturbances, and if $\mu < 1$ or $\lambda < 1/\sqrt{(3\mu)}$ the x-roll solution is unstable. In the next section, consideration is given to what alternative form of steady-state solutions may evolve. It is found that such solutions consisting of a combination of x-rolls and y-rolls exist for $\mu > 1$.

2.6. Steady-state solution for $\mu > 1$

To summarise the results of the previous section, the nonlinear system (2.5.2)-(2.5.5) will evolve to the solution (2.5.16) or (2.5.17) as $\tau \to \infty$ when $\lambda > 1/\sqrt{(3\mu)}$ but when $\lambda < 1/\sqrt{(3\mu)}$ the solution (2.5.16) will be affected by the amplification of y-rolls in the region where $A < 1/\sqrt{(3\mu)}$ and there is the possibility that a new steady-state solution consisting of a combination of x and y-rolls will evolve. To determine the form of this solution, consider the non-zero steady-state solution of (2.5.3),

$$B^2 = \frac{1}{3}(1 - 3\mu A^2) \quad . \tag{2.6.1}$$

Substitution of this into the steady-state form of (2.5.2) gives

$$4\frac{\partial^2 A}{\partial X^2} + 3A^3(\mu^2 - 1) + A(1 - \mu) = 0 \quad , \quad \lambda < A < \frac{1}{\sqrt{3\mu}} \quad . \tag{2.6.2}$$

It is assumed that at the point $X = X_0$ where $A = 1/\sqrt{(3\mu)}$ there is a transition from the steady-state form of (2.5.2) where $B^2 = (1 - 3\mu A^2)/3$ to the steady-state form of (2.5.2) where $B = 0$ which is then valid in the region away from the wall $(X > X_0)$ where $A > 1/\sqrt{(3\mu)}$. Note that if

41

this solution for A increases with X it is necessary that $\mu > 1$ in order that $A \to 1/\sqrt{3}$ as $X \to \infty$.
Substitution of $B=0$ into the steady-state form of (2.5.2) shows that for $X > X_0$ the amplitude
A satisfies

$$4\frac{\partial^2 A}{\partial X^2} + A - 3A^3 = 0 \quad , \quad \frac{1}{\sqrt{3\mu}} < A < \frac{1}{\sqrt{3}} \qquad (2.6.3)$$

and the appropriate solution is

$$A = \frac{1}{\sqrt{3}}\tanh\left[\frac{X-X_0+C_1}{2\sqrt{2}}\right] \quad , \qquad (2.6.4)$$

where $C_1 = 2\sqrt{2}\tanh^{-1}(1/\sqrt{\mu})$.

It is known that $A = 1/\sqrt{(3\mu)}$ at $X=X_0$ and upon differentiation of (2.6.4) it follows that

$$\frac{\partial A}{\partial X} = \frac{1}{2\sqrt{6}}\frac{(\mu-1)}{\mu} \qquad \text{at} \quad X=X_0 \quad . \qquad (2.6.5)$$

Equation (2.6.2) can be integrated once to give

$$2\left(\frac{\partial A}{\partial X}\right)^2 + \frac{3A^4(\mu^2-1)}{4} + \frac{A^2(1-\mu)}{2} = D \qquad (2.6.6)$$

and for continuity of A and $\partial A/\partial X$ at $X=X_0$ it follows that $D=0$. Equation (2.6.6) may then be
integrated again to calculate the constant of integration which leads to the solution

$$A = \frac{2\sqrt{2}\left(\sqrt{2\mu}+\sqrt{\mu-1}\right)e^{\frac{\sqrt{\mu-1}(X-X_0)}{2}}}{\sqrt{3}\left[\left(\sqrt{2\mu}+\sqrt{\mu-1}\right)^2+\left(1+\mu\right)e^{\sqrt{\mu-1}(X-X_0)}\right]} \quad , \quad X < X_0 \quad , \qquad (2.6.7)$$

provided $\mu > 1$. The remaining boundary condition $A=\lambda$ at $X=0$ is used to fix the transition
point X_0 as

42

$$X_0 = \frac{-2}{\sqrt{\mu-1}} \ln \left\{ \frac{\sqrt{3}\,\lambda\left(\sqrt{2\mu}+\sqrt{\mu-1}\right)}{\sqrt{2}\left[1+\left(1-\frac{3\lambda^2(1+\mu)}{2}\right)^{1/2}\right]} \right\} \quad , \quad 0 < \lambda < \frac{1}{\sqrt{3\mu}} \quad . \tag{2.6.8}$$

from (2.6.8) it can be seen that $X_0 \to 0$ as $\lambda \to 1/\sqrt{(3\mu)}$, consistent with the existence of a stable x-roll solution when $\lambda > 1/\sqrt{(3\mu)}$ whereas $X_0 \sim (-2\ln\lambda)/\sqrt{(\mu-1)}$ as $\lambda \to 0$. This means that when λ is small, X_0 is large and the y-rolls extend significantly into the fluid. Values of X_0 for various values of μ and λ are given in Table 2.1 and illustrated in Figure 2.2. Curves are drawn for values of λ in constant proportion to its maximum value of $1/\sqrt{(3\mu)}$ and it can be inferred from these that for a fixed λ, as μ increases from 1 to 14.288, X_0 decreases in value. Therefore as the Prandtl number P increases, X_0 increases. It is also noted that $X_0 \to \infty$ as $\mu \to 1$; solutions for $\mu \le 1$ and for $\lambda=0$ where the y-rolls extend into the fluid will be considered in detail in section 2.8 below.

The steady-state solution obtained here consists of two regions either side of the transition point $X=X_0$ at which $A=1/\sqrt{(3\mu)}$ and the amplitude of the y-rolls falls abruptly to zero. The nature of this abrupt change in the amplitude B can be investigated by considering the local solution near $X=X_0$ as $\tau \to \infty$. Close to X_0, for large time τ, it is expected that

$$A = \frac{1}{\sqrt{3\mu}} + \frac{(\mu-1)}{2\mu\sqrt{6}}(X-X_0) + \dots \tag{2.6.9}$$

and locally B is found to vary on a scale $X-X_0 = O(\tau^{-1})$ as $\tau \to \infty$, with

$$B \sim \tau^{-1/2} g(\zeta) \quad , \tag{2.6.10}$$

where $\zeta=(X-X_0)\tau$. In order to find $g(\zeta)$, (2.6.9) and (2.6.10) are substituted into (2.5.3) to obtain

43

$$\frac{\partial g}{\partial \zeta} + \left(\frac{(\mu - 1)}{\sqrt{2\mu}} - \frac{1}{2\zeta} \right) g + \frac{3g^3}{\zeta} = 0 \quad . \tag{2.6.11}$$

The boundary conditions needed to solve (2.6.11) are found using a matching process. Firstly, matching with the behaviour of $B^2 = (1 - 3\mu A^2)/3$ as $X \to X_0-$ requires

$$g \sim \left(\frac{-(\mu - 1)\zeta}{3\sqrt{2\mu}} \right)^{1/2} \quad \text{as} \quad \zeta \to -\infty \quad . \tag{2.6.12}$$

Secondly, matching with the solution $B = 0$ in $X > X_0$ requires

$$g \to 0 \quad \text{as} \quad \zeta \to \infty \tag{2.6.13}$$

and it follows that for $\mu > 1$

$$g = \left[\frac{\tilde{\zeta}}{6(e^{\tilde{\zeta}} - 1)} \right]^{1/2} \quad \text{where} \quad \tilde{\zeta} = \frac{2(\mu - 1)\zeta}{\sqrt{2\mu}} \quad . \tag{2.6.14}$$

At large times τ the amplitude of y-rolls falls to zero with a square root singularity in the neighbourhood of X_0, which is smoothed out on a length scale of order τ^{-1}.

It is noted that the equation (2.5.3) for B can actually be solved analytically to obtain

$$B = e^{\tau - 6\int_0^\tau \tilde{A}^2(X,\tau')d\tau'} \left\{ 6\int_0^\tau e^{2\tau' - 12\int_0^{\tau'} \tilde{A}^2(X,\tau'')d\tau''} d\tau' + B_0^{-2}(X) \right\}^{-1/2} \tag{2.6.15}$$

where $\tilde{A} = (\mu/2)^{1/2}A$. Among other things this solution confirms that B remains positive for all times.

To summarise the results of this section, it may be concluded that for $\mu > 1$ there is a stable finite amplitude steady-state solution which if $\lambda > 1/\sqrt{(3\mu)}$ at $X = 0$ consists purely of x-rolls, being given by

44

$$A = \frac{1}{\sqrt{3}} \coth \left[\frac{2\sqrt{2} \ \coth^{-1}(\sqrt{3}\lambda) + X}{2\sqrt{2}} \right] \qquad \text{for} \quad \lambda > \frac{1}{\sqrt{3}}$$

(2.6.16)

and

$$A = \frac{1}{\sqrt{3}} \tanh \left[\frac{2\sqrt{2} \ \tanh^{-1}(\sqrt{3}\lambda) + X}{2\sqrt{2}} \right] \qquad \text{for} \quad \lambda < \frac{1}{\sqrt{3}} \ ,$$

(2.6.17)

these being the appropriate solutions of (2.6.3) subject to $A = \lambda$ at $X = 0$. Alternatively, if $\mu > 1$ and $\lambda < 1/\sqrt{(3\mu)}$ the stable steady-state solution is likely to consist of a combination of x and y-rolls in the region $X < X_0$ and x-rolls in the region $X > X_0$, where X_0 is defined by formula (2.6.8). In the next section, numerical solutions of the system (2.5.2)-(2.5.5) are undertaken to confirm these ideas and to investigate the situation where $\mu \leq 1$.

2.7 Numerical solutions

The system (2.5.2)-(2.5.5) was solved numerically using an explicit scheme based on a forward difference approximation in time and a central difference approximation in X. The general process consists of subdividing the X,τ plane into sets of equal rectangles of sides $\delta X = h$, $\delta \tau = k$, by equally spaced grid lines defined by $X = ih$, $i = 0,1,2,...,N$ and $\tau = jk$, $j = 0,1,2,...$ Approximate solutions to the differential equations are found at the grid points (i,j) where the values of $A(X,\tau)$ and $B(X,\tau)$ are denoted by $a_{i,j}$ and $b_{i,j}$ respectively. The solutions for A and B are obtained by approximating the partial differential equations at a given time step by N-1 algebraic equations involving the values of A and B at the internal mesh points, making use of the boundary conditions where necessary.

Solutions were computed at successive time steps starting from initial profiles at $\tau = 0$ given by

45

$$A_0(X) = \frac{1}{\sqrt{3}}\tanh\left(\frac{X}{2\sqrt{2}}\right) + \lambda e^{-X}$$

$$B_0(X) = \delta\operatorname{sech}\left(\frac{X}{2\sqrt{2}}\right) \ .$$

$$(2.7.1)$$

The finite difference approximation to (2.5.2) is

$$\frac{a_{i,j+1}-a_{i,j}}{k} = 4\frac{(a_{i+1,j}-2a_{i,j}+a_{i-1,j})}{h^2} + a_{i,j} - 3a_{i,j}^3 - 3\mu a_{i,j}b_{i,j}^2 \ , \qquad (2.7.2)$$

leading to the explicit formula

$$a_{i,j+1} = \beta\left[4a_{i+1,j}+a_{i,j}\left(h^2-3h^2a_{i,j}^2-8-3h^2\mu b_{i,j}^2+\frac{1}{\beta}\right)+4a_{i-1,j}\right] \qquad (2.7.3)$$

for $j=0,1,2,\ldots$ and $i=1,2,\ldots,N$-1 where $\beta=k/h^2$ and $Nh=X_\infty$. Although (2.5.3) can be solved exactly for B in terms of A to give (2.6.15), it is more convenient to use the discretised form of the differential equation,

$$\frac{b_{i,j+1}-b_{i,j}}{k} = b_{i,j}\left[1-3b_{i,j}^2-3\mu a_{i,j}^2\right] \ , \qquad (2.7.4)$$

which leads to the explicit formula

$$b_{i,j+1} = kb_{i,j}\left[1-3b_{i,j}^2-3\mu a_{i,j}^2+\frac{1}{k}\right] \qquad (2.7.5)$$

for $j=0,1,2,\ldots$ and $i=1,2,\ldots,N$-1.

The two formulae (2.7.3), (2.7.5) determine the unknown amplitudes $a_{i,j+1}$ and $b_{i,j+1}$ at the $i,j+1$ mesh point in terms of known amplitudes along the jth time row. Thus a solution can be found by 'marching forwards' in time, starting from the initial profiles at $\tau=0$,

$$a_{i,0} = A_0(ih) \ , \quad b_{i,0} = B_0(ih) \ , \quad i = 0,\ldots N \ , \qquad (2.7.6)$$

noting that the end values are determined directly from the boundary conditions

46

$$a_{0,j+1} = \lambda \quad ; \quad a_{N,j+1} = \frac{1}{\sqrt{3}} \quad \text{for} \quad j = 0, 1,... \tag{2.7.7}$$

and then applying (2.7.3) and (2.7.5) with $j=0,1,2,...$ to get the solution at successive time steps. Step lengths $h=0.1$ and $k=0.0005$ and an outer boundary $X_\infty=20$ were used for most computations.

The results shown in Figures 2.3-2.24 are for $\delta=0.2$ and various values of μ and λ. In section 2.3 it was found that $1.227<\mu<14.288$ so results were obtained for the end points $\mu=1.227$ and $\mu=14.288$. Computations were also carried out for $\mu=1.246$, equivalent to water at 15°C and 1 atmosphere, and for air where $\mu=1.7$. Additional results were generated for $\mu=2$ to check the numerical procedure against the results of Daniels and Weinstein (1992). It should be noted that in discussing the time evolution of the system, X_0 is regarded as dependent on τ and is defined as the point at which $A=1/\sqrt(3\mu)$. Its value was estimated numerically by applying a linear interpolation procedure.

For $\mu=1.227$, the cases $\lambda=0$, 0.3 and 0.6 were considered. Results for $\lambda=0$ are shown in Figure 2.3 and at $\tau=10$ the y-rolls continue to progress outwards slowly with time, as in the results for $\mu=2$ described by Daniels and Weinstein (1992). A constant value of X_0 is never obtained. For the case $\lambda=0.3$ (Figure 2.4), it is found that A reaches a steady-state solution with y-rolls in the region $X<X_0$ and no y-rolls in the region $X>X_0$, where the value of X_0 at $\tau=10$ is 3.56. This is consistent with the steady-state prediction (2.6.8) which gives $X_0=3.76$ when $\mu=1.227$ and $\lambda=0.3$. For $\lambda=0.6$ it is seen in Figure 2.5 that A again reaches a steady-state solution, this time with the y-rolls completely disappearing, consistent with the fact that here $\lambda>1/\sqrt(3\mu)$. The above numerical solutions thus confirm the analytical results of section 2.6 where it is shown that if $0<\lambda<1/\sqrt(3\mu)$, the stable steady-state solution in the region $X<X_0$ is made up of a mixture of x and y-rolls and in the region $X>X_0$ is made up of x-rolls

47

only (Figure 2.4). The value of X_0 decreases as λ increases and if $\lambda > 1/\sqrt{(3\mu)}$ the stable steady-state solution consists of x-rolls only (Figure 2.5).

For $\mu = 1.246$, the cases $\lambda = 0$, 0.3 and 0.6 were again considered (see Figures 2.6 to 2.8). Similar results were obtained, with X_0 now the point at which $A = 1/\sqrt{(3\mu)} = 0.52$. It was found that $X_0 = 3.39$ for $\lambda = 0.3$ at $\tau = 10$, consistent with the steady-state value of 3.54 predicted by (2.6.8).

Further results were computed for $\mu = 1.7$ with $\lambda = 0$, 0.3, 0.5 (Figures 2.9-2.11), $\mu = 2$ with $\lambda = 0$, 0.2, 0.4, 0.6 (Figures 2.12-2.15) and $\mu = 14.288$ with $\lambda = 0$, 0.1, and 0.2 (Figures 2.16-2.18). These exhibited similar behaviour and in each case for which $0 < \lambda < 1/\sqrt{(3\mu)}$ the value of X_0 at $\tau = 10$ was found to be in good agreement with the steady-state value predicted by (2.6.8) (see Table 2.1). The results for $\mu = 2$ were also found to be in good agreement with the earlier computations by Daniels and Weinstein (1992). For $\lambda = 0$ and general values of $\mu > 1$, the y-rolls continue to propagate outwards with time at a very slow rate, consistent with the fact that the value of X_0 given by (2.6.8) tends to infinity as $\lambda \to 0$.

Computations were also carried out for values of μ less than unity, and here a quite different behaviour was observed. Results for $\lambda = 0$, 0.5 and 1 (Figures 2.19-2.21) all indicate a similar evolution in which the y-rolls propagate steadily outwards with time and a 'plateau' region forms in which the x and y-rolls have equal and virtually constant amplitudes. Beyond this plateau region the amplitude of the y-rolls falls to zero, and the amplitude of the x-rolls rises to $1/\sqrt{3}$, as required by the outer boundary condition (2.5.4). With $\lambda < 1/\sqrt{(3\mu)}$ both x and y-rolls continue to exist near the wall (Figures 2.19 and 2.20) but if $\lambda > 1/\sqrt{(3\mu)}$ (Figure 2.21) the amplitude of the y-rolls decreases to zero there. An analysis of the solution when $\mu < 1$ is undertaken in section 2.8 to explain the markedly different behaviour of the system in this case.

48

Computations were also performed for the marginal case where $\mu = 1$ and results for $\lambda = 0$, 0.5 and 0.7 are shown in Figures 2.22-2.24. Here there is a much slower outward propagation of the y-rolls with time, similar to that which occurs for $\mu > 1$ when $\lambda = 0$. For the case where $\lambda > 1/\sqrt{(3\mu)}$ (Figure 2.24) the y-rolls play only a relatively minor role in the solution.

2.8 Nonlinear evolution with lateral forcing for $\mu \leq 1$

When $\mu < 1$, the x-roll solution $A = 1/\sqrt{3}$, $B = 0$ specified as $X \to \infty$ is no longer stable because the growth rate given by (2.5.19) for this solution is

$$\sigma = 1 - \mu \tag{2.8.1}$$

and this is positive when $\mu < 1$. As a result, a steady-state solution dominated by the form $A = 1/\sqrt{3}$, $B = 0$ at large X can no longer be achieved when $\mu < 1$. The result of this is that the region where $A = 1/\sqrt{3}$, $B = 0$ continues to move outwards as time progresses and a steady-state is never achieved, as shown in the numerical results for $\mu = 0.5$ in Figures 2.19-2.21. The solution instead becomes dominated by a plateau region where the alternative nonlinear solution of

$$0 = A(1 - 3A^2 - 3\mu B^2) \ ,$$
$$0 = B(1 - 3B^2 - 3\mu A^2) \ , \tag{2.8.2}$$

namely

$$A = B = \frac{1}{\sqrt{3(1+\mu)}} \ , \tag{2.8.3}$$

prevails at large values of X. The reason for this can be seen by inserting the time derivatives $\partial A/\partial \tau$ and $\partial B/\partial \tau$ on the left hand sides of (2.5.2) and (2.5.3) and investigating the stability of the solution to small perturbations in A and B. Setting

49

$$A = \frac{1}{\sqrt{3(1+\mu)}} + ae^{\sigma\tau} \quad , \quad B = \frac{1}{\sqrt{3(1+\mu)}} + be^{\sigma\tau} \tag{2.8.4}$$

and linearising in a and b it follows that

$$\sigma^2 + \frac{4}{(1+\mu)}\sigma + \frac{4(1-\mu^2)}{(1+\mu)^2} = 0 \quad , \tag{2.8.5}$$

which has two solutions,

$$\sigma = -2 \quad \text{and} \quad \sigma = \frac{-2(1-\mu)}{(1+\mu)} \quad . \tag{2.8.6}$$

This combination of x and y-rolls of equal amplitude is thus unstable for $\mu > 1$ but becomes stable when $\mu < 1$, and therefore evolves as an extending plateau region in the numerical computations.

Computations for $\mu = 0.5$ and various values of λ are shown in Figures 2.19-2.21, and it is of interest to consider the structure of the solution which evolves at large times when $\mu < 1$. This structure depends partly on whether $\lambda > 1/\sqrt{(3\mu)}$ or $\lambda < 1/\sqrt{(3\mu)}$ at $X=0$. In the former case the region near the wall is dominated by x-rolls, and there is a transition to a combination of x and y-rolls as A descends through the value $1/\sqrt{(3\mu)}$ ahead of the plateau, where $A = 1/\sqrt{[3(1+\mu)]}$ (see Figure 2.21). This structure is shown schematically in Figure 2.25. In the latter case, the region near the wall is dominated by a combination of x and y-rolls which simply extends into the plateau at large values of X (Figure 2.20). Beyond the plateau region the y-rolls subside in order to achieve the outer boundary condition and the plateau itself acts as a 'wavefront' which propagates the combined x and y-roll pattern into the fluid as time progresses.

For the situation of Figures 2.19 and 2.20 where $\lambda < 1/\sqrt{(3\mu)}$ the steady-state solution which develops in the wall region corresponds to $B^2 = (1-3\mu A^2)/3$ and thus, from (2.5.2), A satisfies

$$4\frac{\partial^2 A}{\partial X^2}+(1-\mu)A+3(\mu^2-1)A^3 = 0 \quad , \tag{2.8.7}$$

with boundary conditions

$$A = \lambda \quad (X = 0) \quad , \quad A \rightarrow \frac{1}{\sqrt{3(1+\mu)}} \quad (X \rightarrow \infty) \quad . \tag{2.8.8}$$

The relevant solutions are

$$A = \frac{1}{\sqrt{3(1+\mu)}}\coth\left[\frac{2\sqrt{2}\ \coth^{-1}\!\left(\sqrt{3(1+\mu)}\ \lambda\right) + \sqrt{1-\mu}\ X}{2\sqrt{2}}\right] \quad \text{if} \quad \lambda > \frac{1}{\sqrt{3(1+\mu)}} \quad , \tag{2.8.9}$$

or

$$A = \frac{1}{\sqrt{3(1+\mu)}}\tanh\left[\frac{2\sqrt{2}\ \tanh^{-1}\!\left(\sqrt{3(1+\mu)}\ \lambda\right) + \sqrt{1-\mu}\ X}{2\sqrt{2}}\right] \quad \text{if} \quad \lambda < \frac{1}{\sqrt{3(1+\mu)}} \quad . \tag{2.8.10}$$

For the situation of Figure 2.21, where $\lambda > 1/\sqrt{(3\mu)}$, the solution for A passes through the transition value $1/\sqrt{(3\mu)}$ at $X=X_0$, say, and in the region $X<X_0$, $B=0$ and A is given by the solution of

$$4\frac{\partial^2 A}{\partial X^2}+A-3A^3 = 0 \tag{2.8.11}$$

subject to $A=\lambda$ at $X=0$ and $A=1/\sqrt{(3\mu)}$ at $X=X_0$. For $X>X_0$, $B^2=(1-3\mu A^2)/3$ and A satisfies (2.8.7) with boundary conditions

$$A = \frac{1}{\sqrt{3\mu}} \quad (X = X_0) \quad , \quad A \rightarrow \frac{1}{\sqrt{3(1+\mu)}} \quad (X \rightarrow \infty) \quad . \tag{2.8.12}$$

One integration of (2.8.7) gives

51

$$\frac{2}{(1-\mu)}\left(\frac{\partial A}{\partial X}\right)^2 - \frac{3(1+\mu)A^4}{4} + \frac{A^2}{2} = D \tag{2.8.13}$$

and from the boundary condition as $X \to \infty$ it follows that $D = 1/\{12(1+\mu)\}$. A further integration then yields

$$A = \frac{1}{\sqrt{3(1+\mu)}} \coth\left[\frac{2\sqrt{2}\,\coth^{-1}\left[\sqrt{\frac{1+\mu}{\mu}}\right] + \sqrt{1-\mu}(X-X_0)}{2\sqrt{2}}\right] \tag{2.8.14}$$

and it follows that at $X = X_0$,

$$\frac{\partial A}{\partial X} = -\frac{1}{2\mu}\sqrt{\frac{1-\mu}{6(1+\mu)}} \quad . \tag{2.8.15}$$

Equation (2.8.11) in $X < X_0$ can now be integrated once, using the continuity of A and $\partial A/\partial X$ at $X = X_0$ to give

$$\left(\frac{\partial A}{\partial X}\right)^2 = \frac{3A^4}{8} - \frac{A^2}{4} + \frac{1}{12(1+\mu)} \tag{2.8.16}$$

and application of the boundary condition at $X = 0$ yields

$$\int_\lambda^A \frac{dA}{\left[\left(A^2 - \frac{1}{3}\right)^2 + \frac{(1-\mu)}{9(1+\mu)}\right]^{1/2}} = -\sqrt{\frac{3}{8}}\,X \quad . \tag{2.8.17}$$

Finally, the transition point X_0 is determined by setting $A = 1/\sqrt{(3\mu)}$ to give

$$X_0 = \sqrt{\frac{8}{3}} \int_{\frac{1}{\sqrt{3\mu}}}^\lambda \frac{dA}{\left[\left(A^2 - \frac{1}{3}\right)^2 + \frac{(1-\mu)}{9(1+\mu)}\right]^{1/2}} \quad . \tag{2.8.18}$$

This integral cannot be found analytically but a numerical method of integration yielded the result $X_0 = 0.5801$ when $\lambda = 1$ and $\mu = 0.5$.

52

Close to X_0, A has the form

$$A = \frac{1}{\sqrt{3\mu}} - \frac{1}{2\mu}\sqrt{\frac{1-\mu}{6(1+\mu)}}(X-X_0) + \dots \qquad (2.8.19)$$

and around this point there is a transition region where B increases rapidly from zero. This is similar to the region previously considered in section 2.6 with $B \sim \tau^{-\frac{1}{2}}g(\zeta)$ where $\zeta=(X-X_0)\tau$. The equation for $g(\zeta)$ is obtained from (2.8.19) and (2.5.3) as

$$\frac{dg}{d\zeta} - \left(\sqrt{\frac{1-\mu}{2\mu(1+\mu)}} + \frac{1}{2\zeta}\right)g + \frac{3g^3}{\zeta} = 0 \qquad (2.8.20)$$

and the appropriate boundary conditions are

$$g(\zeta) \to 0 \qquad \text{as} \quad \zeta \to -\infty \qquad (2.8.21)$$

and

$$g(\zeta) \sim \left[\frac{\zeta}{3}\sqrt{\frac{1-\mu}{2\mu(1+\mu)}}\right]^{1/2} \qquad \text{as} \quad \zeta \to \infty \ . \qquad (2.8.22)$$

The required solution is

$$g(\tilde{\zeta}) = \left[\frac{\tilde{\zeta}}{6(e^{\tilde{\zeta}}-1)}\right]^{1/2} \qquad \text{where} \quad \tilde{\zeta} = -2\sqrt{\frac{1-\mu}{2\mu(1+\mu)}}\,\zeta \ . \qquad (2.8.23)$$

The wavefront region distant from X_0 beyond the plateau, where B returns to zero, is not easily analysed, but some insight can be gained here by considering the special case where $\mu=0$. Then the equation for B does not depend on A and is given by

$$\frac{\partial B}{\partial \tau} = B(1-3B^2) \ . \qquad (2.8.24)$$

Thus

$$B^2 = \frac{Ce^{2\tau}}{1+3Ce^{2\tau}} . \qquad (2.8.25)$$

If the initial condition $B=B_0(X)$ at $\tau=0$ is applied it follows that

$$B = \left\{\frac{B_0^2(X)e^{2\tau}}{1+3B_0^2(X)[e^{2\tau}-1]}\right\}^{1/2} . \qquad (2.8.26)$$

The solution for B is displayed in Figure 2.26 for the special case $B_0(X)=\delta\mathrm{sech}(aX)$ and it can be readily seen that, for large X and τ, the y-rolls 'travel' outwards with time and adjust to zero amplitude as $X\to\infty$. The speed of the travelling wave depends on the initial profile of B, $B_0(X)$. This is seen by noticing that for large X, where $B_0(X)\sim 2\delta e^{-aX}$,

$$B^2 \sim \frac{1}{3+e^{-2\tau}\left(\frac{1}{4}\delta^{-2}e^{2aX}-3\right)} \qquad (2.8.27)$$

and so as $\tau\to\infty$,

$$B^2 \sim \frac{1}{3+\frac{1}{4}\delta^{-2}e^{2a\left(X-\frac{1}{a}\tau\right)}} . \qquad (2.8.28)$$

Thus the solution for B is in the form of a travelling wave $B=f(X-c\tau)$ moving in the positive X direction with wave speed $c=1/a$. For the case of Figure 2.26 where $a=1/2\sqrt{2}$, the speed of the travelling wave is $2\sqrt{2}$ and in general it can be expected that the speed will depend upon the initial profile of B. Although it is possible to determine the wave speed of the travelling wave for the case $\mu=0$, it is not attempted here to determine the wave speed for general values of $\mu<1$, although the numerical computations indicate that a similar structure emerges in the region beyond the plateau.

Computations were also performed for the marginal case where $\mu=1$ and here it was found that a steady-state solution was not achieved as $\tau\to\infty$. Results for $\lambda=0$ and $\lambda=0.5$ (Figures

54

2.22 and 2.23) indicate a slow outward propagation of the y-roll pattern with time. A similar slow propagation occurs for general μ when $\lambda=0$ and has been analysed in detail by Daniels and Weinstein (1992).

2.9 Discussion

The solution structure for Rayleigh-Bénard roll patterns in the neighbourhood of a wall subject to lateral forcing of magnitude λ has been determined for general values of a parameter μ depending on the Prandtl number of the fluid. It has been shown analytically and confirmed numerically that for $\mu > 1$ there is a stable finite-amplitude steady-state solution which if $\lambda > 1/\sqrt{(3\mu)}$ consists purely of x-rolls, whereas if $\lambda < 1/\sqrt{(3\mu)}$ it consists of a combination of x and y-rolls in the region $X < X_0$ and x-rolls in the region $X > X_0$, where the transition line $X=X_0$ is determined in terms of λ and μ by the formula (2.6.8). However, for the case $\lambda=0$ no steady-state solution is reached, and the y-rolls progress outwards slowly with time.

For the case $\mu \leq 1$ a steady-state solution is not achieved and instead the y-rolls travel outwards with time. If $\lambda > 1/\sqrt{(3\mu)}$ at $X=0$ the region near the wall is dominated by x-rolls, and there is a transition to a combination of x and y-rolls as A descends through the value $1/\sqrt{(3\mu)}$. When $\lambda < 1/\sqrt{(3\mu)}$, the region near the wall is dominated by a combination of x and y-rolls.

Finally, the evolution of the roll pattern with time is illustrated by contour plots for various λ and μ in Figures 2.27-2.37 using Surfer Version 4 by Golden Software. The program creates a regularly spaced grid from irregularly spaced data based on values of

55

$$\psi = \epsilon^{1/2}\{e^{ix}A(X,\tau) + e^{iy}B(X,\tau)\}+c.c$$

$$= 2\epsilon^{1/2}(A\cos x + B\cos y) \quad ,$$

(2.9.1)

where $x=\epsilon^{-1/2}X$ and the value of ϵ is taken as 0.1. An interpolation method based on minimum curvature is utilised. The grid values are smoothed using a cubic spline interpolation method and the contour map is generated. It should be noted that the contour intervals are automatically selected and vary from 0.1 to 0.2.

P	μ	λ	X_0
∞	1.227	0.3	3.7552
8.00	1.246	0.3	3.5420
0.72	1.700	0.3	1.4377
0.53	2.000	0.2	1.9057
0.53	2.000	0.4	0.0793
0.00	14.288	0.1	0.2929

Table 2.1 : X_0 values for various μ and λ
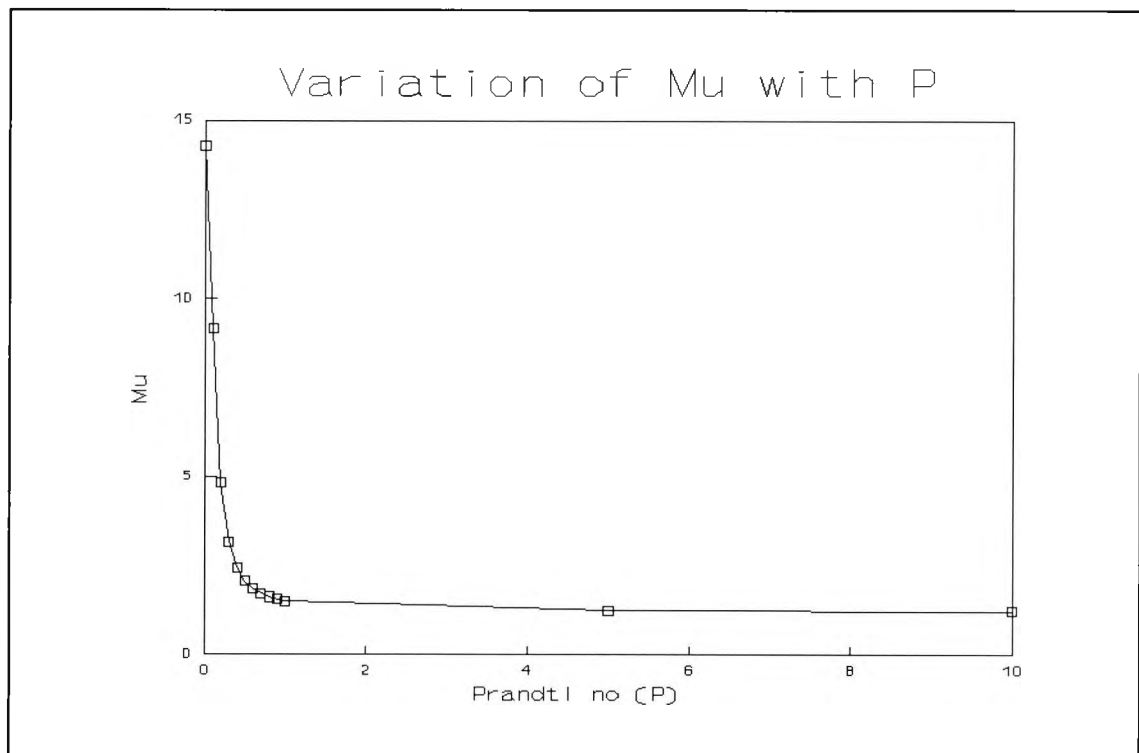
Fig. 2.1 : Variation of μ with the Prandtl number P

57
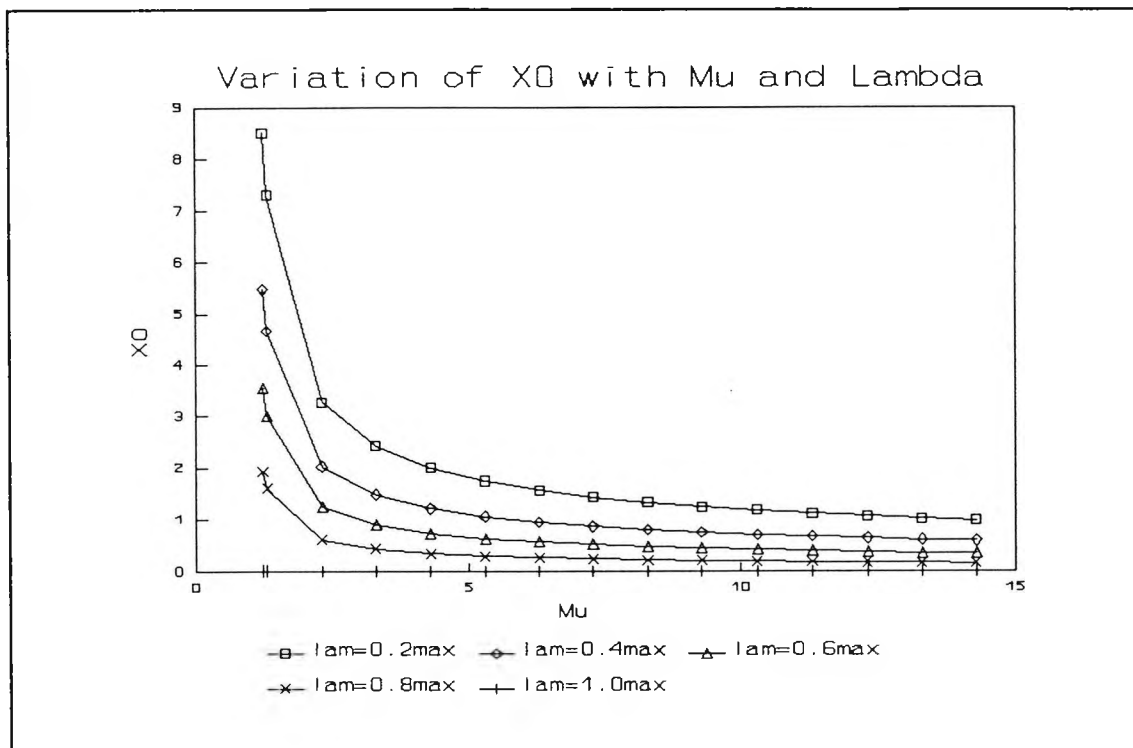
Fig. 2.2 : Variation of X_0 with μ and λ
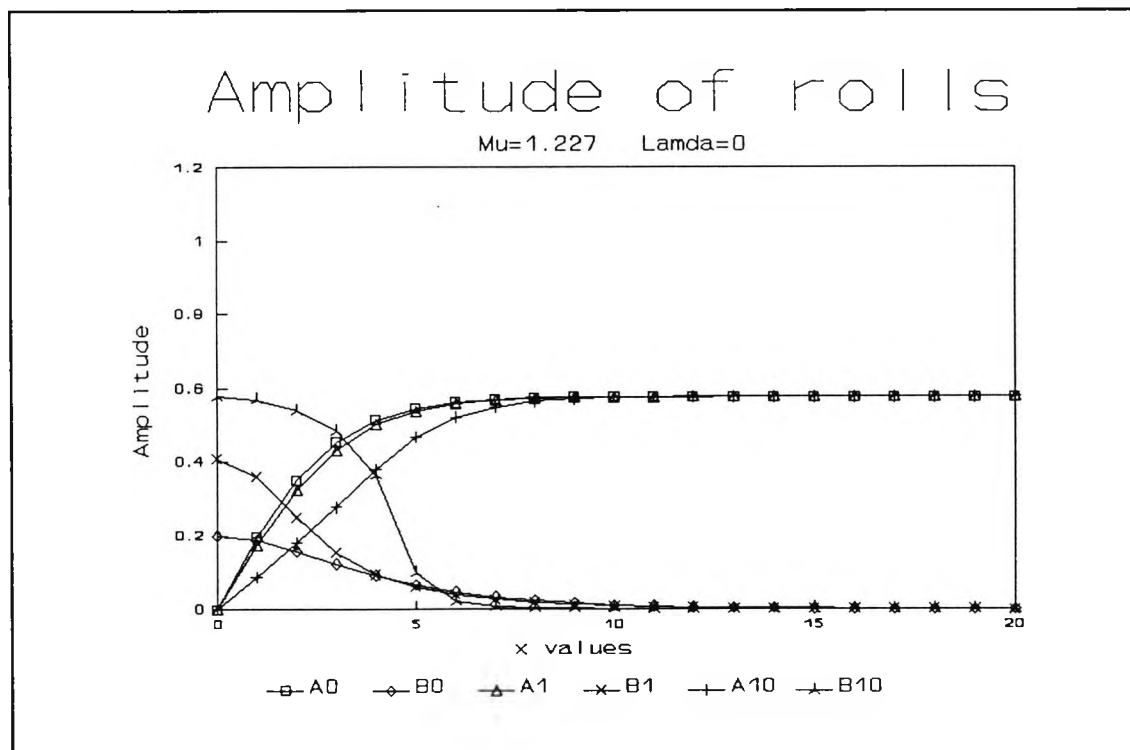
Fig. 2.3 : Numerical evolution for $\mu = 1.227$ and $\lambda = 0$ showing the amplitudes A and B of x-rolls and y-rolls at successive times $\tau = 0$, 1, 10 indicated by $A0$, $B0$, $A1$, $B1$, $A10$, $B10$ respectively
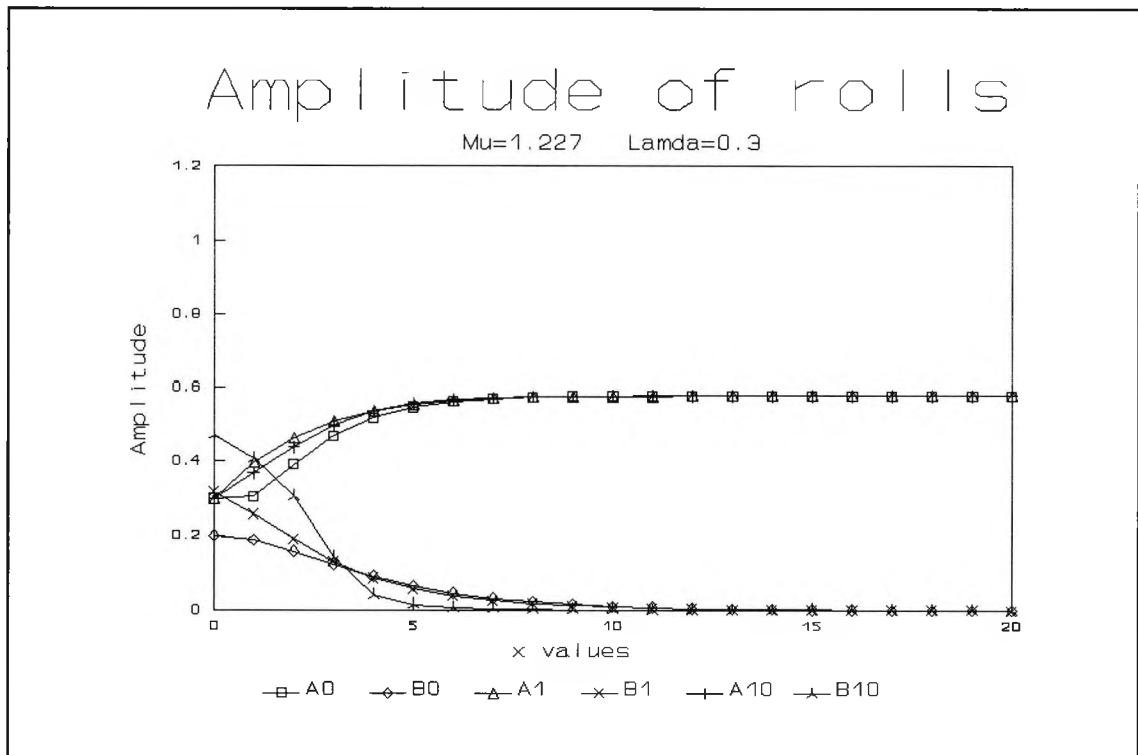
Fig. 2.4 : Numerical evolution for $\mu=1.227$ and $\lambda=0.3$ showing the amplitudes A and B of x-rolls and y-rolls at successive times τ
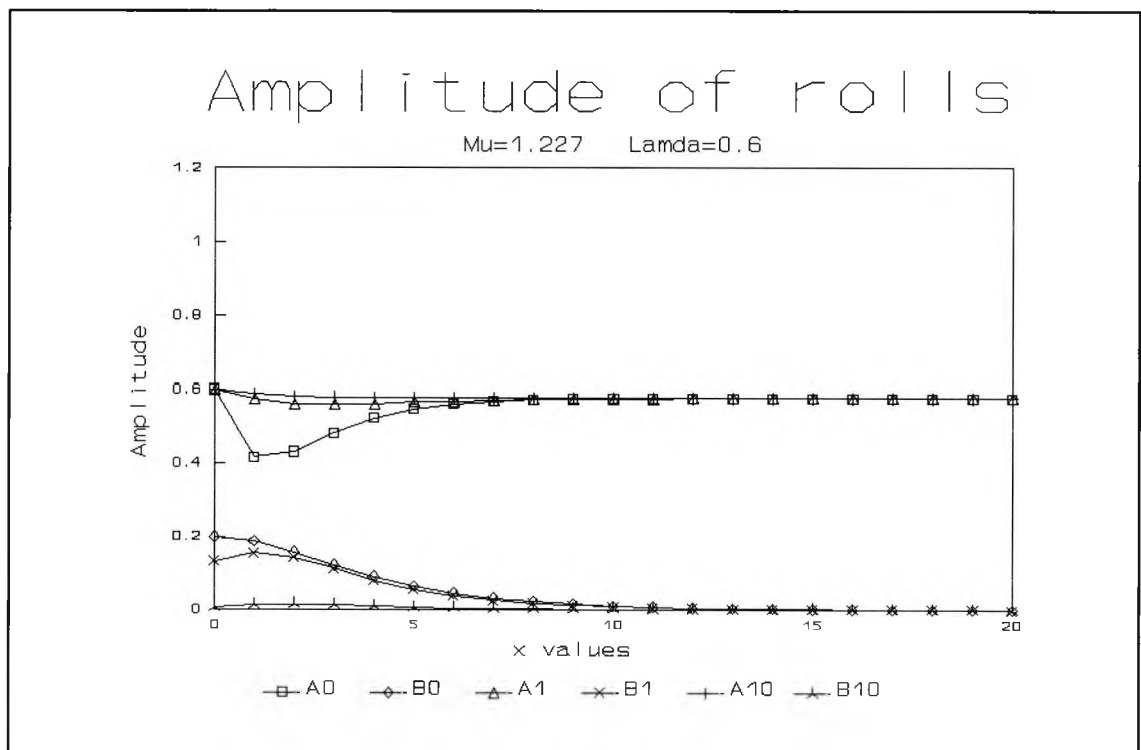
Fig. 2.5 : Numerical evolution for $\mu=1.227$ and $\lambda=0.6$ showing the amplitudes A and B of x-rolls and y-rolls at successive times τ

59
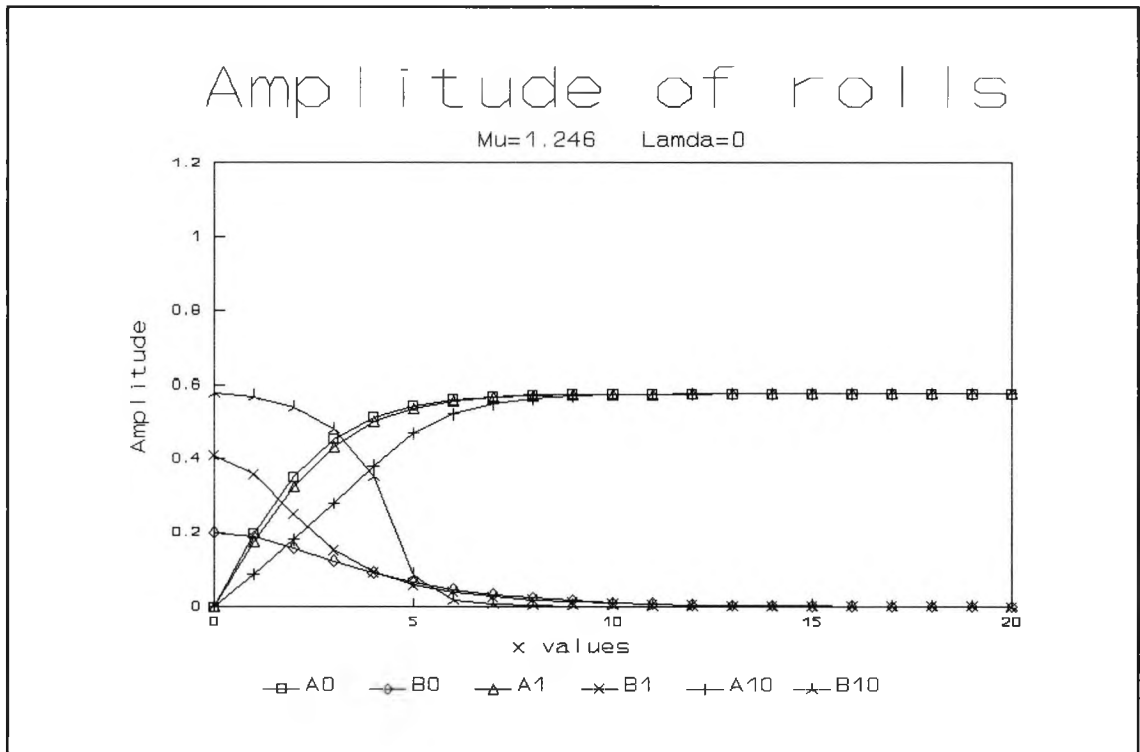
Fig. 2.6 : Numerical evolution for $\mu = 1.246$ and $\lambda = 0$ showing the amplitudes A and B of x-rolls and y-rolls at successive times τ
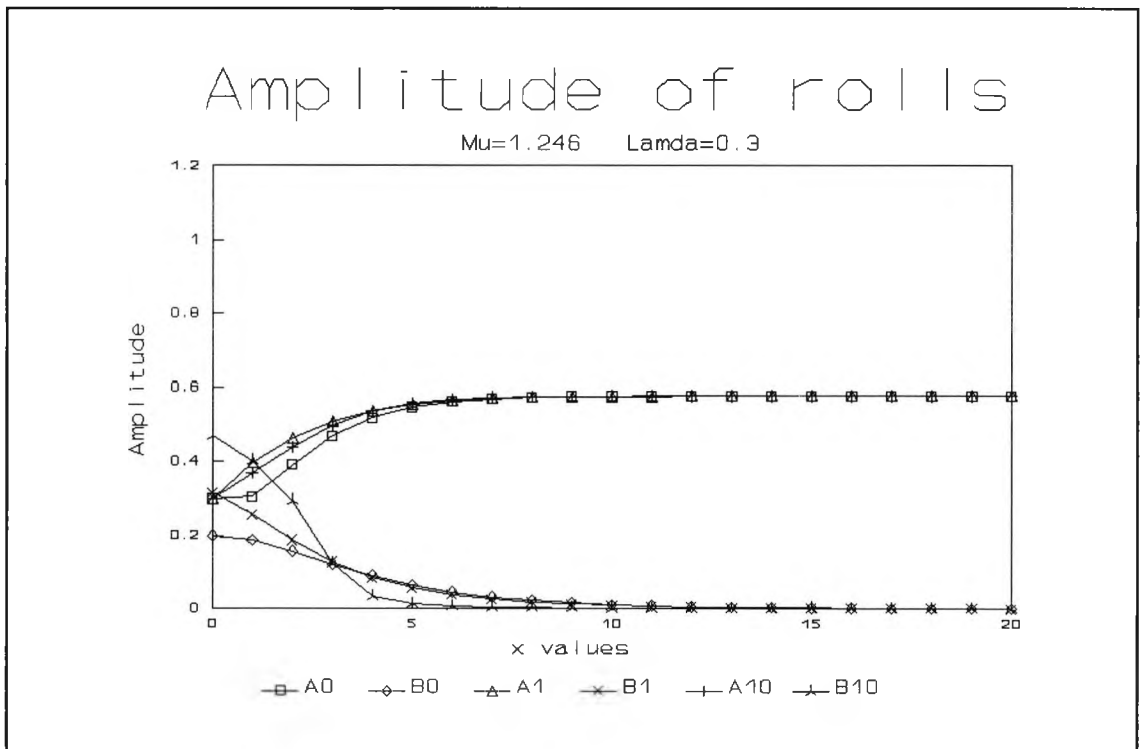
Fig. 2.7 : Numerical evolution for $\mu = 1.246$ and $\lambda = 0.3$ showing the amplitudes A and B of x-rolls and y-rolls at successive times τ
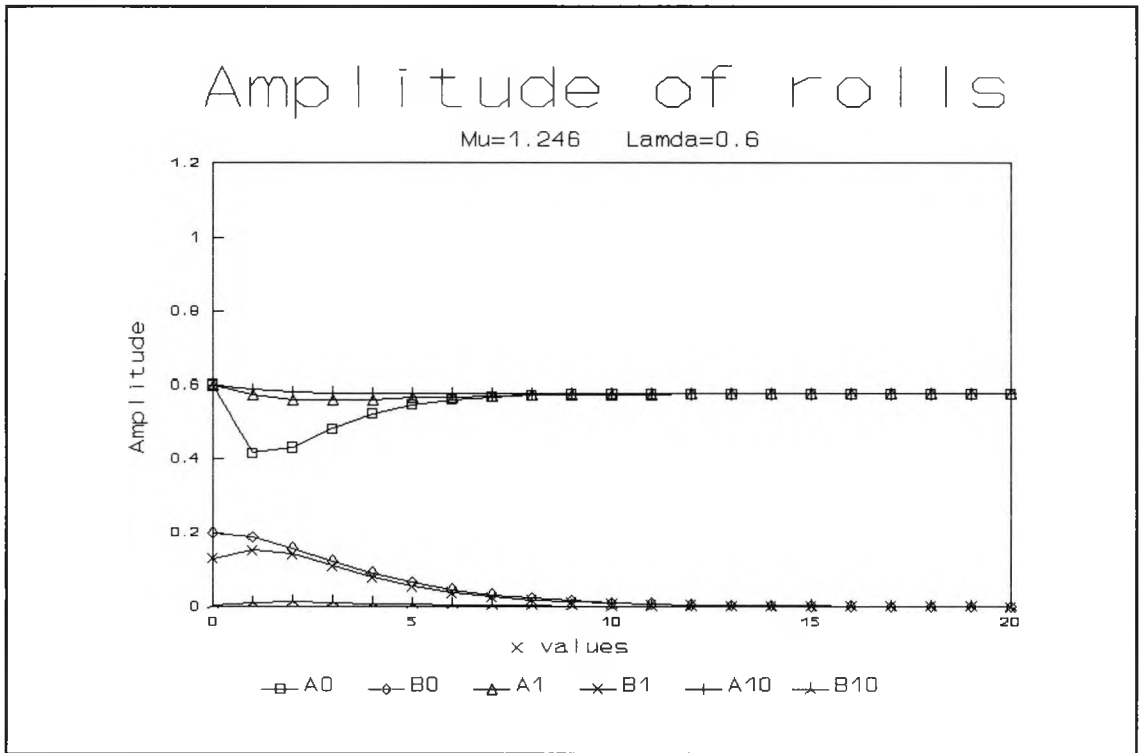
Fig. 2.8 : Numerical evolution for $\mu = 1.246$ and $\lambda = 0.6$ showing the amplitudes A and B of x-rolls and y-rolls at successive times τ
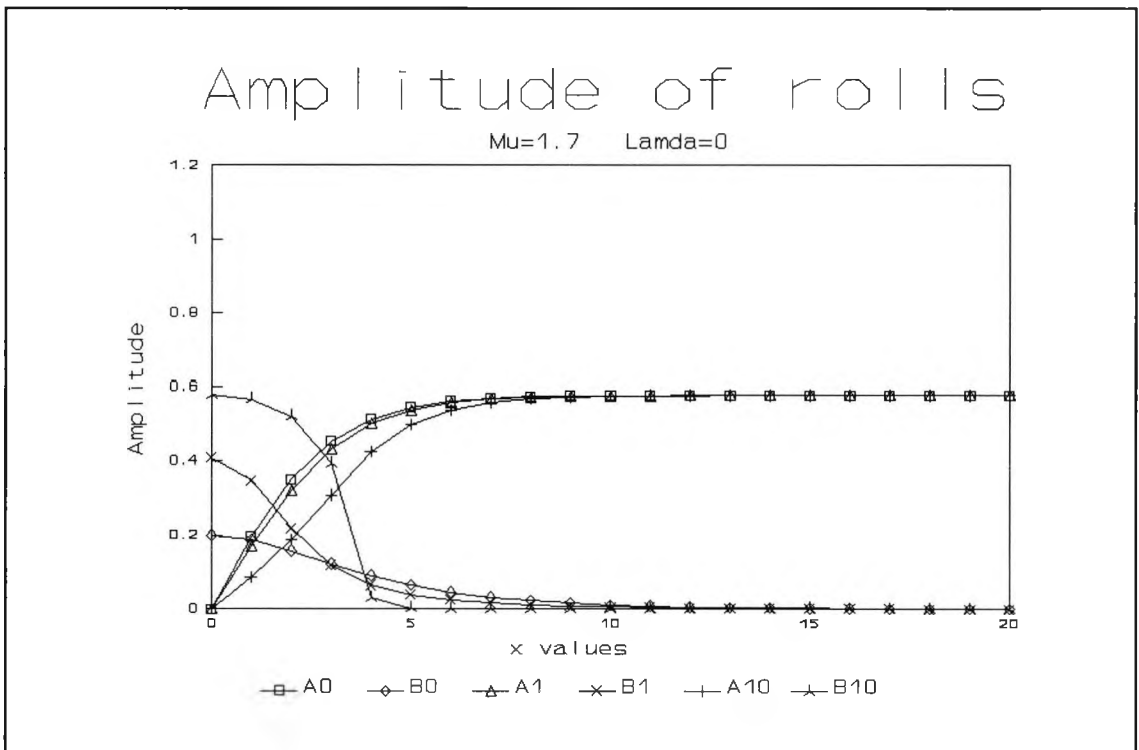
Fig. 2.9 : Numerical evolution for $\mu = 1.700$ and $\lambda = 0$ showing the amplitudes A and B of x-rolls and y-rolls at successive times τ

61
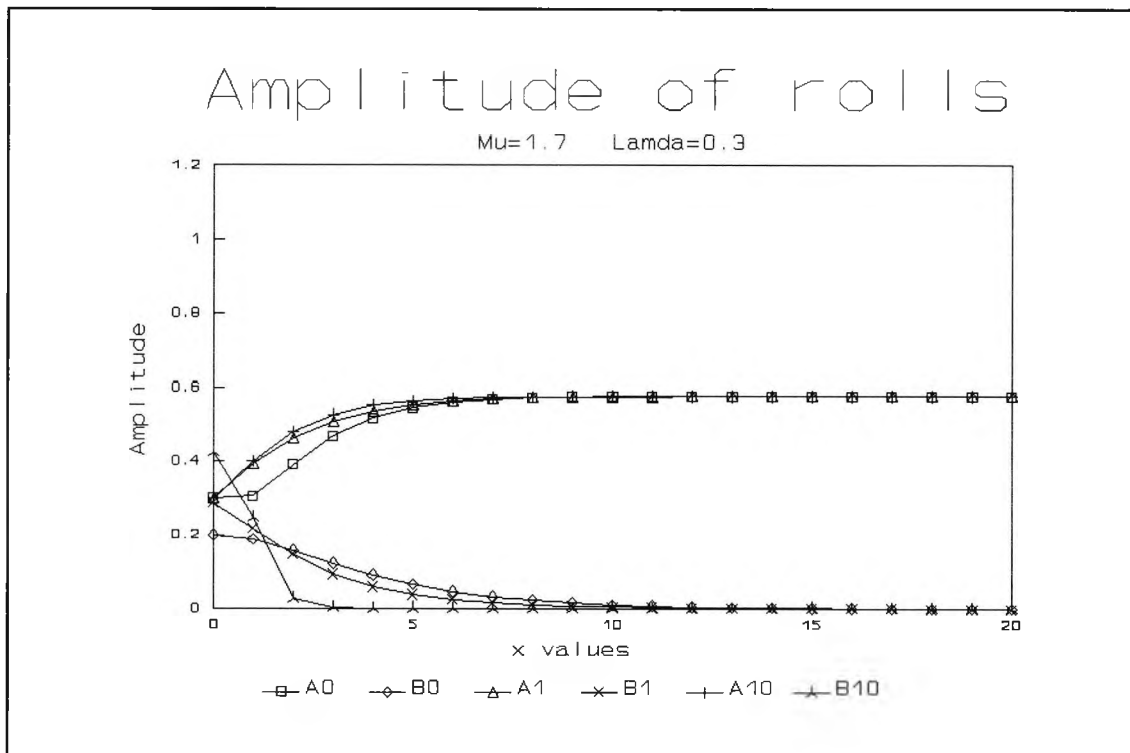
Fig. 2.10 : Numerical evolution for $\mu = 1.700$ and $\lambda = 0.3$ showing the amplitudes A and B of x-rolls and y-rolls at successive times τ
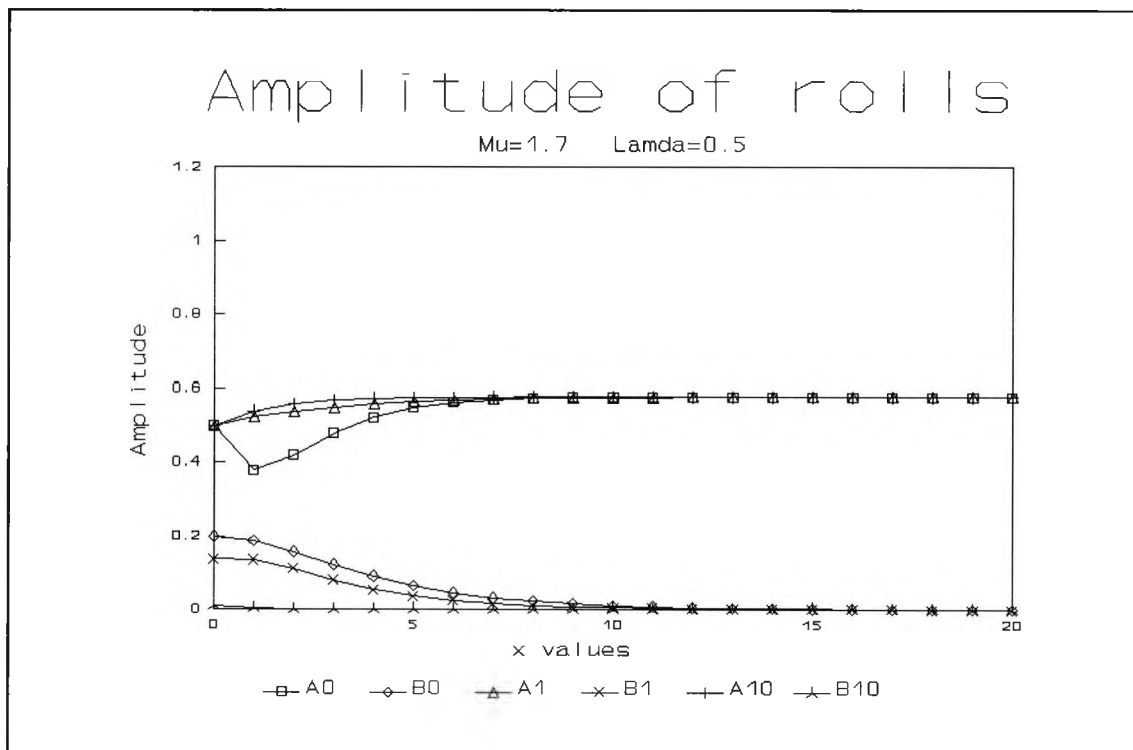
Fig. 2.11 : Numerical evolution for $\mu = 1.700$ and $\lambda = 0.5$ showing the amplitudes A and B of x-rolls and y-rolls at successive times τ

62
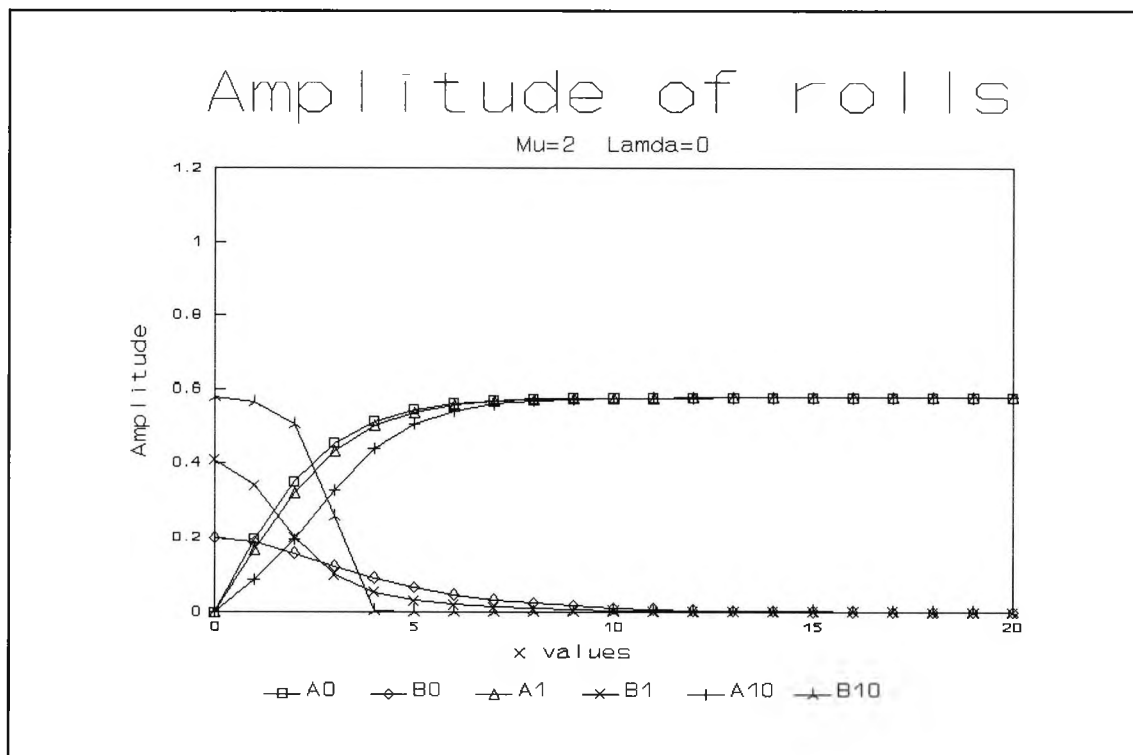
Fig. 2.12 : Numerical evolution for $\mu=2.0$ and $\lambda=0$ showing the amplitudes A and B of x-rolls and y-rolls at successive times τ
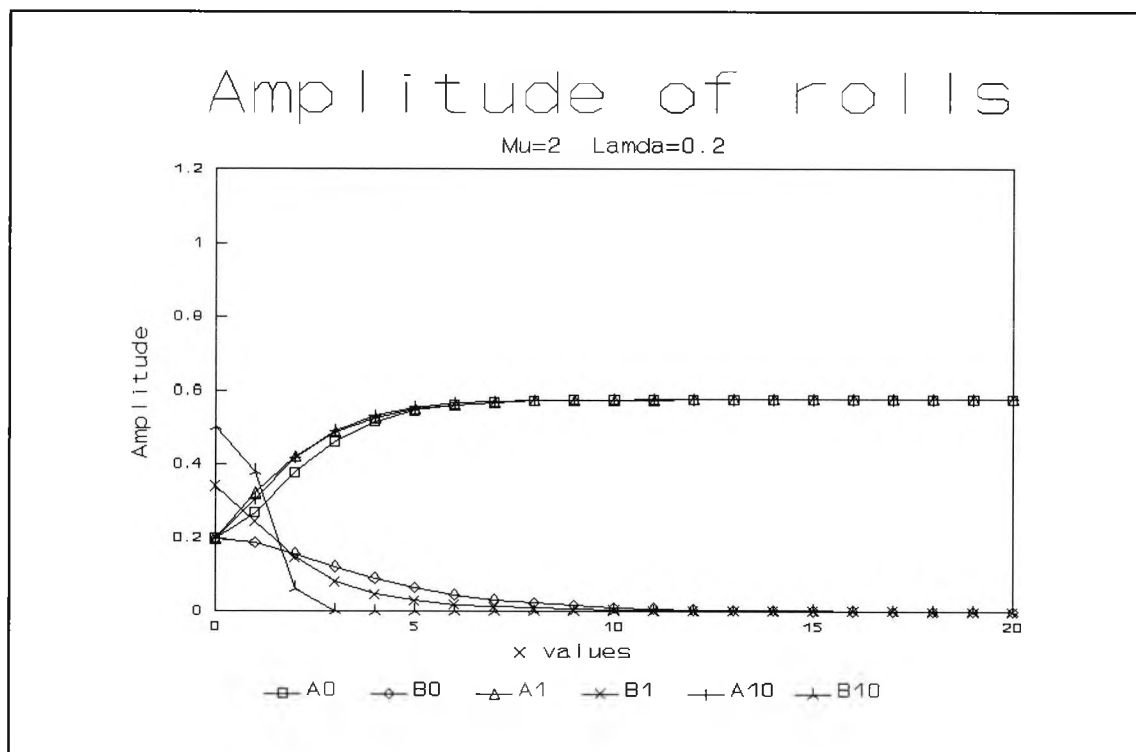
Fig. 2.13 : Numerical evolution for $\mu=2.0$ and $\lambda=0.2$ showing the amplitudes A and B of x-rolls and y-rolls at successive times τ
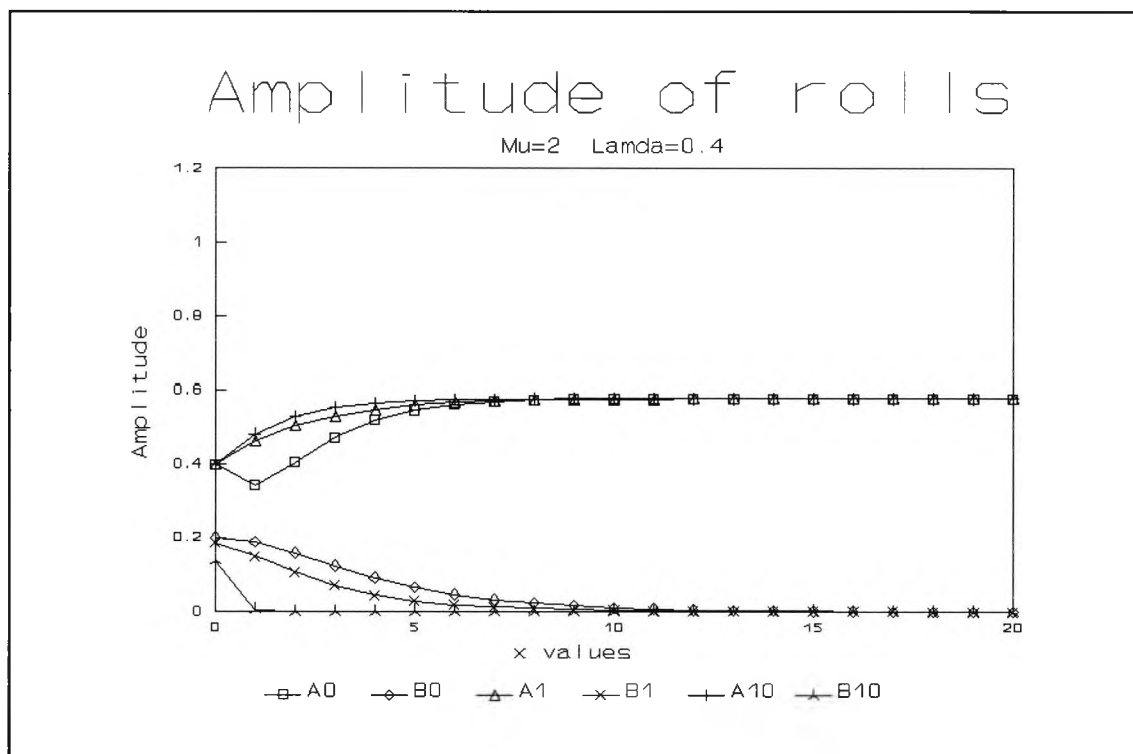
Fig. 2.14 : Numerical evolution for $\mu=2.0$ and $\lambda=0.4$ showing the amplitudes A and B of x-rolls and y-rolls at successive times τ
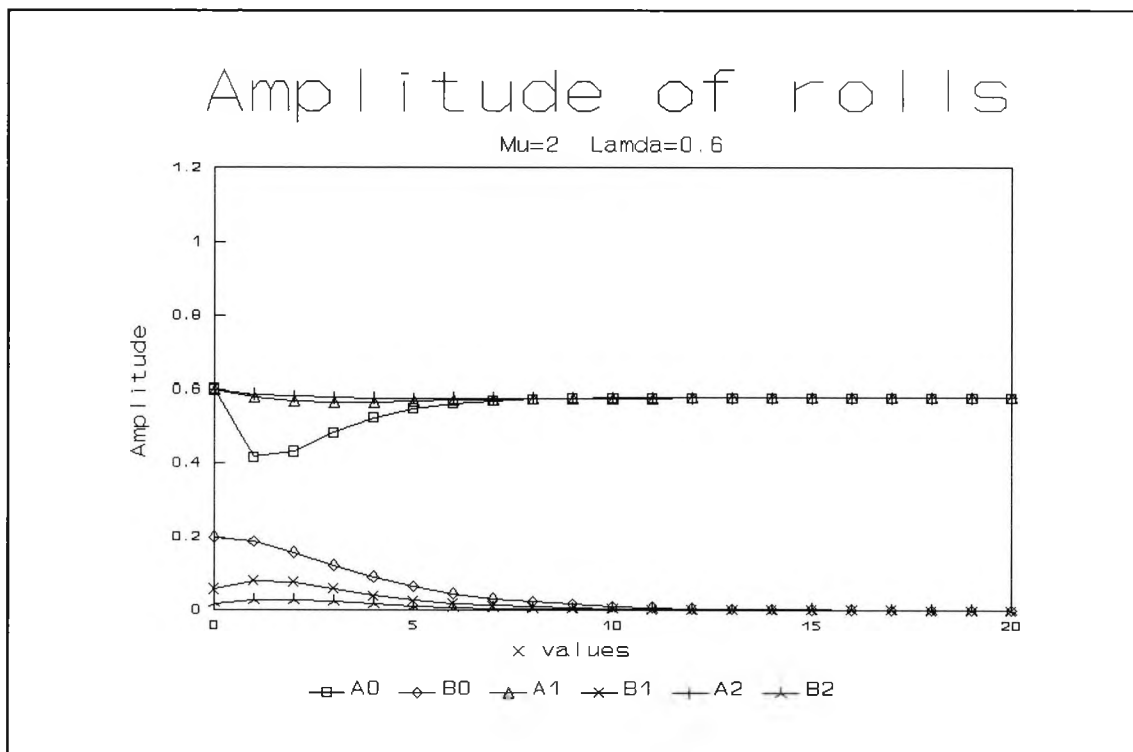
Fig. 2.15 : Numerical evolution for $\mu=2.0$ and $\lambda=0.6$ showing the amplitudes A and B of x-rolls and y-rolls at successive times τ

64
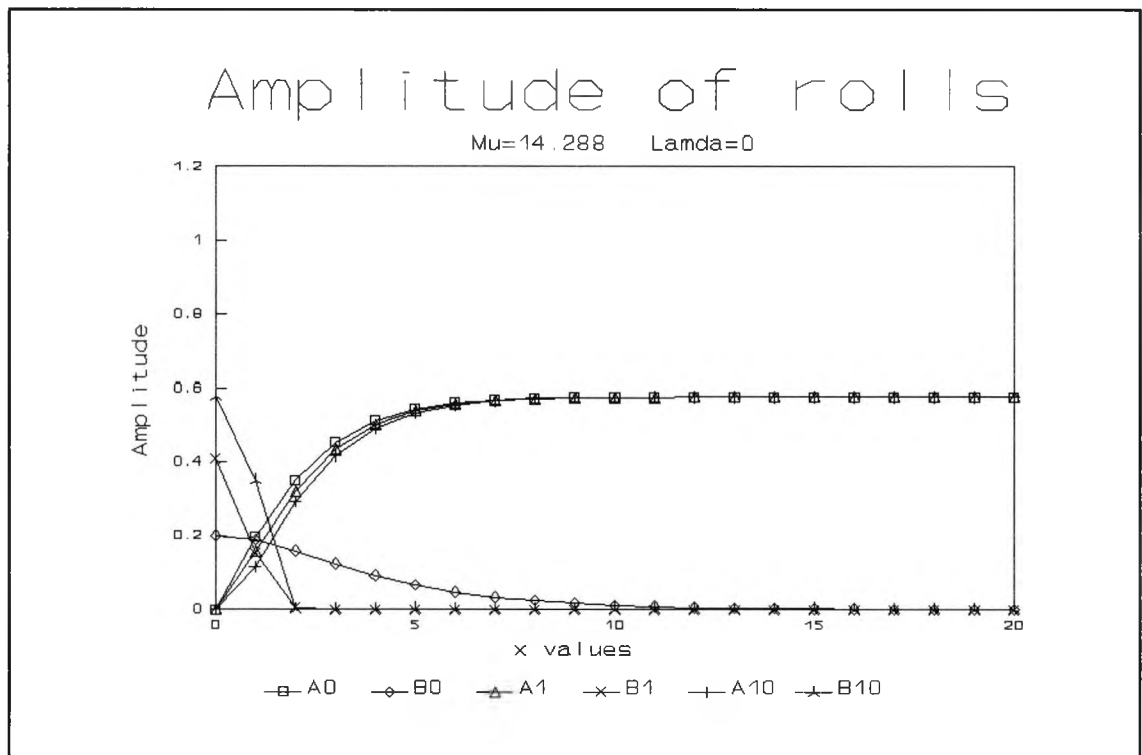
Fig. 2.16 : Numerical evolution for $\mu = 14.288$ and $\lambda = 0$ showing the amplitudes A and B of x-rolls and y-rolls at successive times τ
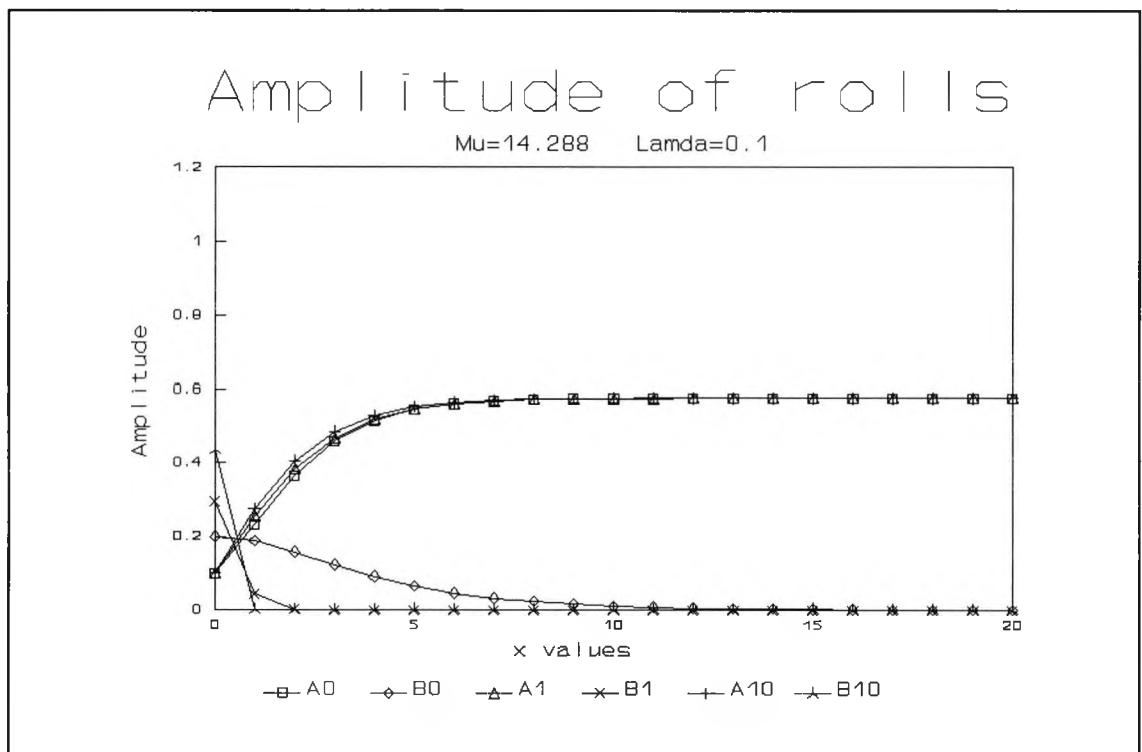
Fig. 2.17 : Numerical evolution for $\mu = 14.288$ and $\lambda = 0.1$ showing the amplitudes A and B of x-rolls and y-rolls at successive times τ

65
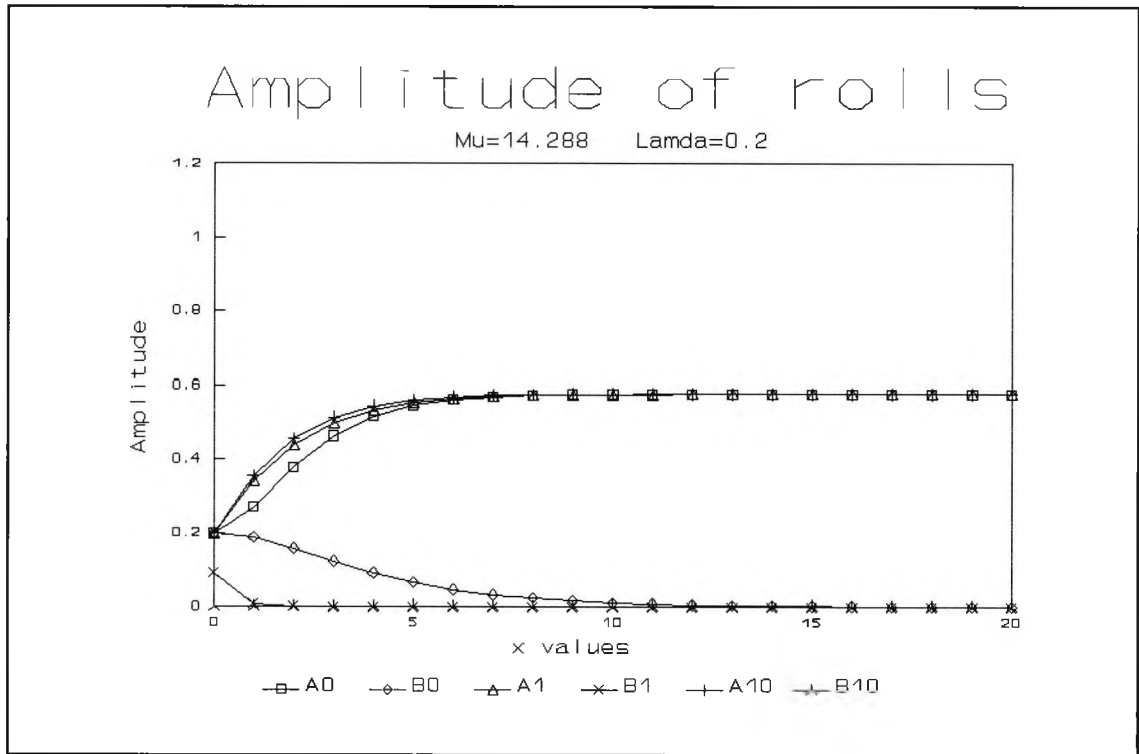
Fig. 2.18 : Numerical evolution for $\mu = 14.288$ and $\lambda = 0.2$ showing the amplitudes A and B of x-rolls and y-rolls at successive times τ
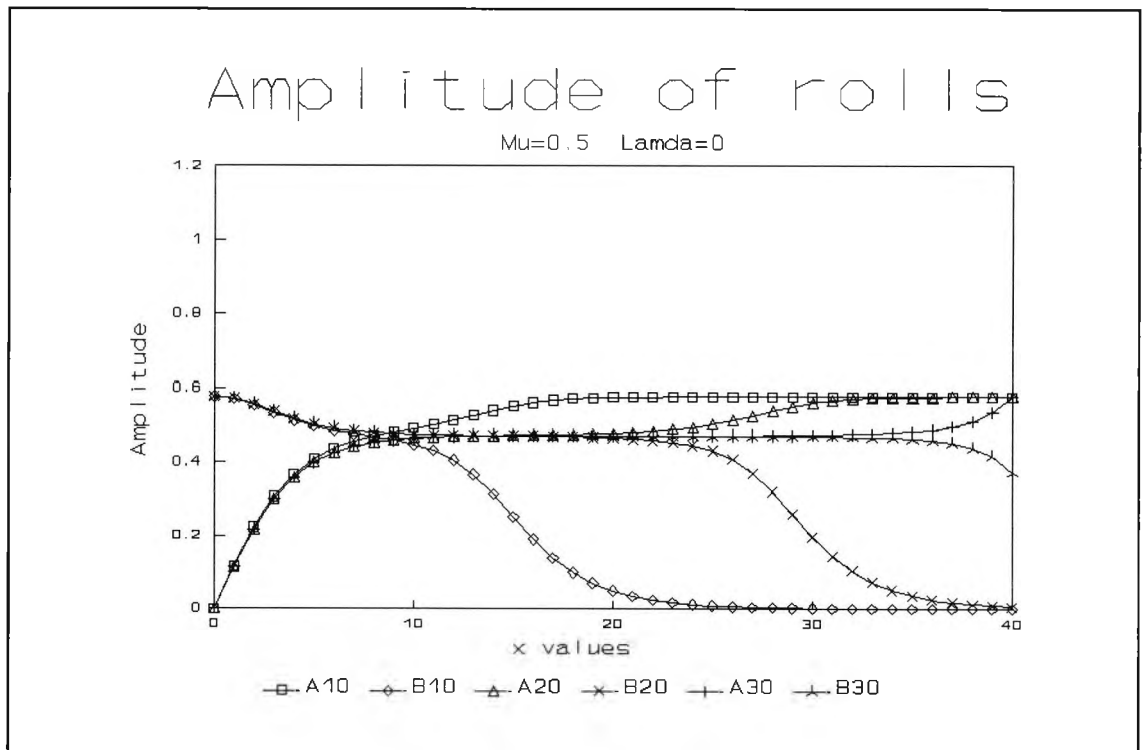
Fig. 2.19 : Numerical evolution for $\mu = 0.5$ and $\lambda = 0$ showing the amplitudes A and B of x-rolls and y-rolls at successive times τ

66
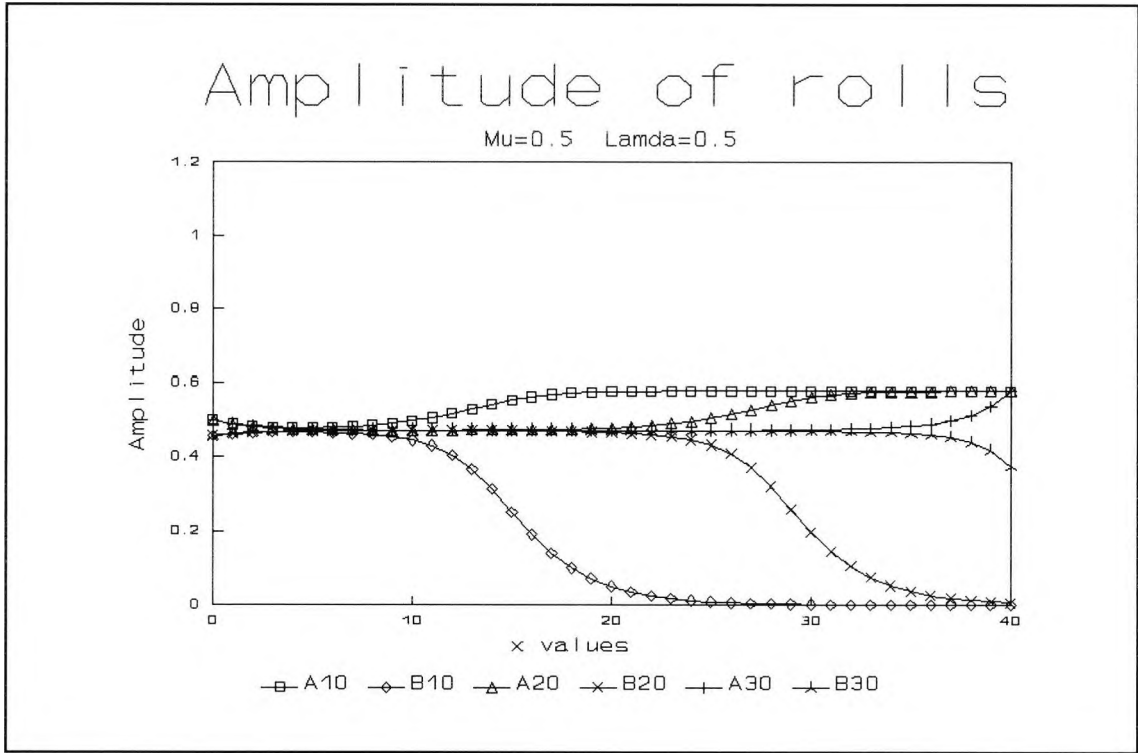
Fig. 2.20 : Numerical evolution for $\mu = 0.5$ and $\lambda = 0.5$ showing the amplitudes A and B of x-rolls and y-rolls at successive times τ
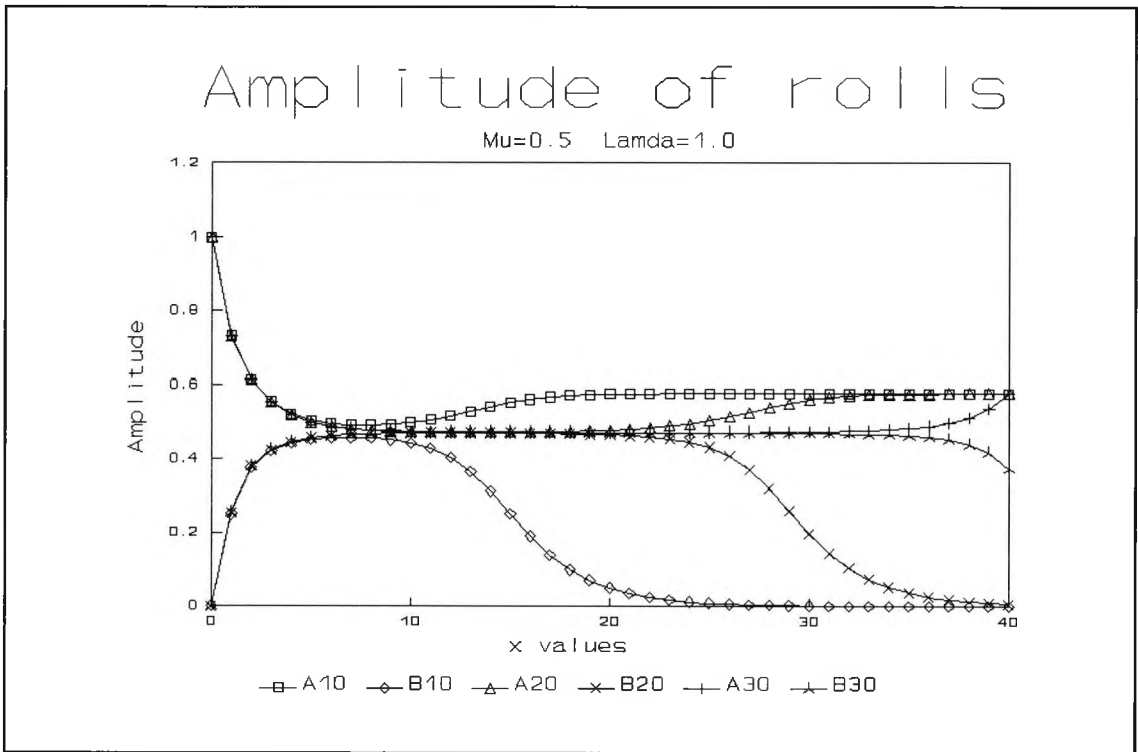
Fig. 2.21 : Numerical evolution for $\mu = 0.5$ and $\lambda = 1.0$ showing the amplitudes A and B of x-rolls and y-rolls at successive times τ
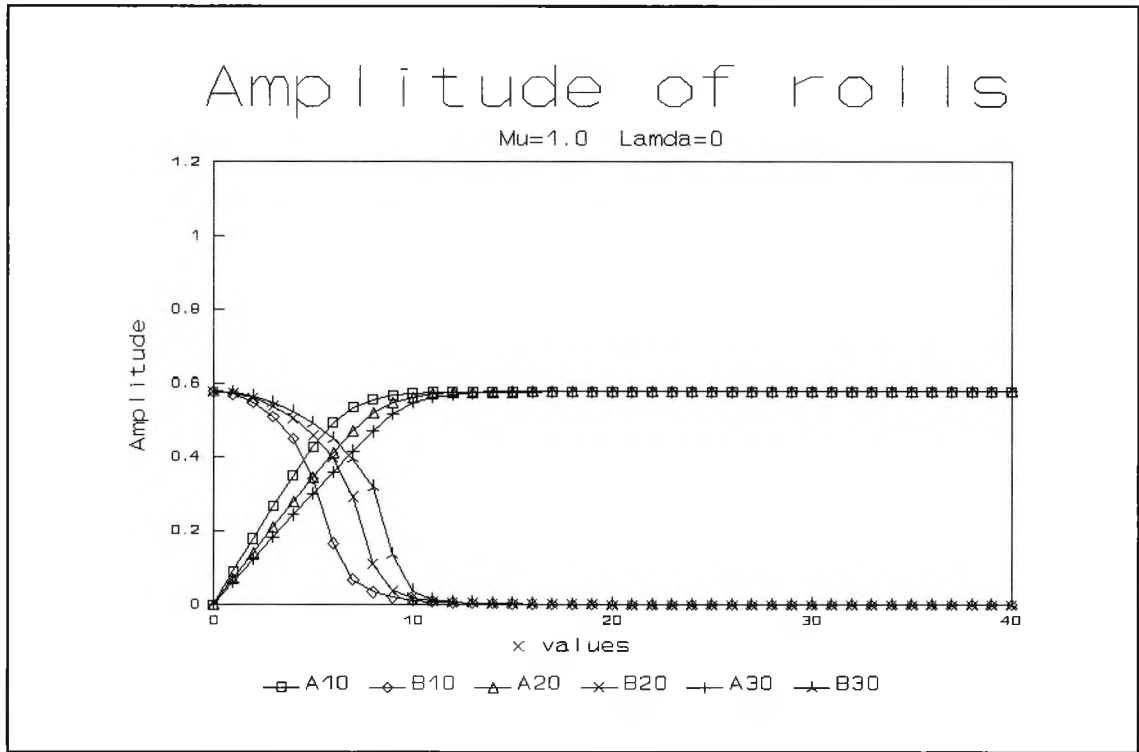
Fig. 2.22 : Numerical evolution for $\mu = 1.0$ and $\lambda = 0$ showing the amplitudes A and B of x-rolls and y-rolls at successive times τ
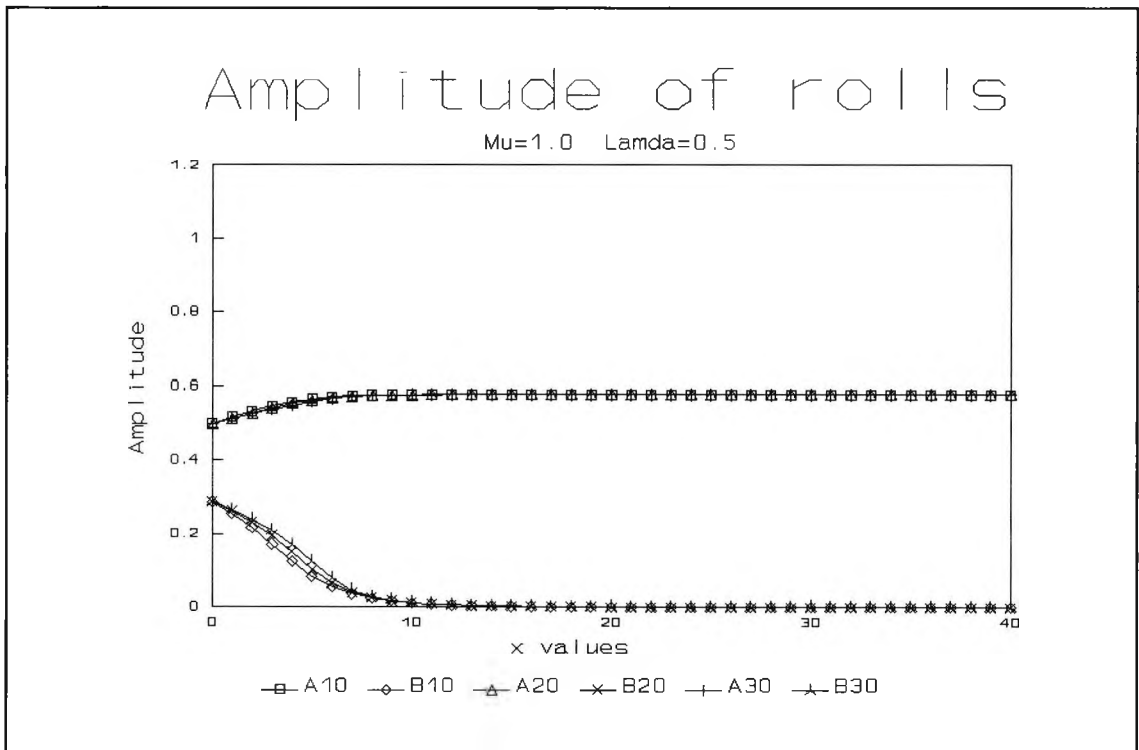
Fig. 2.23 : Numerical evolution for $\mu = 1.0$ and $\lambda = 0.5$ showing the amplitudes A and B of x-rolls and y-rolls at successive times τ

68
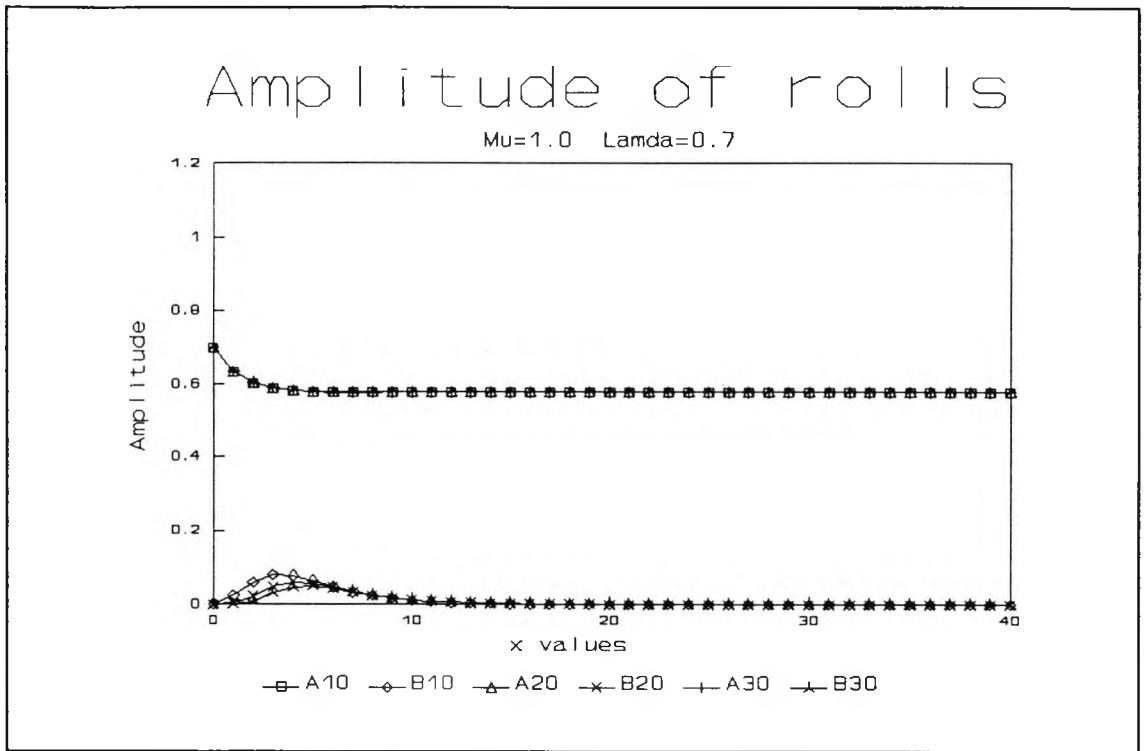
Fig. 2.24 : Numerical evolution for $\mu = 1.0$ and $\lambda = 0.7$ showing the amplitudes A and B of x-rolls and y-rolls at successive times τ
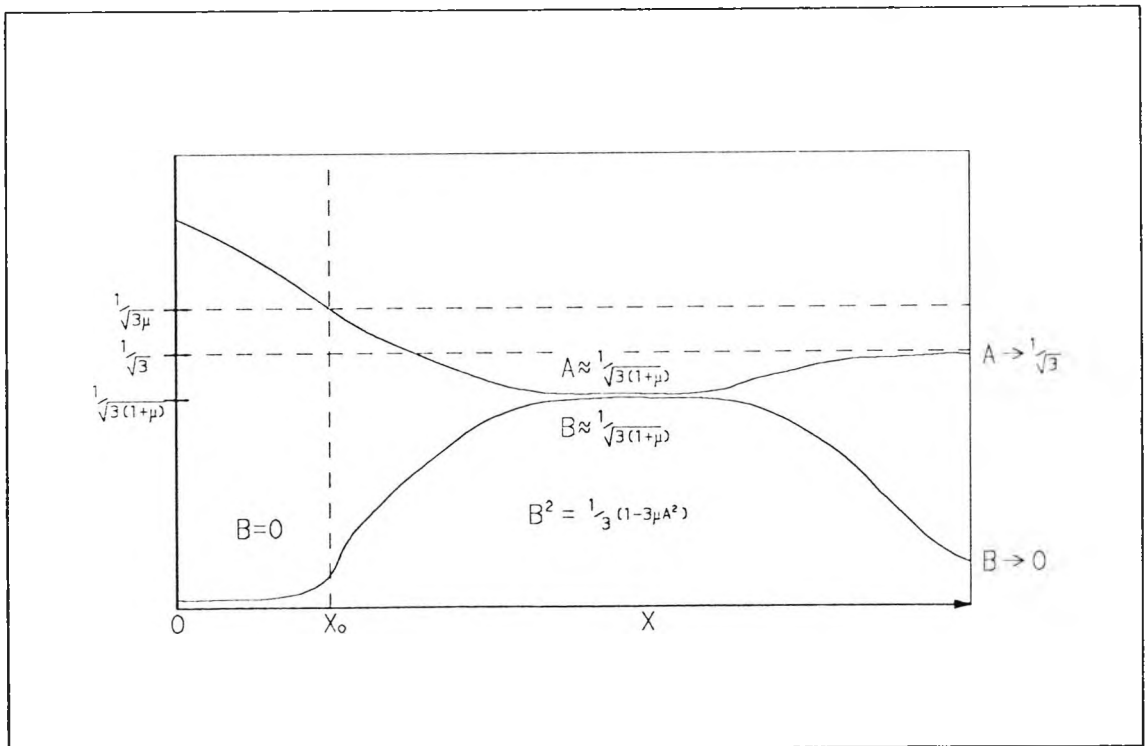
Fig. 2.25 : Schematic diagram showing the main flow regions for $\mu < 1$ and $\lambda > 1/\sqrt{(3\mu)}$

69
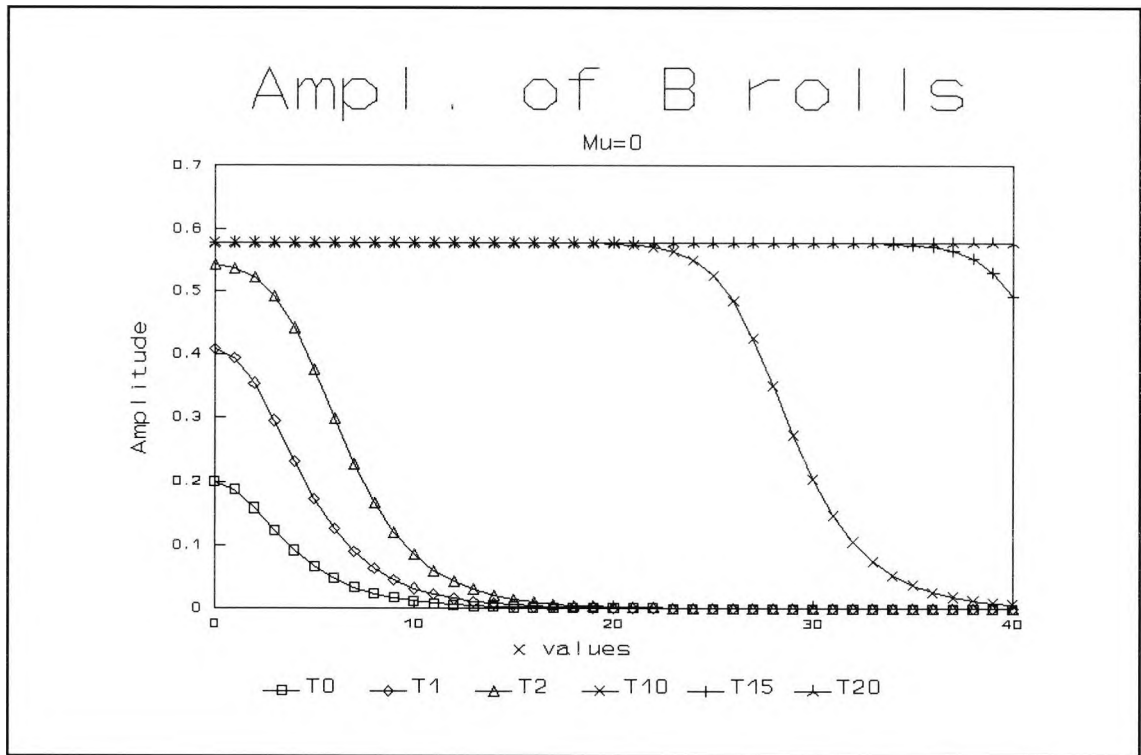
Fig. 2.26 : Analytical solution showing the amplitude B of y-rolls at sucessive times τ
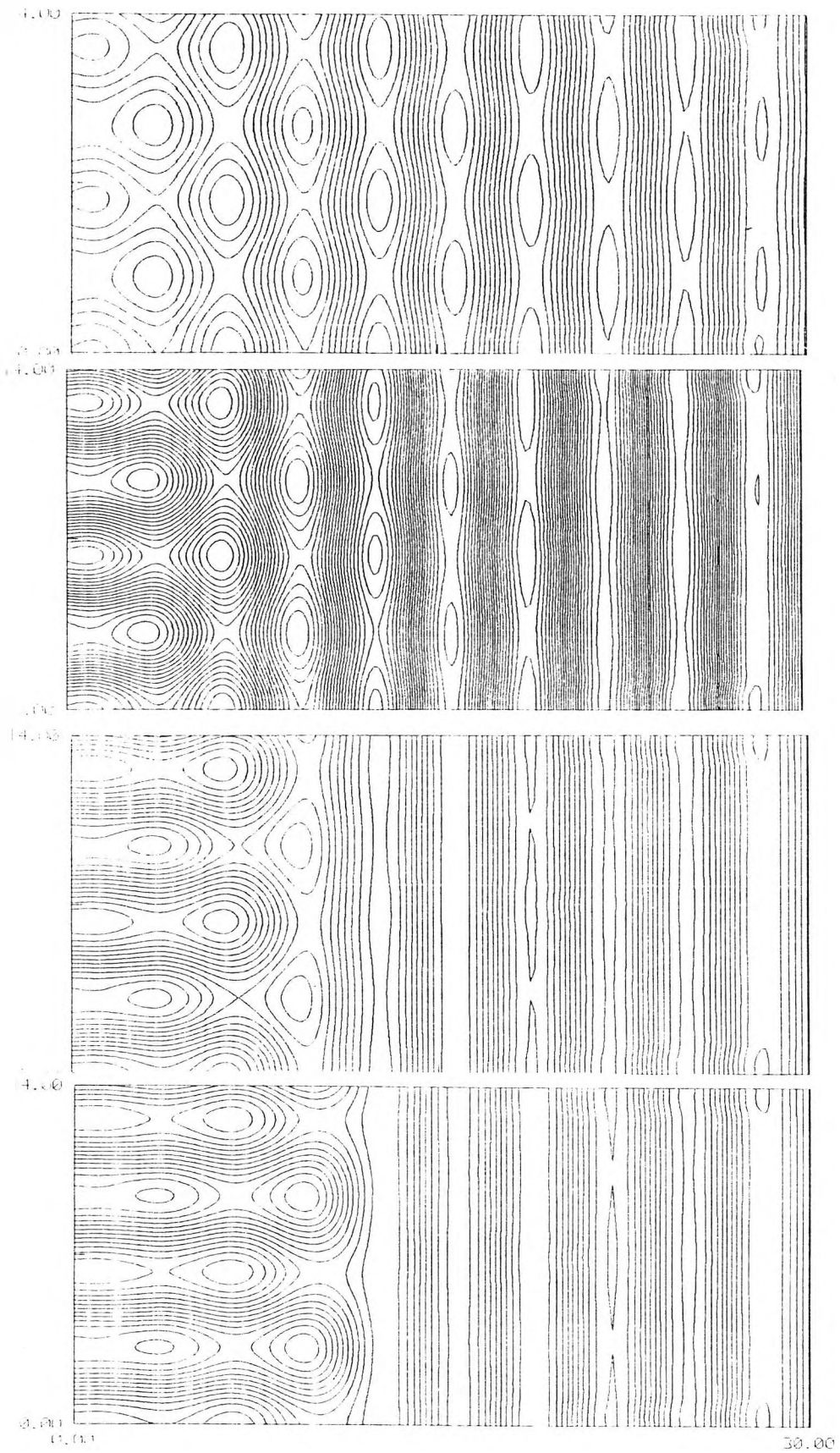
Fig. 2.27 : Contours of ψ at times $\tau=0$, 1, 5 and 20 for $\mu=2.0$, $\lambda=0$

71
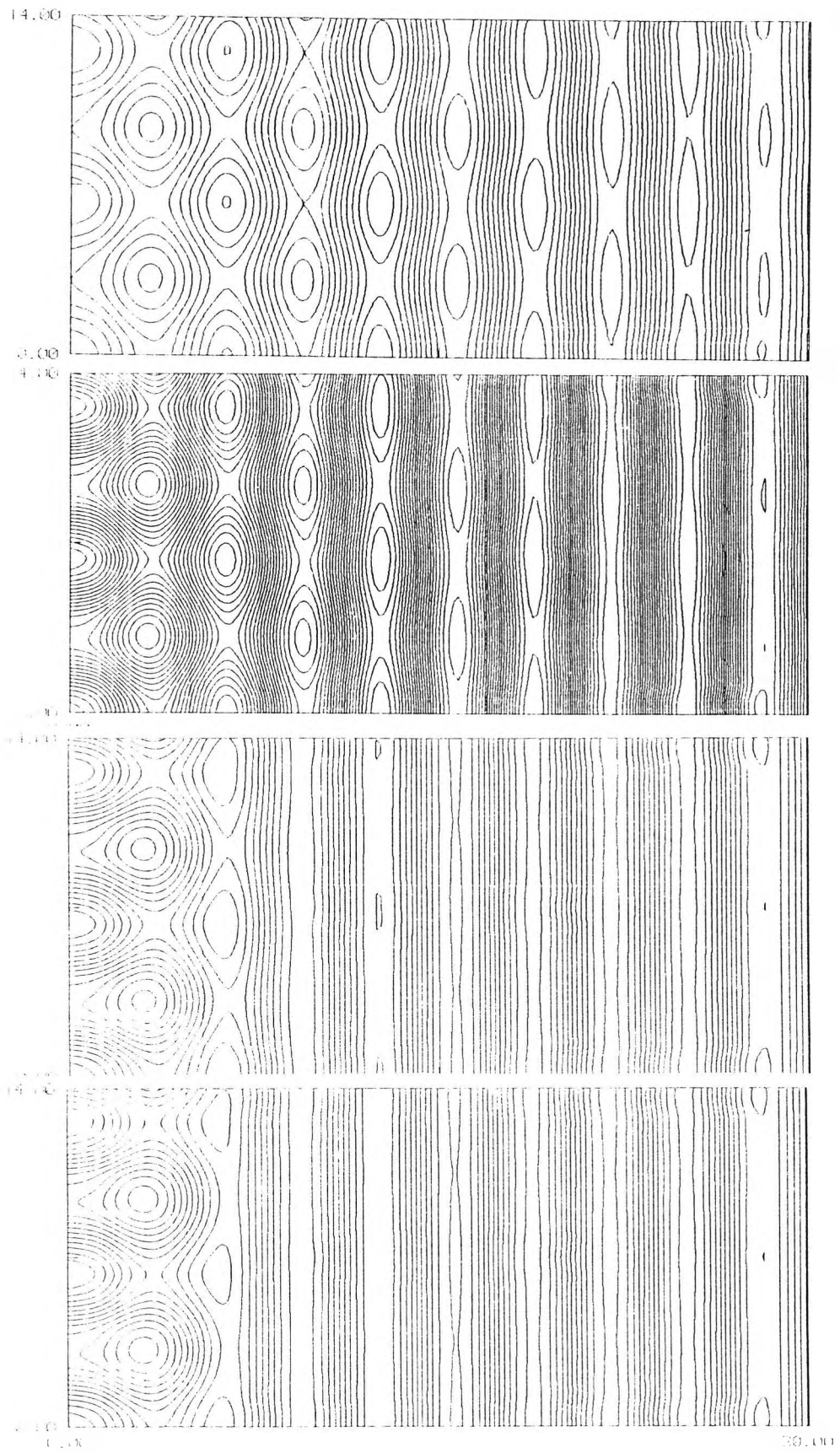
Fig. 2.28 : Contours of ψ at times $\tau = 0$, 1, 5 and 20 for $\mu = 2.0$, $\lambda = 0.2$

72
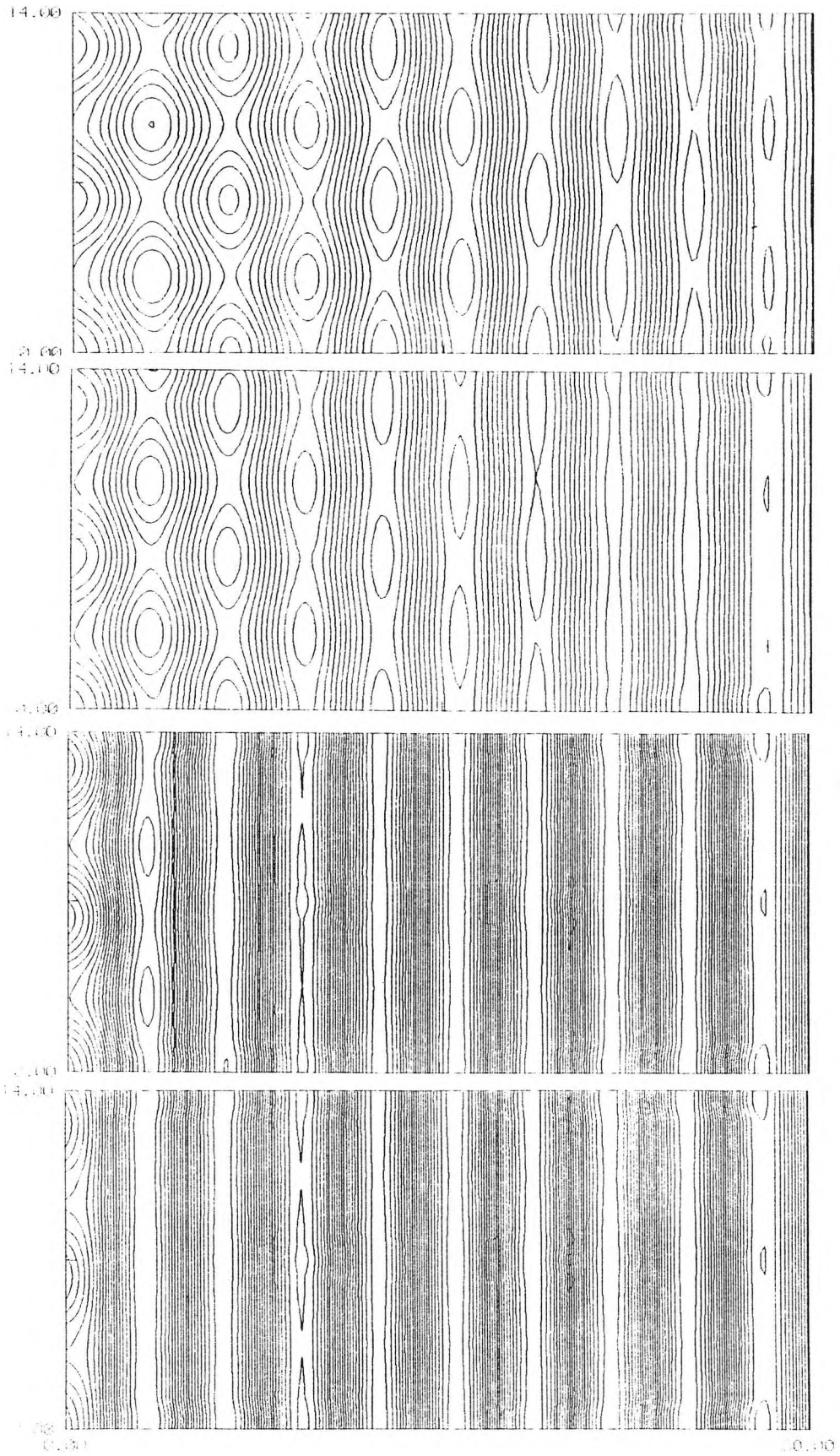
Fig. 2.29 : Contours of ψ at times $\tau=0$, 1, 5 and 20 for $\mu=2.0$, $\lambda=0.4$

73
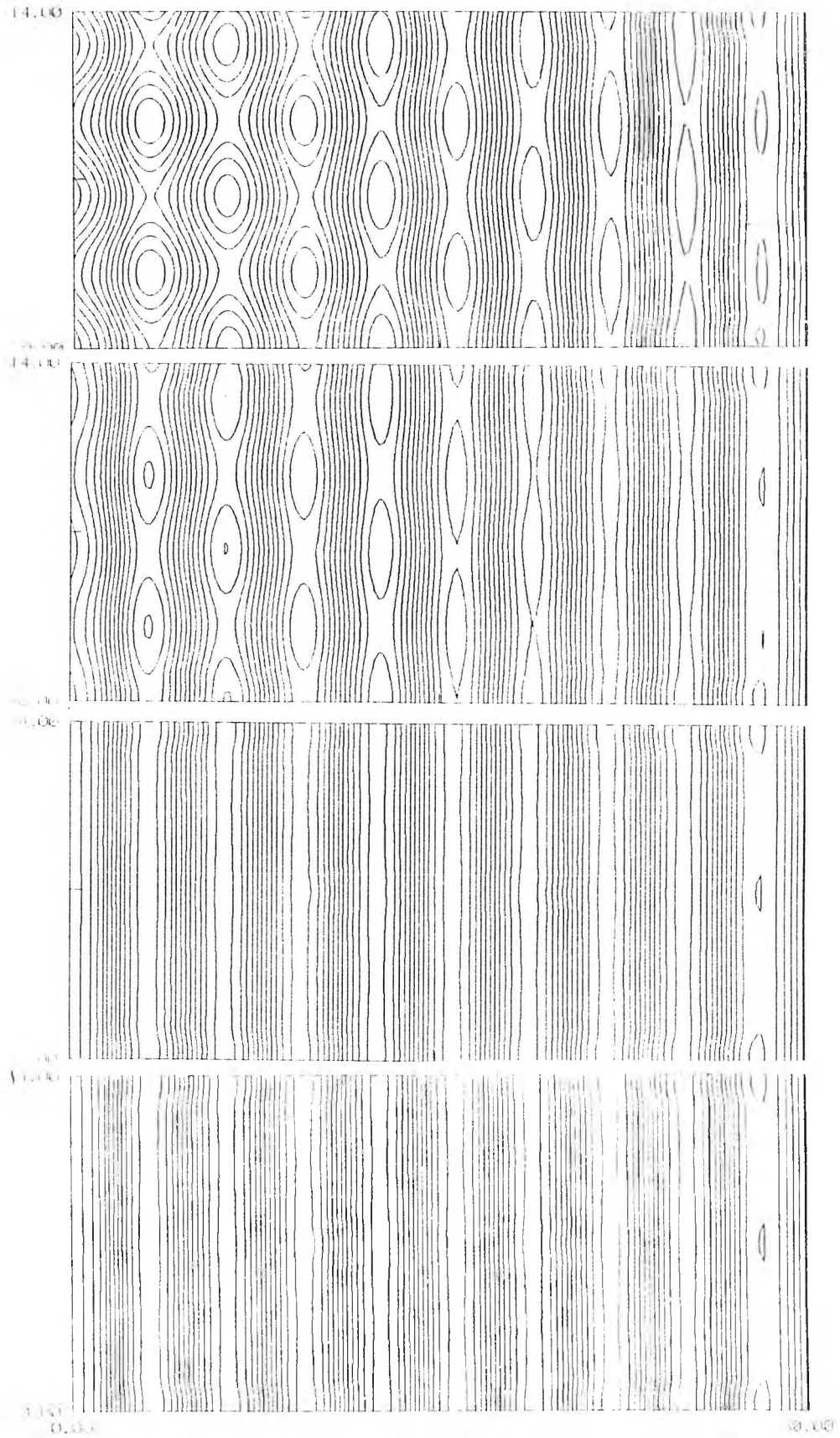
Fig. 2.30 : Contours of ψ at times $\tau=0$, 1, 5 and 20 for $\mu=2.0$, $\lambda=0.6$
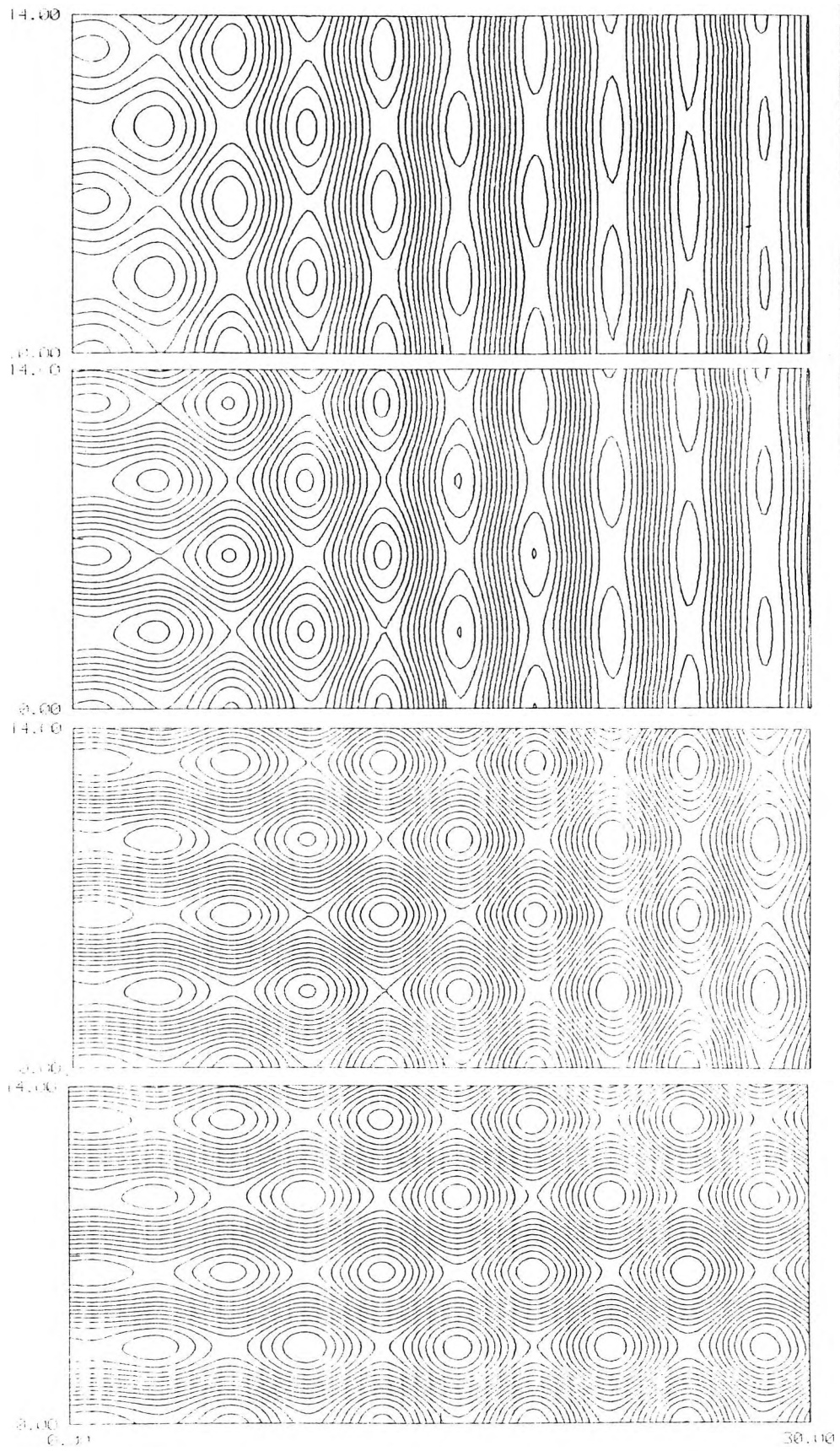
Fig. 2.31 : Contours of ψ at times $\tau=0$, 1, 5 and 20 for $\mu=0.5$, $\lambda=0$
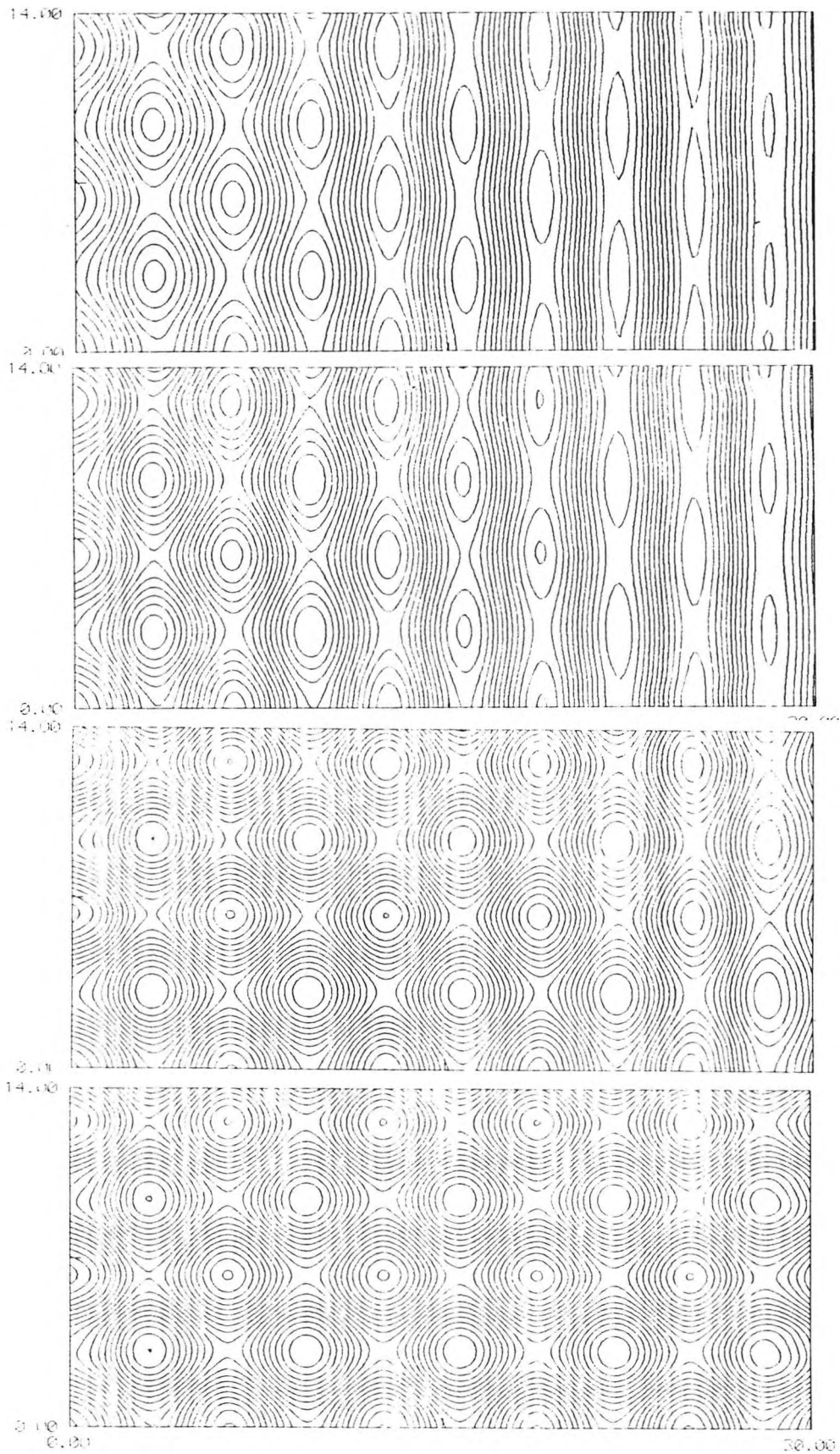
Fig. 2.32 : Contours of ψ at times $\tau=0$, 1, 5 and 20 for $\mu=0.5$, $\lambda=0.5$

76
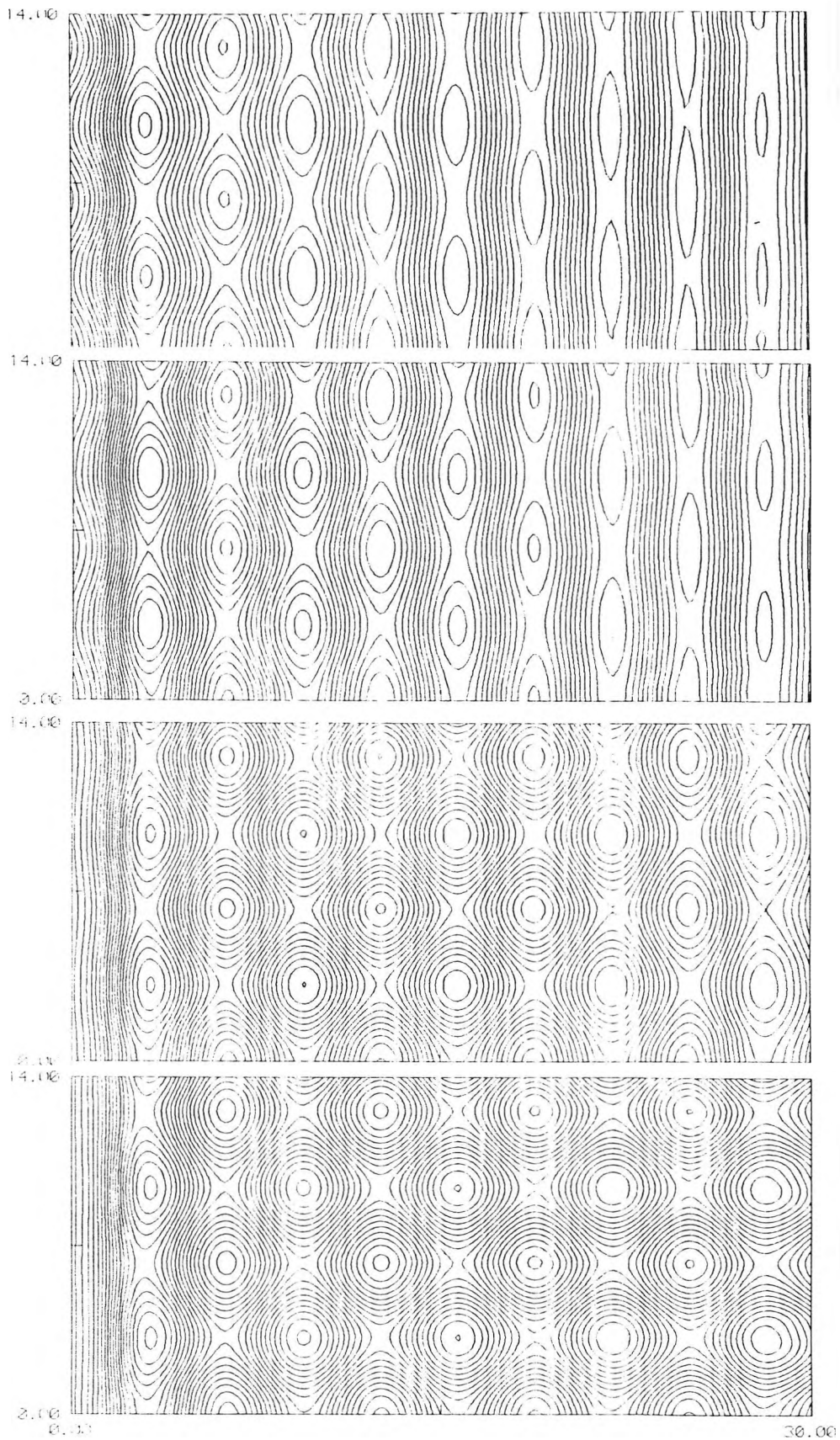
Fig. 2.33 : Contours of ψ at times $\tau=0$, 1, 5 and 20 for $\mu=0.5$, $\lambda=1.0$
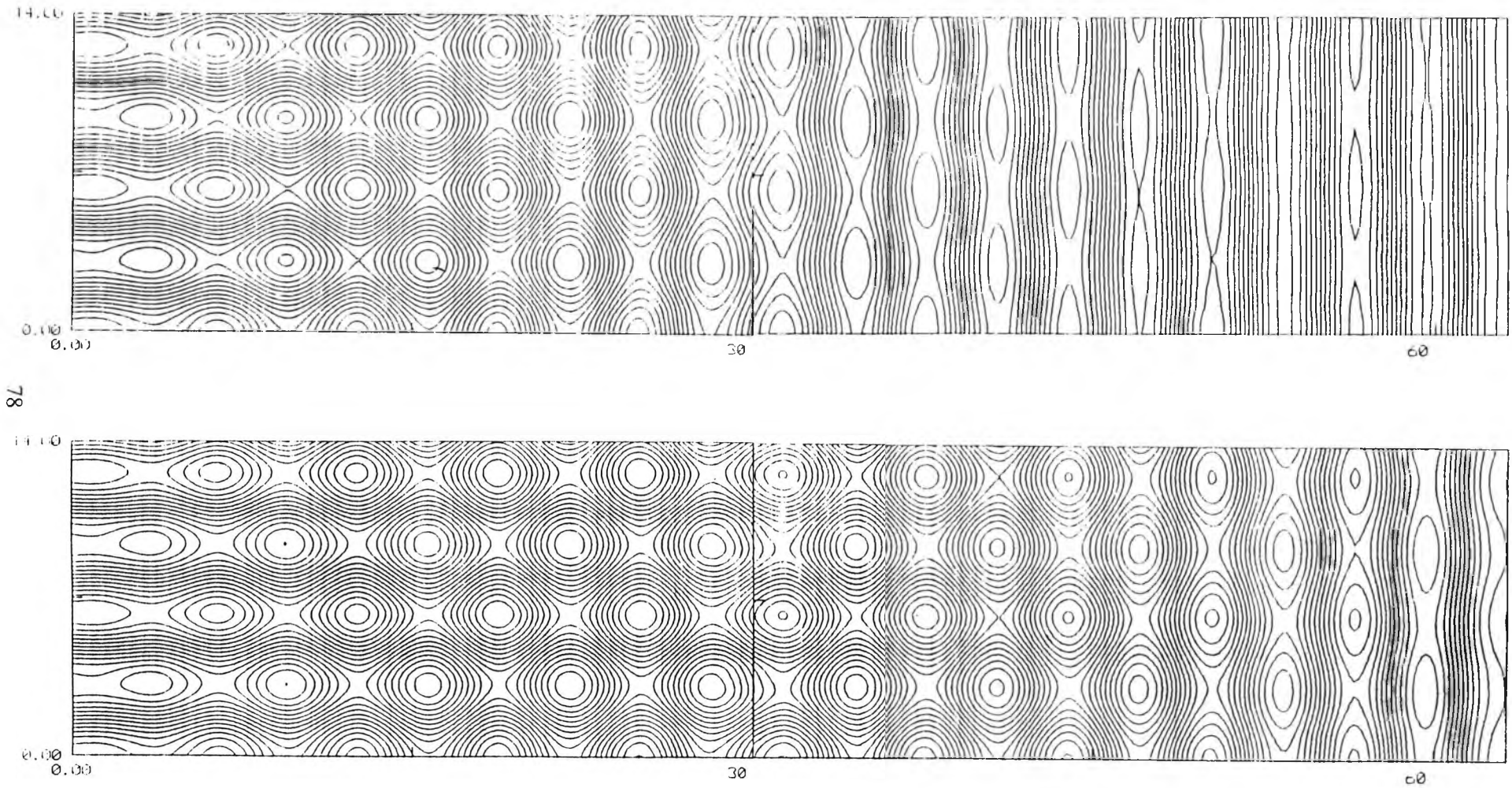
Fig. 2.34 : Contours of ψ at times $\tau=5$ and 10 for $\mu=0.5$, $\lambda=0$ showing the solution structure
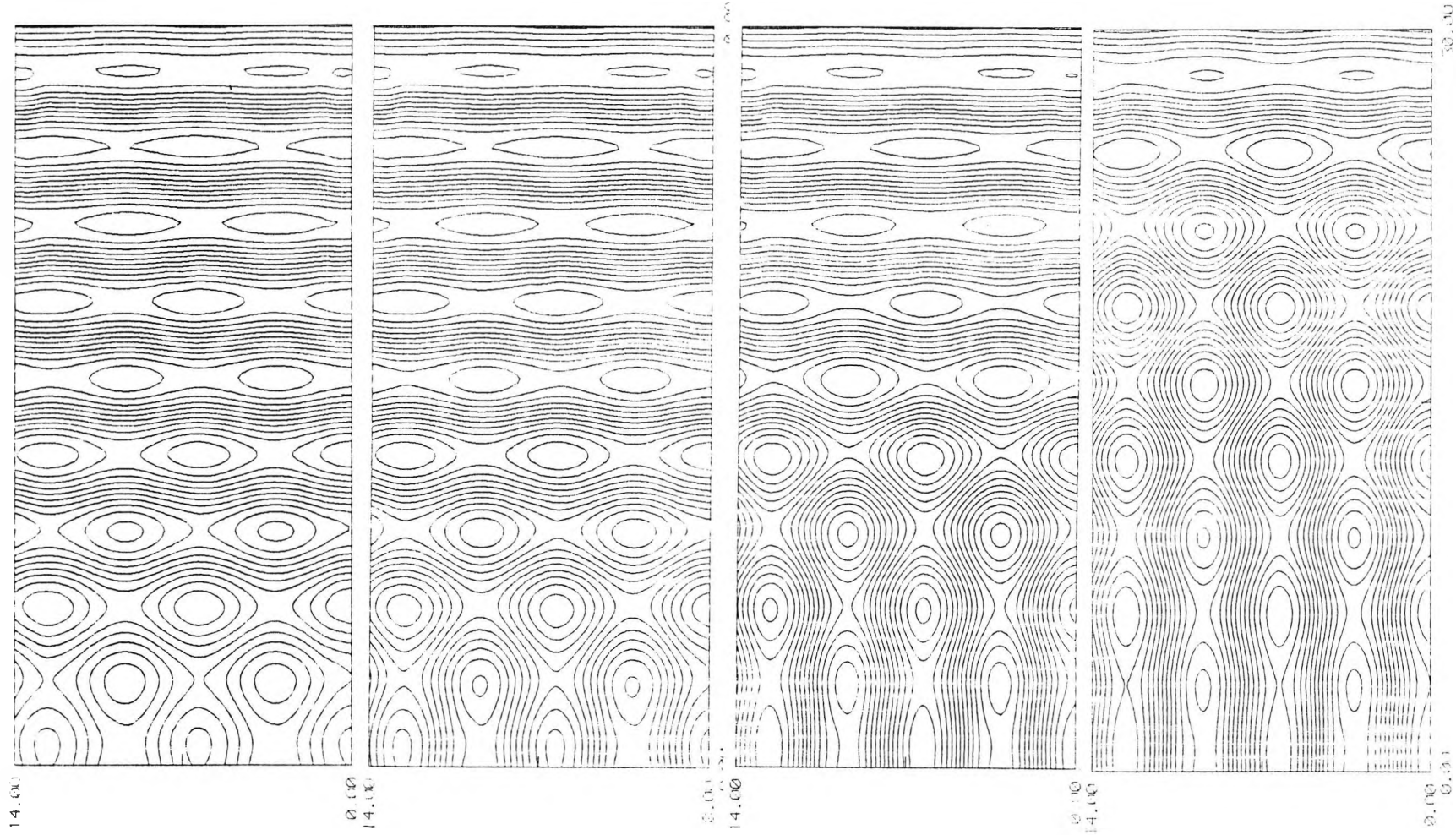
Fig. 2.35 : Contours of ψ at times $\tau = 0$, 1, 5 and 20 for $\mu = 1.0$, $\lambda = 0$

79
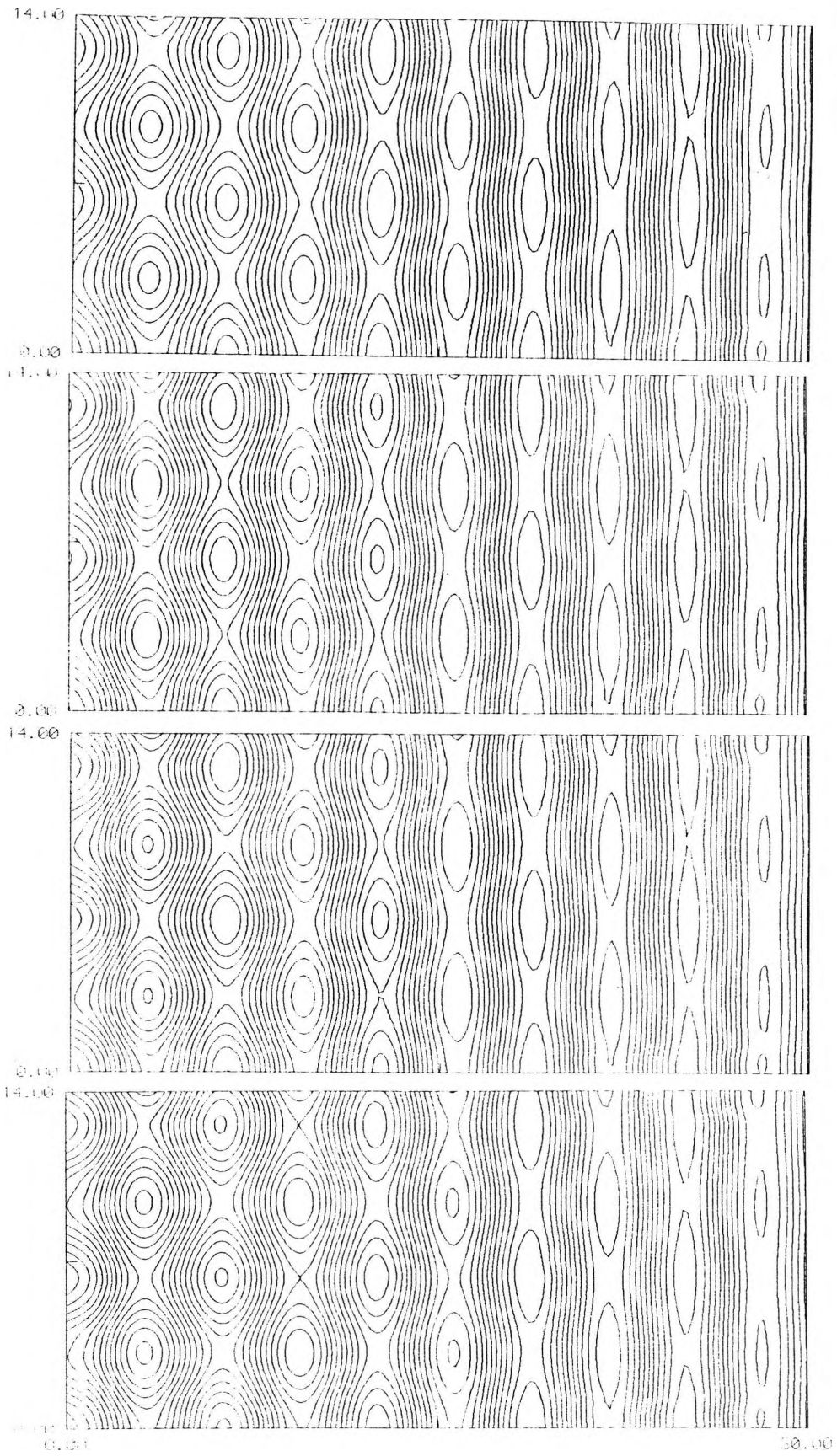
Fig. 2.36 : Contours of ψ at times $\tau=0$, 1, 5 and 20 for $\mu=1.0$, $\lambda=0.5$
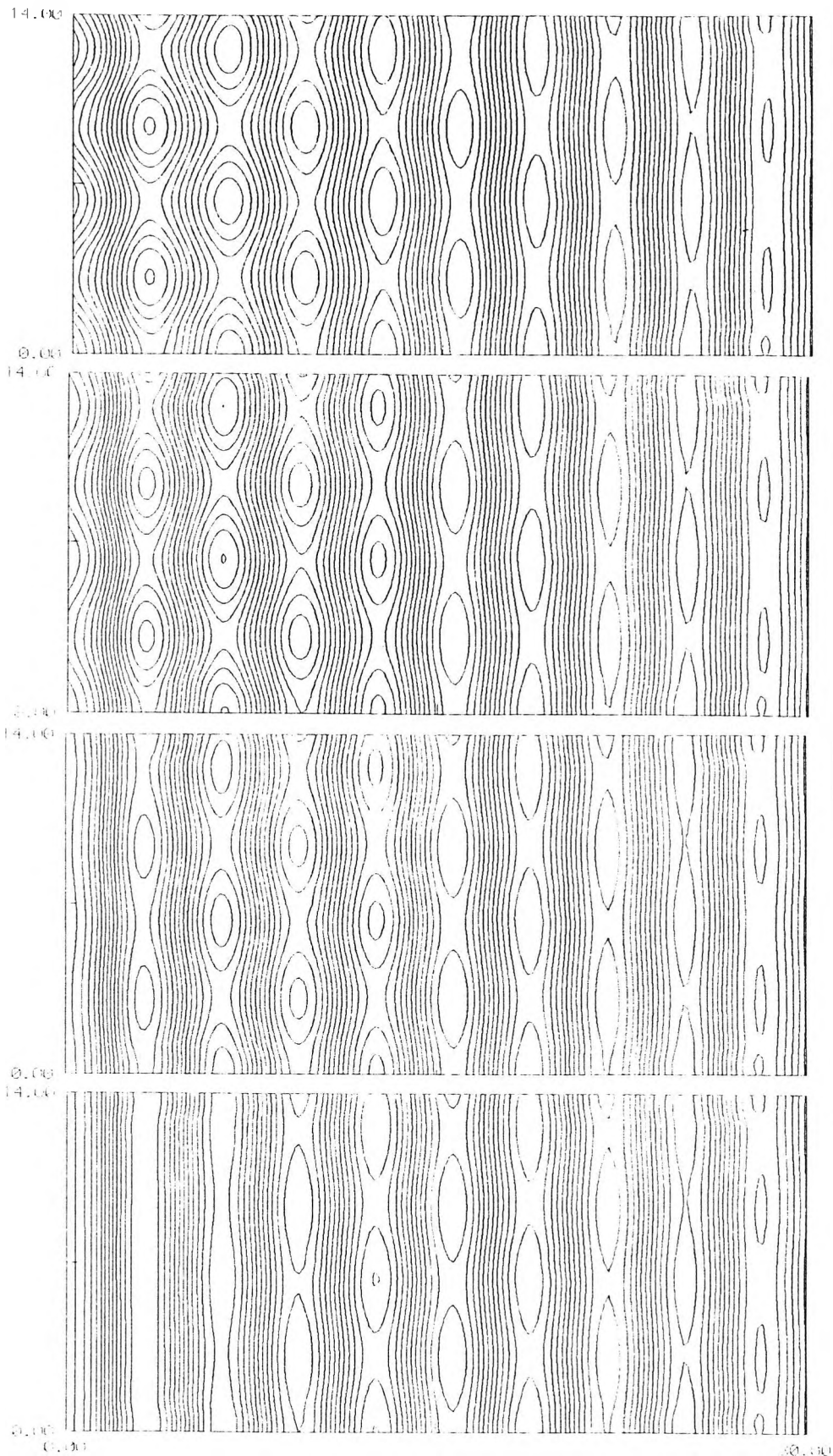
Fig. 2.37 : Contours of ψ at times $\tau=0$, 1, 5 and 20 for $\mu=1.0$, $\lambda=0.7$

81

Chapter 3

Steady-state solution in the transition zone

3.1 Introduction

This chapter considers the solution in the neighbourhood of the transition line $X=X_0$. In chapter 2, it is shown that at large time τ the amplitude of the y-rolls falls to zero with a square root singularity in the neighbourhood of X_0, which is smoothed out on a length scale of order τ^{-1}. When $\tau \to \infty$, the region close to X_0 decreases in size until X gets so small that the $\partial^4 B / \partial X^4$ term can no longer be neglected and in this transition zone a new steady-state solution for B evolves. Clearly for very large times τ the results of chapter 2 are not valid and a separate analysis is needed. In an analysis of grain boundaries in infinite layers, Tesauro and Cross (1987) suggest that the solution for B is smoothed out on an inner boundary layer scale although they did not consider any details of the solution in this inner region. Earlier, Walton (1982) had considered various related problems arising in the transition from longitudinal to transverse rolls in fluid layers subject to horizontal differential heating. This led to a general form of fourth-order equation incorporating effects of variation in the wavelength of the longitudinal roll pattern. He solved the fourth-order equation for B numerically in certain cases using a shooting method and also by expressing B in terms of Tchebychev polynomials over a finite, but large domain. However, no consideration was given to finding various constants arising in the transition zone solution.

In this chapter, the solution of the relevant steady-state transition zone problem is studied for $\mu=2$, assuming that both $\tilde{A}$ and $\tilde{B}$ are real and independent of y. Both analytical and numerical methods are used to obtain solutions. In section 3.2 the leading order outer steady-state solutions for the scaled amplitude functions A and B in the regions $X<X_0$ and $X>X_0$ are set out; these are the solutions obtained in section 2.6 of chapter 2. The limiting forms of these

solutions as $X \rightarrow X_0 \pm$ are determined and this allows the appropriate scalings of B and X in the transition zone to be deduced. In section 3.3 the equations for the transition zone are derived and the problem for $\hat{B}$, the leading term in B, is obtained. This problem is solved in section 3.4 using a fourth-order Runge-Kutta method combined with Newton iteration. In section 3.5, having found $\hat{B}$, it is possible to calculate its effect on the solution for A in the transition zone. This involves integration of the solution for $\hat{B}^2$ across the layer and results are obtained analytically and also numerically using Simpson's rule. These results allow 'bridging' conditions to be obtained for correction terms to the amplitudes of the x-roll patterns in the two outer regions $X < X_0$ and $X > X_0$. These correction terms to A in the outer regions due to the presence of the transitional zone are found to be of order $\epsilon^{3/5}$ and the transition zone itself consists of a region of extent $|X-X_0| \sim \epsilon^{1/5}$ surrounding X_0. The results are discussed in section 3.6 with particular reference to the manner in which they can be extended to general values of μ.

3.2 Formulation

Consider the coupled steady-state system for $\tilde{A}$ and $\tilde{B}$ derived in section 2.2, with both $\tilde{A}$ and $\tilde{B}$ assumed to be real and independent of y, and written in terms of the scaled variables $A = \epsilon^{-1/2}\tilde{A}$, $B = \epsilon^{-1/2}\tilde{B}$, $X = \epsilon^{1/2}x$:

$$4\frac{\partial^2 A}{\partial X^2} + A - 3A^3 - 6AB^2 = 0 \quad , \tag{3.2.1}$$

$$B - 3B^3 - 6BA^2 - \epsilon\frac{\partial^4 B}{\partial X^4} = 0 \quad , \tag{3.2.2}$$

$$A = \lambda \quad \text{at} \quad X = 0 \quad , \tag{3.2.3}$$

$$B = \frac{\partial B}{\partial X} = 0 \quad \text{at} \quad X = 0 \quad , \tag{3.2.4}$$

$$A \to \frac{1}{\sqrt{3}} \quad , \quad B \to 0 \quad \text{as} \quad X \to \infty \quad . \tag{3.2.5}$$

By neglecting the term $\epsilon \partial^4 B / \partial X^4$ in (3.2.2) it is shown in section 2.6 that as $\epsilon \to 0$ a steady-state solution exists for $\lambda < 1/\sqrt{6}$ consisting of only x-rolls in the region $X > X_0$ and a combination of x-rolls and y-rolls in the region $0 < X < X_0$, the position $X = X_0$ being defined by the point at which $A = 1/\sqrt{6}$ and given as a function of λ by (2.6.8) with $\mu = 2$. At X_0 the amplitude of the y-rolls falls abruptly to zero. The nature of this abrupt change in the amplitude B can be seen by considering the local solution near $X = X_0$. For $\mu = 2$ the leading order outer steady-state solutions for A and B where $X < X_0$ and $X > X_0$, found in chapter 2, are as follows. For $X < X_0$,

$$A = \frac{2\sqrt{2}\, e^{\frac{1}{2}(X-X_0)}}{\sqrt{3}\left(3 + e^{X-X_0}\right)} \quad , \quad B^2 = \frac{1}{3}(1 - 6A^2) \tag{3.2.6}$$

and for $X > X_0$,

$$A = \frac{1}{\sqrt{3}} \tanh\left[\frac{X - X_0 + C_1}{2\sqrt{2}}\right] \quad \text{with} \quad C_1 = 2\sqrt{2} \tanh^{-1}\left[\frac{1}{\sqrt{2}}\right] \quad , \quad B = 0 \quad , \tag{3.2.7}$$

where

$$X_0 = -2 \ln \left\{ \frac{3\sqrt{3}\lambda}{\sqrt{2}\left[1 + \left(1 - \frac{9\lambda^2}{2}\right)^{1/2}\right]} \right\} \tag{3.2.8}$$

and $\lambda < 1/\sqrt{6}$. The limiting forms of these outer solutions for A and B as $X \to X_0 \pm$ may now be determined. From (3.2.6) it follows that as $X \to X_0-$,

84

$$A = \frac{1}{\sqrt{6}} + \frac{1}{4\sqrt{6}}(X-X_0) - \frac{1}{16\sqrt{6}}(X-X_0)^2 - \frac{7}{192\sqrt{6}}(X-X_0)^3 + ... \quad , \qquad (3.2.9)$$

$$B \sim \left[\frac{X_0 - X}{6}\right]^{1/2} \quad , \qquad (3.2.10)$$

whereas from (3.2.7) it follows that as $X \to X_0 +$

$$A = \frac{1}{\sqrt{6}} + \frac{1}{4\sqrt{6}}(X-X_0) - \frac{1}{16\sqrt{6}}(X-X_0)^2 + \frac{1}{192\sqrt{6}}(X-X_0)^3 + ... \quad , \qquad (3.2.11)$$

$$B = 0 \quad . \qquad (3.2.12)$$

The scalings for the solution in the transition zone can now be obtained using (3.2.2). Assuming that $X - X_0 = \epsilon^\alpha \hat{X}$ and $B = \epsilon^\beta \hat{B}$ with α and β to be determined, substitution into (3.2.2) gives

$$-\epsilon^{1-4\alpha+\beta}\frac{\partial^4 \hat{B}}{\partial \hat{X}^4} - 3\epsilon^{3\beta}\hat{B}^3 - \epsilon^{\alpha+\beta}\frac{\hat{B}\hat{X}}{2} = 0 \quad , \qquad (3.2.13)$$

where it is assumed that the terms in A which are linear as $X \to X_0$ remain unchanged across the layer. Matching with (3.2.10) requires that $\beta = \alpha/2$ so that the second and third terms are of equal magnitude, and the first term also balances provided that $2\beta = 1 - 4\alpha$, giving

$$\alpha = \frac{1}{5} \quad , \quad \beta = \frac{1}{10} \quad . \qquad (3.2.14)$$

Thus the transition zone is defined by the scalings

$$X - X_0 = \epsilon^{1/5}\hat{X} \quad , \quad B \sim \epsilon^{1/10}\hat{B} \quad , \qquad (3.2.15)$$

with $\hat{X}$ and $\hat{B}$ of order one as $\epsilon \to 0$. Full expansions for both A and B within the transition zone are considered in the next section.

3.3 Transition zone

From (3.2.9) and (3.2.15) it is supposed that in the transition zone

$$A = \hat{A}_0(\hat{X}) + \epsilon^{1/5}\hat{A}_1(\hat{X}) + \epsilon^{2/5}\hat{A}_2(\hat{X}) + \epsilon^{3/5}\hat{A}_3(\hat{X}) + ... \tag{3.3.1}$$

and

$$B = \epsilon^{1/10}\hat{B}(\hat{X}) + ... \quad , \tag{3.3.2}$$

where $X - X_0 = \epsilon^{1/5}\hat{X}$. The expressions (3.3.1) and (3.3.2) are substituted into (3.2.1) and (3.2.2) and orders of ϵ compared, leading to:

$$4\frac{\partial^2 \hat{A}_0}{\partial \hat{X}^2} = 0 \quad , \tag{3.3.3}$$

$$4\frac{\partial^2 \hat{A}_1}{\partial \hat{X}^2} = 0 \quad , \tag{3.3.4}$$

$$4\frac{\partial^2 \hat{A}_2}{\partial \hat{X}^2} + \hat{A}_0 - 3\hat{A}_0^3 = 0 \quad , \tag{3.3.5}$$

$$4\frac{\partial^2 \hat{A}_3}{\partial \hat{X}^2} + \hat{A}_1 - 6\hat{A}_0\hat{B}^2 - 9\hat{A}_0^2\hat{A}_1 = 0 \tag{3.3.6}$$

and

$$\frac{\partial^4 \hat{B}}{\partial \hat{X}^4} + 3\hat{B}^3 + 12\hat{B}\hat{A}_0\hat{A}_1 = 0 \quad . \tag{3.3.7}$$

In order to determine the solutions for successive terms in the transition zone, boundary conditions for $\hat{A}$ as $\hat{X} \rightarrow \pm \infty$ are required. Matching with the outer forms (3.2.9) and (3.2.11) as $X \rightarrow X_0 \pm$ requires

$$\hat{A}_0 \rightarrow \frac{1}{\sqrt{6}} \qquad (\hat{X} \rightarrow \pm \infty) \quad , \tag{3.3.8}$$

86

$$\hat{A}_1 \sim \frac{\hat{X}}{4\sqrt{6}} \qquad (\hat{X} \to \pm\infty) \quad , \qquad\qquad (3.3.9)$$

$$\hat{A}_2 \sim -\frac{\hat{X}^2}{16\sqrt{6}} \qquad (\hat{X} \to \pm\infty) \quad , \qquad\qquad (3.3.10)$$

$$\hat{A}_3 \sim \frac{\hat{X}^3}{192\sqrt{6}} \qquad (\hat{X} \to +\infty) \quad , \quad \hat{A}_3 \sim -\frac{7\hat{X}^3}{192\sqrt{6}} \qquad (\hat{X} \to -\infty) \quad . \qquad (3.3.11)$$

Suitable solutions for $\hat{A}_0$, $\hat{A}_1$ and $\hat{A}_2$ can now be found as

$$\hat{A}_0 = \frac{1}{\sqrt{6}} \quad , \qquad\qquad (3.3.12)$$

$$\hat{A}_1 = \frac{\hat{X}}{4\sqrt{6}} \quad , \qquad\qquad (3.3.13)$$

$$\hat{A}_2 = -\frac{\hat{X}^2}{16\sqrt{6}} \quad , \qquad\qquad (3.3.14)$$

where it is assumed that any constants of integration can be taken as zero. This is valid provided that there are no correction terms in the outer solution for A at order $\epsilon^{1/5}$ or $\epsilon^{2/5}$ and will be discussed in section 3.5 below. Equation (3.3.7) can now be simplified to give

$$\frac{\partial^4 \hat{B}}{\partial \hat{X}^4} + 3\hat{B}^3 + \frac{\hat{B}\hat{X}}{2} = 0 \quad . \qquad\qquad (3.3.15)$$

The boundary conditions for this equation obtained from matching with (3.2.10) and (3.2.12) are

$$\hat{B} \sim \left(-\frac{\hat{X}}{6}\right)^{1/2} \quad \text{as} \quad \hat{X} \to -\infty \qquad\qquad (3.3.16)$$

$$\hat{B} \to 0 \quad \text{as} \quad \hat{X} \to \infty \quad . \qquad\qquad (3.3.17)$$

The solution of the system (3.3.15)-(3.3.17) for $\hat{B}$ is considered in the next section.

3.4 Numerical solution

A fourth-order Runge-Kutta method was used to solve equation (3.3.15). It is convenient to set $\hat{X} = -\check{X}$ and $\hat{B}(\hat{X}) = \check{B}(\check{X})$ to obtain the system

$$\frac{\partial^4 \check{B}}{\partial \check{X}^4} + 3\check{B}^3 - \frac{\check{B}\check{X}}{2} = 0 \quad , \tag{3.4.1}$$

$$\check{B} \sim \left(\frac{\check{X}}{6}\right)^{1/2} \quad \text{as} \quad \check{X} \to \infty \quad , \tag{3.4.2}$$

$$\hat{B} \to 0 \quad \text{as} \quad \check{X} \to -\infty \quad . \tag{3.4.3}$$

The asymptotic expansion of $\check{B}$ as $\check{X} \to \infty$ can be determined to higher order by assuming a correction term to (3.4.2) of the form $k(\check{X}/6)^a$ and then finding a and k by substituting into (3.4.1) and balancing terms. This shows that

$$\check{B} \sim \left(\frac{\check{X}}{6}\right)^{1/2} + \frac{5}{41472}\left(\frac{\check{X}}{6}\right)^{-9/2} \quad \text{as} \quad \check{X} \to \infty \quad . \tag{3.4.4}$$

As $\check{X} \to -\infty$, the solution for $\check{B}$ is exponentially small and can be determined by assuming that $\check{B}$ is proportional to $\exp(-\omega(-\check{X})^{5/4})$ where ω is a constant. This leads to a general solution of the form

$$\check{B} = (-\check{X})^{-3/8} e^{-\omega_r(-\check{X})^{5/4}} \left[a\cos\left(\omega_i(-\check{X})^{5/4}\right) + b\sin\left(\omega_i(-\check{X})^{5/4}\right) \right] \quad \text{as} \quad \check{X} \to -\infty \quad , \tag{3.4.5}$$

where

$$\omega_r = \omega_i = \frac{2^{5/4}}{5} \tag{3.4.6}$$

and a and b are arbitrary constants, the solution in this limit being equivalent to that of the

88

linearised version of the equation studied by Ross (1966) (see also section 2.4).

In order to obtain a numerical solution of (3.4.1)-(3.4.3), equation (3.4.1) is represented as the system of first-order equations

$$y_1' = y_2 \; , \tag{3.4.7}$$

$$y_2' = y_3 \; , \tag{3.4.8}$$

$$y_3' = y_4 \; , \tag{3.4.9}$$

$$y_4' = y_1\left(\frac{\check{X}}{2} - 3y_1^2\right) \; , \tag{3.4.10}$$

where $y_1 = \check{B}$ and this is solved using a fourth-order Runge-Kutta process. The solution is computed on a finite domain $-\check{X}_\infty < \check{X} < \check{X}_\infty$ and the initial values for y_i ($i=1,2,3,4$) at $\check{X} = -\check{X}_\infty$ are specified using the asymptotic form (3.4.5). Correct choice of a and b is needed to ensure the required behaviour of $\check{B}$ given by (3.4.4) is obtained as $\check{X} \to \infty$. Initially the Runge-Kutta method was applied with a range of values of a and b such that a varied from -0.2 to 0.2 and b from -1 to 1 in steps of 0.1. Values of $\check{X}_{\pm\infty}$ were chosen as 1 initially and the solution for $\check{B}$ monitored in order to allow suitable values for a and b to be selected as initial estimates in an iterative scheme. The Runge-Kutta program is run for these estimated values to obtain $\check{B}$ in the range $-\check{X}_{-\infty}$ to $\check{X}_{+\infty}$. At $\check{X} = \check{X}_\infty$ condition (3.4.4) is applied to $\check{B}$ and its first derivative,

$$\frac{\partial \check{B}}{\partial \check{X}} \sim \frac{1}{12}\left(\frac{\check{X}}{6}\right)^{-1/2} - \frac{5}{55296}\left(\frac{\check{X}}{6}\right)^{-11/2} + \ldots \; , \tag{3.4.11}$$

and with f and g defined by

$$f = f(a,b) \equiv y_1 - \left[\left(\frac{\check{X}_\infty}{6}\right)^{1/2} + \frac{5}{41472}\left(\frac{\check{X}_\infty}{6}\right)^{-9/2} + \ldots\right] \; , \tag{3.4.12}$$

$$g = g(a,b) \equiv y_2 - \left[\frac{1}{12}\left(\frac{\check{X}_\infty}{6}\right)^{-1/2} - \frac{5}{55296}\left(\frac{\check{X}_\infty}{6}\right)^{-11/2} + ... \right] , \qquad (3.4.13)$$

it is required that $f(a,b)=0$ and $g(a,b)=0$. When the Runge-Kutta program is first run, $f(a,b)\neq0$ and $g(a,b)\neq0$ so Newton's method is used to adjust the values of a and b by calculating increments δa and δb from the formulae

$$f + \frac{\partial f}{\partial a}\delta a + \frac{\partial f}{\partial b}\delta b = 0 , \qquad (3.4.14)$$

$$g + \frac{\partial g}{\partial a}\delta a + \frac{\partial g}{\partial b}\delta b = 0 . \qquad (3.4.15)$$

In order to calculate δa and δb, the gradients in (3.4.14) and (3.4.15) have to be estimated. The partial derivative $\partial f/\partial a$ is found by dividing the change in f by the change in a for calculations based on fixed b and two neighbouring values of a. Similarly $\partial f/\partial b$ is calculated by fixing a and dividing the change in f by the change in b for two neighbouring values. The gradients of g are calculated in the same way. Once δa and δb are found from (3.4.14) and (3.4.15) the improved estimates

$$a_{new} = a + \delta a \quad , \quad b_{new} = b + \delta b \qquad (3.4.16)$$

are obtained and the Runge-Kutta program run again with these values of a and b to recompute $\check{B}$ from $-\check{X}_{-\infty}$ to $\check{X}_{+\infty}$. The Newton iteration scheme ensures good convergence, with f and g both tending to zero for the given values of $\check{X}_{\pm\infty}$. The values of $\check{X}_{\pm\infty}$ are now gradually increased to obtain better results, using the final values of a and b at the previous $\check{X}_{\pm\infty}$ as initial guesses. In this way results can be achieved for quite large values of $\check{X}_{\pm\infty}$. In addition, final results for a and b were compared for several step sizes h in the Runge-Kutta process in order to estimate the effect of the step size on the accuracy of the solution.

The results of the computations are now discussed. With $a=0.2$, $b=0$, $\check{X}_{\pm\infty}=1$ and

90

$h=0.025$, it was found that $\breve{B} \approx 0.5041$ at $\breve{X}_\infty$ which is quite close to the value $(\breve{X}_\infty/6)^{1/2}=0.408$ given by the leading term of (3.4.4). These values were therefore used to initiate the iterative scheme and after 10 iterations it was found that f and g had decreased to values of order 10^7 with a and b converging to values of 0.928569 and -0.044601 respectively. Using these values as initial guesses it was then found possible to increase the values of $\breve{X}_{\pm\infty}$ to 8.3 and it is noted that $\breve{X}_{\pm\infty}$ had to be increased in steps of only 0.1 when $\breve{X}_{\pm\infty}$ reached 6.0 to ensure convergence. Any further increase in $\breve{X}_{\pm\infty}$ led to slower convergence of f and g. Table 3.1 illustrates the convergence of a and b values with successive iterations when $\breve{X}_{\pm\infty}=3.0$. Table 3.2 shows values of y_i ($i=1,2,3,4$) for various $\breve{X}_{\pm\infty}$ at $\breve{X}=0$ and it can be clearly seen that as $\breve{X}_{\pm\infty}$ increases the values of y_i converge. To investigate the effect of the step size h on the results, the final values of a and b for $\breve{X}_{\pm\infty}=3.0$ are compared for $h=0.025$, 0.05 and 0.1 in Table 3.3. This indicates relatively little dependence on h for values less than or equal to 0.1.

Figure 3.1 shows the final graph of $\hat{B}$ versus $\hat{X}$, representing the smooth decrease in amplitude of the y-rolls across the transition zone from the square root behaviour (3.3.16) as $\hat{X}\to-\infty$ to the exponentially small behaviour associated with (3.3.17) as $\hat{X}\to\infty$. Note that the solution for $\hat{B}$ contains small oscillations in the region where $\hat{X}$ is positive (further detail is shown in Figure 3.2), consistent with the damped oscillatory behaviour given by (3.4.5). For negative $\hat{X}$, the second term in the asymptotic expansion (3.4.4) indicates that $\hat{B}$ is slightly greater than its leading square root form as $\hat{X}\to-\infty$, and this was also correctly reproduced in the computation.

3.5 Reaction in the outer zone

Having found $\hat{B}$, it is now possible to find the solution in the transition zone for $\hat{A}_3$. Equation (3.3.6) can be integrated twice giving

$$4\hat{A}_3 \;=\; \frac{1}{8\sqrt{6}}\left[\frac{\hat{X}^3}{6}+48\int_{\hat{X}}^{\infty}[\int_{\hat{X}}^{\infty}\hat{B}^2 d\hat{X}]d\hat{X}\right]+\alpha_3\hat{X}+\beta_3 \quad, \tag{3.5.1}$$

where α_3 and β_3 are constants. It is convenient to split the integral of $\hat{B}^2$ into two parts such that

$$\int_{\hat{X}}^{\infty}\hat{B}^2 d\hat{X} \;=\; \int_{0}^{\infty}\hat{B}^2 d\hat{X}+\int_{\hat{X}}^{0}(\hat{B}^2+\frac{\hat{X}}{6})d\hat{X}+\frac{\hat{X}^2}{12} \tag{3.5.2}$$

and then it follows from the form of $\hat{B}^2$ as $\hat{X}\to-\infty$ that

$$\int_{\hat{X}}^{\infty}\hat{B}^2 d\hat{X} \;\sim\; \frac{\hat{X}^2}{12}+I_0+I_1+\frac{5}{48}(-\hat{X})^{-3} \quad\text{as}\quad \hat{X}\to-\infty \quad, \tag{3.5.3}$$

where

$$I_0 \;=\; \int_{0}^{\infty}\hat{B}^2 d\hat{X} \tag{3.5.4}$$

and

$$I_1 \;=\; \int_{-\infty}^{0}(\hat{B}^2+\frac{\hat{X}}{6})d\hat{X} \quad. \tag{3.5.5}$$

Now if $G(\hat{X})$ is defined by

$$G(\hat{X}) \;\equiv\; \int_{\hat{X}}^{\infty}\hat{B}^2 d\hat{X} \quad, \tag{3.5.6}$$

then it follows in a similar manner that

$$\int_{\hat{X}}^{\infty}G(\hat{X})d\hat{X} \;=\; \int_{0}^{\infty}G(\hat{X})d\hat{X}+\int_{\hat{X}}^{0}G(\hat{X})d\hat{X} \tag{3.5.7}$$

and that

$$\int_{\hat{X}}^{\infty} G(\hat{X})d\hat{X} \sim -\frac{\hat{X}^3}{36} - (I_0 + I_1)\hat{X} + J_0 + J_1 + \frac{5}{96}(-\hat{X})^{-2} \quad \text{as} \quad \hat{X} \to -\infty \quad , \qquad (3.5.8)$$

where

$$J_0 = \int_0^{\infty} G(\hat{X})d\hat{X} \qquad (3.5.9)$$

and

$$J_1 = \int_{-\infty}^{0} [G(\hat{X}) - \frac{\hat{X}^2}{12} - (I_0 + I_1)]d\hat{X} \quad . \qquad (3.5.10)$$

The form of $\hat{A}_3$ as $\hat{X} \to \pm\infty$ can now be deduced from (3.5.1), with

$$\hat{A}_3 \sim \frac{\hat{X}^3}{192\sqrt{6}} + \frac{\alpha_3 \hat{X}}{4} + \frac{\beta_3}{4} \quad \text{as} \quad \hat{X} \to \infty \qquad (3.5.11)$$

and

$$\hat{A}_3 \sim -\frac{7\hat{X}^3}{192\sqrt{6}} + \left[\frac{\alpha_3}{4} - \frac{3}{2\sqrt{6}}(I_0 + I_1)\right]\hat{X} + \left[\frac{\beta_3}{4} + \frac{3}{2\sqrt{6}}(J_0 + J_1)\right] + \frac{5}{64\sqrt{6}}(-\hat{X})^{-2} \quad \text{as} \quad \hat{X} \to -\infty \quad .$$

$$(3.5.12)$$

In fact it is possible to prove that the value of $I_0 + I_1$ is zero, as follows. Equation (3.3.15) is multiplied by $\partial\hat{B}/\partial\hat{X}$ and integrated from $\hat{X}$ to ∞, resulting in:

$$-\frac{\partial^3\hat{B}}{\partial\hat{X}^3}\frac{\partial\hat{B}}{\partial\hat{X}} + \left(\frac{\partial^2\hat{B}}{\partial\hat{X}^2}\right)^2 + \int_{\hat{X}}^{\infty}\frac{\partial^2\hat{B}}{\partial\hat{X}^2}\frac{\partial^3\hat{B}}{\partial\hat{X}^3}d\hat{X} - \frac{3\hat{B}^4}{4} - \frac{\hat{X}\hat{B}^2}{4} - \frac{1}{4}\int_{\hat{X}}^{\infty}\hat{B}^2 d\hat{X} = C \quad , \qquad (3.5.13)$$

where C is a constant of integration. Further simplification then gives

$$-2\frac{\partial^3\hat{B}}{\partial\hat{X}^3}\frac{\partial\hat{B}}{\partial\hat{X}} - \frac{3\hat{B}^4}{2} + \left(\frac{\partial^2\hat{B}}{\partial\hat{X}^2}\right)^2 - \frac{\hat{X}\hat{B}^2}{2} - \frac{1}{2}\int_{\hat{X}}^{\infty}\hat{B}^2 d\hat{X} = 2C \qquad (3.5.14)$$

and application of the boundary condition (3.3.17) at $\hat{X} = \infty$ gives $C = 0$. Hence

93

$$\frac{1}{2}\int_{\hat{X}}^{\infty}\hat{B}^2 d\hat{X} = -\frac{\hat{X}\hat{B}^2}{2} + \left(\frac{\partial^2\hat{B}}{\partial\hat{X}^2}\right)^2 - \frac{3\hat{B}^4}{2} - 2\frac{\partial^3\hat{B}}{\partial\hat{X}^3}\frac{\partial\hat{B}}{\partial\hat{X}}$$ (3.5.15)

and it follows using (3.3.16) that

$$\int_{\hat{X}}^{\infty}\hat{B}^2 d\hat{X} = \frac{\hat{X}^2}{12} + O(-\hat{X}^{-3}) \quad \text{as} \quad \hat{X} \to -\infty \quad .$$ (3.5.16)

Comparison with (3.5.3) then shows that

$$I_0 + I_1 = 0 \quad .$$ (3.5.17)

This result was also checked from the numerical solution for $\hat{B}$ using Simpson's rule to evaluate the two integrals (3.5.4) and (3.5.5). The calculation was carried out for several step sizes h for $\check{X}_{\pm\infty} = 8.3$ and the results shown in Table 3.4 confirm the analytical prediction.

Since $I_0 + I_1 = 0$, there is no discontinuity in terms proportional to $\hat{X}$ in the expansion of $\hat{A}_3$ as $\hat{X} \to \pm\infty$ and consequently, if there are no other external effects generating terms in A of order $\epsilon^{2/5}$ in the outer regions, it may be assumed that $\alpha_3 = 0$. However, it is expected that $J_0 + J_1$ is not equal to zero, which implies there is a discontinuity in the finite part of $\hat{A}_3$ across the transition zone. This generates terms in the outer regions of order $\epsilon^{3/5}$ such that

$$A = \dot{A}_0 + \epsilon^{3/5}\dot{A}_1 + ... \quad \text{for} \quad X < X_0$$ (3.5.18)

and

$$A = \ddot{A}_0 + \epsilon^{3/5}\ddot{A}_1 + ... \quad \text{for} \quad X > X_0 \quad ,$$ (3.5.19)

where $\dot{A}_0$ and $\ddot{A}_0$ are the leading terms set out in section 3.2. Matching of A as $X \to X_0\pm$ with the solution for A in the transition zone as $\hat{X} \to \pm\infty$ shows that in the outer region, the terms $\dot{A}_1$ and $\ddot{A}_1$ must satisfy the jump condition

94

$$\dot{A}_1 - \ddot{A}_1 = \frac{3}{2\sqrt{6}}(J_0 + J_1) \quad \text{at} \quad X = X_0 \quad . \tag{3.5.20}$$

3.6 Discussion

In the transition zone a smooth steady-state solution for B is obtained which generates terms in the expansions of the outer solutions for A of order $\epsilon^{3/5}$. The results in this chapter have been obtained for $\mu = 2$, but they can be generalised to any positive value of μ in a straightforward way by substituting the general form (2.6.9) for A as $X \to X_0$ into the equation (3.3.7) for $\hat{B}$ giving

$$\frac{\partial^4 \hat{B}}{\partial \hat{X}^4} + 3\hat{B}^3 + \frac{(\mu - 1)\hat{X}\hat{B}}{\sqrt{2\mu}} = 0 \quad . \tag{3.6.1}$$

This can be transformed into (3.3.15) by appropriate scalings for $\hat{B}$ and $\hat{X}$ provided that $\mu > 1$. For $\mu < 1$ it is also necessary to replace $\hat{X}$ by $-\hat{X}$ and then the transition is in the reverse sense, with a combination of x and y-rolls in the region $X > X_0$ and only x-rolls in the region $X < X_0$. This situation is relevant in the structure pertaining to the case $\mu < 1$ described in section 2.8.

It should also be noted that the expansions for A in the outer regions will actually contain effects arising from higher order corrections to the amplitude equations derived in section 2.2, which so far have been neglected. It is expected that these higher order effects in the amplitude equations would generate terms of order $\epsilon^{1/2}$ in the solutions for A in the outer regions, which will therefore be larger than the terms of order $\epsilon^{3/5}$ identified in section 3.5. These terms will be considered in detail in chapter 6 but it is envisaged that they will have no significant effect on the form of the transition zone solution discussed here.

$a(-\breve{X}_{-\infty})^{-3/8}$	$b(-\breve{X}_{-\infty})^{-3/8}$	f	g
0.185059	-0.039785	-0.340894	-0.956241
0.154484	-0.014954	-0.169823	-0.241108
0.130188	-0.023116	-0.020274	-0.020975
0.127428	-0.024760	-0.000406	-0.000569
0.127358	-0.024788	-0.000005	-0.000009
0.127357	-0.024788	-2.536137E-09	-3.789601E-07
0.127357	-0.024788	-2.536137E-09	4.572302E-08

Table 3.1 : Convergence properties of the solution

$\breve{X}_{\pm\infty}$	y_1	y_2	y_3	y_4
1.0	1.018495	0.458799	-0.488236	-1.722706
2.0	0.247718	0.179372	0.042980	-0.054583
3.0	0.214778	0.161838	0.046218	-0.040316
4.0	0.212238	0.159253	0.044635	-0.040467
5.0	0.212253	0.159174	0.044581	-0.040530
6.0	0.212186	0.159142	0.044601	-0.040511
7.0	0.212176	0.159138	0.044599	-0.040512
8.0	0.212173	0.159137	0.044599	-0.040512
8.3	0.212172	0.159137	0.044599	-0.040511

Table 3.2 : Values of y_1, y_2, y_3, y_4 at $X=0$

h	$a(\check{X}_{-\infty})^{-3/8}$	$b(\check{X}_{-\infty})^{-3/8}$	f	g
0.025	0.127357	-0.024788	1.0E-08	1.0E-08
0.05	0.127356	-0.024788	1.0E-07	1.0E-07
0.1	0.127355	-0.024789	1.0E-07	1.0E-08

Table 3.3 : Effect of step size h

h	$I_0 + I_1$	I_0	I_1
0.025	-0.000351	0.023683	-0.024034
0.05	-0.000113	0.023687	-0.023800
0.1	-0.003982	0.019724	-0.023707

Table 3.4 : Integrals I_0, I_1
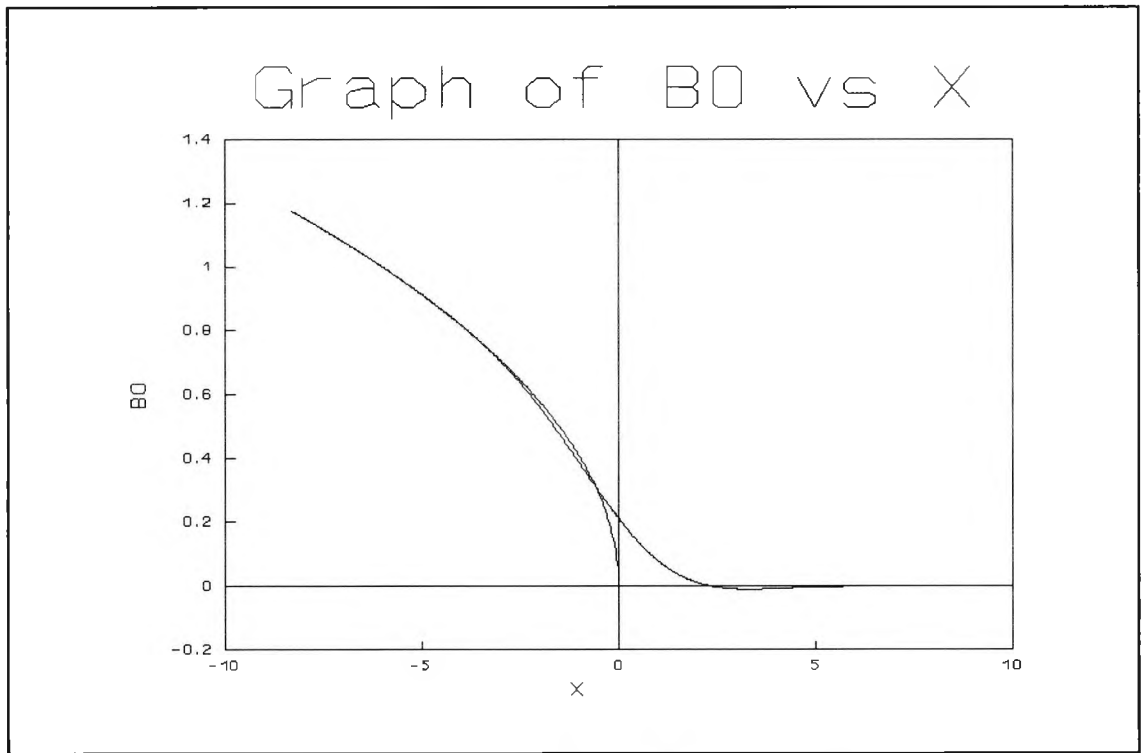
Fig. 3.1 : Graphs of $\hat{B}$ and $(-\hat{X}/6)^{1/2}$ versus $\hat{X}$
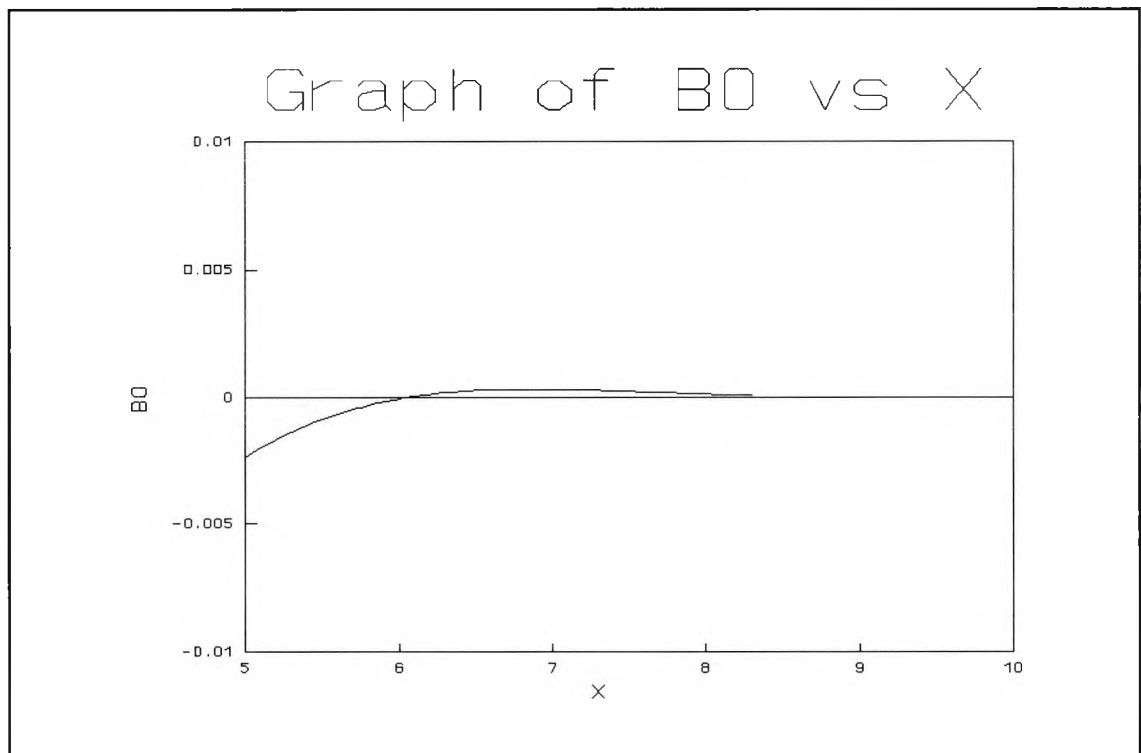
Fig. 3.2 : Detailed graph of $\hat{B}$ vs $\hat{X}$

98

Chapter 4

Variation in the wavelength of the x-roll pattern with lateral forcing

4.1 Introduction

In chapter 2 the amplitudes of the rolls were taken to be real only; here the work will be extended to incorporate complex values of A and B in order to investigate variations in the wavelength of the x-roll pattern. Cross, Daniels, Hohenberg and Siggia (1983) considered the question of allowed wavenumbers of stationary solutions for the two-dimensional Rayleigh-Bénard problem where $B=0$, focusing on the case of stress-free horizontal boundaries. In section 4.2 the case $B=0$ is examined for the model equation where $\mu=2$ and the results are then extended to the case where $B \neq 0$. The presence of the lateral boundary is found to restrict severely the range of allowed wavenumbers and bounds are obtained on the correction q to the critical wavenumber in the x-direction as a function of the parameter λ. Here, as in chapter 2, λ is a parameter equivalent to some kind of imperfection which could describe a finite porosity or thermal conductivity of the lateral boundary.

In section 4.3 the entire steady-state solution structure for the semi-infinite system with B non-zero and one lateral boundary is determined for small values of λ using the method of matched asymptotic expansions. In section 4.4 an explicit finite difference scheme is used to solve the relevant time-dependent amplitude equations for a finite range of values of λ and q and in section 4.5 these numerical results are discussed and compared with the predictions of section 4.2. In section 4.6 the results for small λ are extended to incorporate the presence of a second lateral boundary, leading to the determination of a discrete spectrum of steady-state solutions in which B is non-zero near the two boundaries.

4.2 Bounds on phase-winding in the semi-infinite system

The semi-infinite problem outlined in (2.2.23), (2.2.24), (2.2.29), (2.2.31) and (2.2.32) is now considered with the amplitude functions considered to be complex but still independent of y. The main outer problem is formulated by setting $\tilde{A}=\epsilon^{1/2}A(X,\tau)$, $\tilde{B}=\epsilon^{1/2}B(X,\tau)$, $x=\epsilon^{-1/2}X$, $t=\epsilon^{-1}\tau$ and taking the formal limit as $\epsilon\to0$. Here solutions are considered such that A approaches a form proportional to e^{iqX} as $X\to\infty$. Thus q is effectively equivalent to a correction to the critical wavenumber of the x-roll pattern at large distances from the wall. The full system of equations and boundary conditions is

$$\frac{\partial A}{\partial \tau} = 4\frac{\partial^2 A}{\partial X^2}+A-3A|A|^2-6A|B|^2 \quad, \tag{4.2.1}$$

$$\frac{\partial B}{\partial \tau} = B-3B|B|^2-6B|A|^2 \quad, \tag{4.2.2}$$

$$A = \lambda \quad \text{at} \quad X = 0 \quad, \tag{4.2.3}$$

$$A \to \frac{1}{\sqrt{3}}(1-4q^2)^{1/2}e^{i(qX+C)} \quad, \quad B \to 0 \quad \text{as} \quad X \to \infty \quad, \tag{4.2.4}$$

where C is a constant. In discussing the time evolution of the system in section 4.4 below, initial conditions will be taken of the form

$$A = A_0(X) \quad, \quad B = B_0(X) \quad \text{at} \quad \tau = 0 \quad. \tag{4.2.5}$$

Note that the form of A at $X=\infty$ is equivalent to the steady-state solutions that would exist in an infinite layer, with q restricted to the range

$$|q| < \frac{1}{2} \quad. \tag{4.2.6}$$

Here the intention is to determine how the wall condition (4.2.3) further restricts the allowed values of q. It is convenient to recast the steady-state version of the system (4.2.1)-(4.2.4) in

100

polar form by setting

$$A(X) = r(X)e^{i\theta(X)} \tag{4.2.7}$$

and

$$B(X) = s(X)e^{i\phi(X)} \ , \tag{4.2.8}$$

giving

$$r - 3r^3 - 4r\left(\frac{d\theta}{dX}\right)^2 + 4\frac{d^2r}{dX^2} - 6rs^2 = 0 \ , \tag{4.2.9}$$

$$\frac{d}{dX}\left[r^2\frac{d\theta}{dX}\right] = 0 \ , \tag{4.2.10}$$

$$s(1 - 3s^2 - 6r^2) = 0 \ , \tag{4.2.11}$$

$$r = \lambda \ , \quad \theta = 0 \quad \text{at} \quad X = 0 \ , \tag{4.2.12}$$

$$r \to \frac{1}{\sqrt{3}}(1 - 4q^2)^{1/2} \ , \quad \theta \sim qX + C \ , \quad s \to 0 \quad \text{as} \quad X \to \infty \ . \tag{4.2.13}$$

Bounds on the possible values of q are now determined. It is clear from (4.2.11) that steady-state solutions may exist with $s = 0$ or $s^2 = (1 - 6r^2)/3$. First the case where only x-rolls are present is considered ($s = 0$), equivalent to the earlier analysis by Cross et al (1983).

With $s = 0$, equation (4.2.9) simplifies to

$$r - 3r^3 - 4r\left(\frac{d\theta}{dX}\right)^2 + 4\frac{d^2r}{dX^2} = 0 \tag{4.2.14}$$

and this, together with equation (4.2.10), may be integrated once to give

$$\frac{1}{2}\left(\frac{dr}{dX}\right)^2 - \frac{3r^4}{16} + \frac{r^2}{8} + \frac{Q^2}{2r^2} = E \ , \tag{4.2.15}$$

101

$$r^2 \frac{d\theta}{dX} = Q \quad , \tag{4.2.16}$$

where Q and E are constants of integration. These constants may be written in terms of q using the outer conditions (4.2.13), which imply that

$$Q = \frac{1}{3}(1 - 4q^2)q \tag{4.2.17}$$

and

$$E = \frac{(1 - 4q^2)(1 + 12q^2)}{48} \quad . \tag{4.2.18}$$

General bounds may be determined on the phase-winding in the region away from the wall ($X \to \infty$) by noting that from (4.2.12) and (4.2.15)

$$2E \geq \frac{Q^2}{\lambda^2} + \frac{\lambda^2}{4} - \frac{3\lambda^4}{8} \quad . \tag{4.2.19}$$

Substituting for E and Q from (4.2.17) and (4.2.18), it follows that

$$(8q^2 - 3\lambda^2)(3\lambda^2 - 1 + 4q^2)^2 \leq 0 \quad . \tag{4.2.20}$$

If $3\lambda^2 - 1 + 4q^2 = 0$, the solution is equivalent to an ellipse in the λ, q plane. For a given value of λ this special solution, which corresponds to $r = \lambda$ for all $X \geq 0$, therefore exists for just one value of q^2. More generally, $3\lambda^2 - 1 + 4q^2 > 0$ and (4.2.20) then implies $q^2 \leq 3\lambda^2/8$ which means that only within the wedge $|q| \leq \sqrt{3}\lambda/2\sqrt{2}$ is there a possibility of obtaining a steady-state solution for general λ and q. Thus the amount of phase-winding as $X \to \infty$ is limited by the value of r at the lateral boundary, imposing a severe restriction on the range of wavelengths that can occur away from the lateral boundary when λ is small.

The case where both x and y-rolls are present is now considered. A two-region steady-state structure is envisaged of the kind found for real A and B in chapter 2. Thus it is expected that

there is a region near the wall $(X < X_0$, region I) where s is non-zero and is related to r by $s^2 = (1 - 6r^2)/3$, and a region $X > X_0$ (region II) where $s = 0$. Here, with $\mu = 2$, X_0 is defined as the point at which $r = 1/\sqrt{6}$. At $X = X_0$, it is assumed that r, dr/dX, θ and $d\theta/dX$ are continuous. The equation for r valid in region I, where $s \neq 0$, is

$$4\frac{d^2r}{dX^2} - 4r\left(\frac{d\theta}{dX}\right)^2 - r + 9r^3 = 0 \qquad (4.2.21)$$

and this can be integrated once to give

$$\frac{1}{2}\left(\frac{dr}{dX}\right)^2 + \frac{Q_1^2}{2r^2} - \frac{r^2}{8} + \frac{9r^4}{16} = E_1 \quad , \qquad (4.2.22)$$

where E_1 is a constant of integration. Also, from (4.2.10)

$$r^2\frac{d\theta}{dX} = Q_1 \quad , \qquad (4.2.23)$$

where Q_1 is a constant of integration. Similarly, for region II where $s = 0$, it is found that

$$\frac{1}{2}\left(\frac{dr}{dX}\right)^2 - \frac{3r^4}{16} + \frac{r^2}{8} + \frac{Q_2^2}{2r^2} = E_2 \quad , \qquad (4.2.24)$$

$$r^2\frac{d\theta}{dX} = Q_2 \quad , \qquad (4.2.25)$$

where Q_2 and E_2 are constants of integration. Continuity of r and $d\theta/dX$ at $X = X_0$ requires that

$$Q_1 = Q_2 = Q \quad , \qquad (4.2.26)$$

say, while continuity of dr/dX and r $(= 1/\sqrt{6})$ at X_0 implies from (4.2.22) and (4.2.24) that

$$E_1 - E_2 = -\frac{1}{48} \quad . \qquad (4.2.27)$$

Also, it follows from (4.2.4), (4.2.24) and (4.2.25) that Q and E_2 can be written in terms of q as

$$Q = \frac{1}{3}(1-4q^2)q \quad , \tag{4.2.28}$$

$$E_2 = \frac{(1-4q^2)(12q^2+1)}{48} \quad . \tag{4.2.29}$$

Thus, also

$$E_1 = \frac{q^2(1-6q^2)}{6} \quad . \tag{4.2.30}$$

Bounds on the possible values of q can now be obtained by noting from (4.2.22) and (4.2.3) that

$$2E_1 \geq \frac{Q^2}{\lambda^2} - \frac{\lambda^2}{4} + \frac{9\lambda^4}{8} \tag{4.2.31}$$

and substituting for E_1 and Q from (4.2.30) and (4.2.28) gives

$$C(q^2,\lambda^2) \geq 0 \quad , \tag{4.2.32}$$

where

$$C(q^2,\lambda^2) = \frac{8q^2}{3}(8q^2-1-16q^4) + \lambda^2(8q^2-48q^4) + 6\lambda^4 - 27\lambda^6 \quad . \tag{4.2.33}$$

The roots of the equation

$$C(q^2,\lambda^2) = 0 \tag{4.2.34}$$

can be found using the standard solution for a cubic equation to show that when $\lambda > 0$ there is generally one real root for q^2 and one pair of complex conjugate roots for q^2. When $\lambda = 0$ there are three real roots. For general λ, Figure 4.1 shows the real root which forms the boundary of the region $C(q^2,\lambda^2) \geq 0$ in the q, λ plane. Possible values of q correspond to points below this curve, which touches the straight line $q = \sqrt{3}\lambda/2\sqrt{2}$, corresponding to the pure x-roll solution boundary, at $\lambda = 1/\sqrt{6}$. The combined x and y-roll solution is only relevant for

$\lambda < 1/\sqrt{6}$ and is seen to exist for a more restricted range of values of q than the corresponding pure x-roll solution. Figure 4.2 shows the complex conjugate roots of (4.2.34). Solutions of equation (4.2.34) were also found using Newton's method starting from the point $\lambda = 0$ at which the roots are $q^2 = 0$, 1/4, 1/4 and gradually incrementing the value of λ. Note that for small values of λ, (4.2.32) gives

$$q \leq \frac{3\lambda^2}{2} \qquad\qquad (4.2.35)$$

to a first approximation, which is a much more severe restriction than the linear form in λ associated with the pure x-roll solution.

To summarise the results so far, for the infinite system with $B = 0$ everywhere it is required that $|q| < 1/2$; for the semi-infinite system with the boundary condition (4.2.3) at the wall and $B = 0$ everywhere it is required that $|q| \leq \sqrt{3}\lambda/2\sqrt{2}$ (apart from one exceptional case); and for the semi-infinite system with the boundary condition (4.2.3) at the wall and $B \neq 0$ it is required that $|q|$ must be less than the real root of the cubic equation (4.2.34). The results for the semi-infinite system are summarised in Figure 4.1 where the existence and stability of the solution depends on the values of q and λ. Above the line $q = \sqrt{3}\lambda/2\sqrt{2}$ no steady-state solution is found unless $3\lambda^2 + 4q^2 = 1$. Below the same line, steady-state solutions exist with $B = 0$. The growth rate of a y-roll perturbation $e^{\sigma \tau} B_0(X)$ is given by $\sigma = 1 - 6r^2$ from (4.2.2) and so it is expected that when $\lambda < 1/\sqrt{6}$, y-rolls will grow with time so that the x-roll solution is unstable, whereas if $\lambda > 1/\sqrt{6}$, y-rolls will decay with time so that the x-roll solution is stable. Below the lower curve in Figure 4.1, steady-state solutions exist with A and B both non-zero provided $\lambda < 1/\sqrt{6}$ and these are expected to be the stable finite amplitude states of the system for this range of λ.

4.3 Solution structure for small λ

In this section an explicit steady-state solution of the semi-infinite system with one lateral boundary consisting of both x and y-rolls is found for the case where λ is small, incorporating the range of values of $q \leq 3\lambda^2/2$ identified in the previous section. The boundary condition (4.2.3) with $\lambda \ll 1$ ensures that the amplitude r is small at the lateral boundary. Explicit analytical solutions of the amplitude equations can be found in the limit as $\lambda \rightarrow 0$ using the method of matched asymptotic expansions. It follows from (4.2.28) that $|Q| = O(\lambda^2)$ for small λ and the solution for r can be calculated using

$$Q = \lambda^2 Q_0 + \dots \tag{4.3.1}$$

as a small parameter. The phase variation θ is then given in terms of Q by (4.2.23) or (4.2.25), given that $Q_1 = Q_2 = Q$.

Following the structure of the solution identified in chapter 2 for small values of λ and real A and B, it is expected that the domain can be divided into a wall region where r is small and of order λ, a region distant from the wall (region I) where $s^2 = (1-6r^2)/3$ and $r \leq 1/\sqrt{6}$, and another region beyond this (region II) where $s = 0$ and $r \geq 1/\sqrt{6}$ (see Figure 4.3). The point at which $r = 1/\sqrt{6}$ is defined as $X = X_0$ and from the results of chapter 2, it is expected that $X_0 \sim -2\ln\lambda$ as $\lambda \rightarrow 0$. Since λ is small, r can be found analytically in all three regions and the constants of integration determined by the boundary conditions and by matching between the regions. With $q = O(\lambda^2)$, it follows from (4.2.29) and (4.2.30) that

$$E_1 = E_{10} + \lambda^2 E_{11} + \dots , \tag{4.3.2}$$

$$E_2 = E_{20} + \lambda^2 E_{21} + \dots , \tag{4.3.3}$$

where

$$E_{10} = 0 \quad , \quad E_{20} = \frac{1}{48} \tag{4.3.4}$$

106

and

$$E_{11} = E_{21} = 0 \quad .$$ (4.3.5)

The appropriate orders of magnitude of the variables in each region are now determined consistent with (4.2.22)-(4.2.25). Regions I and II are considered first, and here r is of order one and from (4.2.23) the variation in θ is of order λ^2; thus in region I,

$$r = \dot{r}_0(\tilde{X}) + \lambda^2 \dot{r}_1(\tilde{X}) + \dots \quad ,$$ (4.3.6)

$$\theta = \dot{C}_0 + \lambda^2 \dot{\theta}_1(\tilde{X}) + \dots$$ (4.3.7)

and in region II,

$$r = \ddot{r}_0(\tilde{X}) + \lambda^2 \ddot{r}_1(\tilde{X}) + \dots \quad ,$$ (4.3.8)

$$\theta = \ddot{C}_0 + \lambda^2 \ddot{\theta}_1(\tilde{X}) + \dots \quad ,$$ (4.3.9)

where it is convenient to set $\tilde{X} = X - X_0$.

In order to find r and θ in each region, it is necessary to substitute the expansions for r, θ, E_1, E_2 and Q into (4.2.22)-(4.2.25). In region II, the term $Q^2/2r^2$ in (4.2.24) is small and may be neglected so that at leading order

$$\left(\frac{d\ddot{r}_0}{d\tilde{X}}\right)^2 = \frac{1}{24} + \frac{3\ddot{r}_0^4}{8} - \frac{\ddot{r}_0^2}{4} \quad ,$$ (4.3.10)

with solution

$$\ddot{r}_0 = \frac{1}{\sqrt{3}} \tanh\left[\frac{\sqrt{2}\ddot{C} + \tilde{X}}{2\sqrt{2}}\right] \quad .$$ (4.3.11)

The requirement that $\ddot{r}_0 = 1/\sqrt{6}$ at $\tilde{X} = 0$ gives $\ddot{C} = 2\tanh^{-1}(1/\sqrt{2})$. Similarly, in region I at leading

107

order

$$\left(\frac{d\dot{r}_0}{d\tilde{X}}\right)^2 = \frac{\dot{r}_0^2}{4} - \frac{9\dot{r}_0^4}{8} \quad , \tag{4.3.12}$$

with solution

$$\dot{r}_0 = \frac{2\sqrt{2}\dot{C}e^{\tilde{X}/2}}{3\left(\dot{C}^2 e^{\tilde{X}} + 1\right)} \quad . \tag{4.3.13}$$

The requirement that $\dot{r}_0 = 1/\sqrt{6}$ at $\tilde{X}=0$, together with continuity of $d\dot{r}_0/d\tilde{X}$, gives $\dot{C}=1/\sqrt{3}$.

In order to determine θ in region II, the expansions for r, θ and Q are substituted into (4.2.25), giving

$$\dot{r}_0^2 \frac{d\ddot{\theta}_1}{d\tilde{X}} = Q_0 \quad , \tag{4.3.14}$$

which has a solution

$$\ddot{\theta}_1 = 6\sqrt{2}Q_0 \left\{ \frac{\sqrt{2}\ddot{C} + \tilde{X}}{2\sqrt{2}} - \coth\left[\frac{\sqrt{2}\ddot{C} + \tilde{X}}{2\sqrt{2}}\right] \right\} + \ddot{C}_1 \quad . \tag{4.3.15}$$

Similarly, for region I,

$$\dot{r}_0^2 \frac{d\dot{\theta}_1}{d\tilde{X}} = Q_0 \quad , \tag{4.3.16}$$

$$\dot{\theta}_1 = \frac{27Q_0}{8}\left[\frac{1}{9}e^{\tilde{X}} - e^{-\tilde{X}} + \frac{2\tilde{X}}{3}\right] + \dot{C}_1 \quad . \tag{4.3.17}$$

Continuity of θ at $\tilde{X}=0$ requires that

108

$$\dot{C}_0 = \ddot{C}_0 \qquad (4.3.18)$$

and

$$\dot{C}_1 - 3Q_0 = 6\sqrt{2}Q_0\left[\tanh^{-1}\left(\frac{1}{\sqrt{2}}\right) - \sqrt{2}\right] + \ddot{C}_1 \quad . \qquad (4.3.19)$$

The correction terms of order λ^2 in r in each region can also be determined as follows. In region II, $\ddot{r}_1$ is found to satisfy

$$\frac{d\ddot{r}_0}{d\tilde{X}}\frac{d\ddot{r}_1}{d\tilde{X}} = -\frac{\ddot{r}_0\ddot{r}_1}{4} + \frac{3\ddot{r}_0^3\ddot{r}_1}{4} \quad , \qquad (4.3.20)$$

with solution

$$\ddot{r}_1 = \frac{\ddot{K}}{2\sqrt{6}}\operatorname{sech}^2\left[\frac{\sqrt{2}\ddot{C} + \tilde{X}}{2\sqrt{2}}\right] \quad , \qquad (4.3.21)$$

while in region I, $\dot{r}_1$ is found to satisfy

$$2\frac{d\dot{r}_0}{d\tilde{X}}\frac{d\dot{r}_1}{d\tilde{X}} = \frac{\dot{r}_0\dot{r}_1}{2} - \frac{9\dot{r}_0^3\dot{r}_1}{2} \quad , \qquad (4.3.22)$$

with solution

$$\dot{r}_1 = \frac{\sqrt{2}\dot{K}\left(e^{\tilde{X}/2} - \frac{1}{3}e^{3\tilde{X}/2}\right)}{3\sqrt{3}\left(\frac{1}{3}e^{\tilde{X}} + 1\right)^2} \quad . \qquad (4.3.23)$$

However, the requirement that $r = 1/\sqrt{6}$ at $\tilde{X} = 0$ implies that $\dot{K} = \ddot{K} = 0$, so that in fact

$$\dot{r}_1 = \ddot{r}_1 = 0 \qquad (4.3.24)$$

and there is no order λ^2 correction to r in regions I and II.

109

To summarise, in region I,

$$r = \frac{2\sqrt{2}e^{\bar{X}/2}}{\sqrt{3}\left(e^{\bar{X}}+3\right)} + o(\lambda^2)$$

(4.3.25)

and in region II,

$$r = \frac{1}{\sqrt{3}}\tanh\left[\tanh^{-1}\left(\frac{1}{\sqrt{2}}\right) + \frac{\bar{X}}{2\sqrt{2}}\right] + o(\lambda^2) \ .$$

(4.3.26)

The relevant scaling of the solution in the wall region is investigated by studying the form of the solution in region I as $\bar{X}\to-\infty$. As $\bar{X}\to-\infty$, (4.3.25) becomes

$$r = \frac{2\sqrt{2}}{3\sqrt{3}}e^{\bar{X}/2}\left[1-\frac{e^{\bar{X}}}{3}+\frac{e^{2\bar{X}}}{9}+...\right] \ .$$

(4.3.27)

Rewriting the above expression in terms of X gives

$$r = \frac{2\sqrt{2}}{3\sqrt{3}}e^{(X-X_0)/2}\left[1-\frac{e^{(X-X_0)}}{3}+\frac{e^{2(X-X_0)}}{9}-...\right] \ .$$

(4.3.28)

It is known that in the wall region r must be of order λ which requires that $X_0 \sim -2\ln\lambda$ and by studying (4.2.22) it is clear that within the wall region X is of order one. Also, equation (4.2.23) implies that θ is of order one. Therefore, expansions for r and θ in the wall region are

$$r = \lambda\bar{r}(X) + ... \ ,$$

(4.3.29)

$$\theta = \bar{\theta}_0(X) + \lambda^2\bar{\theta}_1(X) + ...$$

(4.3.30)

and it is assumed that X_0 can be written as

$$X_0 = -2\ln\lambda + a + ... \ ,$$

(4.3.31)

where a is to be determined. The expansions for r and Q are substituted into (4.2.22), giving

110

$$\left(\frac{d\bar{r}}{dX}\right)^2 = \frac{\bar{r}^2}{4} - \frac{Q_0^2}{\bar{r}^2} \quad , \tag{4.3.32}$$

which has solution

$$\bar{r}^2 = Q_0 \left[\frac{1 + \bar{C}^2 e^{2X}}{\bar{C} e^X}\right] \tag{4.3.33}$$

where $\bar{C}$ is a constant. Since $\bar{r} = 1$ at $X = 0$, it follows from (4.3.32) that $|Q_0| \leq 1/2$ and it is convenient to define a new parameter γ by the relation

$$Q_0 = \frac{1}{2} \sin\gamma \quad . \tag{4.3.34}$$

The boundary condition at the wall then implies that

$$\bar{C} = \frac{1 \pm \cos\gamma}{2Q_0} \tag{4.3.35}$$

and it follows that in the wall region

$$r = \lambda \left\{\frac{\sin^2\gamma + e^{2X}(1 + \cos\gamma)^2}{2e^X(1 + \cos\gamma)}\right\}^{1/2} + \ldots \quad , \quad \lambda \rightarrow 0 \quad . \tag{4.3.36}$$

Matching between the wall region and region I allows a to be found in (4.3.31). From (4.3.36),

$$r^2 \sim \frac{\lambda^2(1 + \cos\gamma)e^X}{2} \quad , \quad X \rightarrow \infty \tag{4.3.37}$$

and (4.3.28) is written in terms of a using (4.3.31) and matched with (4.3.37) to obtain

$$a = \ln\left[\frac{16}{27(1 + \cos\gamma)}\right] \quad . \tag{4.3.38}$$

Hence

$$X_0 = -2\ln\lambda + \ln\left[\frac{16}{27(1+\cos\gamma)}\right] + \dots \quad , \quad \lambda \to 0 \quad . \tag{4.3.39}$$

Note that when the solution for A is real, γ is zero and then (4.3.39) reduces to

$$X_0 = -2\ln\lambda + \ln\left[\frac{8}{27}\right] + \dots \quad , \tag{4.3.40}$$

which agrees with the formula (2.6.8) for X_0 in the limit as $\lambda \to 0$ when $\mu = 2$.

In the wall region, θ is found by substituting the expansions for r, θ and Q into (4.2.23), leading to

$$\frac{d\bar{\theta}_0}{dX} = \frac{Q_0}{r^2} \quad , \tag{4.3.41}$$

which gives

$$\theta = \left\{ \tan^{-1}\left[\frac{(1+\cos\gamma)e^X}{\sin\gamma}\right] + C_W \right\} + O(\lambda^2) \quad . \tag{4.3.42}$$

and the condition on θ at the wall $(X=0)$ gives

$$C_W = -\frac{Q_0[\pi-\gamma]}{\sin\gamma} = \frac{\gamma-\pi}{2} \quad . \tag{4.3.43}$$

Matching between the wall region and region I now determines the constant $\dot{C}_0$. The form of the solution for θ in region I as $\tilde{X} \to -\infty$, rewritten in terms of X, is

$$\theta = \dot{C}_0 + \frac{27Q_0}{8}\left[-e^{(a-X)} + \frac{2\lambda^2(X+2\ln\lambda-a)}{3} + \frac{\lambda^4 e^{(X-a)}}{9}\right] + \lambda^2\dot{C}_1 + \dots \tag{4.3.44}$$

and as $X \to \infty$, (4.3.42) becomes

$$\theta = \left[\frac{\pi}{2} - \frac{\sin\gamma}{(1+\cos\gamma)e^X}\right] + C_W + \dots \quad . \tag{4.3.45}$$

112

Thus matching requires

$$\dot{C}_0 = \frac{\pi}{2} + C_W = \frac{\gamma}{2} \ .$$

(4.3.46)

The main features of the solution structure for small λ are now complete and can be summarised as follows. In region I:

$$r = \frac{2\sqrt{2}e^{\tilde{X}/2}}{\sqrt{3}\left(e^{\tilde{X}}+3\right)} + O(\lambda^2) \ ,$$

(4.3.47)

$$\theta = \frac{\gamma}{2} + \lambda^2 \left\{ \frac{27\sin\gamma}{16} \left[\frac{1}{9}e^{\tilde{X}} - e^{-\tilde{X}} + \frac{2\tilde{X}}{3} \right] + \dot{C}_1 \right\} + \ldots \ .$$

(4.3.48)

In region II:

$$r = \frac{1}{\sqrt{3}}\tanh\left[\tanh^{-1}\left(\frac{1}{\sqrt{2}}\right) + \frac{\tilde{X}}{2\sqrt{2}}\right] + O(\lambda^2) \ ,$$

(4.3.49)

$$\theta = \frac{\gamma}{2} + \lambda^2 \left\{ 3\sqrt{2}\sin\gamma\left(\tanh^{-1}\left(\frac{1}{\sqrt{2}}\right) + \frac{\tilde{X}}{2\sqrt{2}} - \coth\left[\tanh^{-1}\left(\frac{1}{\sqrt{2}}\right) + \frac{\tilde{X}}{2\sqrt{2}}\right]\right) + \ddot{C}_1 \right\} + \ldots \ .$$

(4.3.50)

In the wall region:

$$r = \lambda \left\{ \frac{\sin^2\gamma + e^{2X}(1+\cos\gamma)^2}{2e^{X}(1+\cos\gamma)} \right\}^{1/2} + \ldots \ ,$$

(4.3.51)

$$\theta = \left\{ \tan^{-1}\left[\frac{(1+\cos\gamma)e^{X}}{\sin\gamma} \right] + \frac{1}{2}(\gamma-\pi) \right\} + \ldots \ .$$

(4.3.52)

In region II, θ is represented by (4.3.50) and it follows that

$$\theta \sim \frac{\gamma}{2} + \left(\frac{3\lambda^2 \sin\gamma}{2}\right)\tilde{X} \quad , \quad \tilde{X} \to \infty \quad . \tag{4.3.53}$$

In order for θ to change by a finite amount, equivalent to a change in the number of x-rolls in the system, it is seen to be necessary for $\tilde{X}$ to increase to values of order λ^{-2}. In section 4.6 the above result is used to estimate how solutions for ψ corresponding to different numbers of x-rolls can occur in a finite container of large aspect ratio.

4.4 Numerical solution for finite λ

The predicted evolution of the system for $\lambda > 0$ and general values of q was tested by a numerical solution of the system based on an extension of the explicit finite difference scheme used for the case of real amplitude functions in chapter 2. Here the governing equations and boundary conditions are

$$\frac{\partial A}{\partial \tau} = 4\frac{\partial^2 A}{\partial X^2} + A - 3A(|A|^2 + 2|B|^2) \quad , \tag{4.4.1}$$

$$\frac{\partial B}{\partial \tau} = B - 3B(|B|^2 + 2|A|^2) \quad , \tag{4.4.2}$$

$$A = \lambda \quad \text{at} \quad X = 0 \quad , \tag{4.4.3}$$

$$A \to \frac{1}{\sqrt{3}}(1 - 4q^2)^{1/2}e^{i(qX+C)} \quad , \quad B \to 0 \quad \text{as} \quad X \to \infty \tag{4.4.4}$$

and initial profiles are taken of the form

$$A = A_0(X) = \left\{\frac{1}{\sqrt{3}}(1 - 4q^2)^{1/2}\tanh\left[\frac{X}{2\sqrt{2}}\right] + \lambda e^{-X}\right\}e^{iqX} \quad \text{at} \quad \tau = 0 \tag{4.4.5}$$

and

$$B = B_0(X) = \delta \operatorname{sech}\left[\frac{X}{2\sqrt{2}}\right] \quad \text{at} \quad \tau = 0 \quad . \tag{4.4.6}$$

114

It is assumed that $\lambda \geq 0$.

The amplitude functions are written in polar form as

$$A(X,\tau) = r(X,\tau)e^{i\theta(X,\tau)} \quad , \tag{4.4.7}$$

$$B(X,\tau) = s(X,\tau)e^{i\phi(X,\tau)} \quad , \tag{4.4.8}$$

and substitution of (4.4.7) and (4.4.8) into (4.4.1)-(4.4.6) and comparison of real and imaginary parts yields the equations

$$\frac{\partial r}{\partial \tau} = 4\frac{\partial^2 r}{\partial X^2} - 4r\left(\frac{\partial \theta}{\partial X}\right)^2 + r - 3r^3 - 6rs^2 \quad , \tag{4.4.9}$$

$$r\frac{\partial \theta}{\partial \tau} = 4r\frac{\partial^2 \theta}{\partial X^2} + 8\frac{\partial r}{\partial X}\frac{\partial \theta}{\partial X} \quad , \tag{4.4.10}$$

$$\frac{\partial s}{\partial \tau} = s - 3s^3 - 6r^2 s \quad , \tag{4.4.11}$$

$$s\frac{\partial \phi}{\partial \tau} = 0 \quad , \tag{4.4.12}$$

with boundary conditions

$$r = \lambda \quad \text{at} \quad X = 0 \quad , \tag{4.4.13}$$

$$\theta = 0 \quad \text{at} \quad X = 0 \quad , \tag{4.4.14}$$

$$r \rightarrow \frac{1}{\sqrt{3}}(1 - 4q^2)^{1/2} \quad \text{as} \quad X \rightarrow \infty \quad , \tag{4.4.15}$$

$$\frac{\partial \theta}{\partial X} \rightarrow q \quad \text{as} \quad X \rightarrow \infty \tag{4.4.16}$$

and initial conditions

115

$$r = \bar{r}_0(X) = \frac{1}{\sqrt{3}}(1-4q^2)^{1/2}\tanh\left(\frac{X}{2\sqrt{2}}\right) + \lambda e^{-X} \quad \text{at} \quad \tau = 0 \quad , \tag{4.4.17}$$

$$\theta = \bar{\theta}_0(X) = qX \quad \text{at} \quad \tau = 0 \quad , \tag{4.4.18}$$

$$s = \bar{s}_0(X) = \delta\,\text{sech}\left[\frac{X}{2\sqrt{2}}\right] \quad \text{at} \quad \tau = 0 \quad , \tag{4.4.19}$$

$$\phi = \bar{\phi}_0(X) = 0 \quad \text{at} \quad \tau = 0 \quad . \tag{4.4.20}$$

Approximate solutions to the differential equations are found in the finite difference scheme by denoting the values of $r(X,\tau)$, $s(X,\tau)$, $\theta(X,\tau)$ and $\phi(X,\tau)$ at $X=ih$, $\tau=jk$ by $r_{i,j}$, $s_{i,j}$, $\theta_{i,j}$ and $\phi_{i,j}$ respectively. The finite difference approximation to (4.4.9) is obtained by using a forward difference approximation for $\partial r/\partial\tau$ and a central difference approximation for $\partial^2 r/\partial X^2$ and $\partial\theta/\partial X$. The discretised system for the explicit scheme then has the form

$$r_{i,j+1} = \beta\left[4r_{i+1,j} + r_{i,j}\left(h^2 - 3h^2 r_{i,j}^2 - 6h^2 s_{i,j}^2 - 8 - (\theta_{i+1,j} - \theta_{i-1,j})^2 + \frac{1}{\beta}\right) + 4r_{i-1,j}\right]$$

$$(4.4.21)$$

for $i=1,2,\dots N\text{-}1$ and $j=0,1,2\dots$, where $\beta=k/h^2$ and $Nh=X_\infty$. Using a similar representation of equation (4.4.10), it is found that

$$\theta_{i,j+1} = \frac{\beta}{r_{i,j}}\left[\theta_{i+1,j}(4r_{i,j} + 2r_{i+1,j} - 2r_{i-1,j}) + r_{i,j}\theta_{i,j}\left(\frac{1}{\beta} - 8\right) + \theta_{i-1,j}(4r_{i,j} - 2r_{i+1,j} + 2r_{i-1,j})\right]$$

$$(4.4.22)$$

for $i=1,2,\dots N\text{-}1$ and $j=0,1,2\dots$. Similarly for (4.4.11), it is deduced that

$$s_{i,j+1} = ks_{i,j}\left[1 - 3s_{i,j}^2 - 6r_{i,j}^2 + \frac{1}{k}\right] \tag{4.4.23}$$

for $i=1,2,\dots N\text{-}1$ and $j=0,1,2\dots$. Equation (4.4.12), together with (4.4.20), implies that ϕ is

116

zero for all times and so there is no need to include this equation in the numerical scheme.

The end values of r and θ are determined directly from the boundary conditions:

$$r_{0,j+1} = \lambda \quad , \quad r_{N,j+1} = \frac{1}{\sqrt{3}}(1-4q^2)^{1/2} \quad \text{for} \quad j = 0,1,\ldots \quad , \qquad (4.4.24)$$

$$\theta_{0,j+1} = 0 \quad , \quad \theta_{N,j+1} = \theta_{N-1,j+1} + qh \quad \text{for} \quad j = 0,1\ldots \quad . \qquad (4.4.25)$$

The above formulae (4.4.21)-(4.4.25) allow the unknown amplitudes $r_{i,j+1}$, $s_{i,j+1}$ and phase $\theta_{i,j+1}$ at the $(j+1)$th time step to be determined in terms of the known amplitudes and phase at the jth time step. Thus a solution can be found by moving forward with time, starting from the initial profiles at $\tau=0$:

$$r_{i,0} = \overline{r}_0(ih) \quad , \quad \theta_{i,0} = \overline{\theta}_0(ih) \quad , \quad s_{i,0} = \overline{s}_0(ih) \quad , \quad i = 0,1,\ldots N \quad . \qquad (4.4.26)$$

It should be noted that $\lambda=0$ must be treated as a special case since the boundary condition at the wall becomes $r=0$ at $X=0$. The condition $\theta=0$ at $X=0$ is then not appropriate and singular behaviour there can be avoided by using the alternative condition

$$\frac{\partial \theta}{\partial X} = 0 \quad \text{at} \quad X = 0 \quad . \qquad (4.4.27)$$

In discretised form this is approximated by

$$\theta_{0,j+1} = \theta_{1,j+1} \quad . \qquad (4.4.28)$$

4.5 Numerical results

Using the numerical method described in the previous section, results were obtained for various values of q and λ. Values of the parameters were chosen to test the predictions of the

117

analysis described in sections 4.2 and 4.3 concerning the existence and stability of steady-state solutions. For each evolution from the given initial conditions (4.4.17)-(4.4.19), the location X_0 of the position at which $r = 1/\sqrt{6}$ was monitored as a function of time. Results were obtained for values of q in the range 0.005 to 0.25, in each case investigating the effect of different values of λ.

For $q = 0.05$, the cases $\lambda = 0$, 0.1, 0.1826, 0.3, 0.4 and 0.5 were considered. For $\lambda = 0$ (Figures 4.4-4.6) the y-rolls continue to travel outwards with increasing time and θ continues to increase. A steady-state solution for A and B is not obtained, as expected from Figure 4.1. It was found that $X_0 = 4.04$ for $\tau = 20$ and the value of X_0 continues to increase as τ increases. For $X < X_0$ the y-rolls are increasing in amplitude and affect the x-roll amplitude while for $X > X_0$ the y-rolls decay, as illustrated in Figure 4.6. For $\lambda = 0.1$ (Figures 4.7-4.9) the y-rolls again travel outwards with increasing time and θ also increases with time. Again a steady-state solution is not reached, consistent with the expectation from Figure 4.1. Here $X_0 = 3.16$ for $\tau = 20$ and the y-rolls are confined to a region slightly nearer the wall than in the case $\lambda = 0$. For $\lambda = 0.1826$, and large times (Figures 4.10-4.12) the solutions for r, s and θ appear to attain almost constant forms. From Figure 4.1 it can be seen that these values of λ and q lie on the boundary between an unstable x-roll solution and a stable x-roll/y-roll solution which is why an almost steady-state solution is reached. Here $X_0 = 2.20$ at $\tau = 20$ and the y-rolls are confined to a region much nearer the wall as $\tau \to \infty$ than in the previous two cases. For $\lambda = 0.3$ (Figures 4.13-4.18) r, θ and s attain constant forms for large times and a steady-state x-roll/y-roll solution is obtained consistent with the prediction of Figure 4.1. To verify the attainment of a steady-state, r, θ and s were found for very large times (up to $\tau = 200$) and were indeed found to be constant, with $X_0 = 1.00$ at $\tau = 200$. Thus the cross-rolls are confined to a region relatively close to the wall. For $\lambda = 0.4$ (Figures 4.19-4.21) r, θ and s are again constant for large times and a stable steady-state solution is obtained consisting of a combination of x-rolls and y-rolls.

118

At $\tau=20$, $X_0=0.08$ which means that the region where y-rolls occur is very small. This is expected because λ is close to $1/\sqrt{6}$. For $\lambda=0.5$ (Figures 4.22-4.24) r, θ and s are again constant for large times but here $\lambda>1/\sqrt{6}$ and so s decays to zero as $\tau\to\infty$ and no value of X_0 exists for large times. The final steady-state solution consists entirely of x-rolls, as expected from Figure 4.1.

For $q=0.2$, results were obtained for $\lambda=0$, 0.3, 0.3651, 0.4 and 0.5. For $\lambda=0$ (Figures 4.25-4.30) a steady-state solution is not reached, with $X_0=5.16$ at $\tau=200$ and still increasing. There is an ever-expanding region near the wall where y-rolls occur. For $\lambda=0.3$ (Figures 4.31-4.33) again a steady-state solution is not reached and $X_0=2.34$ at $\tau=20$. For $\lambda=0.3651$ (Figures 4.34-4.36) an almost steady-state solution is reached because these values of λ and q lie on the boundary between an unstable x-roll solution and a stable x-roll/y-roll solution (see Figure 4.1). In this case $X_0=0.82$ at $\tau=20$. For $\lambda=0.4$ (Figures 4.37-4.39) a stable steady-state solution is obtained with $X_0=0.16$ at $\tau=20$ so that the region where cross-rolls occur is very close to the wall, consistent with the proximity of λ to the value $1/\sqrt{6}$. For $\lambda=0.5$ (Figures 4.40-4.42) a stable steady-state solution is attained and $s\to0$ as $\tau\to\infty$ consistent with a solution in the region to the right of the vertical line in Figure 4.1.

For $q=0.25$, results were obtained for $\lambda=0$, 0.39, 0.4082 and 0.45. As expected, when $\lambda=0$ no steady-state solution is reached and $X_0=4.32$ at $\tau=20$ (Figures 4.43-4.45). When $\lambda=0.39$ and $\lambda=0.4082$ (Figures 4.46-4.51), the values of λ and q lie near the boundary between the unstable steady-state x-roll solution and the stable x-roll/y-roll solution and an almost steady-state solution is reached. When $\lambda=0.39$, $X_0=0.69$ at $\tau=20$ whereas when $\lambda=0.4082$, $X_0\approx0$ at $\tau=20$ which is expected because X_0 should be zero when $\lambda=1/\sqrt{6}=0.4082$. For $\lambda=0.45$ (Figures 4.52-4.54) a stable steady-state solution is attained as $\tau\to\infty$ and since $\lambda>1/\sqrt{6}$ this consists entirely of x-rolls.

119

Further results for $q=0.1$ and $\lambda=0.2$ (Figures 4.55-4.57) and $q=0.005$, $\lambda=0.02$ (Figures 4.58-4.60) indicate that no steady-state is achieved, consistent with the predictions of Figure 4.1.

The various solution regions found in Figure 4.1 were confirmed by the numerical solutions for different q and λ in all cases. Above the line $q=\sqrt{3}\lambda/2\sqrt{2}$ no steady-state solution was found to exist. Below the line and above the curve the y-rolls grow with time for $\lambda<1/\sqrt{6}$ so that although a steady-state x-roll solution exists it is unstable and again no steady-state is achieved. Below the curve where $\lambda<1/\sqrt{6}$ a stable steady-state x-roll/y-roll solution is attained whereas when $\lambda>1/\sqrt{6}$ a stable steady-state solution is attained consisting entirely of x-rolls.

The evolution of the roll pattern with time is represented graphically by contour plots of ψ for various values of q and λ in Figures 4.61-4.63 using Surfer Version 4 by Golden Software. Here ψ is obtained from the formula

$$\psi = 2\epsilon^{1/2}[r\cos(\theta+x) + s\cos y] \quad , \tag{4.5.1}$$

and the value of ϵ was taken to be 0.1.

Finally, the steady-state prediction (4.3.39) of X_0 for small λ was compared with the results of the numerical computations. This result suggests that as $\lambda\rightarrow0$,

$$X_0 \sim -2\ln\lambda + \ln\left[\frac{16}{27\left(1+\left[1-\frac{4q^2}{9\lambda^4}\right]^{1/2}\right)}\right] \quad , \tag{4.5.2}$$

provided $q\leq3\lambda^2/2$. To compare this with the value of X_0 determined in the numerical computation, X_0 was calculated for $q=0.0005$ and $\lambda=0.02$. The formula (4.5.2) gives $X_0=6.86$ whereas the numerical computation gave $X_0=4.72$ at $\tau=200$. The discrepancy may well be due

120

to the fact that a very small value of λ is needed in order for the asymptotic result (4.5.2) to be applicable - the logarithmic dependence on λ of the leading term suggests that this may be the case. A further cause of discrepancy is the proximity of the x-roll/y-roll solution boundary, which suggests that the solution must be computed to very large times in order to achieve the steady-state value of X_0 at these small values of λ and q.

4.6 Finite systems

The results of section 4.3 can be used to obtain phase-winding solutions in the finite region between two lateral boundaries, in a similar fashion to the analysis undertaken by Cross et al (1983) for the case where only x-rolls are present. In this way it is possible to obtain the whole spectrum of solutions for a finite container of large aspect ratio, provided the lateral forcing at the boundaries is small ($\lambda \ll 1$). This family of solutions represents roll patterns with different numbers of rolls in the container. The present analysis allows for the existence of y-rolls near the two lateral boundaries and is therefore an improvement on the analysis of Cross et al (1983) which took no account of the cross-roll instability. The finite region is taken to be defined by $-\delta \leq \hat{X} \leq \delta$ where $X = \hat{X} + \delta$.

The boundary condition at the left-hand wall $\hat{X} = -\delta$ is assumed to be

$$r = r_- = \lambda \quad , \quad \theta = \theta_- = 0 \qquad (4.6.1)$$

and at the right-hand wall $\hat{X} = \delta$ is assumed to be

$$r = r_+ = \lambda \quad , \quad \theta = \theta_+ = 0 \quad , \qquad (4.6.2)$$

where r and θ are interpreted as the magnitude and phase of the complex amplitude A of the x-roll pattern, as in the preceding sections of this chapter.

The solution near the left-hand wall consists of the structure identified in section 4.3 (Figure

4.3) with a wall region where r is small and of order λ, and regions I and II centred on the point $X=X_0 \sim -2\ln\lambda$ where r is of order one, the position X_0 marking the extent of the y-roll pattern from the wall. A similar structure exists near the right-hand wall and the intervening region, or core, extends for most of the length of the container and consists of x-rolls for which to a first approximation

$$A = re^{i\theta} \sim \frac{1}{\sqrt{3}} e^{i(qX + C)} \quad , \tag{4.6.3}$$

with $q \leq 3\lambda^2/2$. Since the value of q is small, of order λ^2, it is necessary for the length of the container $X=2\delta$ to be large, of order λ^{-2}, in order that phase-winding effects are significant. A change in θ of $m\pi$ across the container is equivalent to the addition or subtraction of m rolls from the number which would exist in the case when θ is constant across the container.

The change in θ across the container is estimated by considering the left and right-hand sides separately and then combining the results. The left-hand side has been studied in detail in section 4.3 and in this section the parameter γ is replaced by γ_-. Then the result (4.3.53) of section 4.3 shows that as X increases from 0 to δ across the left-hand side of the container the increase in θ is to a first approximation

$$\Delta\theta = q\delta + \frac{\gamma_-}{2} \quad , \tag{4.6.4}$$

where $q=3\lambda^2\sin\gamma_-/2$. For the right-hand side, a similar calculation shows that the increase in θ from the centre of the container to the right-hand wall is

$$\Delta\theta = q\delta + \frac{\gamma_+}{2} \quad , \tag{4.6.5}$$

where $q=3\lambda^2\sin\gamma_+/2$. Thus the total change in θ across the finite container is

$$\Delta\theta_{total} = \frac{\gamma_-}{2} + 2q\delta + \frac{\gamma_+}{2} \qquad (4.6.6)$$

and from (4.6.1) and (4.6.2) this must be equal to $\theta_+ - \theta_- + 2n\pi$ where n is any integer. Thus

$$\theta_+ - \theta_- + 2n\pi = \frac{\gamma_-}{2} + \frac{\gamma_+}{2} + 2q\delta \quad . \qquad (4.6.7)$$

In addition, the relations

$$q = \frac{3\lambda^2}{2}\sin\gamma_- = \frac{3\lambda^2}{2}\sin\gamma_+ \qquad (4.6.8)$$

imply that

$$\sin\gamma_+ = \sin\gamma_- \quad . \qquad (4.6.9)$$

The results (4.6.7) and (4.6.9) together with the assumption that $\theta_+ = -\theta_- = 0$ leads to two classes

of solutions. Firstly, if from (4.6.9), $\gamma_+ = \gamma_- = \gamma$, say, then (4.6.7) becomes

$$2n\pi = \gamma + 2q\delta \qquad (4.6.10)$$

and using (4.6.8) it follows that

$$\frac{q}{3} = \frac{\lambda^2}{2}\sin[2n\pi - 2q\delta] = -\frac{\lambda^2}{2}\sin[2q\delta] \quad . \qquad (4.6.11)$$

This represents an implicit equation for q, defining an infinite spectrum of solutions similar to

those discussed by Cross et al (1983).

Secondly, if from (4.6.9), $\gamma_+ + \gamma_- = \pm\pi$ then (4.6.7) becomes

$$2q_n\delta = 2n\pi \pm \frac{\pi}{2} \qquad (4.6.12)$$

and this defines a second infinite spectrum of solutions, each with a constant value of $q = q_n$

limited by $|q_n| \le 3\lambda^2/2$ for each value of λ. This is similar to the second class of solutions

discussed by Cross et al (1983).

123

The two results (4.6.11) and (4.6.12) represent the discrete spectrum of solutions for a finite container equivalent to the continuous spectrum $|q| \leq 3\lambda^2/2$ identified for the semi-infinite problem in section 4.2.

4.7 Discussion

In this chapter it has been shown that for both finite and semi-infinite systems, the presence of a lateral boundary parallel to the y direction restricts the band of wavelengths that can occur in the x-roll pattern at large distances from the boundary. For small imperfections measured by the parameter λ, the presence of cross-rolls near the boundary leads to a larger restriction than that previously determined for pure x-roll patterns. In particular, the available steady-state wavenumbers for the x-roll pattern around the critical wavenumber are reduced from a band of order $\epsilon^{1/2}\lambda$ to a band of order $\epsilon^{1/2}\lambda^2$ as $\lambda \rightarrow 0$. Both of these are small compared with the band of order $\epsilon^{1/2}$ available for an infinite layer, and the results obtained here suggest that for 'perfect' lateral boundaries a stable configuration with cross-rolls will have a main x-roll pattern with wavelength even closer to the critical value than was suggested by previous two-dimensional theories (Cross et al 1983). It is clear from the logarithmic structure identified in section 4.3 that the special case where $\lambda = 0$ will require separate consideration and this is not attempted here.
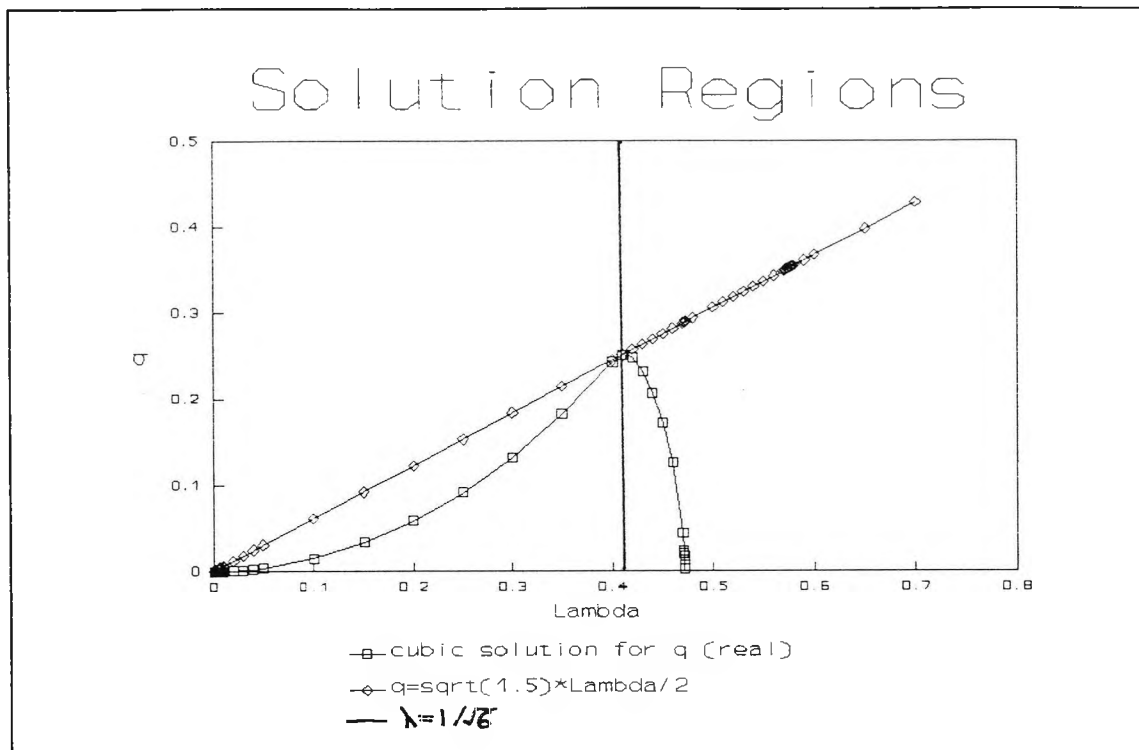
Fig. 4.1 : Real root of $C(q^2,\lambda^2)=0$ and the lines $q=\sqrt{3}\lambda/2\sqrt{2}$ and $\lambda=1/\sqrt{6}$, defining the existence and stability of steady-state solutions
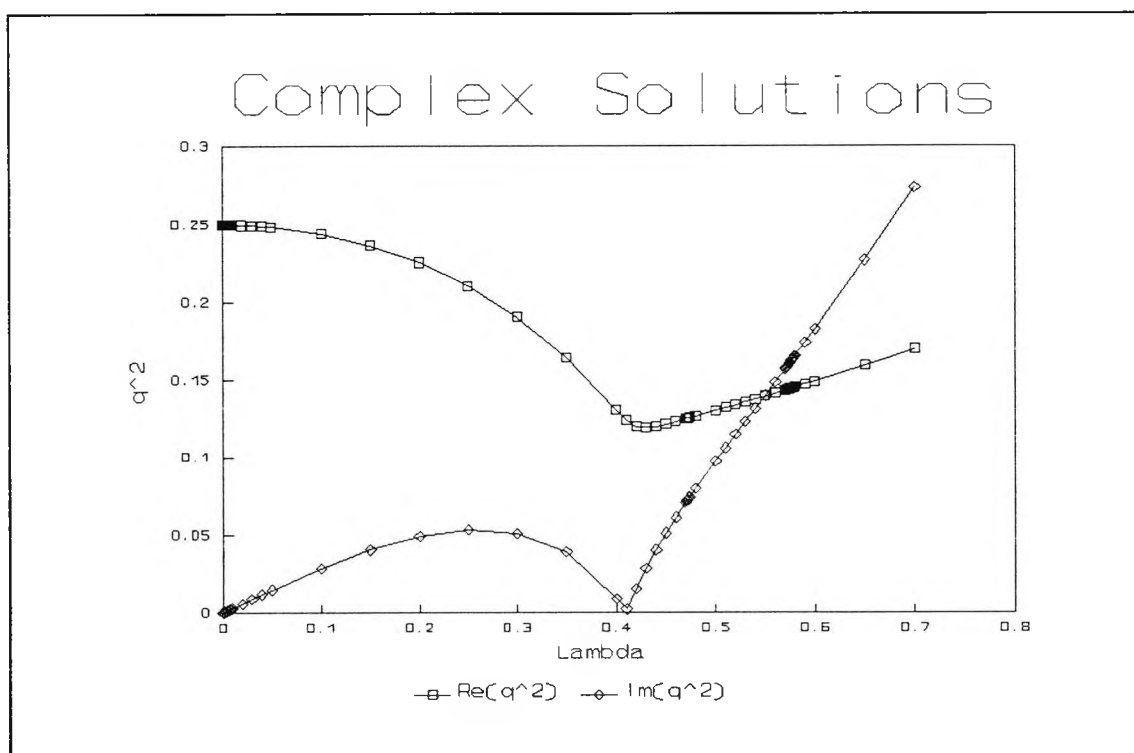
Fig. 4.2 : Complex conjugate roots of $C(q^2,\lambda^2)=0$
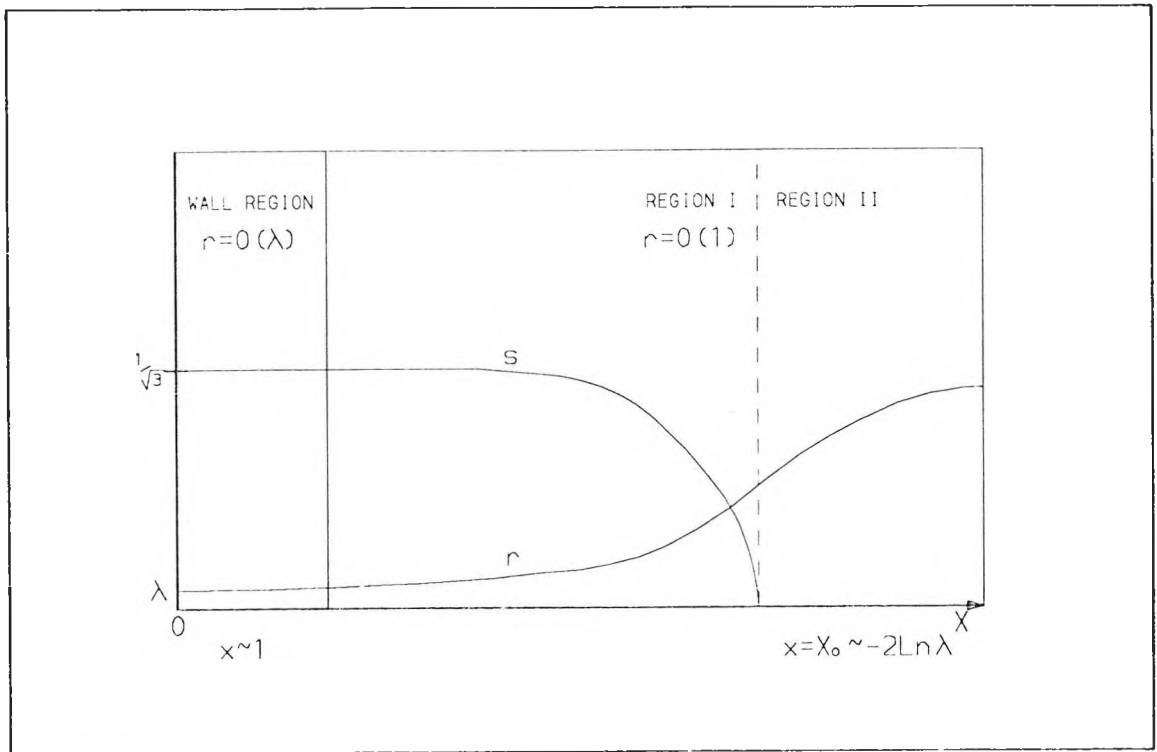
Fig. 4.3 : Schematic diagram showing the main flow regions for small λ
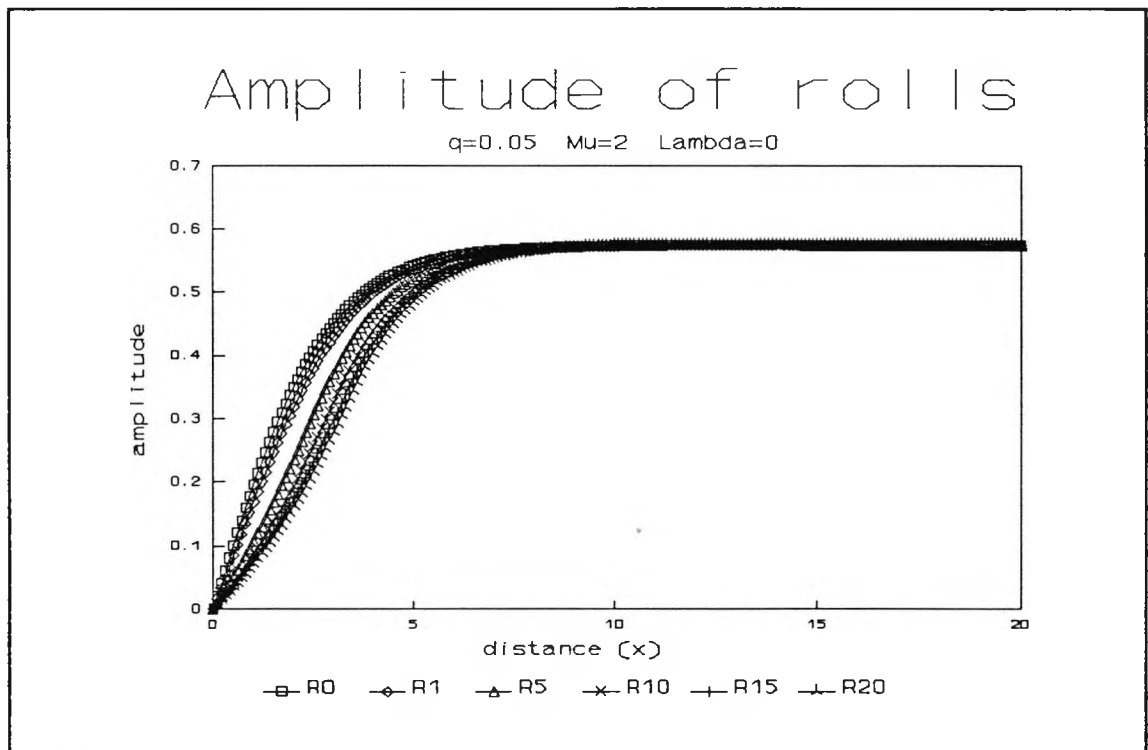
Fig. 4.4 : Numerical evolution for $q=0.05$, $\mu=2$ and $\lambda=0$ showing the amplitude of x-rolls at successive times τ
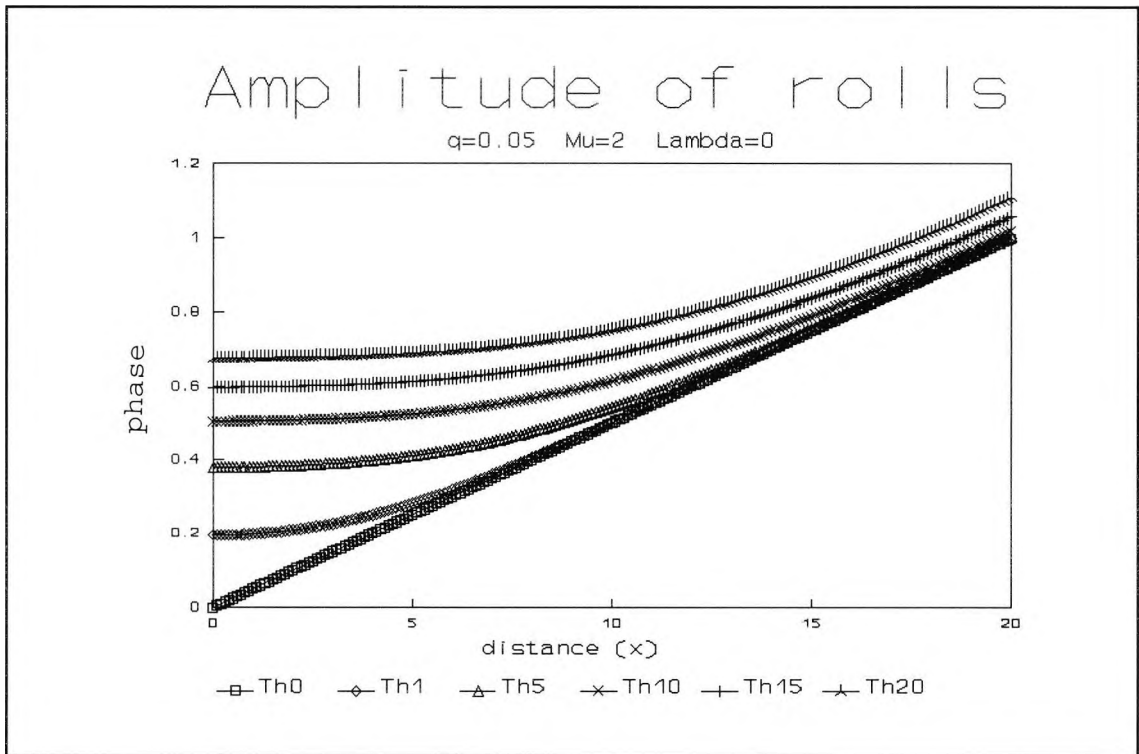
Fig. 4.5 : Numerical evolution for $q=0.05$, $\mu=2$ and $\lambda=0$ showing the phase of x-rolls at successive times τ
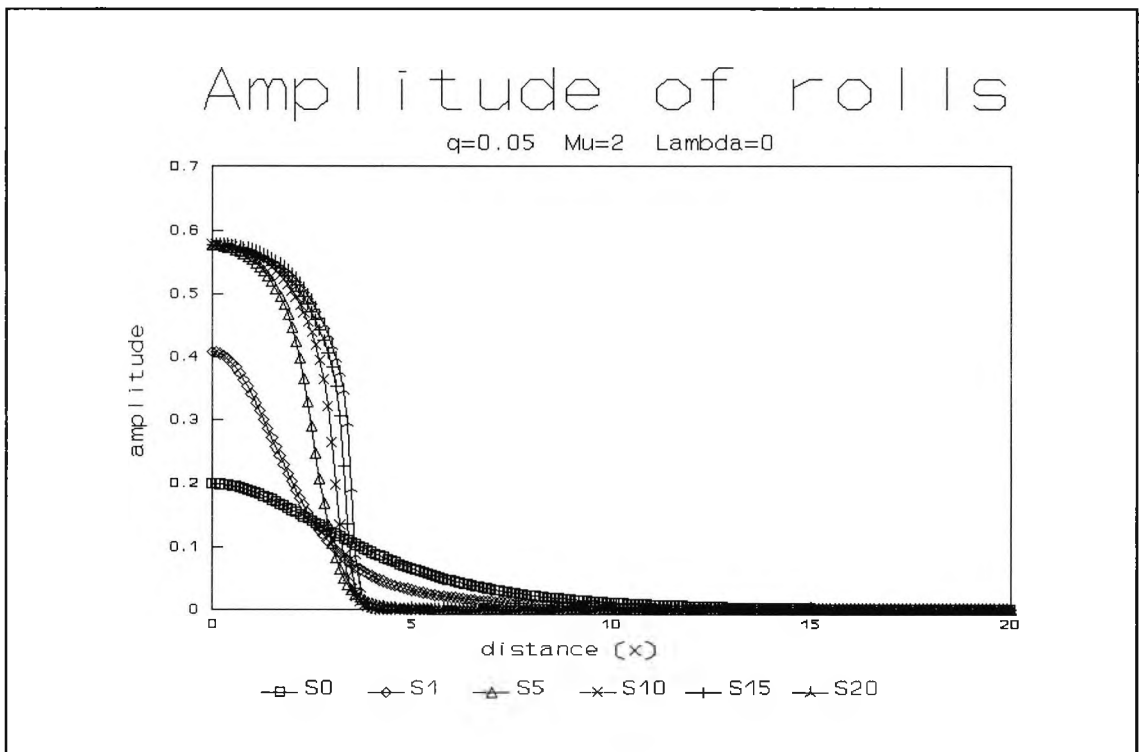
Fig. 4.6 : Numerical evolution for $q=0.05$, $\mu=2$ and $\lambda=0$ showing the amplitude of y-rolls at successive times τ

127
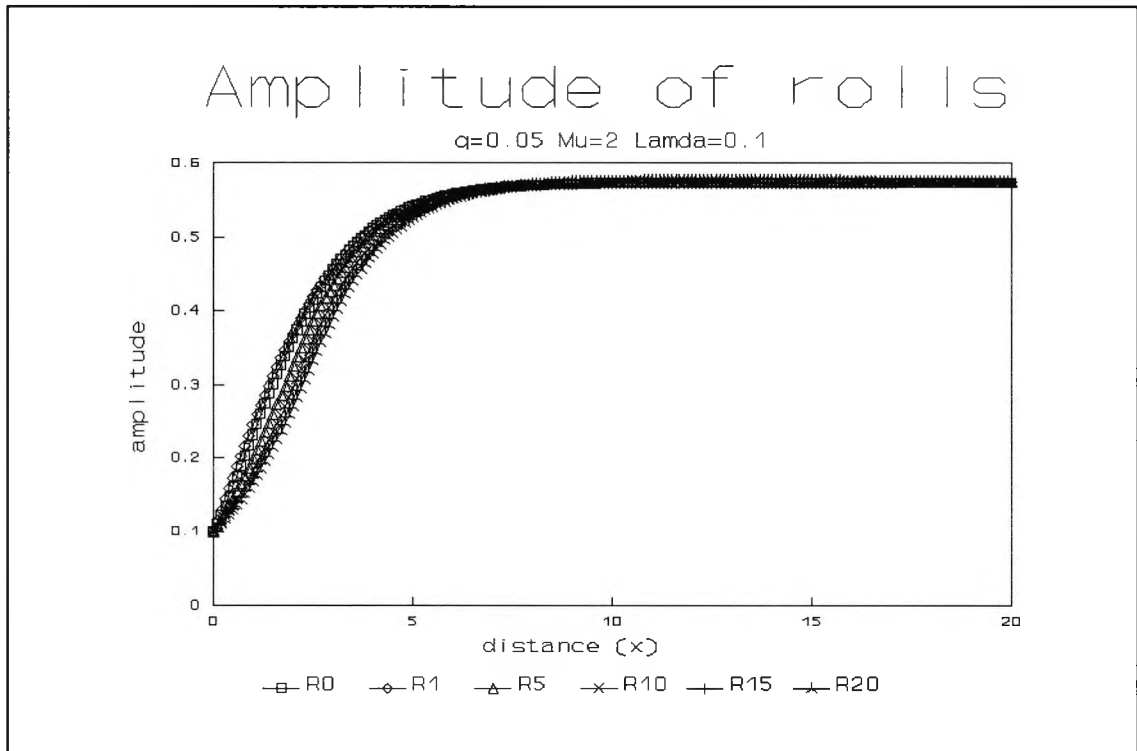
Fig. 4.7 : Numerical evolution for $q=0.05$, $\mu=2$ and $\lambda=0.1$ showing the amplitude of x-rolls at successive times τ
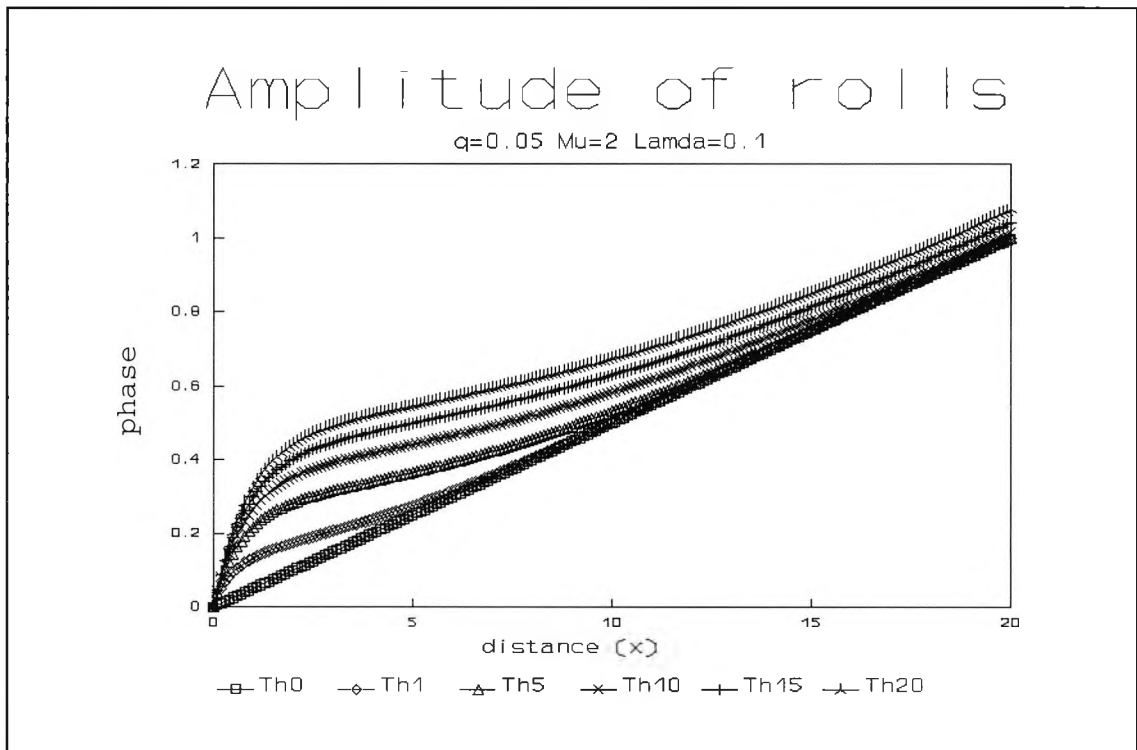
Fig. 4.8 : Numerical evolution for $q=0.05$, $\mu=2$ and $\lambda=0.1$ showing the phase of x-rolls at successive times τ

128
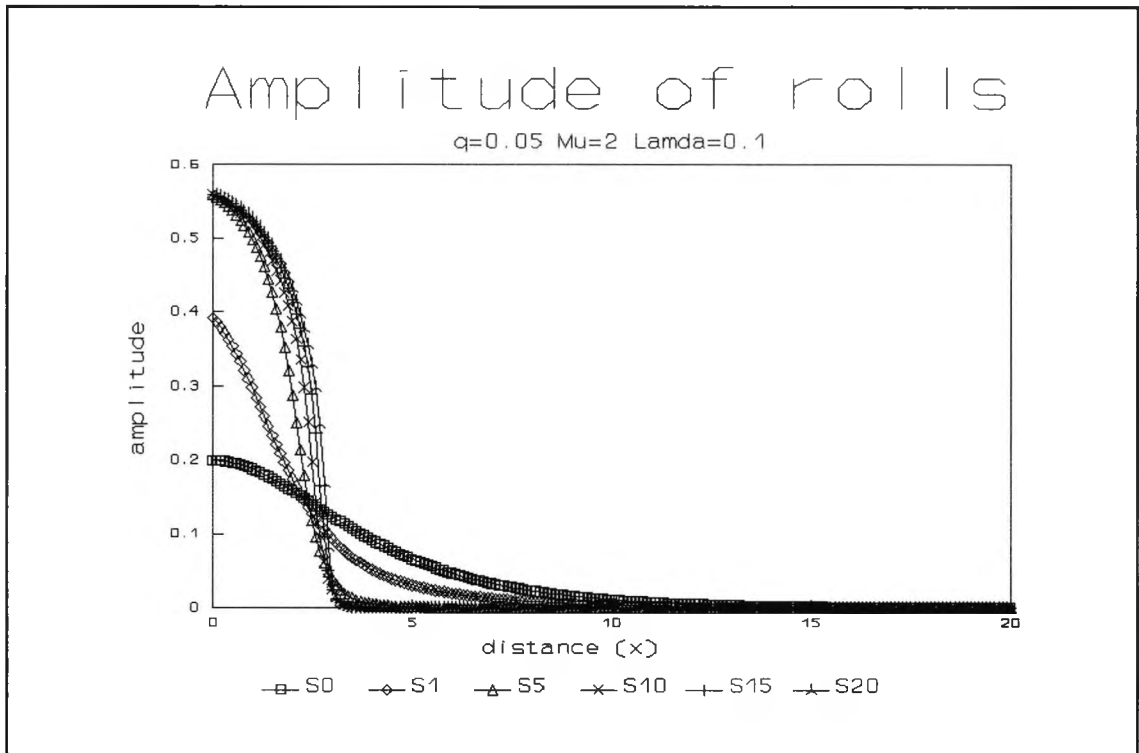
Fig. 4.9 : Numerical evolution for $q=0.05$, $\mu=2$ and $\lambda=0.1$ showing the amplitude of y-rolls at successive times τ
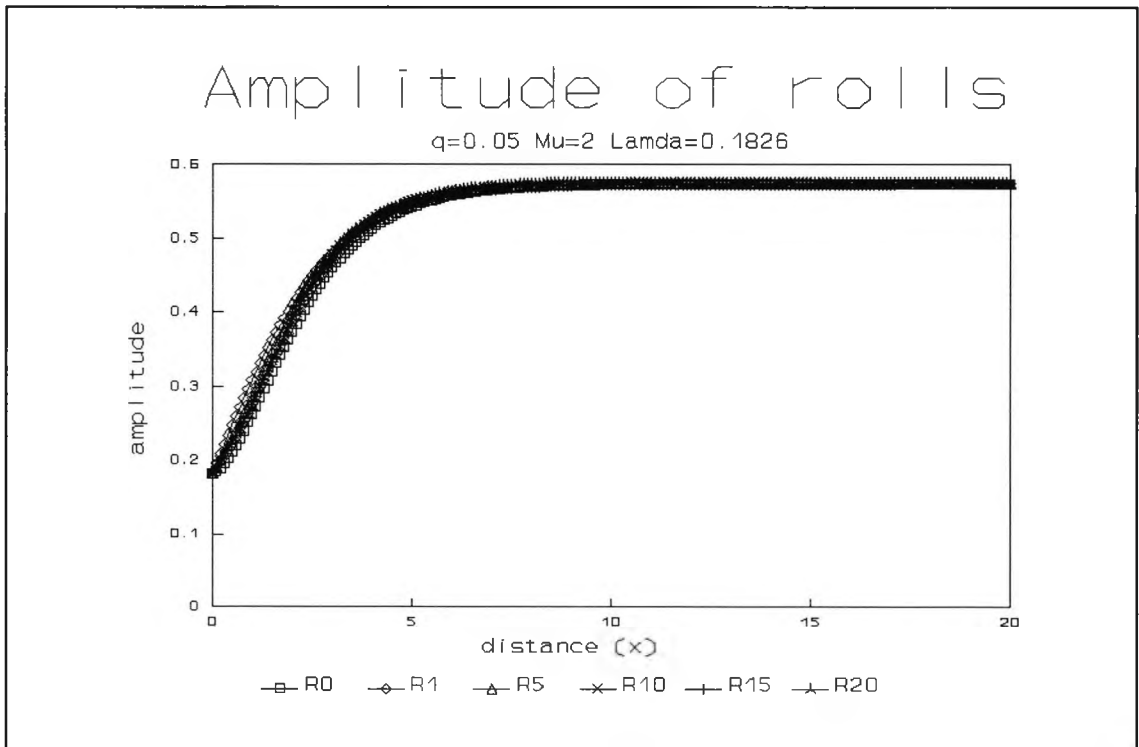
Fig. 4.10 : Numerical evolution for $q=0.05$, $\mu=2$ and $\lambda=0.1826$ showing the amplitude of x-rolls at successive times τ

129
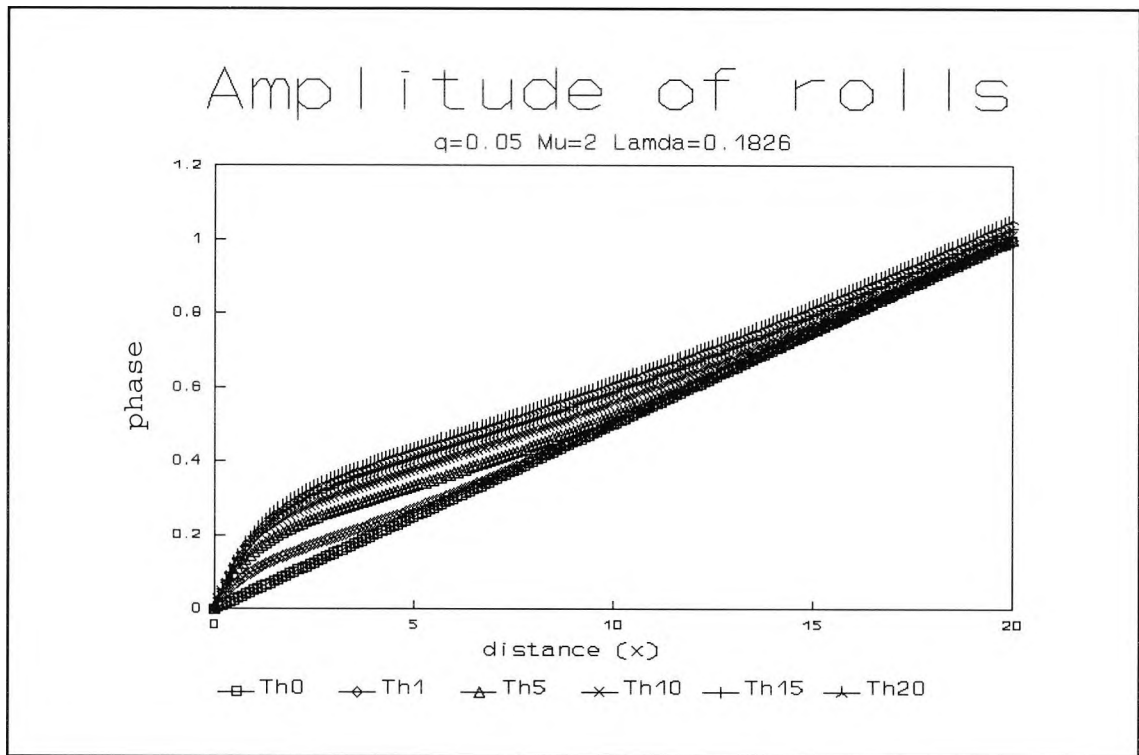
Fig. 4.11 : Numerical evolution for $q=0.05$, $\mu=2$ and $\lambda=0.1826$ showing the phase of x-rolls at successive times τ
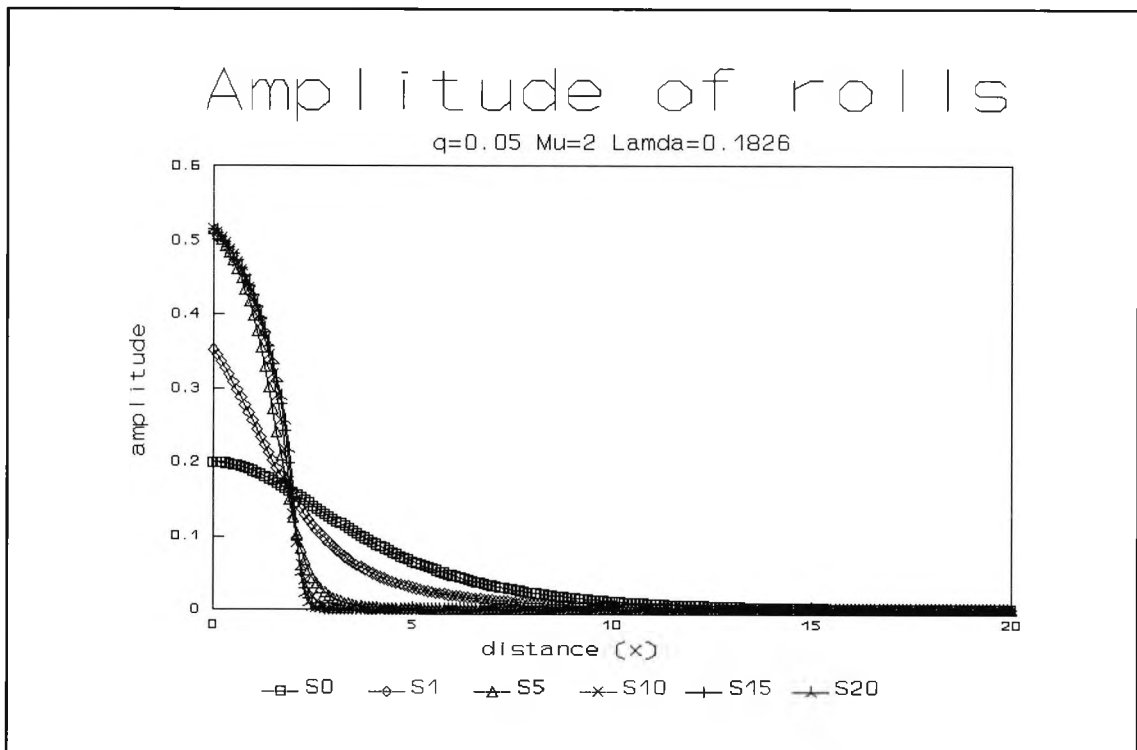
Fig. 4.12 : Numerical evolution for $q=0.05$, $\mu=2$ and $\lambda=0.1826$ showing the amplitude of y-rolls at successive times τ

130
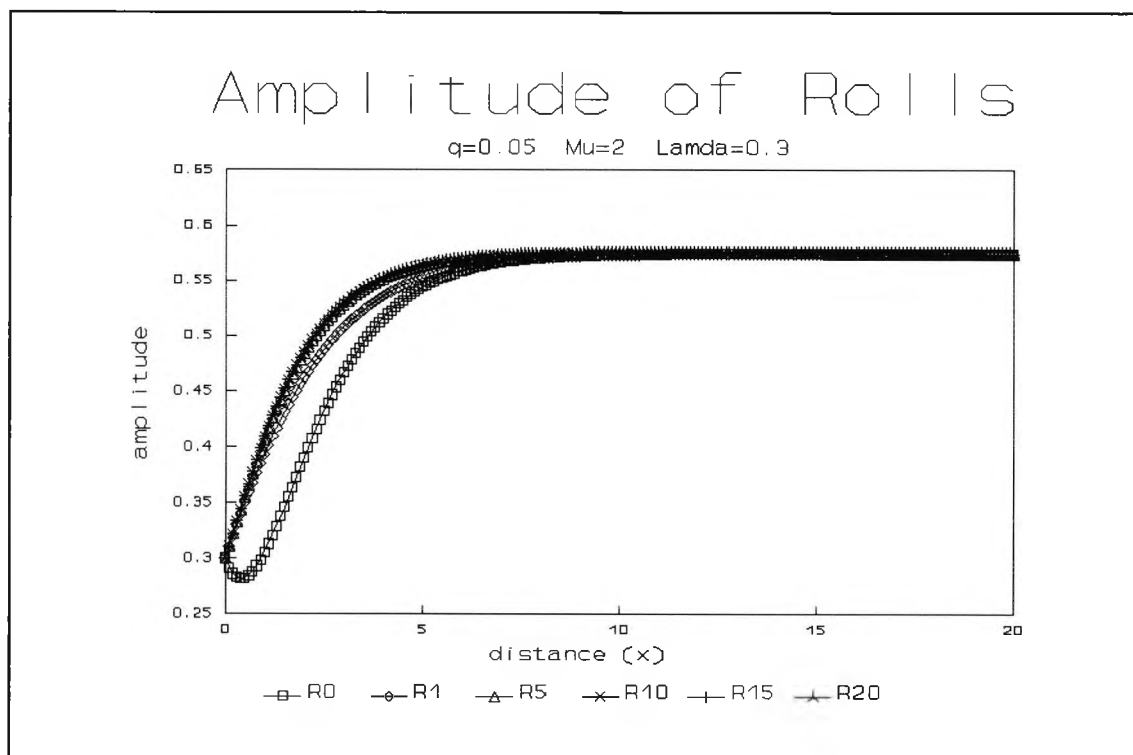
Fig. 4.13 : Numerical evolution for $q=0.05$, $\mu=2$ and $\lambda=0.3$ showing the amplitude of x-rolls at successive times τ
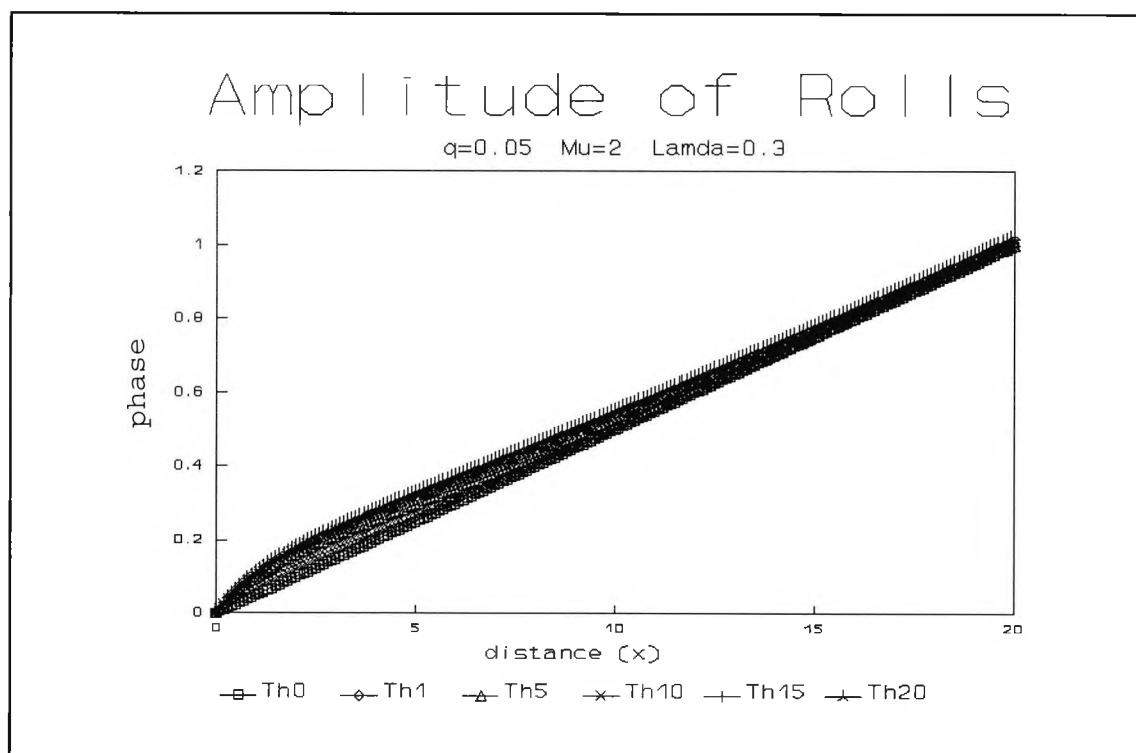
Fig. 4.14 : Numerical evolution for $q=0.05$, $\mu=2$ and $\lambda=0.3$ showing the phase of x-rolls at successive times τ
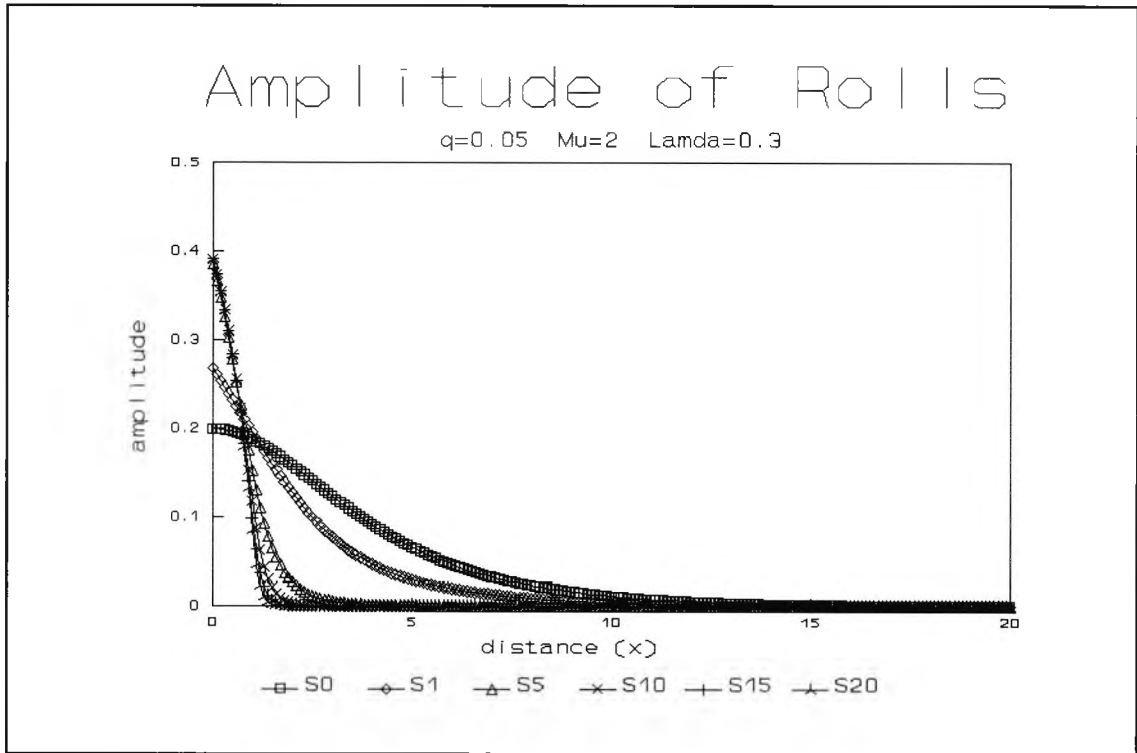
Fig. 4.15 : Numerical evolution for $q=0.05$, $\mu=2$ and $\lambda=0.3$ showing the amplitude of y-rolls at successive times τ
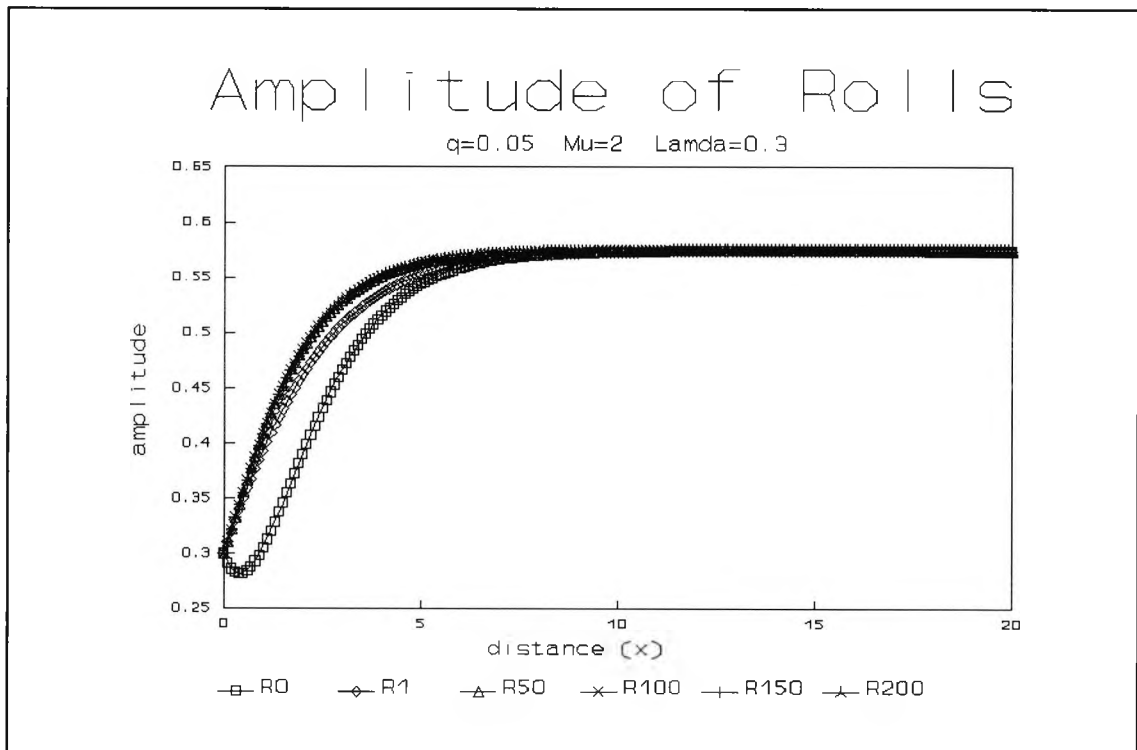
Fig. 4.16 : Numerical evolution for $q=0.05$, $\mu=2$ and $\lambda=0.3$ showing the amplitude of x-rolls at successive times τ
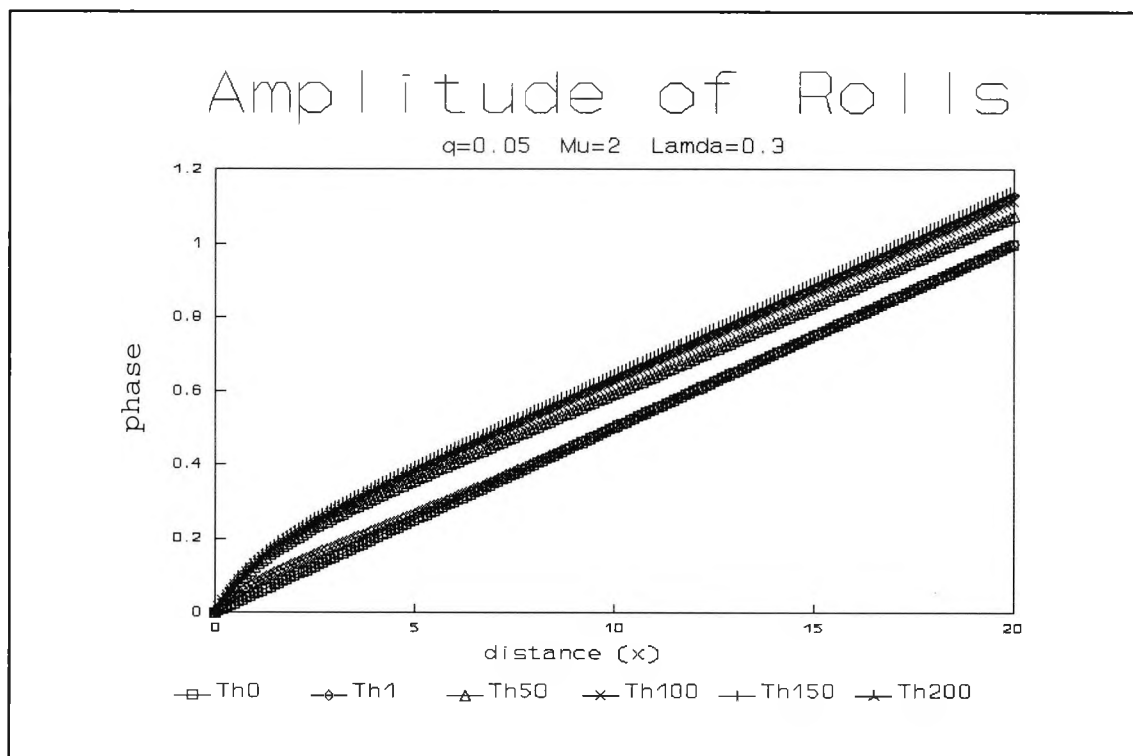
Fig. 4.17 : Numerical evolution for $q=0.05$, $\mu=2$ and $\lambda=0.3$ showing the phase of x-rolls at successive times τ
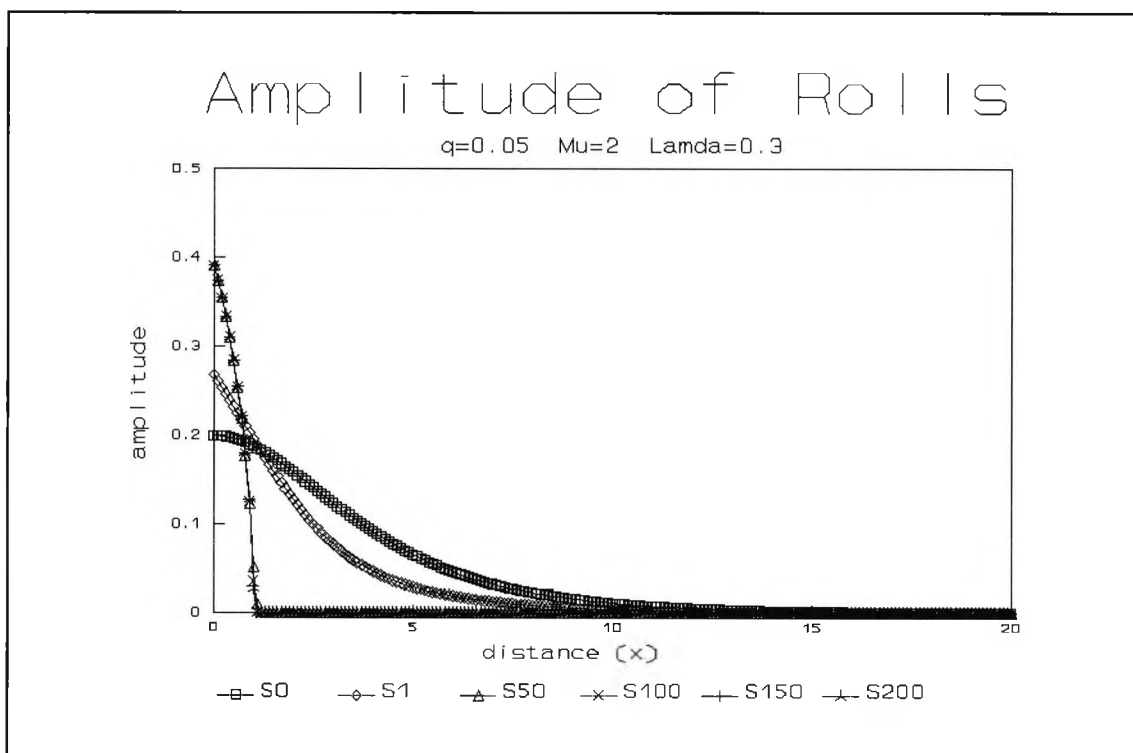
Fig. 4.18 : Numerical evolution for $q=0.05$, $\mu=2$ and $\lambda=0.3$ showing the amplitude of y-rolls at successive times τ

133
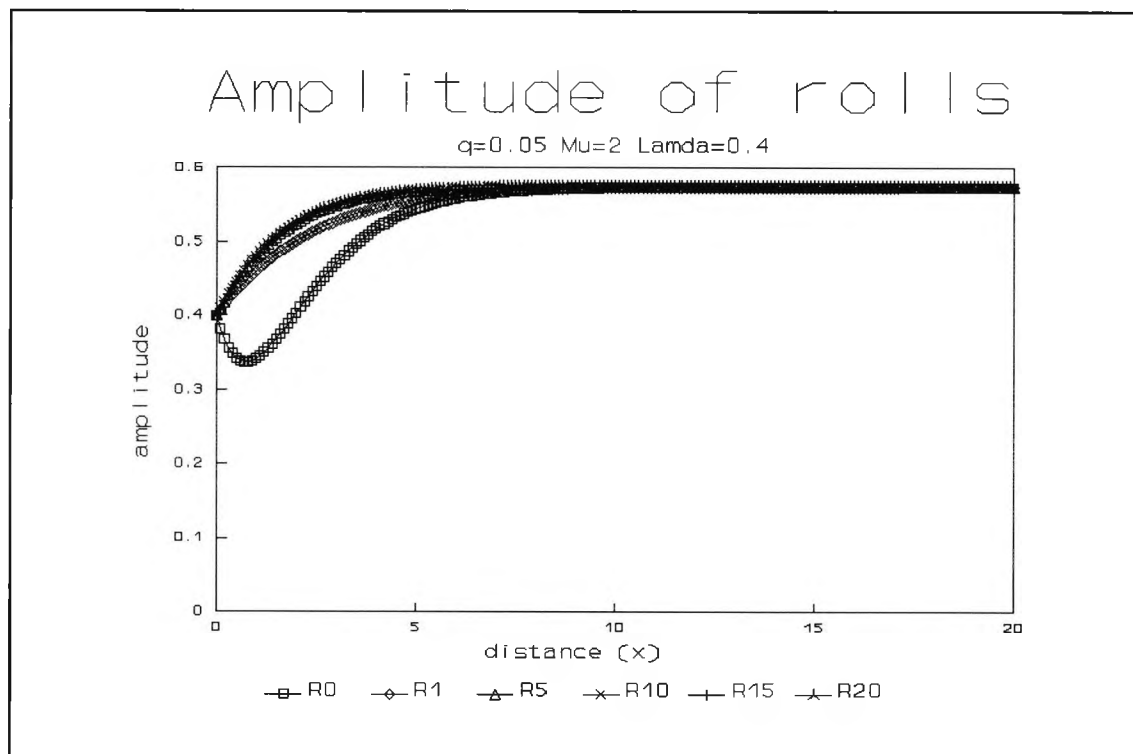
Fig. 4.19 : Numerical evolution for $q=0.05$, $\mu=2$ and $\lambda=0.4$ showing the amplitude of x-rolls at successive times τ
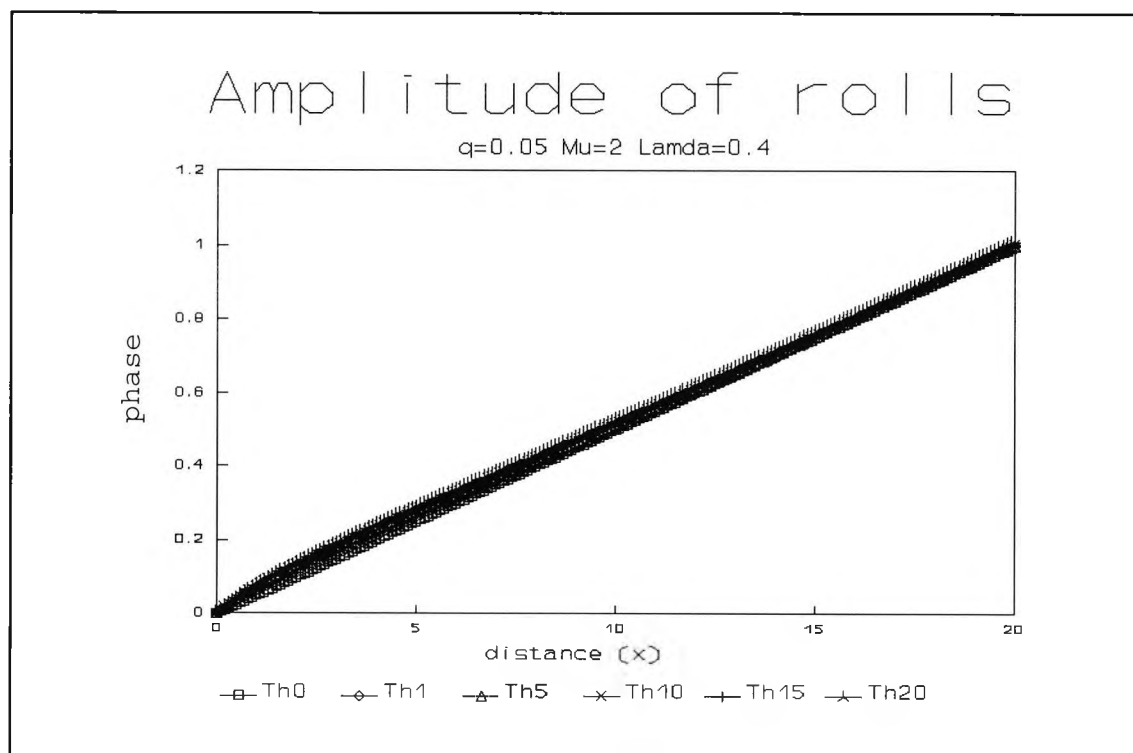
Fig. 4.20 : Numerical evolution for $q=0.05$, $\mu=2$ and $\lambda=0.4$ showing the phase of x-rolls at successive times τ

134
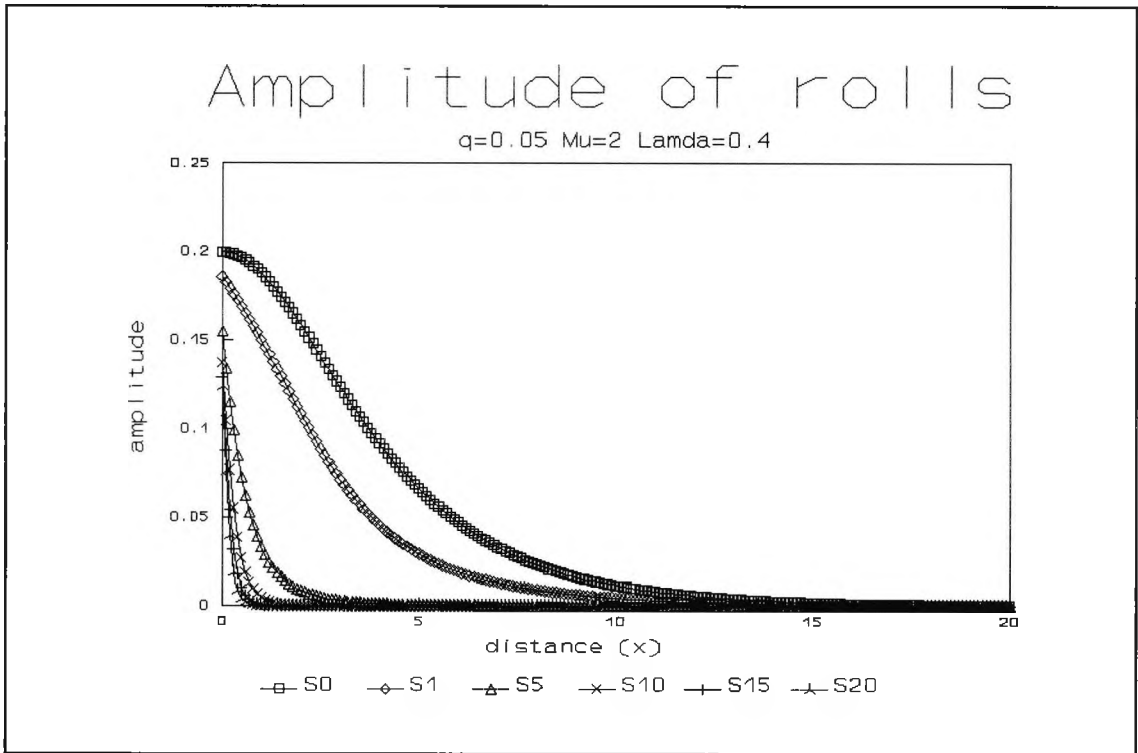
Fig. 4.21 : Numerical evolution for $q=0.05$, $\mu=2$ and $\lambda=0.4$ showing the amplitude of y-rolls at successive times τ
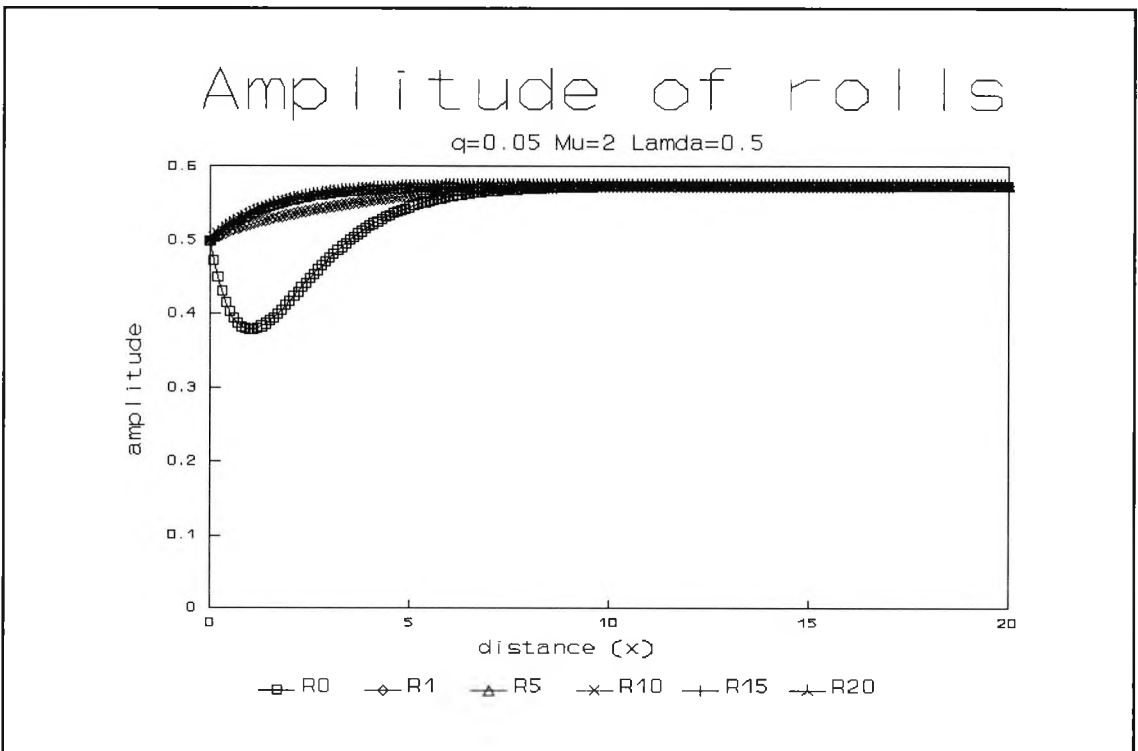
Fig. 4.22 : Numerical evolution for $q=0.05$, $\mu=2$ and $\lambda=0.5$ showing the amplitude of x-rolls at successive times τ

135
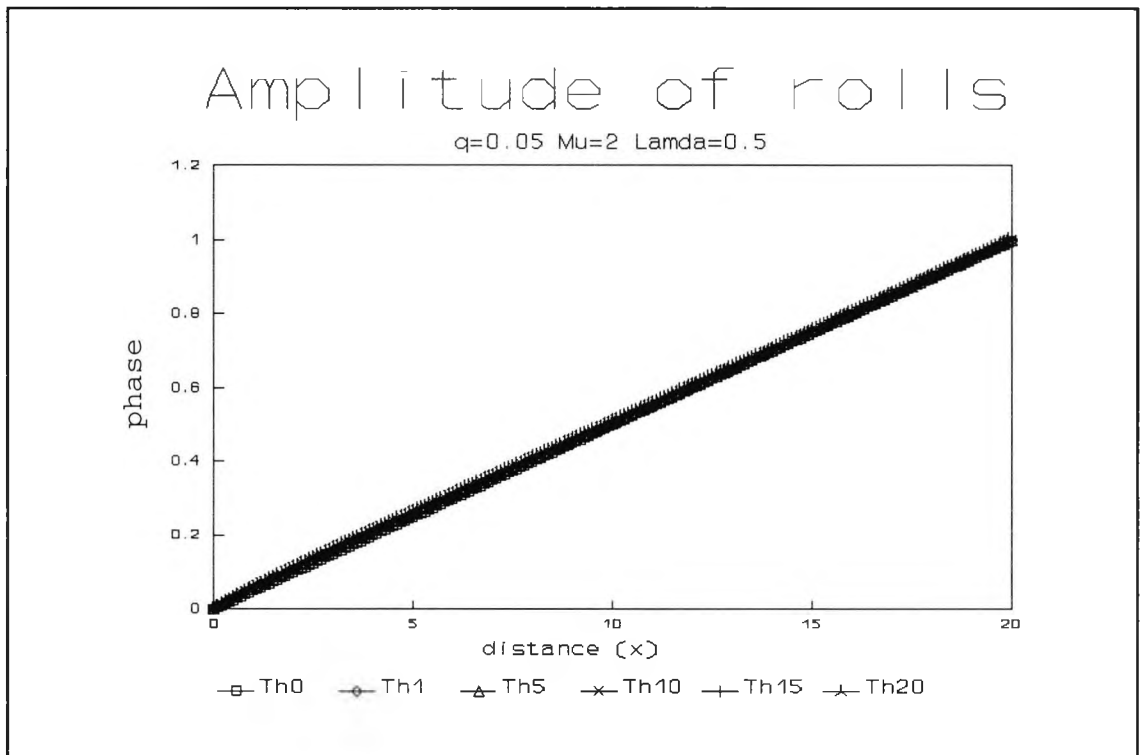
Fig. 4.23 : Numerical evolution for $q=0.05$, $\mu=2$ and $\lambda=0.5$ showing the phase of x-rolls at successive times τ
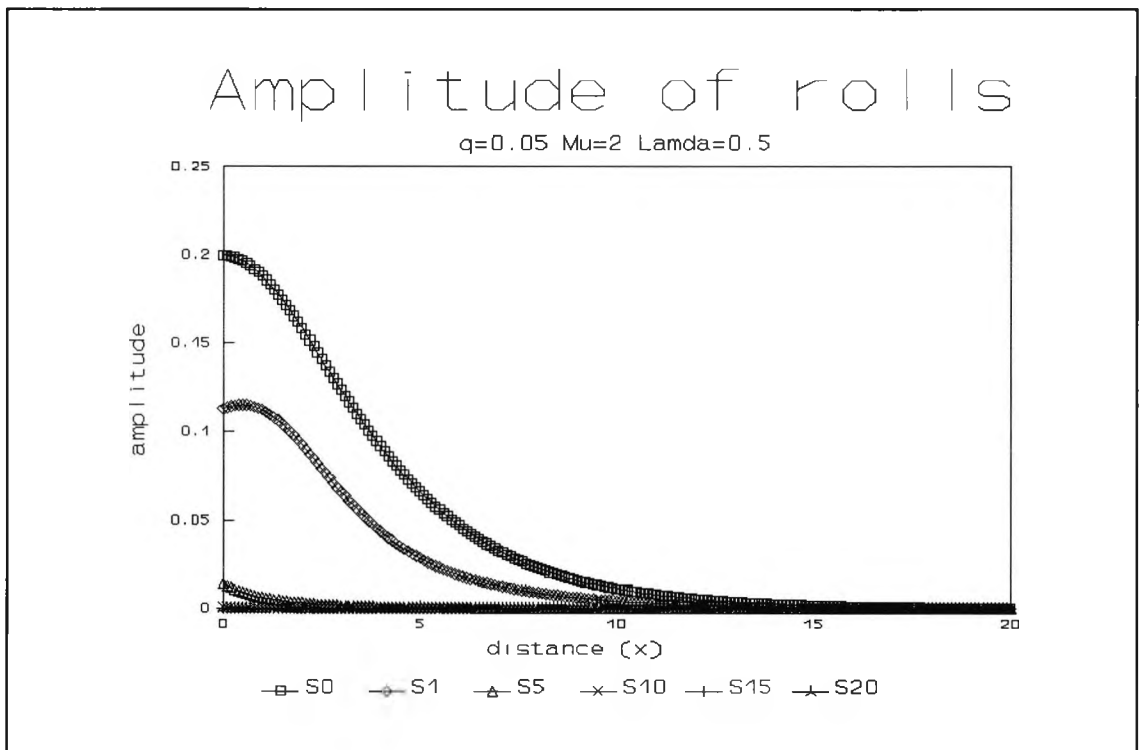
Fig. 4.24 : Numerical evolution for $q=0.05$, $\mu=2$ and $\lambda=0.5$ showing the amplitude of y-rolls at successive times τ

136
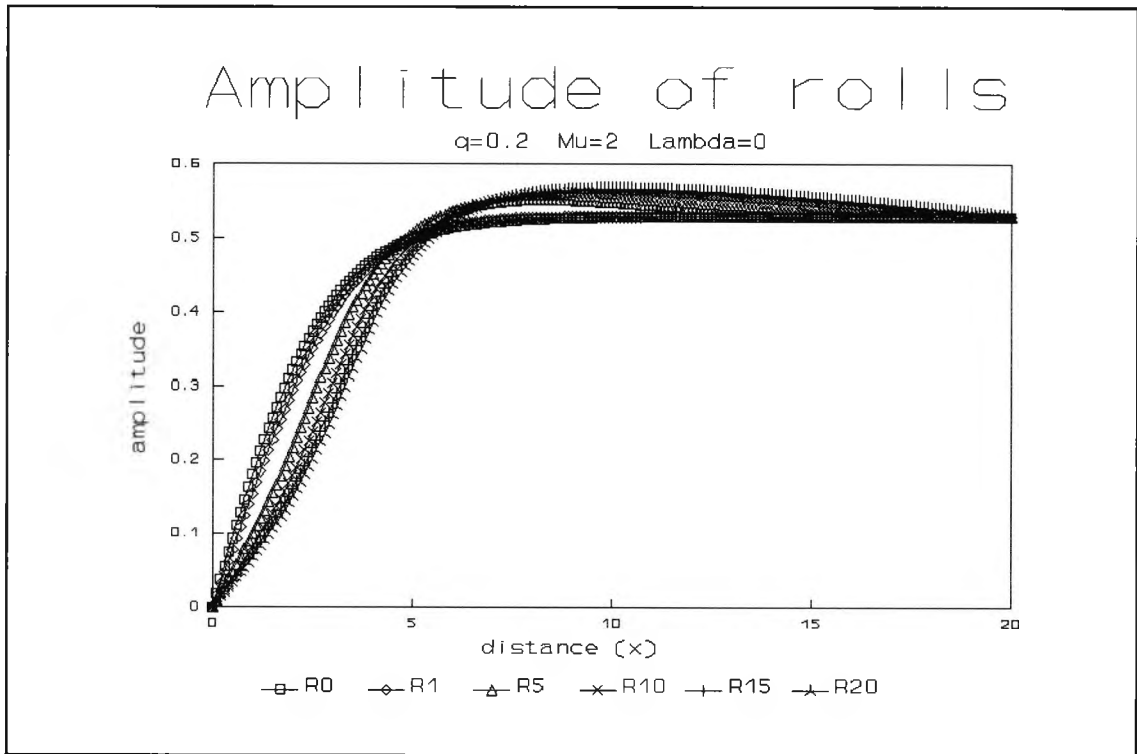
Fig. 4.25 : Numerical evolution for $q=0.2$, $\mu=2$ and $\lambda=0$ showing the amplitude of x-rolls at successive times τ
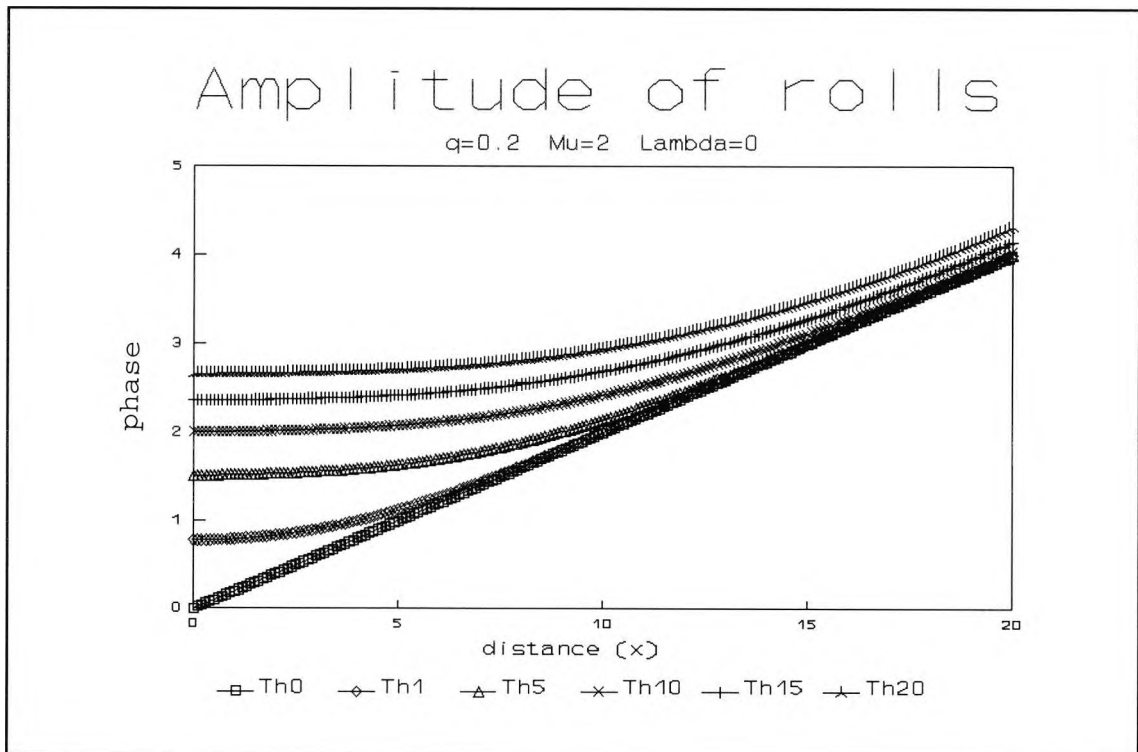
Fig. 4.26 : Numerical evolution for $q=0.2$, $\mu=2$ and $\lambda=0$ showing the phase of x-rolls at successive times τ

137
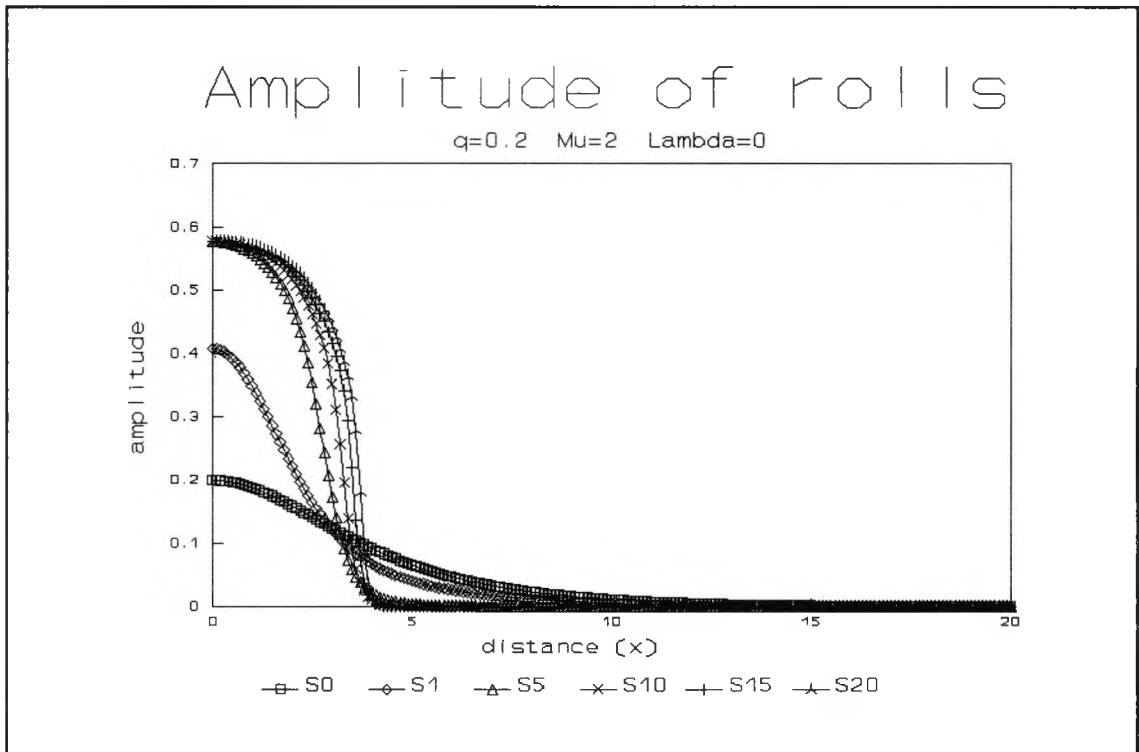
Fig. 4.27 : Numerical evolution for $q=0.2$, $\mu=2$ and $\lambda=0$ showing the amplitude of y-rolls at successive times τ
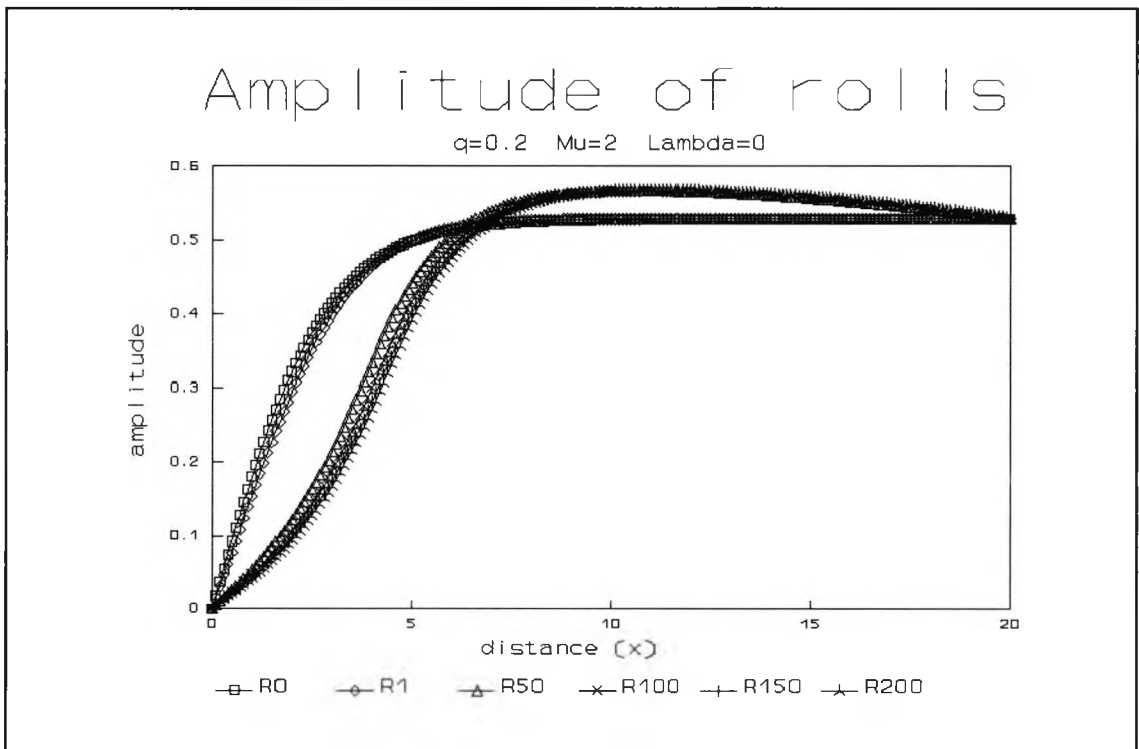
Fig. 4.28 : Numerical evolution for $q=0.2$, $\mu=2$ and $\lambda=0$ showing the amplitude of x-rolls at successive times τ

138
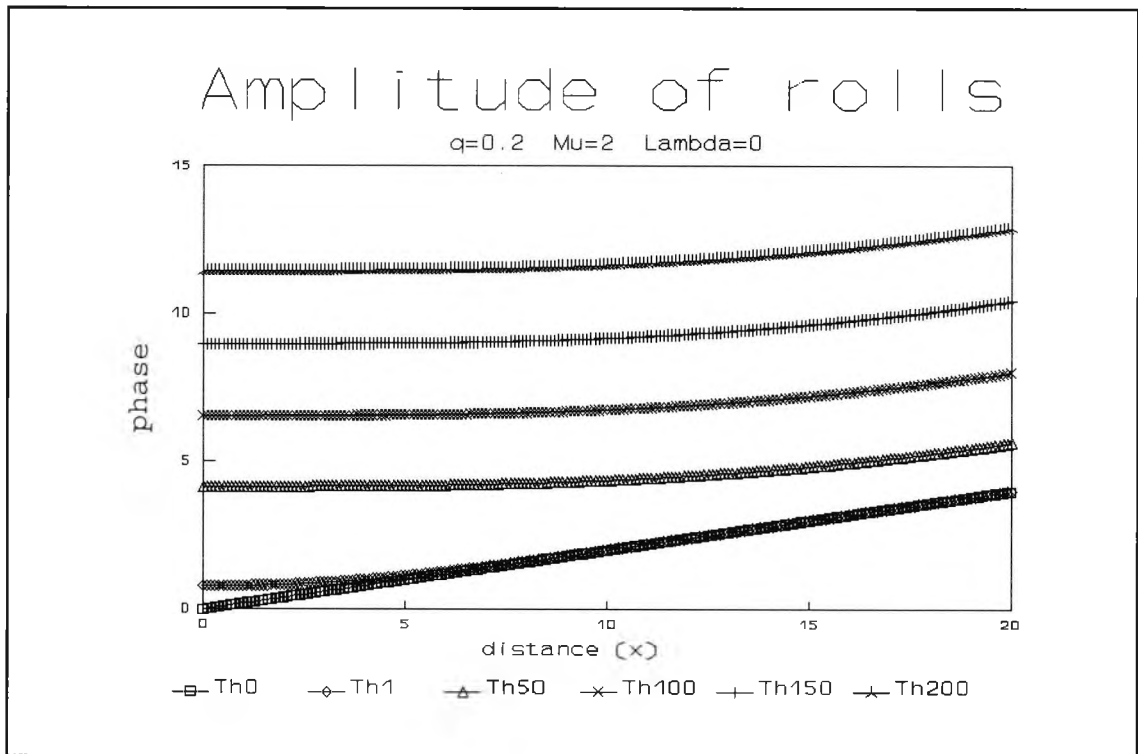
Fig. 4.29 : Numerical evolution for $q=0.2$, $\mu=2$ and $\lambda=0$ showing the phase of x-rolls at successive times τ
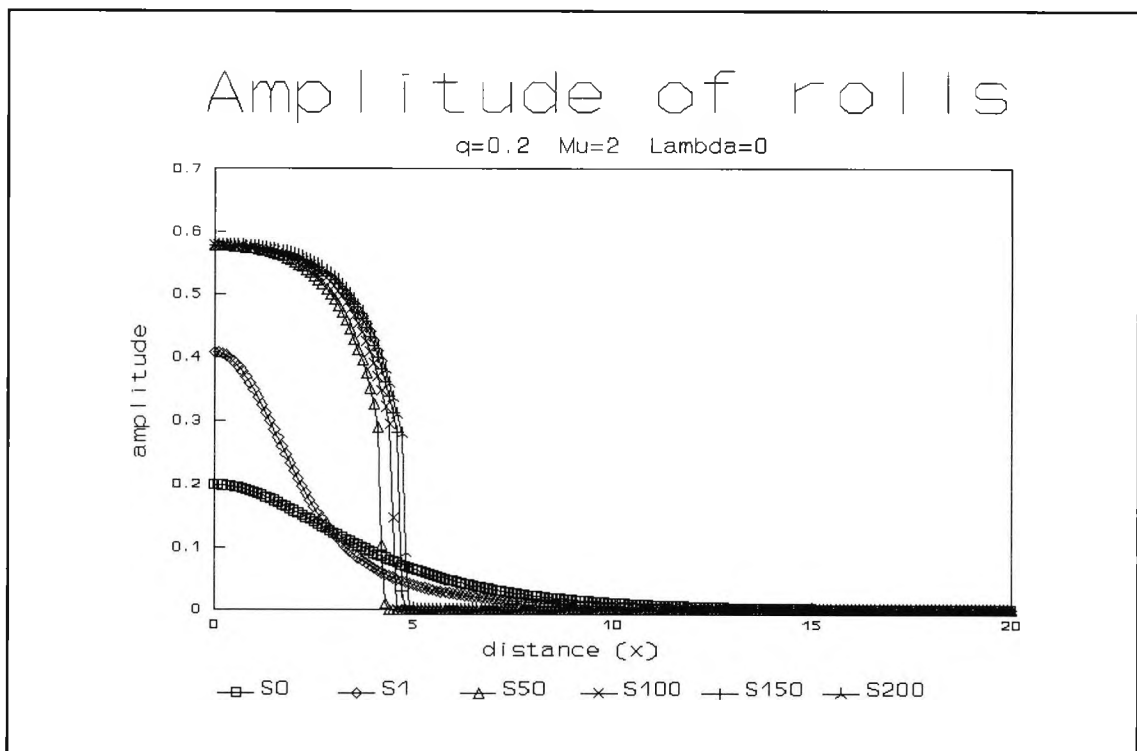
Fig. 4.30 : Numerical evolution for $q=0.2$, $\mu=2$ and $\lambda=0$ showing the amplitude of y-rolls at successive times τ

139
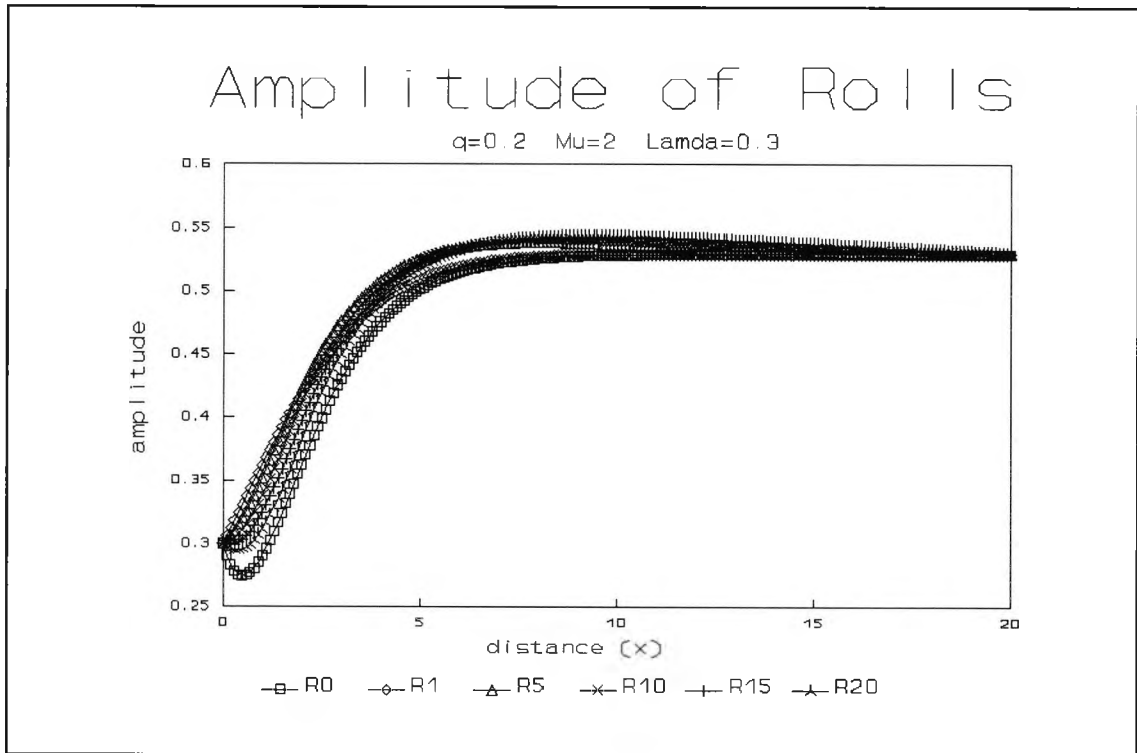
Fig. 4.31 : Numerical evolution for $q=0.2$, $\mu=2$ and $\lambda=0.3$ showing the amplitude of x-rolls at successive times τ
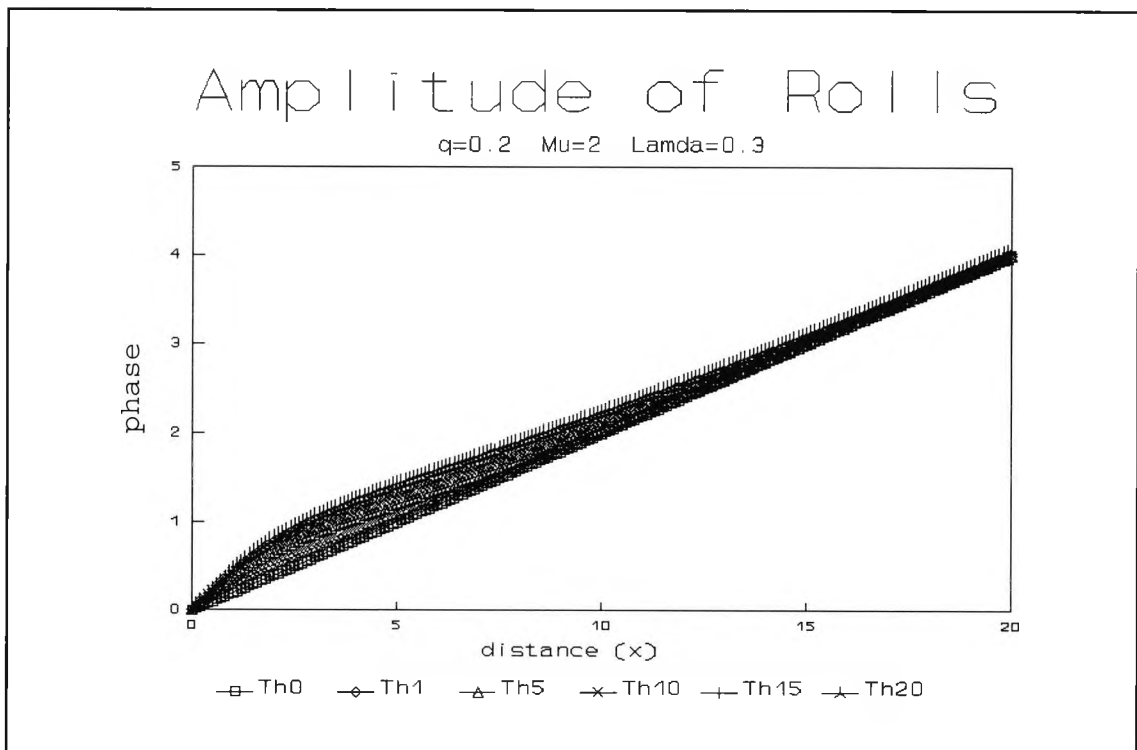
Fig. 4.32 : Numerical evolution for $q=0.2$, $\mu=2$ and $\lambda=0.3$ showing the phase of x-rolls at successive times τ

140
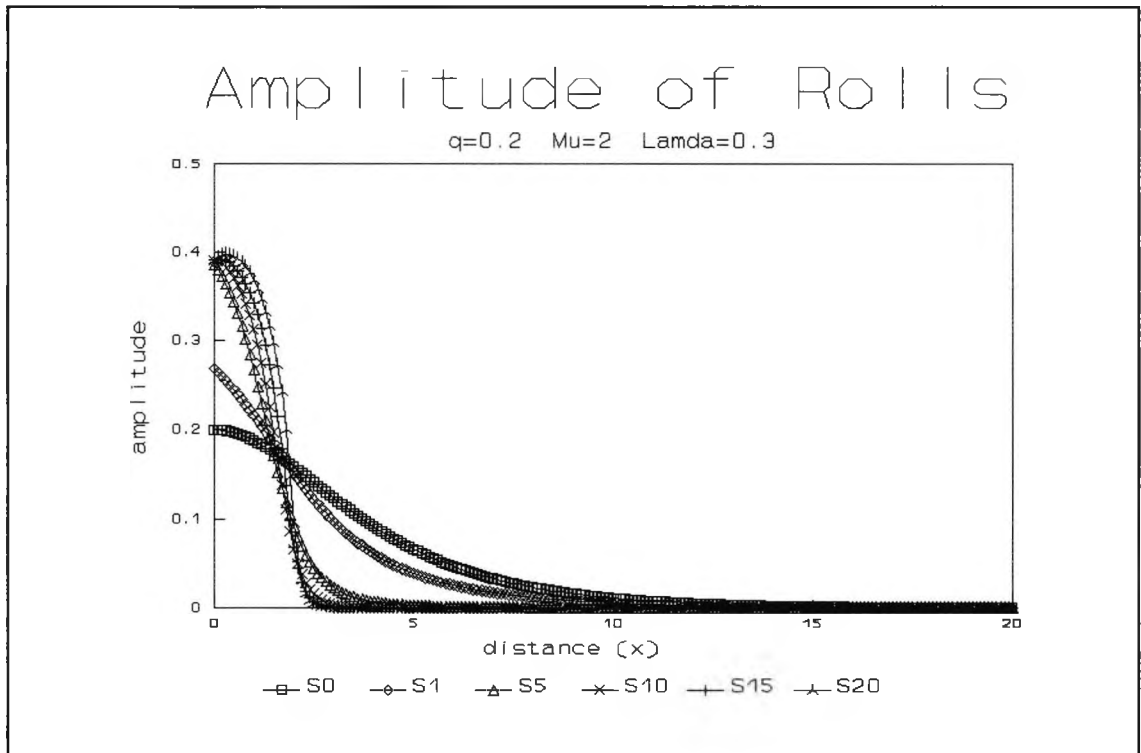
Fig. 4.33 : Numerical evolution for $q=0.2$, $\mu=2$ and $\lambda=0.3$ showing the amplitude of y-rolls at successive times τ
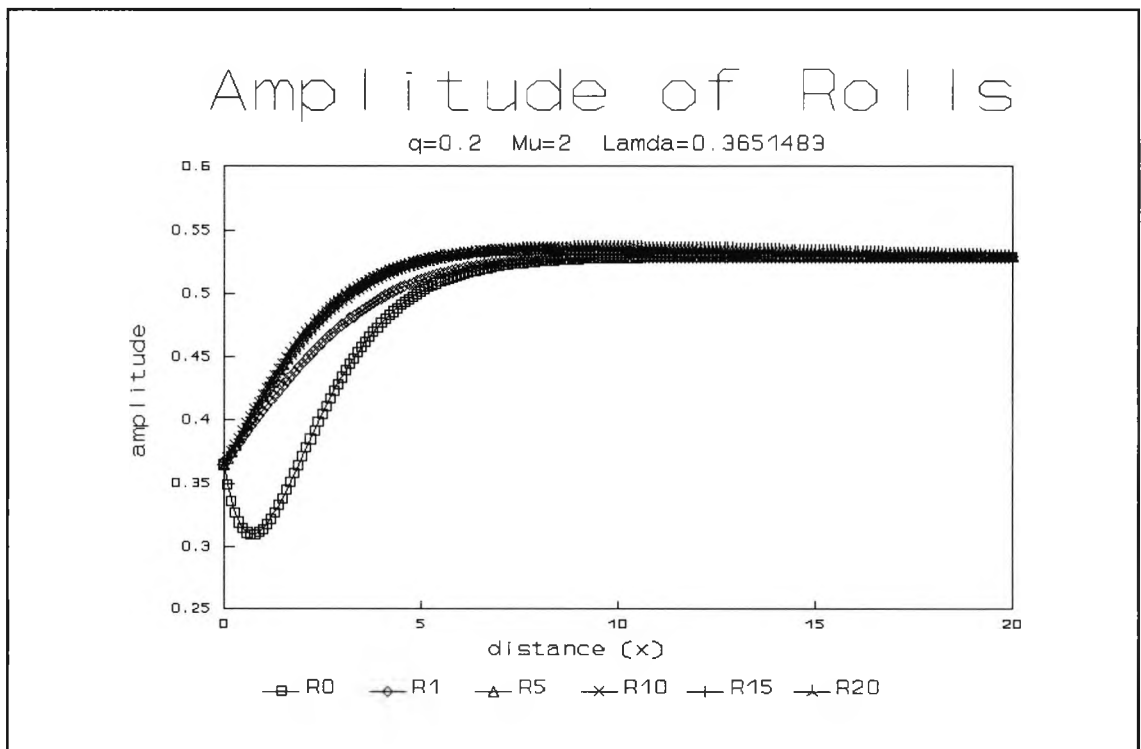
Fig. 4.34 : Numerical evolution for $q=0.2$, $\mu=2$ and $\lambda=0.3651$ showing the amplitude of x-rolls at successive times τ
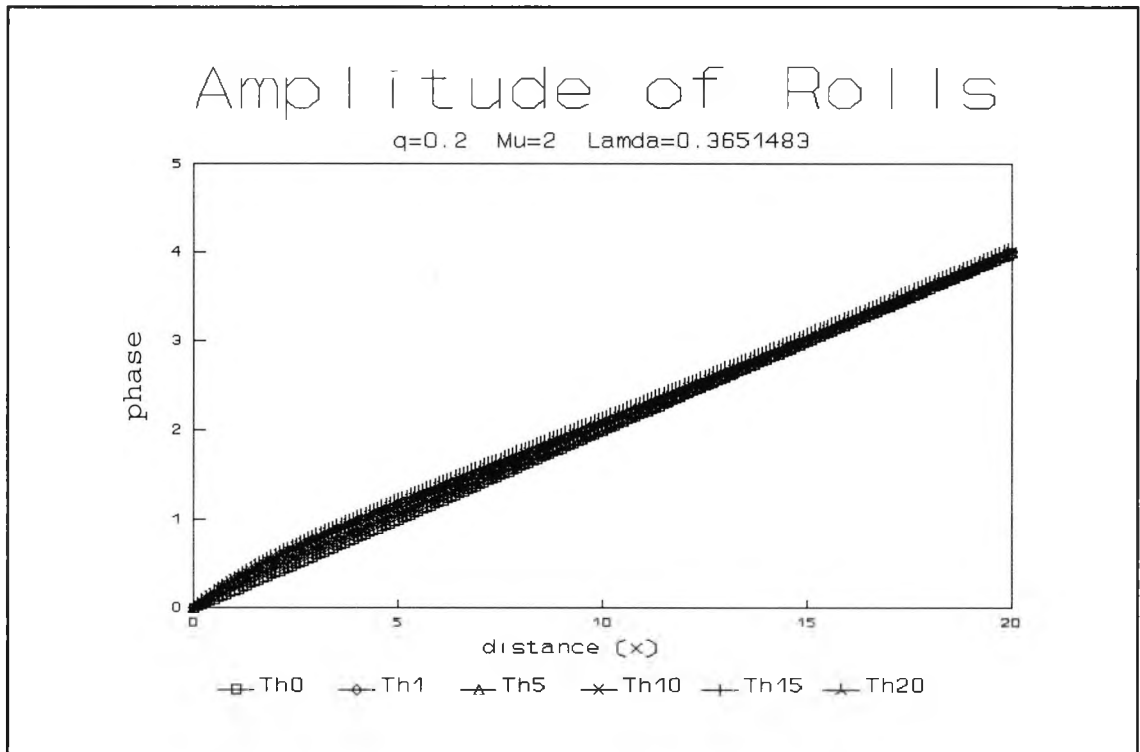
Fig. 4.35 : Numerical evolution for $q=0.2$, $\mu=2$ and $\lambda=0.3651$ showing the phase of x-rolls at successive times τ
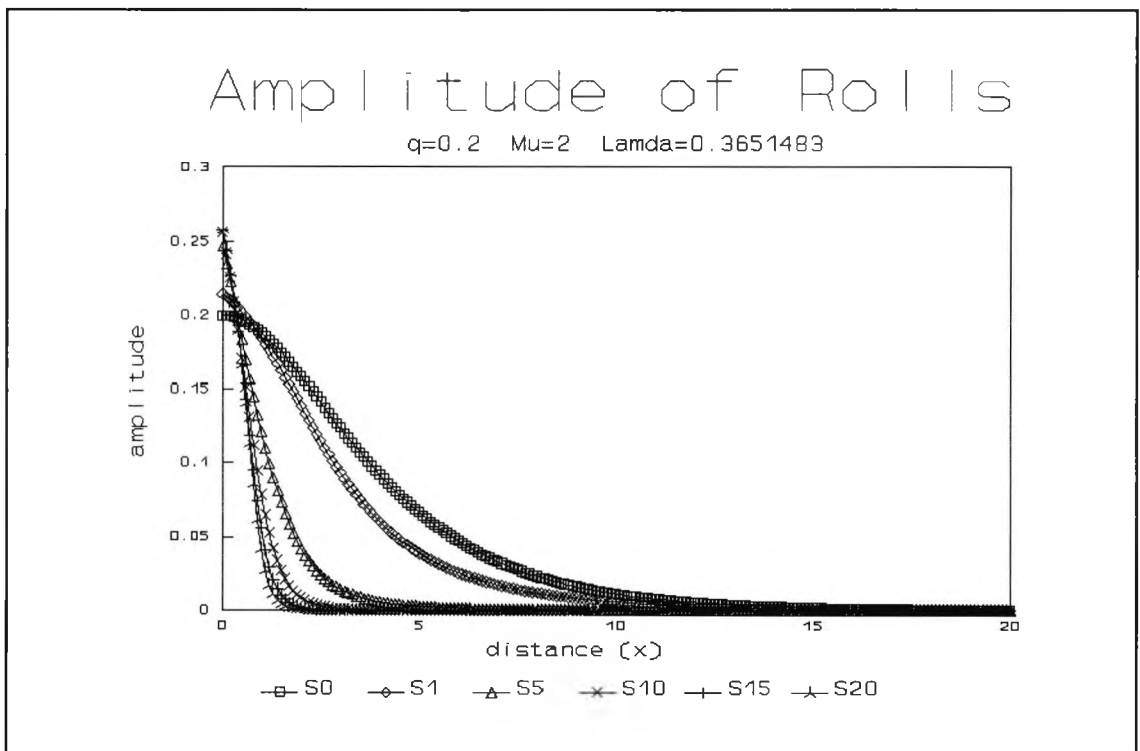
Fig. 4.36 : Numerical evolution for $q=0.2$, $\mu=2$ and $\lambda=0.3651$ showing the amplitude of y-rolls at successive times τ

142
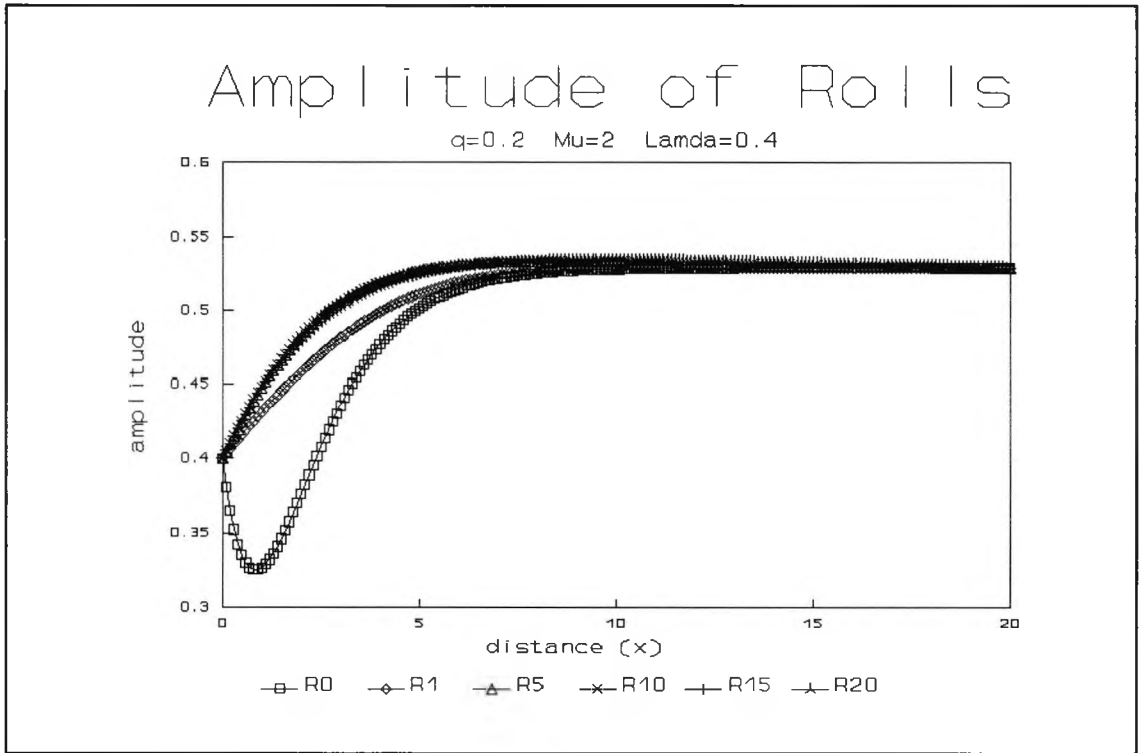
Fig. 4.37 : Numerical evolution for $q=0.2$, $\mu=2$ and $\lambda=0.4$ showing the amplitude of x-rolls at successive times τ
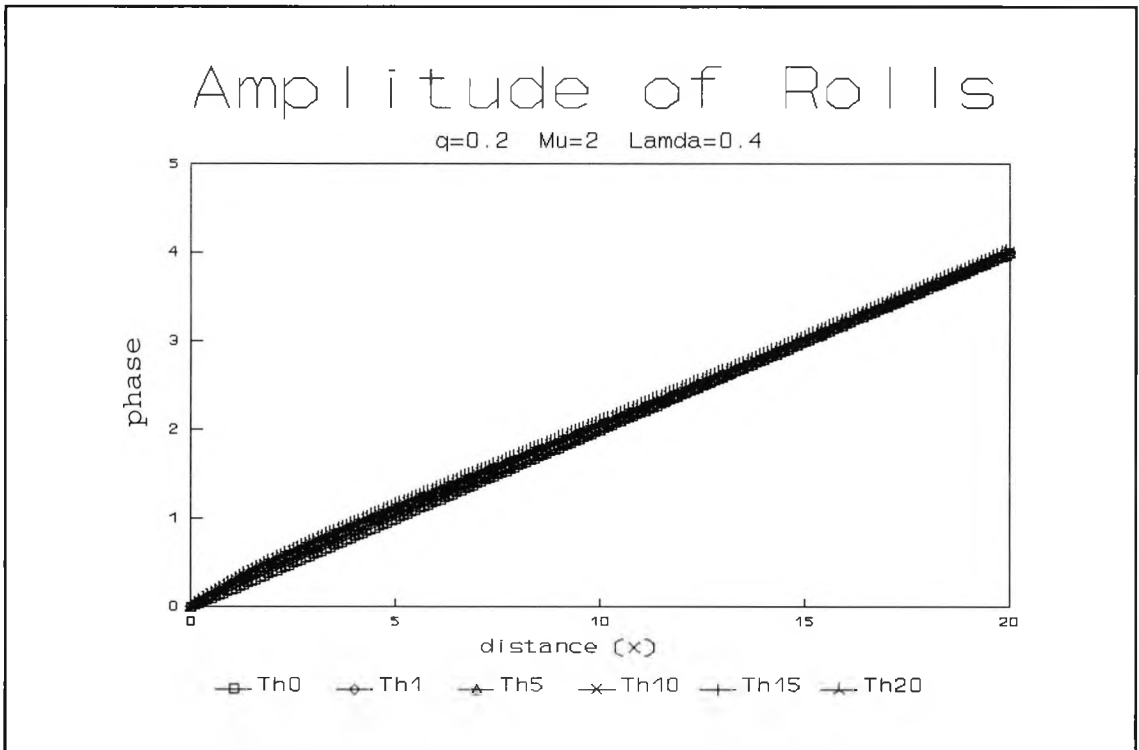
Fig. 4.38 : Numerical evolution for $q=0.2$, $\mu=2$ and $\lambda=0.4$ showing the phase of x-rolls at successive times τ

143
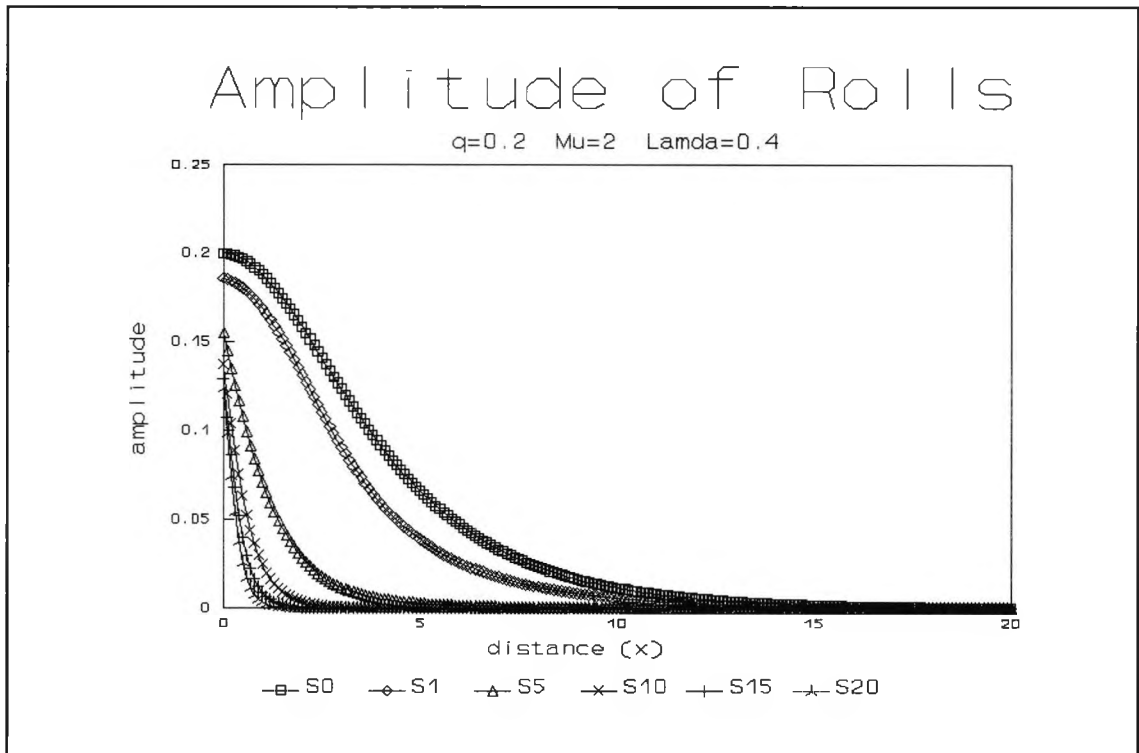
Fig. 4.39 : Numerical evolution for $q=0.2$, $\mu=2$ and $\lambda=0.4$ showing the amplitude of y-rolls at successive times τ
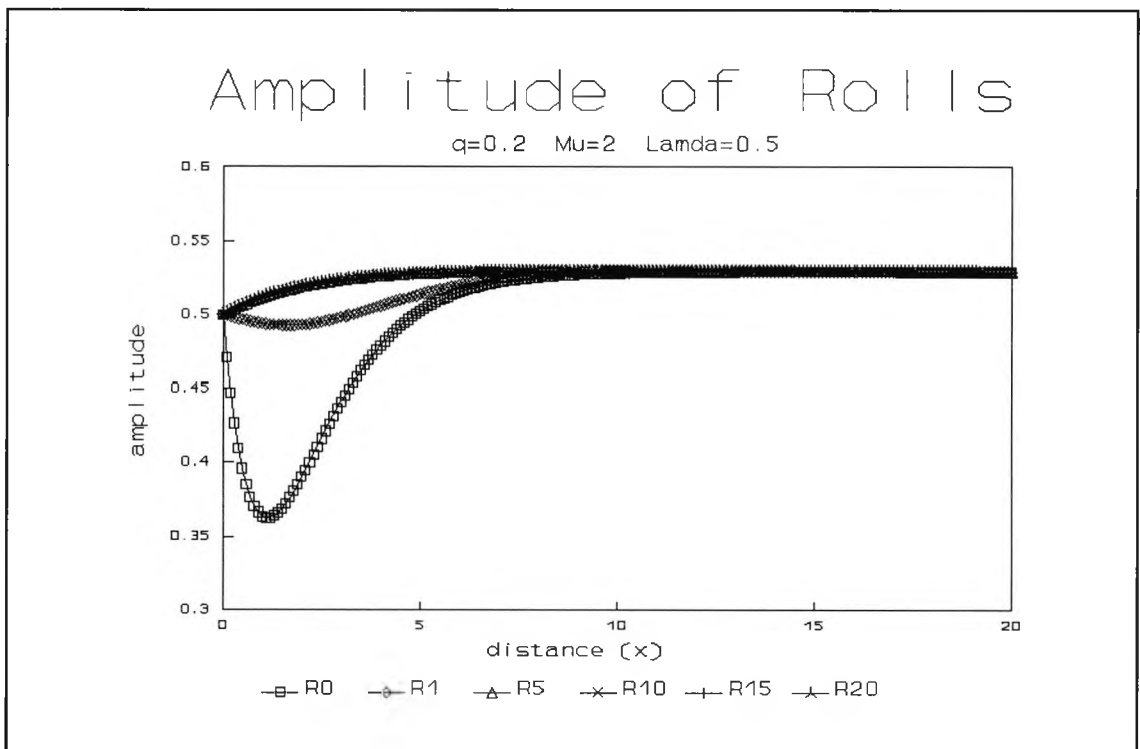
Fig. 4.40 : Numerical evolution for $q=0.2$, $\mu=2$ and $\lambda=0.5$ showing the amplitude of x-rolls at successive times τ

144
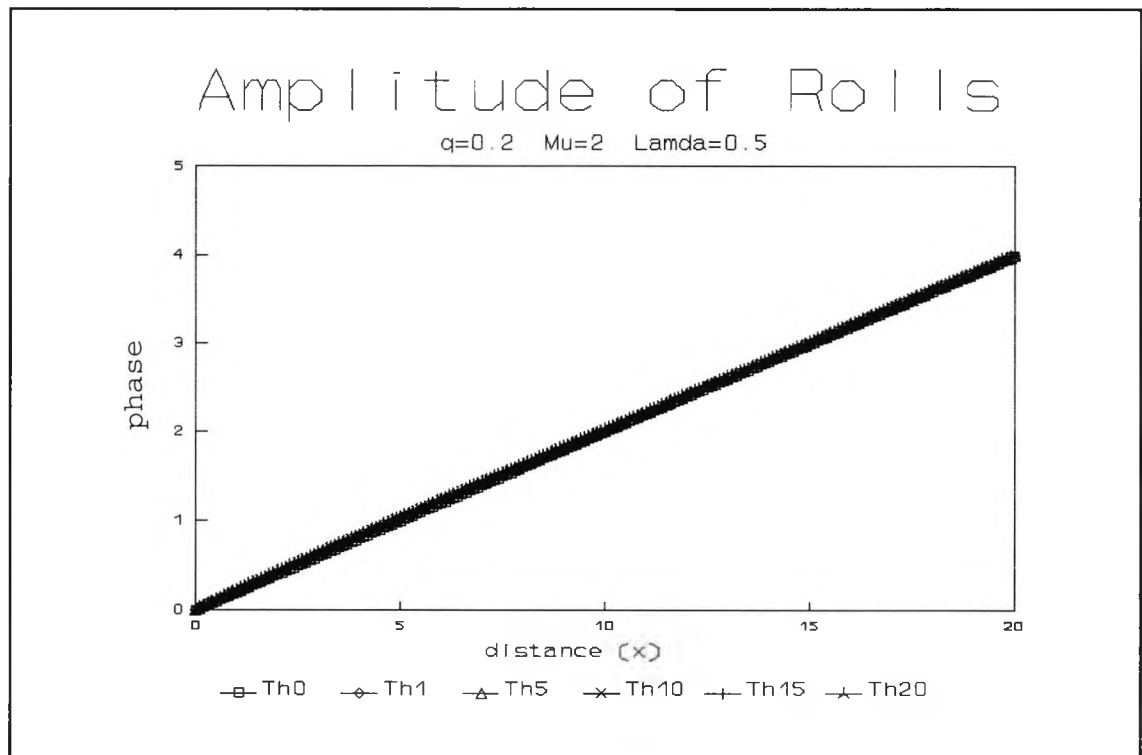
Fig. 4.41 : Numerical evolution for $q=0.2$, $\mu=2$ and $\lambda=0.5$ showing the phase of x-rolls at successive times τ
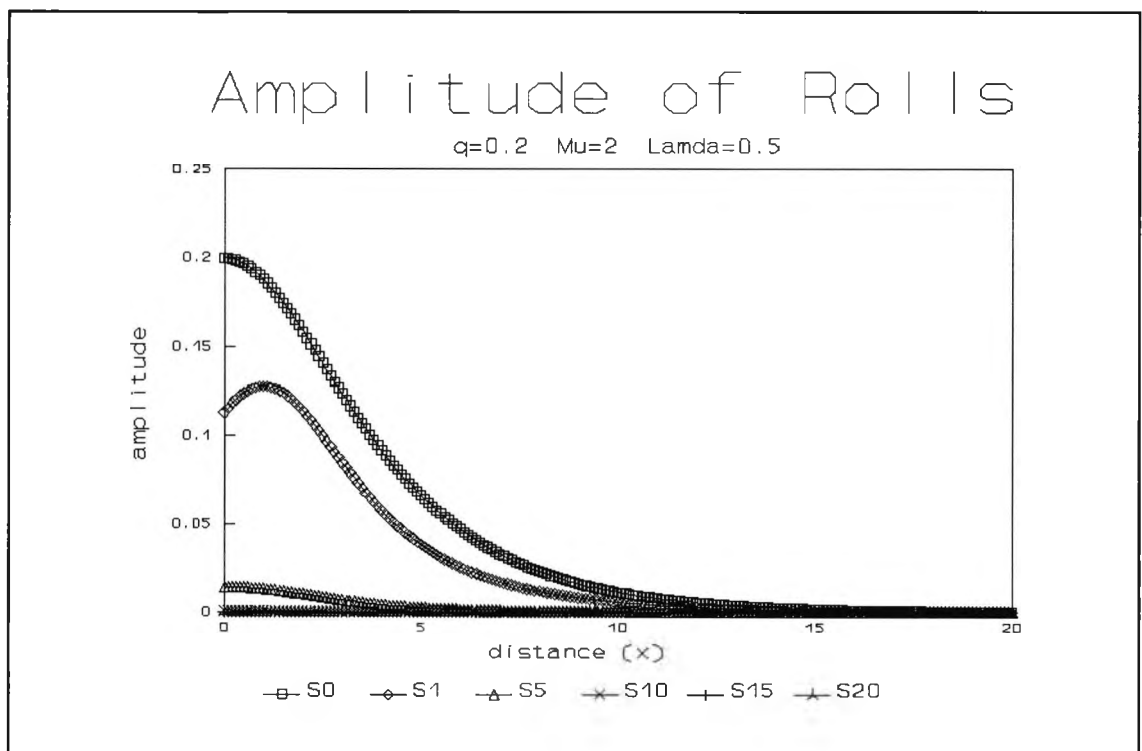
Fig. 4.42 : Numerical evolution for $q=0.2$, $\mu=2$ and $\lambda=0.5$ showing the amplitude of y-rolls at successive times τ

145
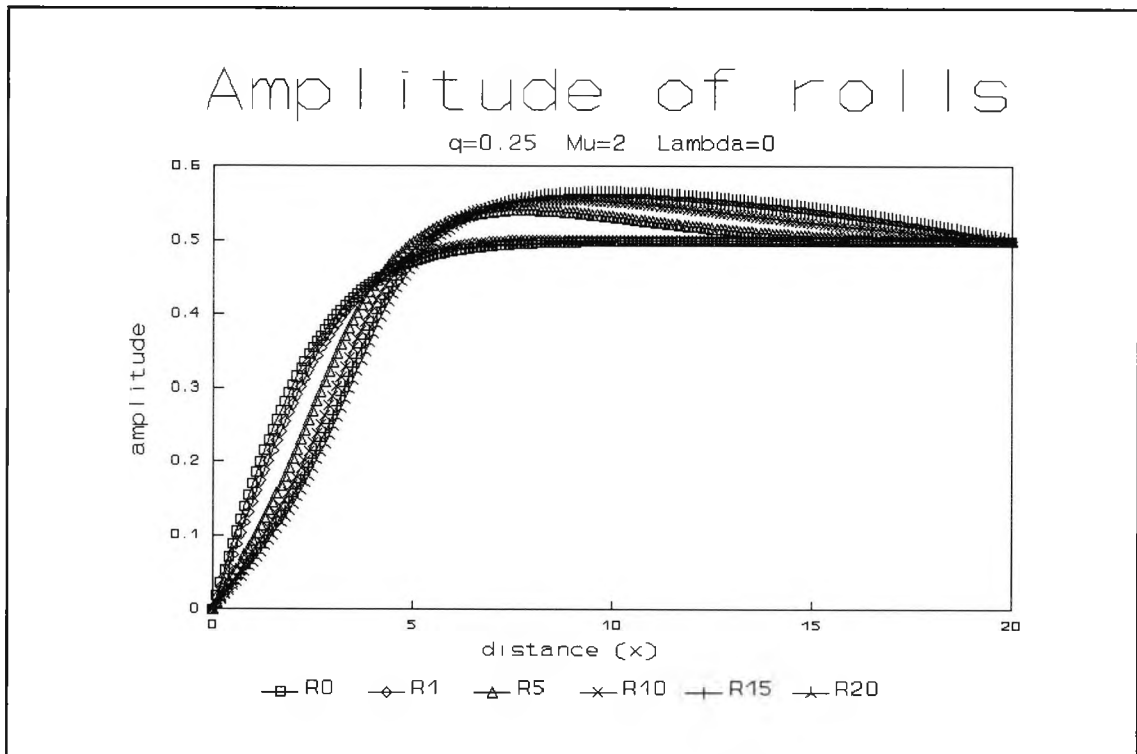
Fig. 4.43 : Numerical evolution for $q=0.25$, $\mu=2$ and $\lambda=0$ showing the amplitude of x-rolls at successive times τ
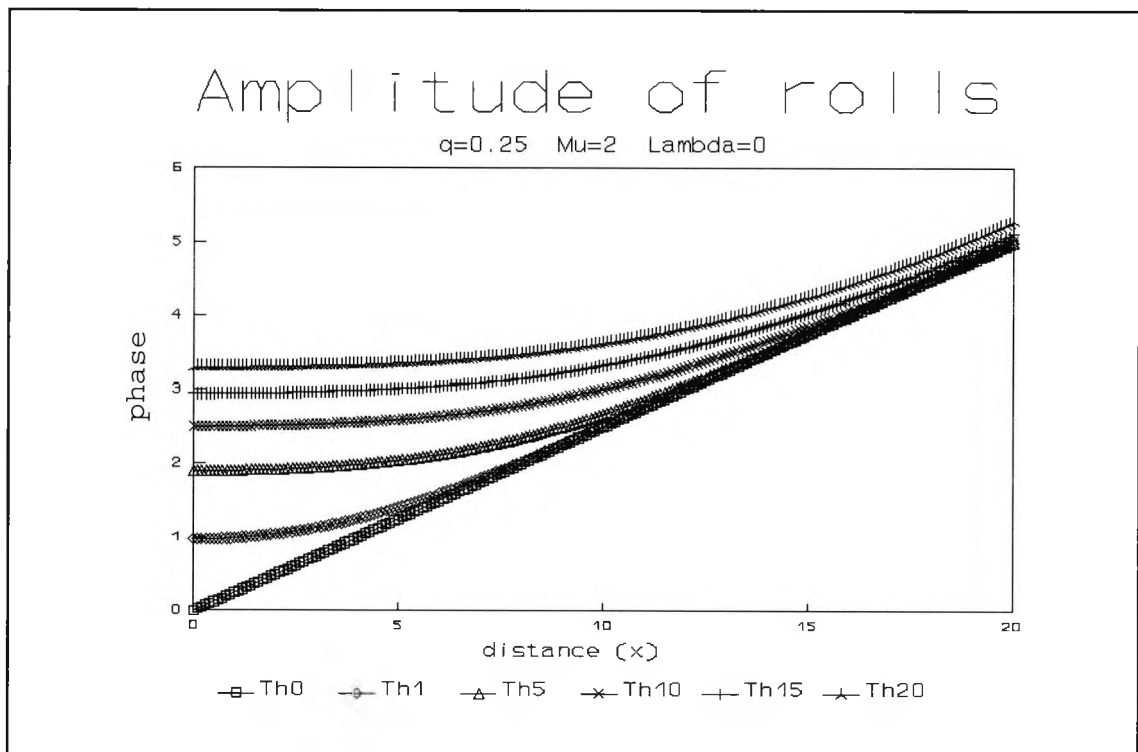
Fig. 4.44 : Numerical evolution for $q=0.25$, $\mu=2$ and $\lambda=0$ showing the phase of x-rolls at successive times τ

146
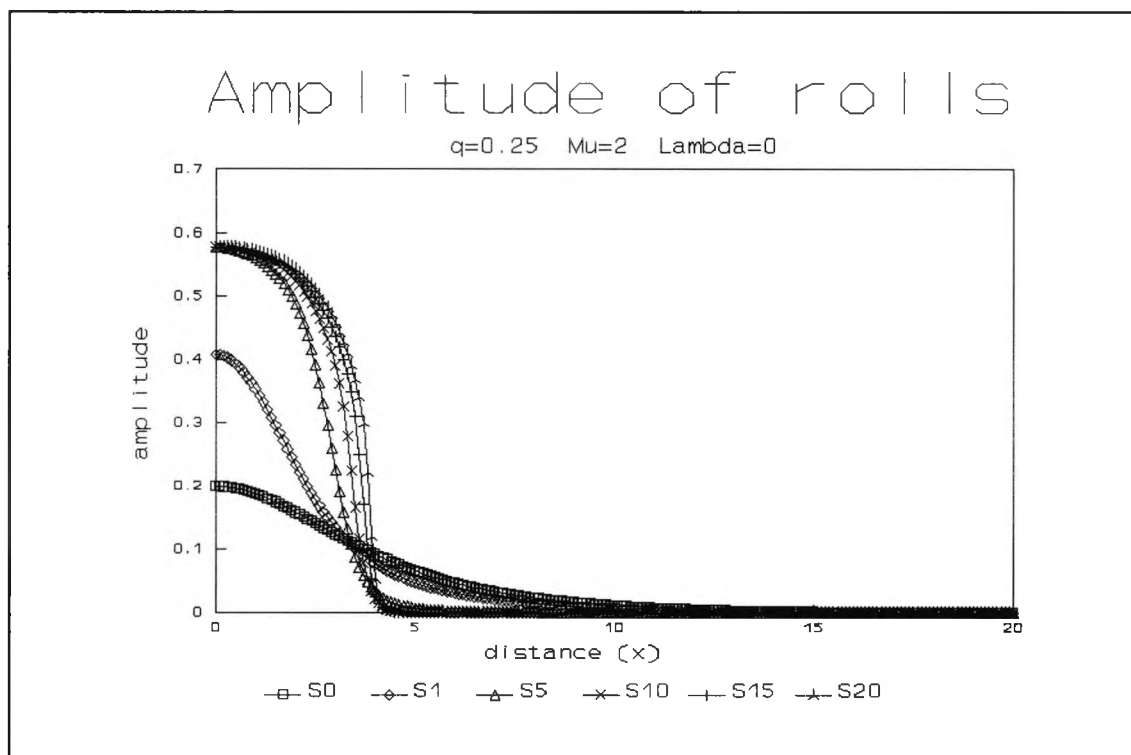
Fig. 4.45 : Numerical evolution for $q=0.25$, $\mu=2$ and $\lambda=0$ showing the amplitude of y-rolls at successive times τ
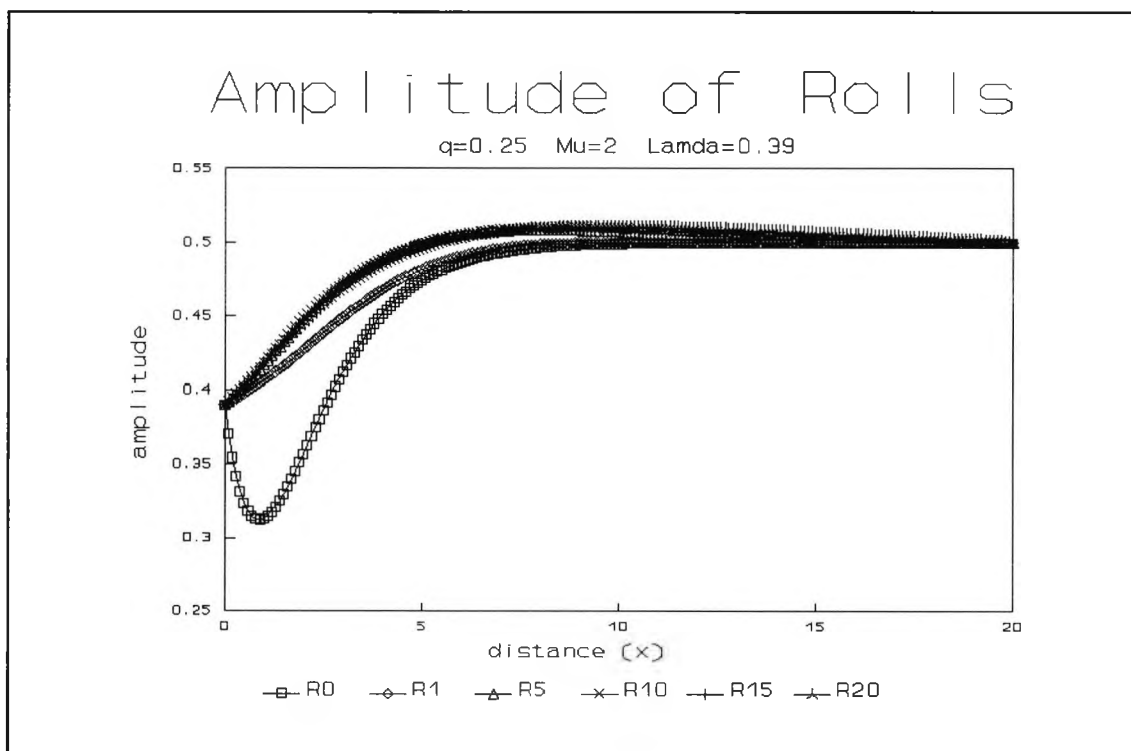
Fig. 4.46 : Numerical evolution for $q=0.25$, $\mu=2$ and $\lambda=0.39$ showing the amplitude of x-rolls at successive times τ

147
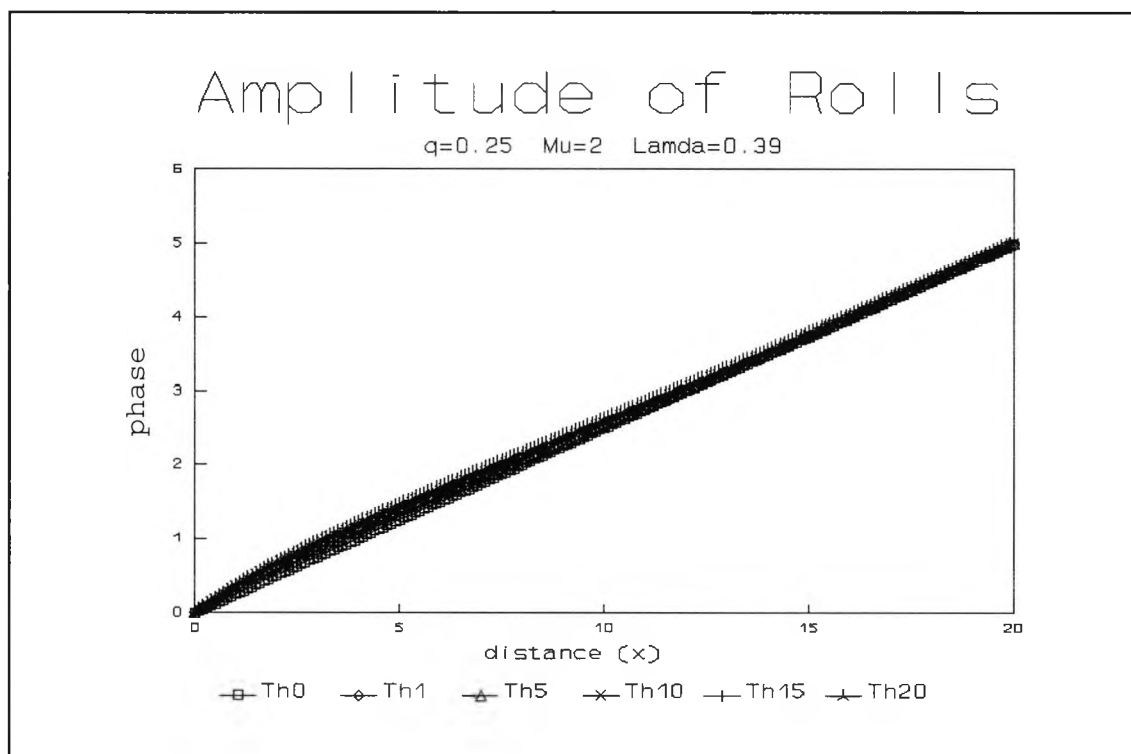
Fig. 4.47 : Numerical evolution for $q=0.25$, $\mu=2$ and $\lambda=0.39$ showing the phase of x-rolls at successive times τ
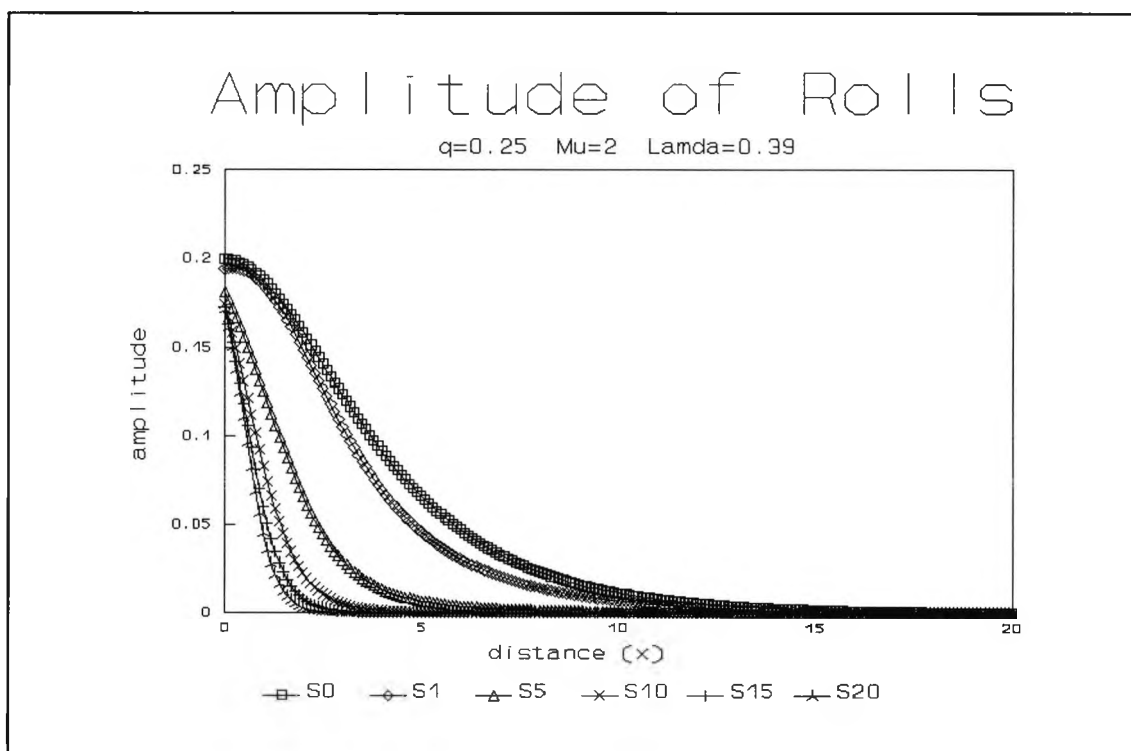
Fig. 4.48 : Numerical evolution for $q=0.25$, $\mu=2$ and $\lambda=0.39$ showing the amplitude of y-rolls at successive times τ

148
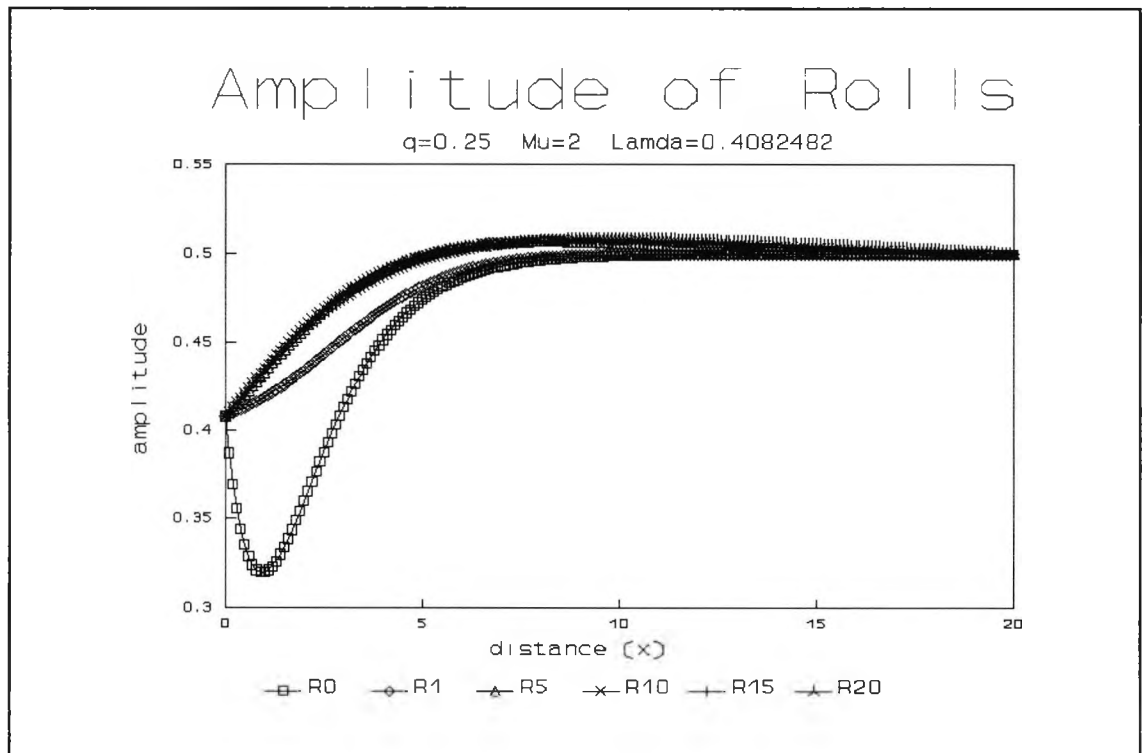
Fig. 4.49 : Numerical evolution for $q=0.25$, $\mu=2$ and $\lambda=0.4082$ showing the amplitude of x-rolls at successive times τ
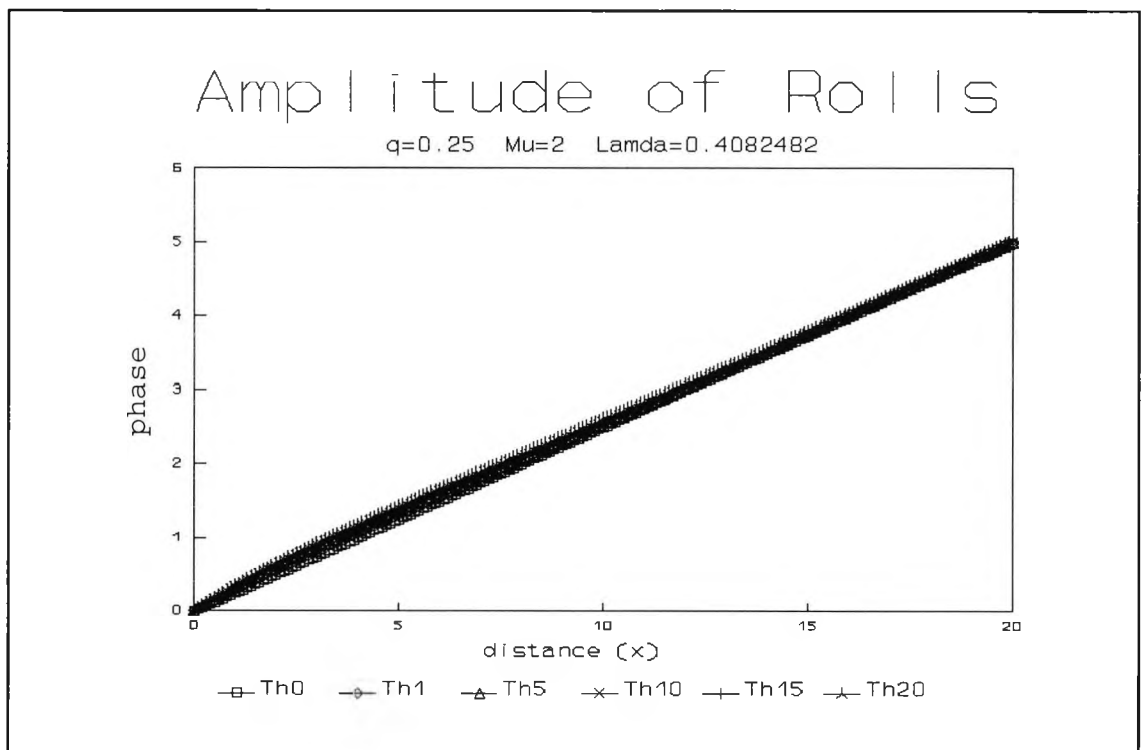
Fig. 4.50 : Numerical evolution for $q=0.25$, $\mu=2$ and $\lambda=0.4082$ showing the phase of x-rolls at successive times τ

149
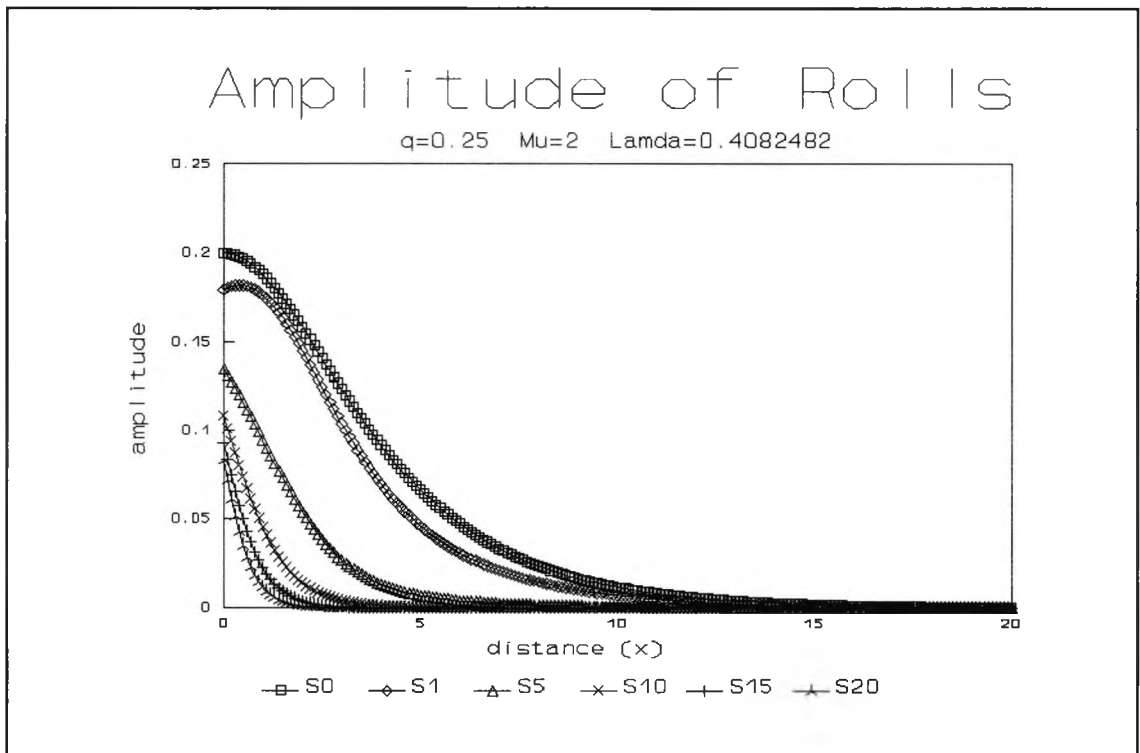
Fig. 4.51 : Numerical evolution for $q=0.25$, $\mu=2$ and $\lambda=0.4082$ showing the amplitude of y-rolls at successive times τ
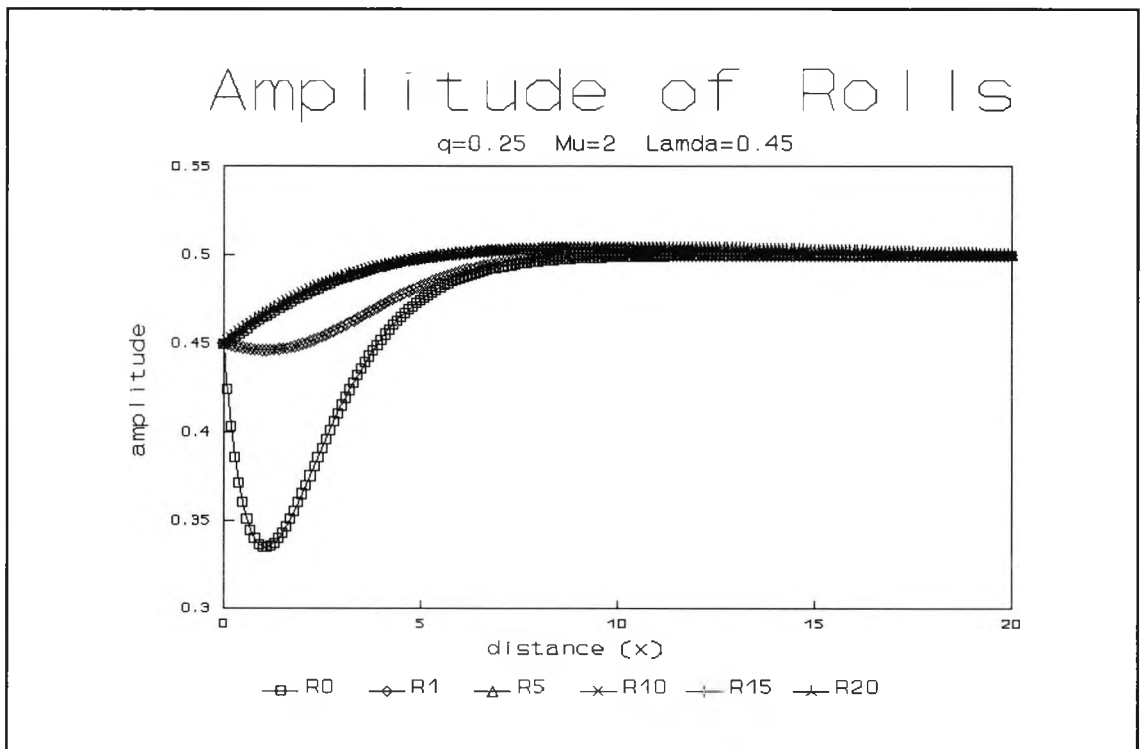
Fig. 4.52 : Numerical evolution for $q=0.25$, $\mu=2$ and $\lambda=0.45$ showing the amplitude of x-rolls at successive times τ

150
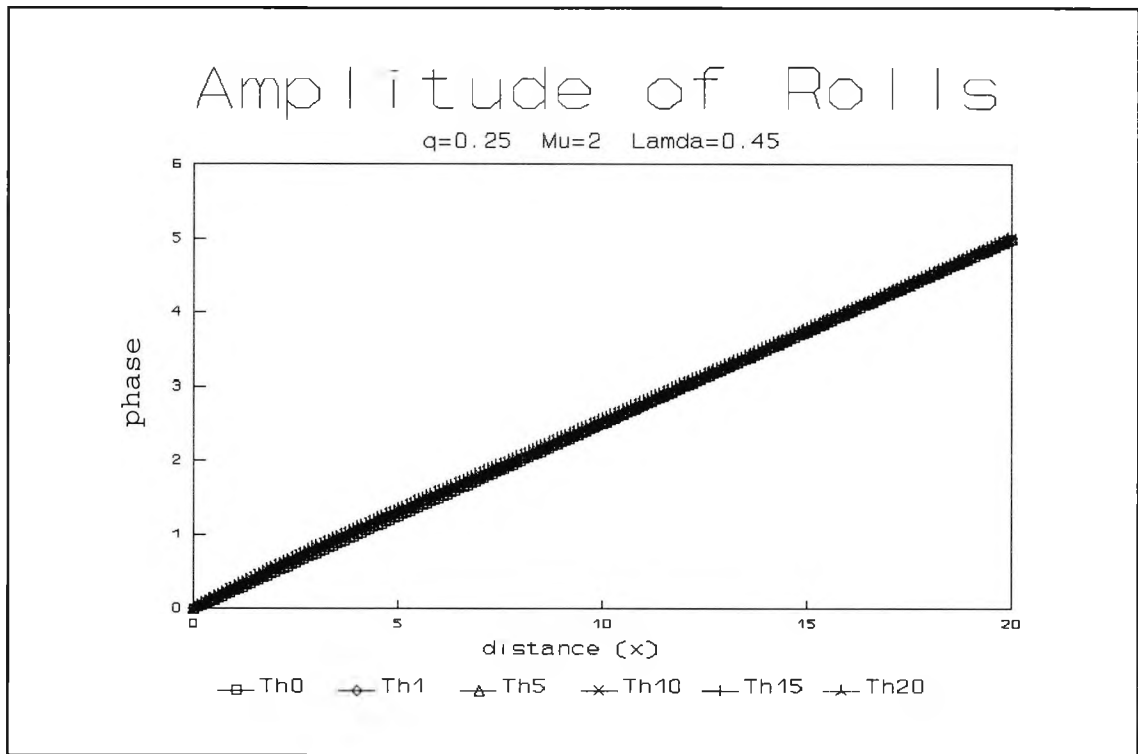
Fig. 4.53 : Numerical evolution for $q=0.25$, $\mu=2$ and $\lambda=0.45$ showing the phase of x-rolls at successive times τ
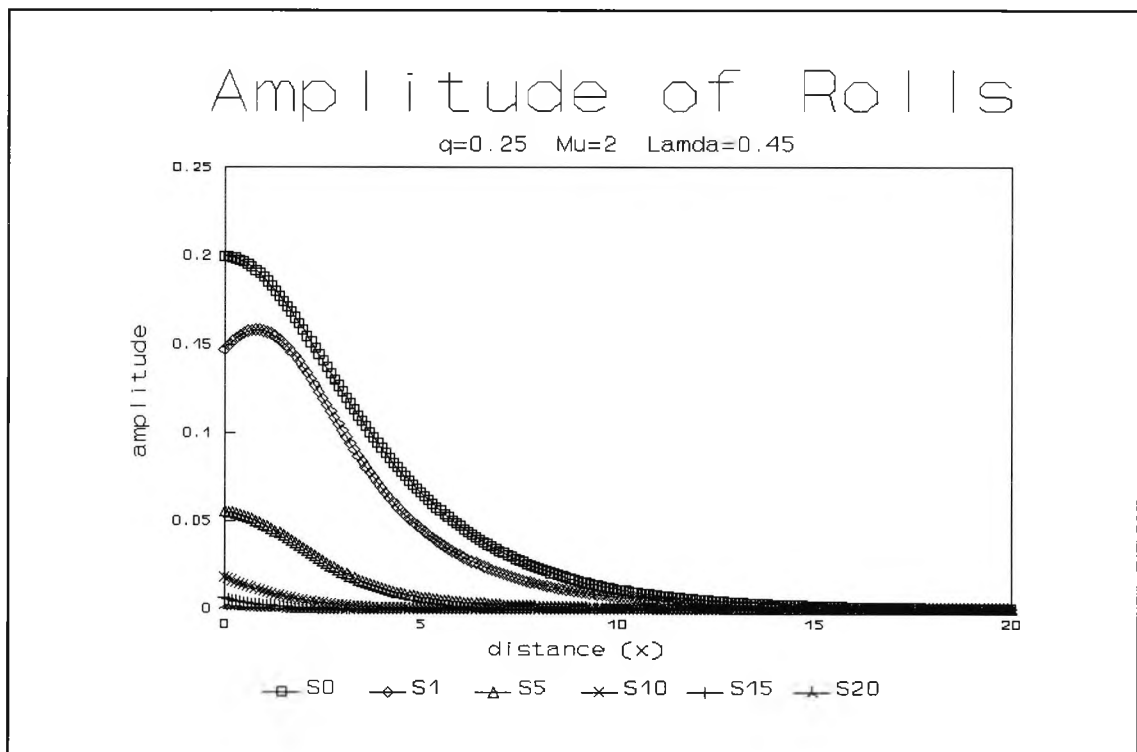
Fig. 4.54 : Numerical evolution for $q=0.25$, $\mu=2$ and $\lambda=0.45$ showing the amplitude of y-rolls at successive times τ

151
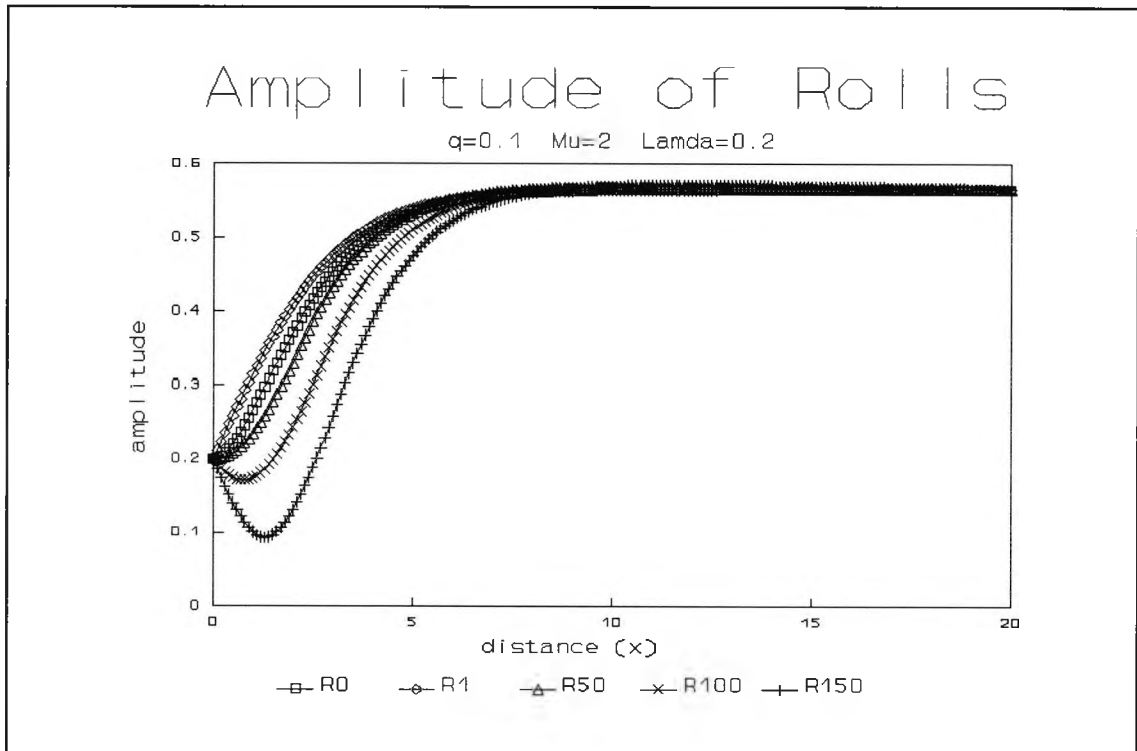
Fig. 4.55 : Numerical evolution for $q=0.1$, $\mu=2$ and $\lambda=0.2$ showing the amplitude of x-rolls at successive times τ
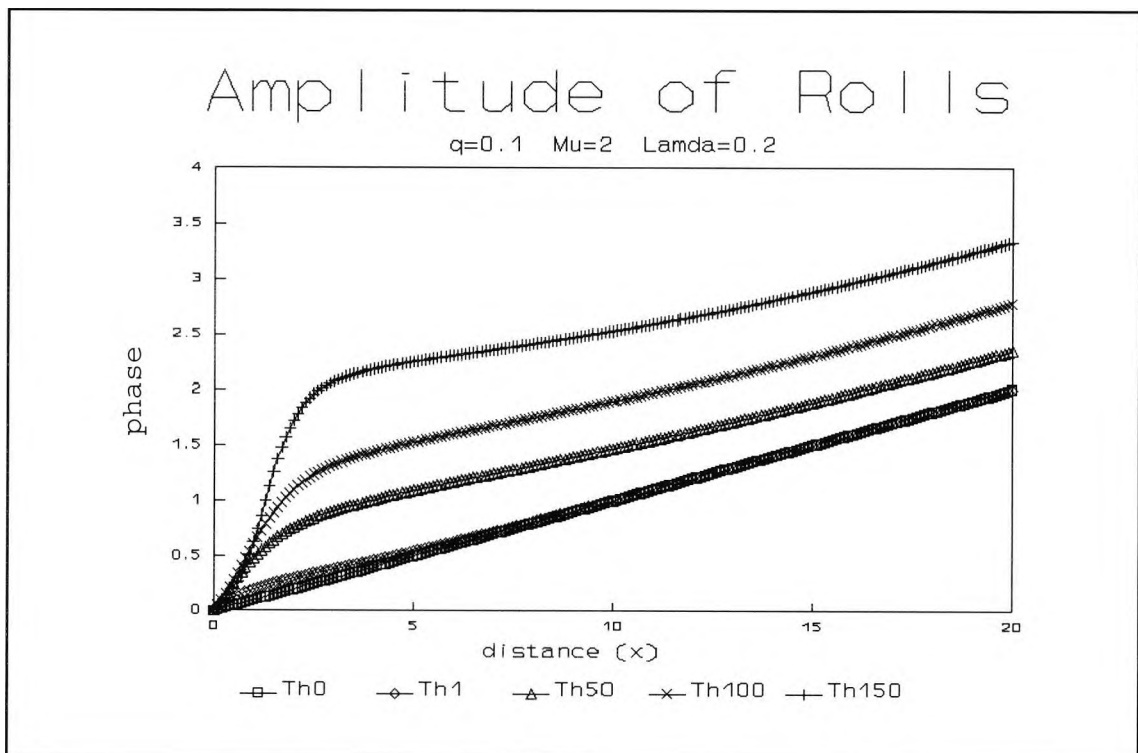
Fig. 4.56 : Numerical evolution for $q=0.1$, $\mu=2$ and $\lambda=0.2$ showing the phase of x-rolls at successive times τ

152
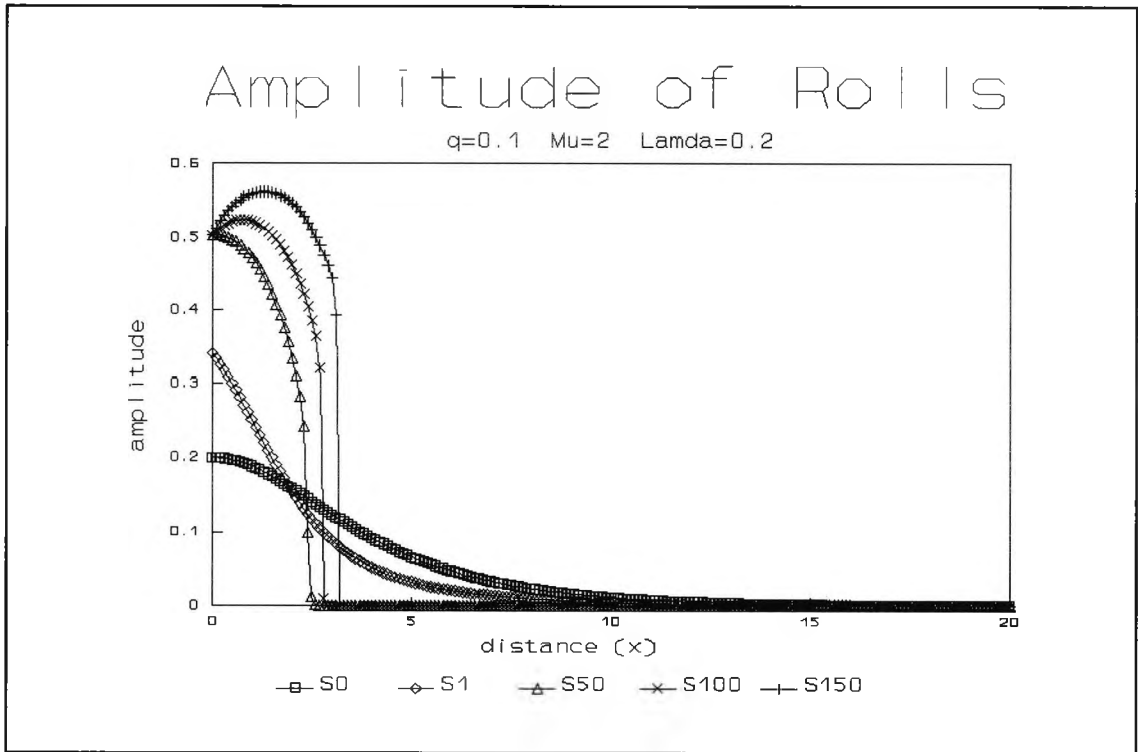
Fig. 4.57 : Numerical evolution for $q=0.1$, $\mu=2$ and $\lambda=0.2$ showing the amplitude of y-rolls at successive times τ
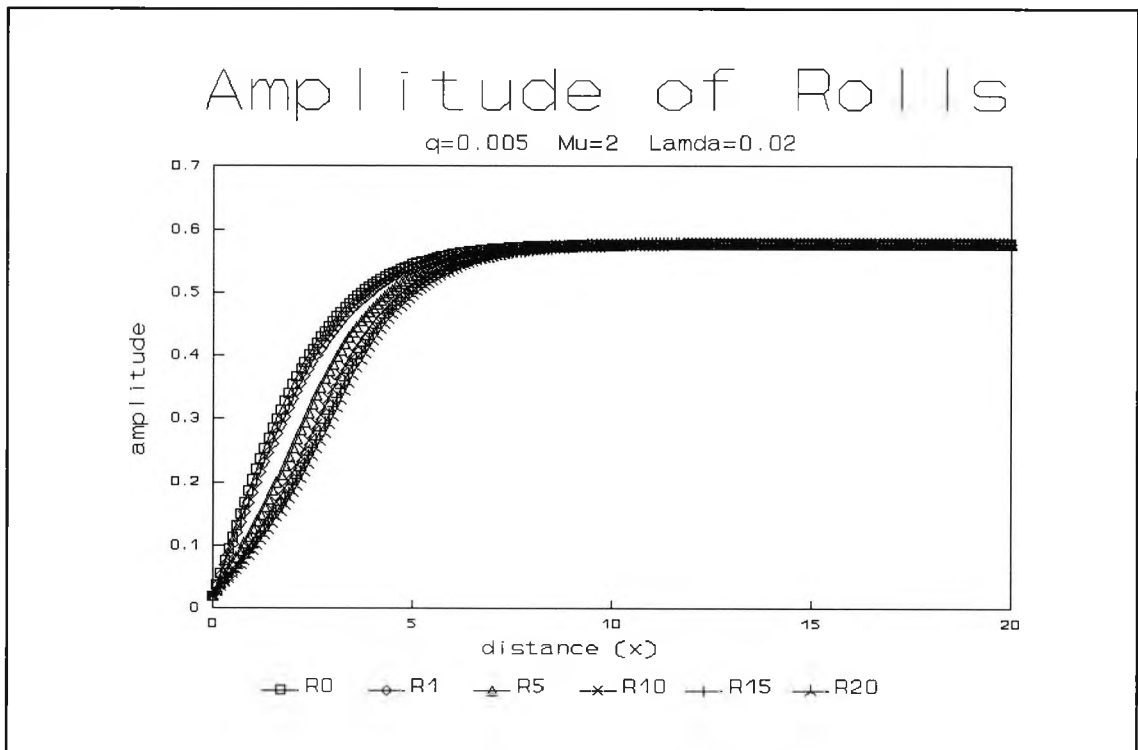
Fig. 4.58 : Numerical evolution for $q=0.005$, $\mu=2$ and $\lambda=0.02$ showing the amplitude of x-rolls at successive times τ

153
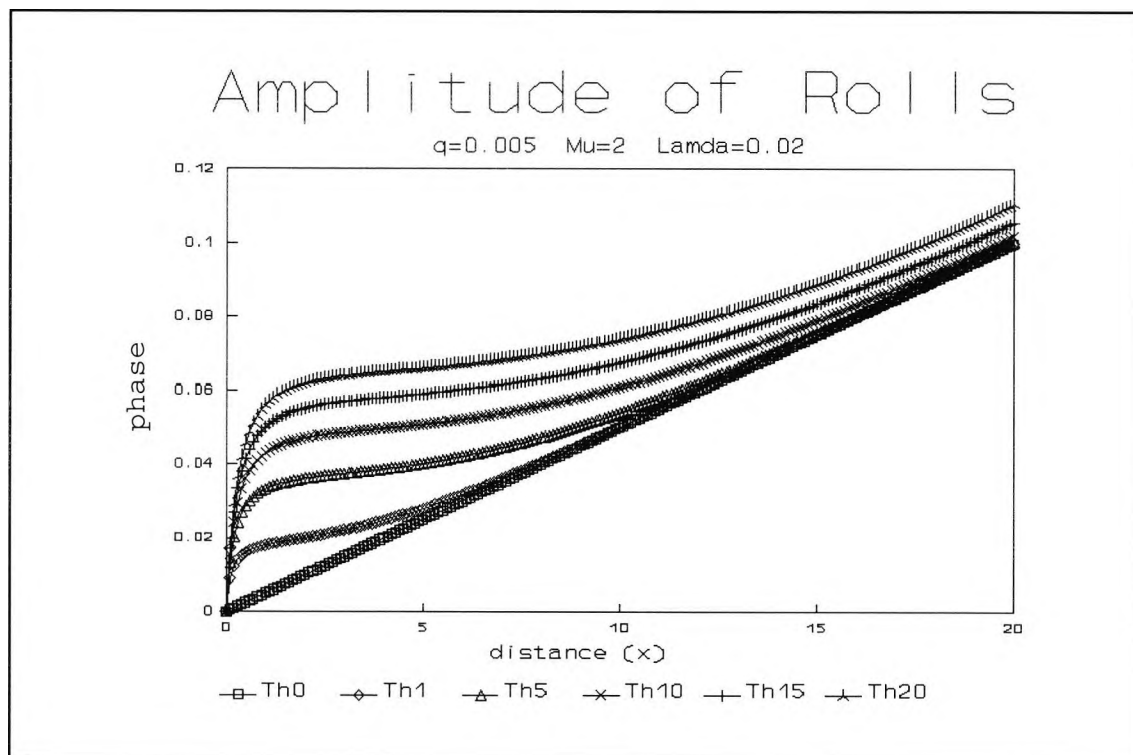
Fig. 4.59 : Numerical evolution for $q=0.005$, $\mu=2$ and $\lambda=0.02$ showing the phase of x-rolls at successive times τ
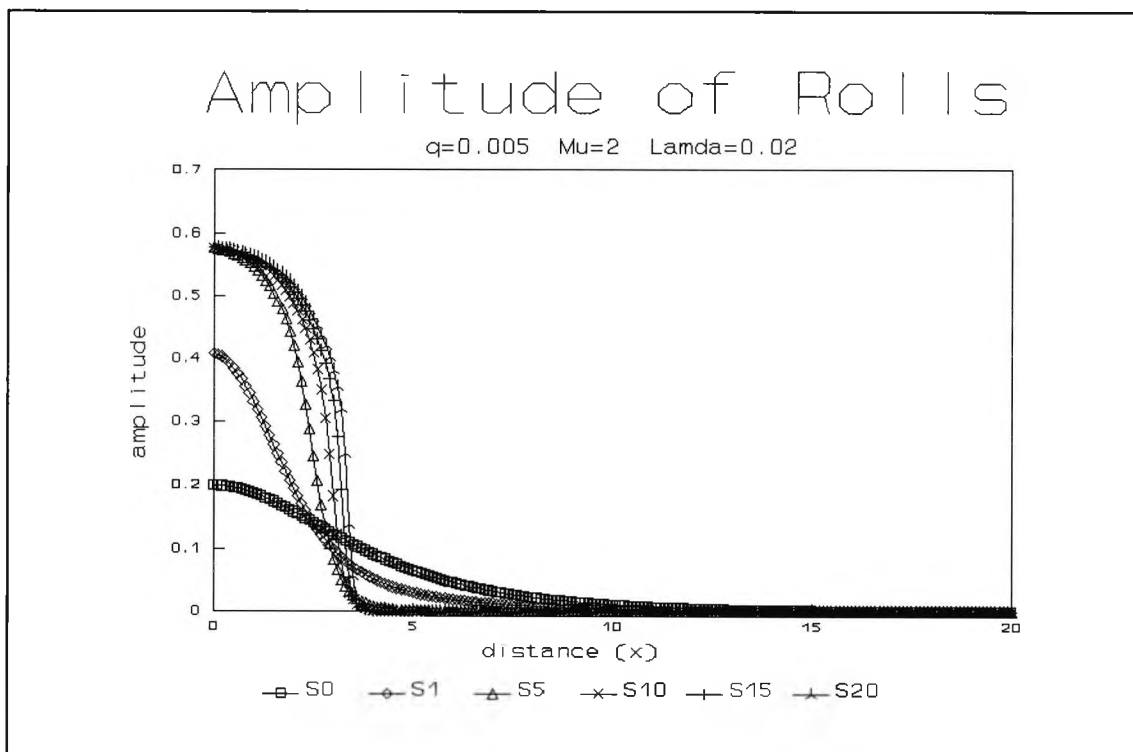
Fig. 4.60 : Numerical evolution for $q=0.005$, $\mu=2$ and $\lambda=0.02$ showing the amplitude of y-rolls at successive times τ

154
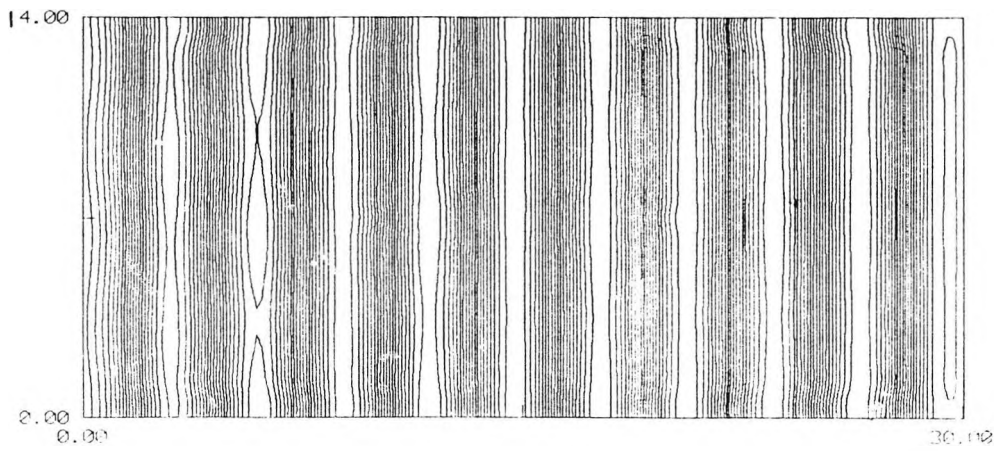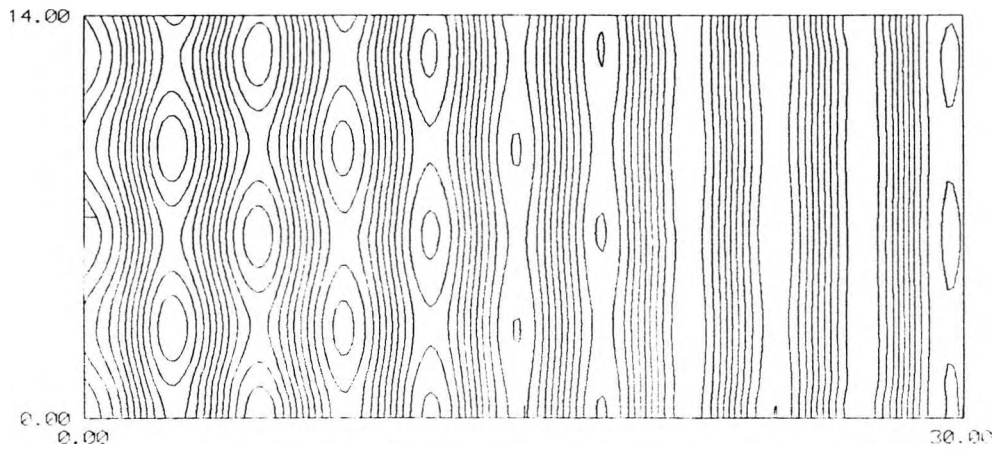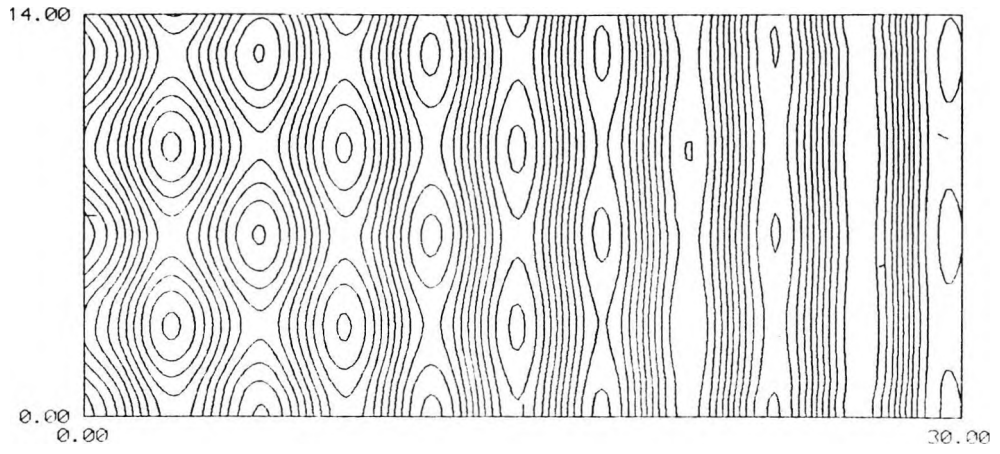
Fig. 4.61 : Contours of ψ at times $\tau=0$, 1 and 5 for q=0.2, $\mu=2.0$, $\lambda=0.5$

155
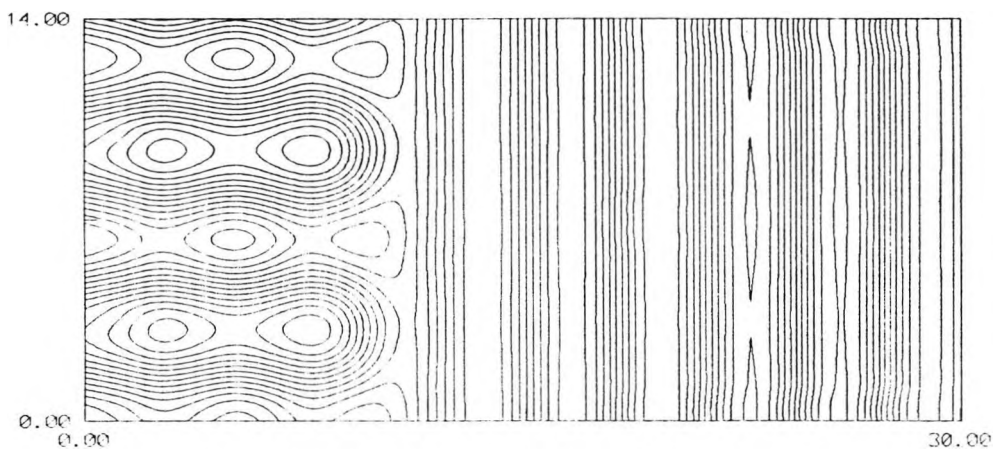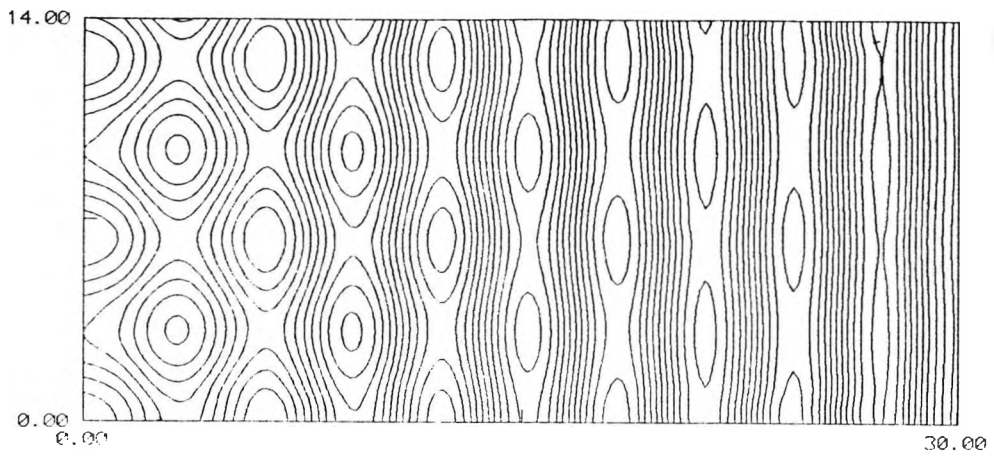
Fig. 4.62 : Contours of ψ at times $\tau=0$ and 150 for q=0.1, $\mu=2.0$, $\lambda=0.2$

156
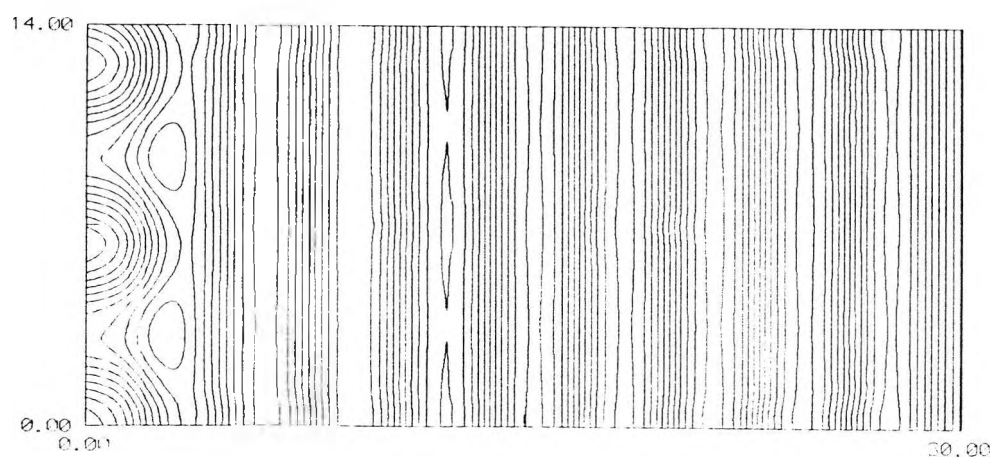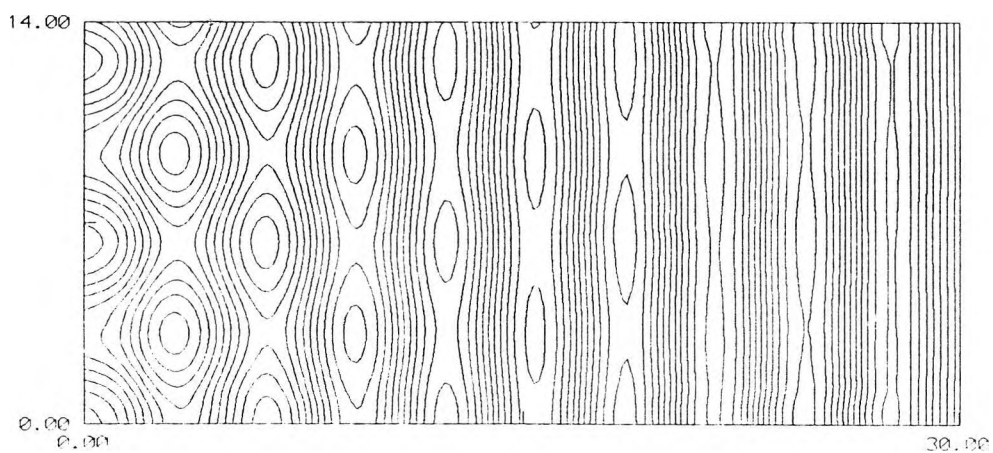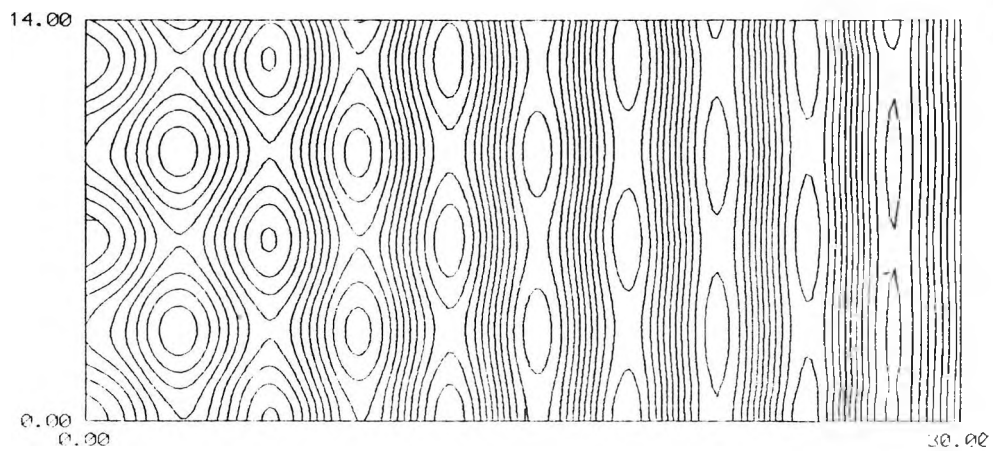
Fig. 4.63 : Contours of ψ at times $\tau=0$, 1 and 50 for q=0.05, $\mu=2.0$, $\lambda=0.3$

Chapter 5

Variation in the wavelength of the *y*-roll pattern with lateral forcing

5.1 Introduction

The nonlinear evolution of the system (2.2.23), (2.2.24), (2.2.29), (2.2.31) and (2.2.32) was investigated in chapter 2 allowing for only amplitude modulation of the orthogonal roll solutions. In this chapter frequency modulation of the *y*-roll pattern is incorporated to determine how the transition point X_0 and the solutions for A and B are affected for a range of wavenumbers in the *y* direction close to the critical value.

In section 5.2 the relevant amplitude equations and boundary conditions are set out. Attention is focused on the case where A is real and $\mu = 2$ although the results could easily be extended to include other values of μ and complex amplitude functions in the manner described in chapters 2 and 4. The nonlinear evolution of an initial disturbance is studied in section 5.3, together with the determination of steady-state solutions for A and B. In section 5.4 the nonlinear evolution of an initial disturbance is studied numerically using an explicit finite difference scheme. Section 5.5 contains a discussion of the results of this chapter.

5.2 Formulation

The amplitude equations derived in sections 2.2 and 2.3 were studied in chapters 2, 3 and 4 assuming $\tilde{A}$ and $\tilde{B}$ to be independent of *y*. The main outer problem is now formulated by setting $\tilde{A} = \epsilon^{1/2} A(X,Y,\tau)$, $\tilde{B} = \epsilon^{1/2} B(X,Y,\tau)$, $x = \epsilon^{-1/2} X$, $y = \epsilon^{-1/2} Y$ and $t = \epsilon^{-1}\tau$ so that the amplitude functions A and B are allowed to depend on the slow spatial variable Y as well as X and τ. With $\mu = 2$, it follows from (2.2.23), (2.2.24), (2.2.29) and (2.2.32) that to a first approximation A and B satisfy the equations

158

$$\frac{\partial A}{\partial \tau} = 4\frac{\partial^2 A}{\partial X^2} + A - 3A|A|^2 - 6A|B|^2 \quad , \tag{5.2.1}$$

$$\frac{\partial B}{\partial \tau} = 4\frac{\partial^2 B}{\partial Y^2} + B - 3B|B|^2 - 6B|A|^2 \quad , \tag{5.2.2}$$

to be solved subject to the boundary conditions

$$A = \lambda \quad \text{at} \quad X = 0 \quad , \tag{5.2.3}$$

$$A \rightarrow \frac{1}{\sqrt{3}} \quad , \quad B \rightarrow 0 \quad \text{as} \quad X \rightarrow \infty \quad . \tag{5.2.4}$$

Note that as in the analysis of chapter 2, the fourth derivative of B with respect to X can be neglected at leading order in (2.2.24) and thus no boundary conditions are applied on B at $X=0$ in the solution of (5.2.2). The adjustment of $\bar{B}$ to the boundary conditions $\bar{B} = \partial\bar{B}/\partial x = 0$ at $x=0$ will again occur within a boundary layer region where $\bar{X} = O(1)$, or $x = O(\epsilon^{-1/4})$ on which scale the term $\partial^4 B/\partial\bar{X}^4$ and others will come into play in (5.2.2). Similarly, on the assumption that Y is of order one, the derivatives of A with respect to Y are neglected at leading order in (5.2.1).

In order to investigate the effect of frequency modulation of the y-roll pattern in the y direction, it is assumed that B is of the form

$$B = \dot{B}(X,\tau)e^{i\delta Y} \quad , \tag{5.2.5}$$

where $\dot{B}$ is real, and it follows that a solution for A may be assumed in the form

$$A = A(X,\tau) \quad , \tag{5.2.6}$$

where A is real. The parameter δ represents an adjustment to the wavelength of the y-roll pattern in the neighbourhood of the critical value. Substitution of (5.2.5) and (5.2.6) into (5.2.1) and (5.2.2) shows that A and $\dot{B}$ satisfy

$$\frac{\partial A}{\partial \tau} = 4\frac{\partial^2 A}{\partial X^2} + A - 3A^3 - 6A\dot{B}^2 \quad , \tag{5.2.7}$$

$$\frac{\partial \dot{B}}{\partial \tau} = \dot{B}(1 - 4\delta^2 - 6A^2) - 3\dot{B}^3 \quad , \tag{5.2.8}$$

with boundary conditions

$$A = \lambda \quad \text{at} \quad X = 0 \quad , \tag{5.2.9}$$

$$A \to \frac{1}{\sqrt{3}} \quad , \quad \dot{B} \to 0 \quad \text{as} \quad X \to \infty \quad . \tag{5.2.10}$$

Solutions for positive initial profiles

$$A = A_0(X) \quad , \quad \dot{B} = \dot{B}_0(X) \quad \text{at} \quad \tau = 0 \tag{5.2.11}$$

and positive values of λ, will be studied.

5.3 Nonlinear evolution and steady-state solutions

Steady-state solutions of the system (5.2.7)-(5.2.11) exist when $\dot{B}=0$ and are given by

$$A = A_0(X) = \frac{1}{\sqrt{3}}\tanh\left[\frac{c_1 + X}{2\sqrt{2}}\right] \quad \text{for} \quad \lambda < \frac{1}{\sqrt{3}} \quad , \tag{5.3.1}$$

$$A = A_0(X) = \frac{1}{\sqrt{3}}\coth\left[\frac{c_2 + X}{2\sqrt{2}}\right] \quad \text{for} \quad \lambda > \frac{1}{\sqrt{3}} \quad , \tag{5.3.2}$$

where $c_1 = 2\sqrt{2}\tanh^{-1}(\sqrt{3}\lambda)$ and $c_2 = 2\sqrt{2}\coth^{-1}(\sqrt{3}\lambda)$, as in the analysis of chapter 2.

The instability of this x-roll solution to cross-rolls is shown by considering a small y-roll disturbance of the form

$$\dot{B} = \dot{B}_0(X)e^{\sigma(X)\tau} \quad , \quad \text{where} \quad \dot{B}_0 \ll 1 \quad . \tag{5.3.3}$$

Substitution into (5.2.8) shows that

$$\sigma(X) = 1 - 4\delta^2 - 6A_0^2(X) \quad . \tag{5.3.4}$$

Clearly y-rolls will grow in any region where $A_0 < [(1-4\delta^2)/6]^{1/2}$ and the x-roll solution will be unstable. Hence the nonlinear system (5.2.7)-(5.2.11) can be expected to evolve to the solution (5.3.1) or (5.3.2) as $\tau \to \infty$ when $\lambda > [(1-4\delta^2)/6]^{1/2}$, but when $\lambda < [(1-4\delta^2)/6]^{1/2}$ the solution (5.3.1) will be affected by the amplification of y-rolls in the region where $A_0 < [(1-4\delta^2)/6]^{1/2}$. In this case, a new steady solution consisting of a combination of x and y-rolls is expected to evolve in the region near the wall (region I), where the relevant steady-state solution of (5.2.8) is

$$\dot{B}^2 = \frac{1}{3}(1 - 4\delta^2 - 6A^2) \quad . \tag{5.3.5}$$

Substitution of this into the steady-state form of (5.2.7) results in the equation

$$4\frac{\partial^2 A}{\partial X^2} - A + 9A^3 + 8\delta^2 A = 0 \quad , \quad \lambda < A < \left[\frac{1-4\delta^2}{6}\right]^{1/2} \quad . \tag{5.3.6}$$

It is expected that a position $X = X_0$ exists at which $A = [(1-4\delta^2)/6]^{1/2}$ and there is a transition from the steady-state form of (5.2.7) where (5.3.5) is valid to the steady-state form of (5.2.7) where $\dot{B} = 0$ and $A > [(1-4\delta^2)/6]^{1/2}$. Substitution of $\dot{B} = 0$ into the steady-state form of (5.2.7) shows that in this region away from the wall where $X > X_0$ (region II), A satisfies

$$4\frac{\partial^2 A}{\partial X^2} + A - 3A^3 = 0 \quad , \quad \left[\frac{1-4\delta^2}{6}\right]^{1/2} < A < \frac{1}{\sqrt{3}} \tag{5.3.7}$$

and the relevant solution is

$$A = \frac{1}{\sqrt{3}}\tanh\left[\frac{X-X_0+c}{2\sqrt{2}}\right] \quad , \tag{5.3.8}$$

where $c = 2\sqrt{2}\tanh^{-1}\{\sqrt{[(1-4\delta^2)/2]}\}$. At $X = X_0$, $A = [(1-4\delta^2)/6]^{1/2}$ and differentiation of (5.3.8) gives

161

$$\frac{\partial A}{\partial X} = \frac{1}{4\sqrt{6}}(1+4\delta^2) \quad \text{at} \quad X = X_0 \quad . \tag{5.3.9}$$

Equation (5.3.6) for $X < X_0$ can now be integrated once to give

$$\left(\frac{\partial A}{\partial X}\right)^2 = \frac{(1-8\delta^2)A^2}{4} - \frac{9A^4}{8} + D \tag{5.3.10}$$

and, by using continuity of A and $\partial A/\partial X$ at X_0, it is found that

$$D = \frac{\delta^2}{3}(1-2\delta^2) \quad . \tag{5.3.11}$$

A further integration of (5.3.6), together with application of the boundary condition at $X=0$, yields

$$\int_\lambda^A \frac{dA}{\left(\dfrac{\delta^2(1-2\delta^2)}{3} + \dfrac{(1-8\delta^2)A^2}{4} - \dfrac{9A^4}{8}\right)^{1/2}} = X \quad . \tag{5.3.12}$$

Finally, the transition point X_0 is determined by setting $A = [(1-4\delta^2)/6]^{1/2}$ to give

$$\int_\lambda^{\sqrt{\frac{1-4\delta^2}{6}}} \frac{dA}{\left(\dfrac{\delta^2(1-2\delta^2)}{3} + \dfrac{(1-8\delta^2)A^2}{4} - \dfrac{9A^4}{8}\right)^{1/2}} = X_0 \quad . \tag{5.3.13}$$

This integral cannot be found analytically in general, but a numerical method of integration based on a Romberg technique gives the results shown in Table 5.1 for a range of values of λ and δ^2.

It is seen that $X_0 \to 0$ as $\lambda \to [(1-4\delta^2)/6]^{1/2}$ and the y-rolls are then confined to a region close to the wall. For $\delta = 0$ the result of Daniels and Weinstein (1992) is recovered, equivalent to the formula (2.6.8) for X_0 obtained in chapter 2 with $\mu = 2$. As δ^2 increases in value, X_0 decreases and reaches zero when $\delta^2 = 1/4$. For values of δ^2 close to 1/4, so that $\delta = (1/2)-\bar{\delta}$ with $\bar{\delta} \ll 1$, it

162

may be assumed that $\lambda = \lambda_0 \bar{\delta}^{1/2}$ with λ_0 finite and then the result (5.3.13) shows that to a first approximation the transition point is located at

$$X_0 \approx \bar{\delta}^{1/2}(4 - 2\sqrt{6}\lambda_0) \quad , \quad \lambda_0 < 2/\sqrt{6} \quad . \tag{5.3.14}$$

Note that if $\delta^2 > 0$, X_0 does not tend to infinity as $\lambda \to 0$, unlike the situation considered in chapter 2 where $\delta = 0$ and X_0 has a logarithmic behaviour as $\lambda \to 0$. With $\delta^2 > 0$ the transition point is located at a finite distance from the wall when $\lambda = 0$ and the gradient of A at $X = 0$ remains non-zero, being given from (5.3.10) by

$$\frac{\partial A}{\partial X}(X=0) = \left(\frac{\delta^2(1-2\delta^2)}{3} + \frac{(1-8\delta^2)\lambda^2}{4} - \frac{9\lambda^4}{8} \right)^{1/2} , \tag{5.3.15}$$

for general values of λ. Figure 5.1 shows X_0 and $\partial A/\partial X$ ($X=0$) as functions of δ^2 for $\lambda = 0$.

5.4 Numerical solution

The system (5.2.7)-(5.2.11) was solved numerically using the explicit finite difference scheme of chapter 2, modified to incorporate the term involving δ^2. The finite difference approximations to (5.2.7) and (5.2.8) become

$$a_{i,j+1} = \beta \left[4a_{i+1,j} + a_{i,j}\left(h^2 - 3h^2 a_{i,j}^2 - 8 - 6h^2 b_{i,j}^2 + \frac{1}{\beta} \right) + 4a_{i-1,j} \right] , \tag{5.4.1}$$

$$b_{i,j+1} = k b_{i,j}\left[1 - 4\delta^2 - 3b_{i,j}^2 - 6a_{i,j}^2 + \frac{1}{k} \right] , \tag{5.4.2}$$

where $\beta = k/h^2$ and h and k are the step sizes in X and τ respectively, with $a_{i,j}$ and $b_{i,j}$ now denoting the values of A and B at $X = ih$ and $\tau = jk$. The end values are found from the boundary conditions

$$a_{0,j+1} = \lambda \quad , \quad a_{N,j+1} = \frac{1}{\sqrt{3}} \qquad \text{for} \quad j = 0,1... \tag{5.4.3}$$

and then (5.4.1) and (5.4.2) are applied with $j = 0,1,2...$ to obtain the solution at successive

163

time steps. Thus the solution is computed by marching forwards in time, starting from appropriate initial profiles at $\tau=0$. These were chosen to be

$$A_0(X) = \frac{1}{\sqrt{3}}\tanh\left(\frac{X}{2\sqrt{2}}\right)+\lambda e^{-X} \quad , \quad \dot{B}_0(X) = \dot{\delta}\operatorname{sech}\left(\frac{X}{2\sqrt{2}}\right) \quad . \tag{5.4.4}$$

Results are represented graphically in Figures 5.2 and 5.3 for $\dot{\delta}=0.2$, $\delta^2=0.1$ and $\lambda=0$. As $\tau\to\infty$, A reaches a steady-state solution, as seen in Figure 5.2, and X_0, defined as the point at which $A=[(1-4\delta^2)/6]^{1/2}=0.3162$ was found to be 1.9628 for $\tau=30$. For $X<X_0$, the y-rolls grow with time whereas for $X>X_0$ the y-rolls decay with time, in the manner anticipated from the analysis of section 5.3. For $X<X_0$ the stable steady-state solution consists of a combination of x and y-rolls whereas for $X>X_0$ the stable steady-state solution consists only of x-rolls. The value of X_0 obtained in the computation for $\tau=30$ compares well with the value $X_0=1.9612$ predicted by the analysis of section 5.3 (see Table 5.1).

Finally, the evolution of the roll pattern with time is illustrated graphically by contour plots of ψ for $\delta^2=0.1$ and $\lambda=0$ in Figure 5.4 using Surfer Version 4 by Golden Software. Here ψ is obtained from the formula

$$\psi = 2\epsilon^{1/2}\left[A\cos x + \dot{B}\cos\{(1+\delta\epsilon^{1/2})y\}\right] \tag{5.4.5}$$

and the value of ϵ was taken to be 0.1, with δ taking its positive value.

5.5 Discussion

When frequency modulation of y-rolls is incorporated in the theory, equivalent to an overall y-dependence in ψ of the form

$$\exp(iy+i\delta Y) = \exp[i(1+\delta\epsilon^{1/2})y] \quad , \tag{5.5.1}$$

it is found that for $0 \le \delta^2 \le 1/4$, the transition point X_0 at which the y-rolls disappear is a function of both λ and δ. For fixed δ, it has been shown analytically and confirmed numerically that if $0 \le \lambda < [(1-4\delta^2)/6]^{1/2}$, a stable steady-state solution will be obtained consisting of a combination of x and y-rolls in the region where $X < X_0$, and where $X > X_0$ the solution consists of x-rolls only. The transition point X_0 is given by (5.3.13), from which it can be deduced that as $\lambda \to [(1-4\delta^2)/6]^{1/2}$, $X_0 \to 0$ and the y-rolls then disappear.

The results show that if the value of δ can be freely selected, then the highest growth rate (5.3.4) corresponds to disturbances with the critical wavenumber ($\delta=0$) and that these also correspond to the situation where the transition point is located at the greatest distance from the wall; in general a solution of the type described here with δ non-zero will be unstable to y-rolls in the region where $[(1-4\delta^2)/6]^{1/2} < A < 1/\sqrt{6}$. Nevertheless, the influence of the wavelength of the roll pattern perpendicular to the wall is of intrinsic interest and the solutions described here may be relevant in situations where the value of δ is selected by the presence of lateral boundaries parallel to the x direction. The results of this chapter have only been obtained for $\mu=2$ and it has been assumed that A is real but they can be generalised in a straightforward manner to any value of μ and to complex values of A using the methods described in chapters 2 and 4.

δ^2	λ	X_0	$\partial A/\partial X\ (X=0)$
0.00	0.00	∞	0
0.00	0.20	1.9057	0.0906
0.00	0.40	0.0793	0.1058
0.00	0.60	-	-
0.05	0.00	2.7575	0.1225
0.05	0.20	1.2034	0.1386
0.05	0.36	0.0417	0.1247
0.05	0.40	-	-
0.10	0.00	1.9612	0.1633
0.10	0.20	0.7434	0.1639
0.10	0.30	0.1113	0.1485
0.10	0.32	-	-
0.15	0.00	1.4266	0.1871
0.15	0.20	0.3411	0.1766
0.15	0.25	0.0498	0.1658
0.15	0.30	-	-
0.20	0.00	0.9364	0.2000
0.20	0.10	0.4331	0.1959
0.20	0.18	0.0140	0.1843
0.20	0.20	-	-
0.24	0.00	0.4029	0.2040
0.24	0.05	0.1572	0.2025
0.24	0.08	0.0082	0.2002
0.24	0.10	-	-
0.25	0.00	0	0.2041

Table 5.1 : X_0 and $\partial A/\partial X\ (X=0)$ for a range of values of λ and δ^2

166
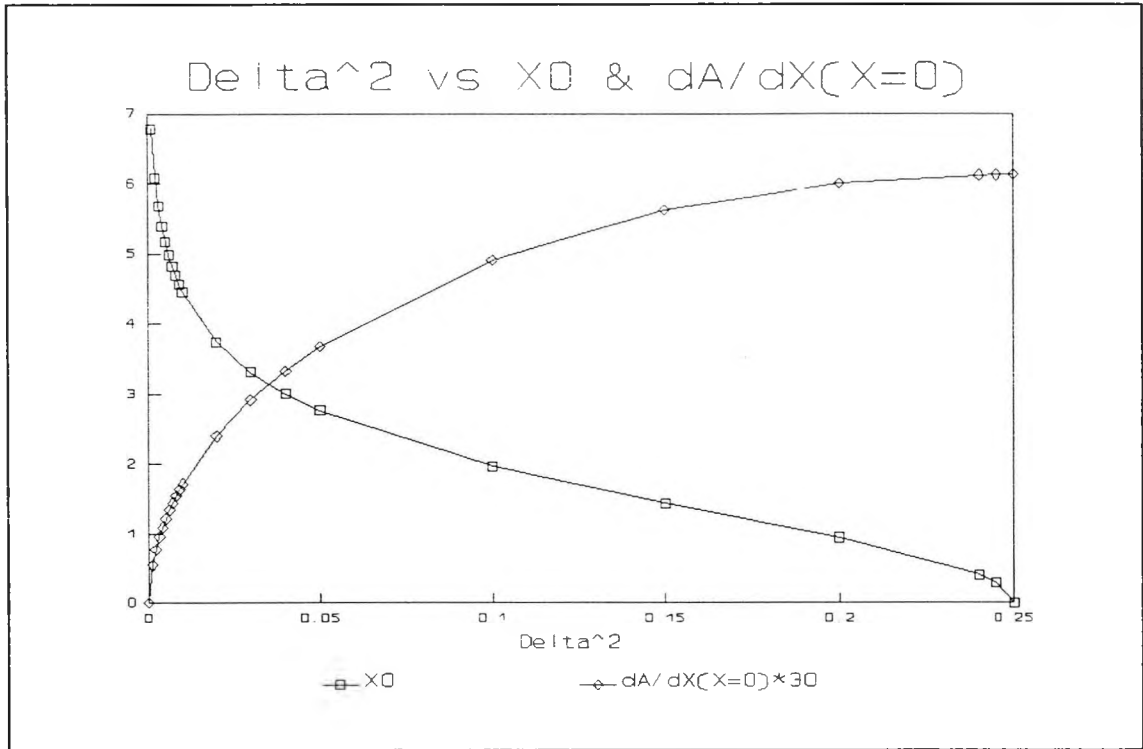
Fig. 5.1 : Graphs of X_0 and $\partial A/\partial X$ ($X=0$) versus δ^2 for $\lambda=0$
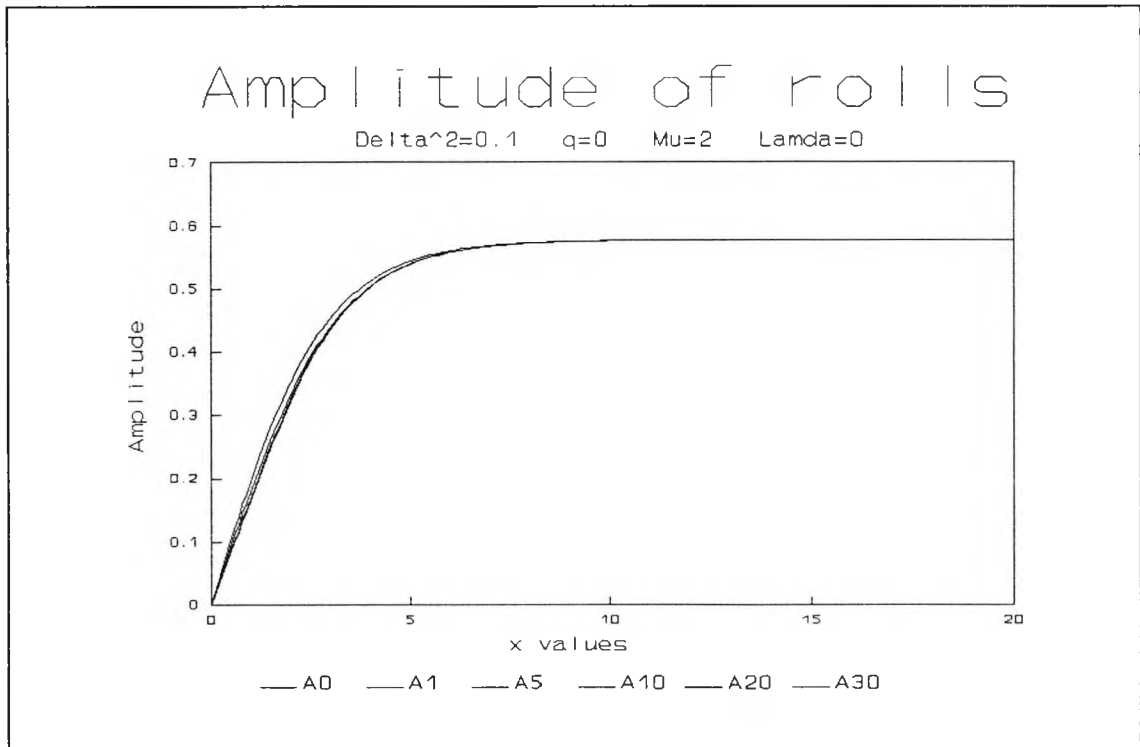
Fig. 5.2 : Amplitude of x-rolls when $\delta^2=0.1$, $q=0$, $\mu=2$ and $\lambda=0$ at successive times $\tau=0$, 1, 5, 10, 20, 30 indicated by $A0$, $A1$, $A5$, $A10$, $A20$, $A30$ respectively

167
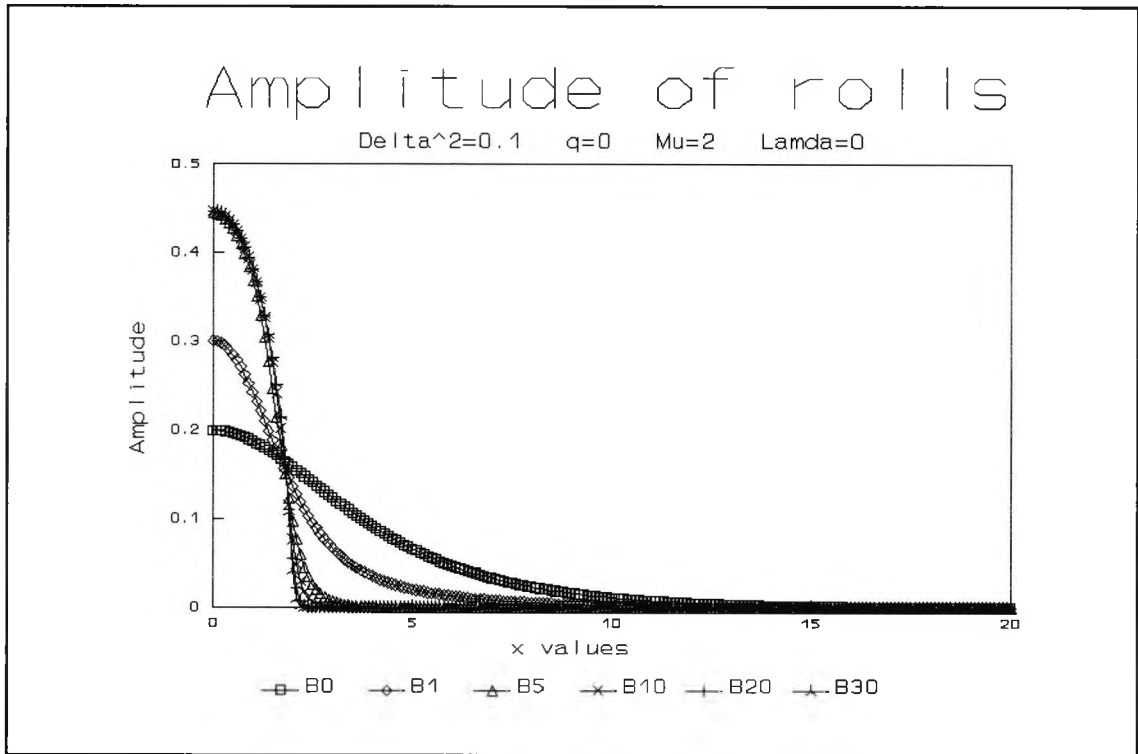
Fig. 5.3 : Amplitude of y-rolls with time when $\delta^2=0.1$, $q=0$, $\mu=2$ and $\lambda=0$
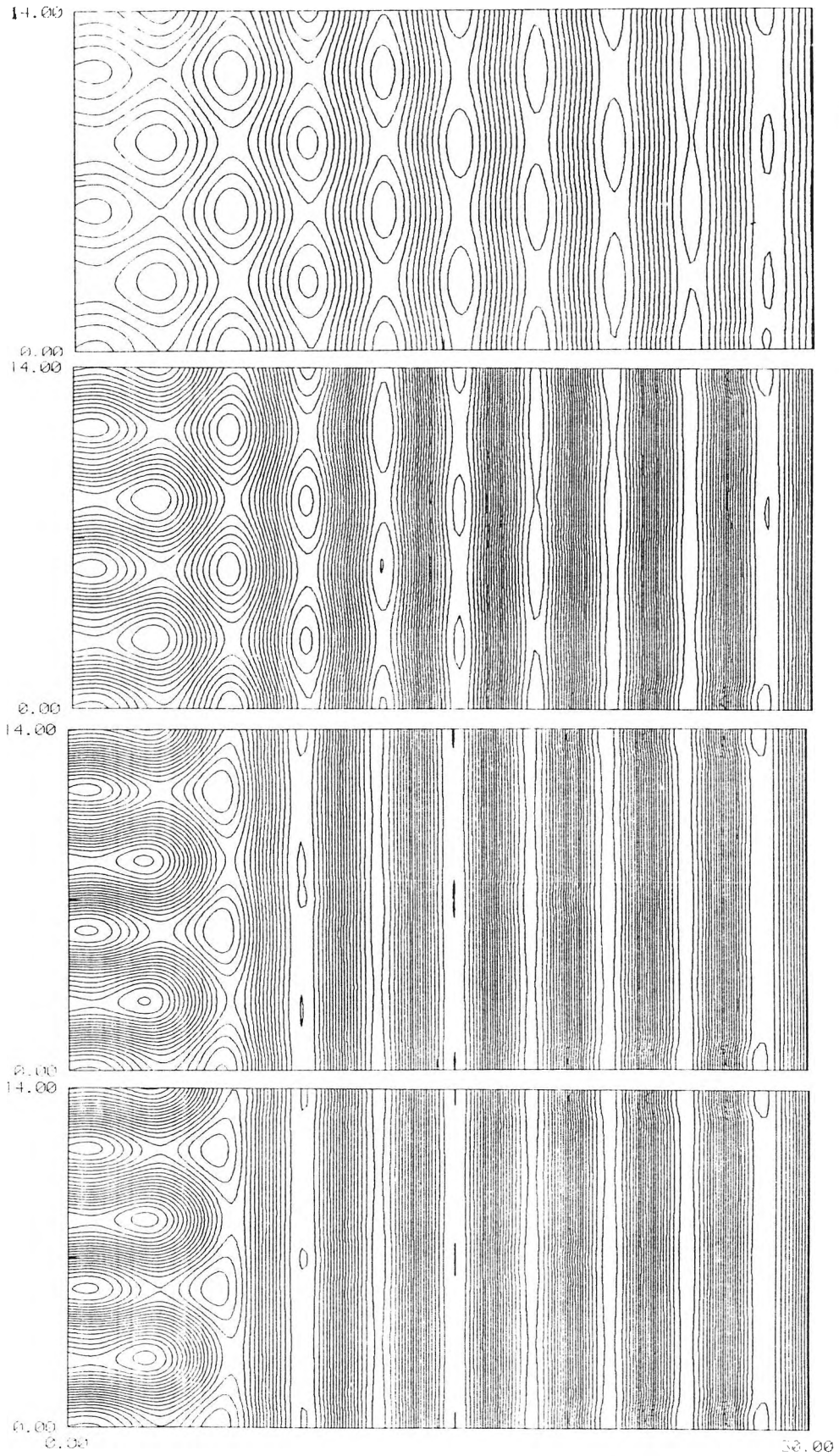
Fig. 5.4 : Contours of ψ at times $\tau=0$, 1, 5 and 20 for $\delta^2=0.1$, $\mu=2.0$, $\lambda=0$

169

Chapter 6

Variation in the wavelength of the x and y-roll pattern

without lateral forcing

6.1 Introduction

This chapter discusses the possibility of phase-winding solutions for the semi-infinite problem with one lateral wall for the case where there is no lateral forcing, $\lambda=0$. With no frequency modulation of the y-roll pattern ($\delta=0$) the logarithmic behaviour of the transition point X_0 as $\lambda\to0$ identified in chapter 4 makes a study of the situation where $\lambda=0$ particularly difficult. However, from chapter 5, it is known that when $\delta\neq0$, $\partial A/\partial X$ remains non-zero at the wall and the location of the transition point X_0 remains finite as $\lambda\to0$. This makes an investigation of phase-winding solutions for $\lambda=0$ more straightforward when $\delta\neq0$ than in the case where $\delta=0$. This investigation is the subject of the present chapter.

In order to discuss phase-winding for $\lambda=0$ it is necessary to consider higher order terms in the derivation of the amplitude equations than those considered in chapter 2. Specifically, terms of order ϵ^2 are studied, i.e. of order $\epsilon^{1/2}$ relative to the smallest terms considered in chapter 2. For this reason, attention is restricted to the simpler model system (2.2.1)-(2.2.2) introduced in chapter 2 and the required amplitude equations are derived in section 6.2. In section 6.3 the overall solution structure is set out, based on the leading order solutions obtained in chapter 5 and incorporating the possibility of complex amplitude functions A and B. This structure consists of two wall regions ($x\sim1$ and $x\sim\epsilon^{-1/4}$) together with the two main outer regions ($x\sim\epsilon^{-1/2}$) discussed in chapter 5. These outer regions are separated by a transition zone at the point where the amplitude of the y-rolls falls to zero. The leading terms in the expansion of the solution in the outer regions are given in section 6.3 and, in section 6.4,

higher order terms are discussed. In section 6.5 the scalings of the transition region are determined together with the appropriate expansions for A and B. Solutions in the transition region are found which lead to the relevant continuity conditions for the outer solution at $X = X_0$. The solutions in the wall regions are discussed in section 6.6 and matching leads to conditions to be applied at $X = 0$ to complete the determination of the various constants arising in the outer solutions. In particular, in section 6.7, the constant associated with phase-winding is determined, leading to a prediction of how the lateral wall restricts the allowed band of wavelengths in the main x-roll pattern. The results are discussed with ideas for future work in section 6.8.

6.2 Higher order amplitude equations

The amplitude equations derived in chapter 2 are now extended to incorporate higher order terms. Attention is restricted to the model equation

$$\frac{\partial \psi}{\partial t} = \left\{ \epsilon - (\nabla^2 + 1)^2 \right\} \psi - \psi^3 \quad , \tag{6.2.1}$$

where $\nabla^2 = \partial^2 / \partial x^2 + \partial^2 / \partial y^2$, and as in chapter 2, a semi-infinite domain $x \geq 0$ is considered. At the lateral boundary it is assumed that

$$\psi = 2\lambda \epsilon^{1/2} \quad , \quad \frac{\partial \psi}{\partial x} = 0 \quad , \quad x = 0 \tag{6.2.2}$$

and subsequently λ will be taken as zero. The amplitude equations are derived by assuming an expansion for ψ of the form

$$\psi = \epsilon^{1/2} \psi_0 + \epsilon \psi_1 + \epsilon^{3/2} \psi_2 + \epsilon^2 \psi_3 + \dots \quad , \quad \epsilon \to 0 \quad . \tag{6.2.3}$$

The most general form of the amplitude equations for the model system is determined by allowing the semi-infinite domain $x \geq 0$ to contain x-rolls which have slow spatial modulation on length scales X, $\tilde{Y}$ defined by

$$X = \epsilon^{1/2}x \quad , \quad \bar{Y} = \epsilon^{1/4}y \tag{6.2.4}$$

and y-rolls which have slow spatial modulation on length scales $\bar{X}$ and Y defined by

$$\bar{X} = \epsilon^{1/4}x \quad , \quad Y = \epsilon^{1/2}y \quad . \tag{6.2.5}$$

Also both sets of rolls are allowed to vary on a slow time scale τ defined by

$$\tau = \epsilon t \quad . \tag{6.2.6}$$

These scales are the same as those introduced in chapter 2 and, as before, the method of multiple scales is applied to obtain a succession of problems for ψ_i ($i=0,1,2...$). The solutions for ψ_0 and ψ_1 are precisely as given in chapter 2, except that it is now convenient to replace A by A_0 and B by B_0. Then at order $\epsilon^{3/2}$, it follows that ψ_2 satisfies

$$(\nabla^2+1)^2\psi_2 = -\frac{\partial\psi_0}{\partial\tau} - \left[\frac{4\partial^4}{\partial x\partial X\partial\bar{Y}^2} + \frac{\partial^4}{\partial\bar{Y}^4} + \frac{4\partial^4}{\partial x^2\partial X^2}\right]\psi_0^A$$

$$- \left[\frac{4\partial^4}{\partial\bar{X}^2\partial y\partial Y} + \frac{\partial^4}{\partial\bar{X}^4} + \frac{4\partial^4}{\partial y^2\partial Y^2}\right]\psi_0^B + \psi_0 - \psi_0^3 \quad ,$$

$$\tag{6.2.7}$$

where

$$\psi_0 = \psi_0^A(x,X,\bar{Y},\tau) + \psi_0^B(y,\bar{X},Y,\tau) \quad , \tag{6.2.8}$$

with

$$\psi_0^A = A_0(X,\bar{Y},\tau)e^{ix} + c.c \tag{6.2.9}$$

and

$$\psi_0^B = B_0(\bar{X},Y,\tau)e^{iy} + c.c \quad , \tag{6.2.10}$$

where $c.c$ denotes complex conjugate. Terms proportional to $e^{\pm ix}$ and $e^{\pm iy}$ lead to the amplitude equations for A_0 and B_0 equivalent to those for A and B given in (2.2.20), (2.2.21) and the complete solution for ψ_2 may be written in the form

$$\psi_2 = \psi_2^A(x,X,\overline{Y},\tau) + \psi_2^B(y,\overline{X},Y,\tau)$$

$$- \frac{1}{64}\Big[A_0^3(X,\overline{Y},\tau)e^{3ix} + B_0^3(\overline{X},Y,\tau)e^{3iy}\Big]$$

$$- \frac{3}{16}\Big[A_0^2(X,\overline{Y},\tau)B_0(\overline{X},Y,\tau)e^{i(2x+y)}\Big]$$

$$- \frac{3}{16}\Big[A_0^2(X,\overline{Y},\tau)B_0^\star(\overline{X},Y,\tau)e^{i(2x-y)}\Big]$$

$$- \frac{3}{16}\Big[A_0(X,\overline{Y},\tau)B_0^2(\overline{X},Y,\tau)e^{i(x+2y)}\Big]$$

$$- \frac{3}{16}\Big[A_0(X,\overline{Y},\tau)B_0^{\star 2}(\overline{X},Y,\tau)e^{i(x-2y)}\Big] + c.c \quad,$$

$$(6.2.11)$$

where

$$\psi_2^A = A_2(X,\overline{Y},\tau)e^{ix} + c.c \qquad (6.2.12)$$

and

$$\psi_2^B = B_2(\overline{X},Y,\tau)e^{iy} + c.c \quad. \qquad (6.2.13)$$

At order ϵ^2, ψ_3 is found to satisfy

$$(\nabla^2 + 1)^2\psi_3 = \psi_1 - \frac{\partial\psi_1}{\partial\tau} - \left[\frac{2\partial^4}{\partial x^2\partial\overline{Y}^2} + \frac{2\partial^4}{\partial\overline{X}^2\partial y^2}\right]\psi_2$$

$$- \left[\frac{4\partial^4}{\partial x^3\partial X} + \frac{4\partial^4}{\partial y^3\partial Y} + \frac{2\partial^2}{\partial\overline{Y}^2} + \frac{4\partial^2}{\partial x\partial X} + \frac{2\partial^2}{\partial\overline{X}^2} + \frac{4\partial^2}{\partial y\partial Y}\right]\psi_2$$

$$- \left[\frac{4\partial^4}{\partial x\partial X\partial\overline{Y}^2} + \frac{\partial^4}{\partial\overline{Y}^4} + \frac{4\partial^4}{\partial x^2\partial X^2}\right]\psi_1^A$$

$$- \left[\frac{4\partial^4}{\partial\overline{X}^2\partial y\partial Y} + \frac{\partial^4}{\partial\overline{X}^4} + \frac{4\partial^4}{\partial y^2\partial Y^2}\right]\psi_1^B$$

$$- \left[\frac{4\partial^4}{\partial x\partial X^3} + \frac{2\partial^4}{\partial X^2\partial\overline{Y}^2}\right]\psi_0^A - \left[\frac{4\partial^4}{\partial y\partial Y^3} + \frac{2\partial^4}{\partial\overline{X}^2\partial Y^2}\right]\psi_0^B - 3\psi_0^2\psi_1 \quad,$$

$$(6.2.14)$$

173

where

$$\psi_1 = \psi_1^A(x,X,\bar{Y},\tau) + \psi_1^B(y,\bar{X},Y,\tau) \quad , \tag{6.2.15}$$

with

$$\psi_1^A = A_1(X,\bar{Y},\tau)e^{ix} + c.c \tag{6.2.16}$$

and

$$\psi_1^B = B_1(\bar{X},Y,\tau)e^{iy} + c.c \quad . \tag{6.2.17}$$

The right hand side of (6.2.14) contains terms proportional to $e^{\pm ix}$, $e^{\pm 3ix}$, $e^{\pm iy}$, $e^{\pm 3iy}$, $e^{\pm i(2x\pm y)}$ and $e^{\pm i(x\pm 2y)}$. In order that the solution for ψ_2 does not grow with x or y, the secular terms proportional to $e^{\pm ix}$ and $e^{\pm iy}$ must be avoided, and after substitution for ψ_0 and ψ_1 from (6.2.8) and (6.2.15) this requires that

$$\frac{\partial A_1}{\partial \tau} = A_1 - \frac{4i\partial^3 A_1}{\partial X \partial \bar{Y}^2} - \frac{\partial^4 A_1}{\partial \bar{Y}^4} + \frac{4\partial^2 A_1}{\partial X^2} - \frac{4i\partial^3 A_0}{\partial X^3} - \frac{2\partial^4 A_0}{\partial X^2 \partial \bar{Y}^2} - 3A_0^2 A_1^*$$
$$-6|A_0|^2 A_1 - 6A_0 B_0 B_1^* - 6A_0 B_0^* B_1 - 6|B_0|^2 A_1 \quad ,$$

$$\tag{6.2.18}$$

$$\frac{\partial B_1}{\partial \tau} = B_1 - \frac{4i\partial^3 B_1}{\partial \bar{X}^2 \partial Y} - \frac{\partial^4 B_1}{\partial \bar{X}^4} + \frac{4\partial^2 B_1}{\partial Y^2} - \frac{4i\partial^3 B_0}{\partial Y^3} - \frac{2\partial^4 B_0}{\partial \bar{X}^2 \partial Y^2} - 3B_0^2 B_1^*$$
$$-6|A_0|^2 B_1 - 6A_0 B_0 A_1^* - 6A_0^* B_0 A_1 - 6|B_0|^2 B_1 \quad .$$

$$\tag{6.2.19}$$

The results for A_0, B_0 and A_1, B_1 may be combined in a pair of 'general' amplitude equations which can be formulated by setting

$$A = A_0 + \epsilon^{1/2} A_1 + ... \tag{6.2.20}$$

and

$$B = B_0 + \epsilon^{1/2} B_1 + ... \tag{6.2.21}$$

174

and by using the equations for A_0 and B_0 derived in chapter 2. This leads to the 'general' amplitude equation for A,

$$\frac{\partial A}{\partial \tau} = A + 4\left(\frac{\partial}{\partial X} - \frac{i}{2}\frac{\partial^2}{\partial \overline{Y}^2}\right)^2 A - 4\epsilon^{1/2}i\frac{\partial^3 A}{\partial X^3} - 2\epsilon^{1/2}\frac{\partial^4 A}{\partial X^2 \partial \overline{Y}^2} - 3A|A|^2 - 6A|B|^2 \quad , \quad (6.2.22)$$

which can be considered correct up to terms in A and B of relative order $\epsilon^{1/2}$. Similarly, the 'general' amplitude equation for B correct to terms of relative order $\epsilon^{1/2}$ is

$$\frac{\partial B}{\partial \tau} = B + 4\left(\frac{\partial}{\partial Y} - \frac{i}{2}\frac{\partial^2}{\partial \overline{X}^2}\right)^2 B - 4\epsilon^{1/2}i\frac{\partial^3 B}{\partial Y^3} - 2\epsilon^{1/2}\frac{\partial^4 B}{\partial \overline{X}^2 \partial Y^2} - 3B|B|^2 - 6B|A|^2 \quad \cdot \quad (6.2.23)$$

Finally, it is worth noting that these amplitude equations can be rewritten in terms of functions $\tilde{A}$ and $\tilde{B}$ of the original spatial and temporal variables x, y and t by writing

$$\psi \sim \{\tilde{A}(x,y,t)e^{ix} + \tilde{B}(x,y,t)e^{iy}\} + c.c \quad , \quad (6.2.24)$$

and then the amplitude equations are

$$\frac{\partial \tilde{A}}{\partial t} = \epsilon\tilde{A} + 4\left(\frac{\partial}{\partial x} - \frac{i}{2}\frac{\partial^2}{\partial y^2}\right)^2 \tilde{A} - 4i\frac{\partial^3 \tilde{A}}{\partial x^3} - \frac{2\partial^4 \tilde{A}}{\partial x^2 \partial y^2} - 3\tilde{A}|\tilde{A}|^2 - 6\tilde{A}|\tilde{B}|^2 \quad (6.2.25)$$

and

$$\frac{\partial \tilde{B}}{\partial t} = \epsilon\tilde{B} + 4\left(\frac{\partial}{\partial y} - \frac{i}{2}\frac{\partial^2}{\partial x^2}\right)^2 \tilde{B} - 4i\frac{\partial^3 \tilde{B}}{\partial y^3} - \frac{2\partial^4 \tilde{B}}{\partial x^2 \partial y^2} - 3\tilde{B}|\tilde{B}|^2 - 6\tilde{B}|\tilde{A}|^2 \quad , \quad (6.2.26)$$

again correct to relative order $\epsilon^{1/2}$.

6.3 Solution structure and leading order terms

In chapter 5 the amplitude functions A and B are allowed to depend on the slow spatial variables X and Y where $x = \epsilon^{-1/2}X$ and $y = \epsilon^{-1/2}Y$, as well as the slow time scale τ. A similar

175

assumption is made here although other regions of the flow, near the wall where $x \sim 1$ and $x \sim \epsilon^{-1/4}$, and near the transition point, $X = X_0$, will also be considered in some detail. A schematic diagram of the main flow regions is shown in Figure 6.1. Apart from the region adjacent to the wall, the amplitude equations (6.2.22) and (6.2.23) can be used as a basis for finding the solution, even though scalings for x and y will be used which are not necessarily the same as those used in deriving the equations.

In order to incorporate the effect of frequency modulation in the y direction, it is assumed that

$$B = \dot{B}(X,\tau)e^{i\delta Y} \quad , \tag{6.3.1}$$

where $\dot{B}$ is independent of Y, and it follows that a solution for A may be assumed in the form

$$A = A(X,\tau) \quad , \tag{6.3.2}$$

where A is complex. Substitution of (6.3.1) and (6.3.2) into (6.2.22) and (6.2.23) and the assumption of a steady-state solution, results in the following amplitude equations for A and $\dot{B}$:

$$A + 4\frac{\partial^2 A}{\partial X^2} - 3A|A|^2 - 6A|\dot{B}|^2 - 4i\epsilon^{1/2}\frac{\partial^3 A}{\partial X^3} = 0 \quad , \tag{6.3.3}$$

$$\dot{B}(1-4\delta^2) - 3\dot{B}|\dot{B}|^2 - 6\dot{B}|A|^2 - \epsilon\frac{\partial^4 \dot{B}}{\partial X^4} + 4\epsilon^{1/2}\delta\frac{\partial^2 \dot{B}}{\partial X^2} - 4\delta^3\epsilon^{1/2}\dot{B} + 2\epsilon\delta^2\frac{\partial^2 \dot{B}}{\partial X^2} = 0 \quad . \tag{6.3.4}$$

The equation for A depends only on the modulus of $\dot{B}$ and it is possible to assume without loss of generality that $\dot{B}$ is real.

The main outer region where $X = O(1)$ is divided into two parts, $X < X_0$ (region I) and $X > X_0$ (region II), by a transition region centred at X_0 where there is a smooth adjustment in the amplitude of the y-rolls such that for $X > X_0$, B is zero. The transition region is similar to that

176

described in chapter 3 but has some significant differences because when δ is non-zero the term $\epsilon\delta^2\partial^2\dot{B}/\partial X^2$ in (6.3.4) is more important than the term $\epsilon\partial^4 B/\partial X^4$. The transition region is considered in detail in section 6.5. In the two main outer regions, expansions for A and $\dot{B}$ must be taken in the following forms.

Region I:

$$A = \dot{A}_0 + \epsilon^{1/3}\dot{A}_1 + \epsilon^{1/2}\ln\epsilon\,\dot{A}_{20} + \epsilon^{1/2}\dot{A}_2 + \dots\ ,\qquad (6.3.5)$$

$$\dot{B} = \dot{B}_0 + \epsilon^{1/3}\dot{B}_1 + \epsilon^{1/2}\ln\epsilon\,\dot{B}_{20} + \epsilon^{1/2}\dot{B}_2 + \dots\ .\qquad (6.3.6)$$

Region II:

$$A = \ddot{A}_0 + \epsilon^{1/3}\ddot{A}_1 + \epsilon^{1/2}\ln\epsilon\,\ddot{A}_{20} + \epsilon^{1/2}\ddot{A}_2 + \dots\ ,\qquad (6.3.7)$$

$$\dot{B} = 0\ .\qquad (6.3.8)$$

Here the leading terms are similar to those considered in chapter 5 and justification for the higher order terms will be given in full below; the terms of order $\epsilon^{1/3}$ are associated with the presence of the transition zone, while those of order $\epsilon^{1/2}$ and $\epsilon^{1/2}\ln\epsilon$ are related to the existence of the higher order terms which appear in (6.3.3) and (6.3.4).

Since $\lambda=0$, it is expected that the leading terms $\dot{A}_0$ and $\ddot{A}_0$ must have constant complex arguments, so that

$$\dot{A}_0 = \dot{R}_0(X)e^{iC}\ ,\qquad (6.3.9)$$

$$\ddot{A}_0 = \ddot{R}_0(X)e^{iC}\ ,\qquad (6.3.10)$$

where $\dot{R}_0$ and $\ddot{R}_0$ are real and satisfy

$$4\frac{d^2\ddot{R}_0}{dX^2} + \ddot{R}_0 - 3\ddot{R}_0^3 = 0 \quad , \tag{6.3.11}$$

$$4\frac{d^2\dot{R}_0}{dX^2} + (8\delta^2 - 1)\dot{R}_0 + 9\dot{R}_0^3 = 0 \quad . \tag{6.3.12}$$

The relevant solutions, subject to the requirement that $\ddot{R}_0 \rightarrow 1/\sqrt{3}$ as $X \rightarrow \infty$, the continuity of $\ddot{R}_0$ and $\dot{R}_0$ and their first derivatives at $X = X_0$ (defined as the point at which $\dot{R}_0 = \ddot{R}_0 = [(1-4\delta^2)/6]^{1/2}$) and the condition $\dot{R}_0 = 0$ at $X = 0$, are identical to those given for A and $\dot{B}$ in chapter 5 for the case where $\lambda = 0$. Thus $\dot{R}_0$ is defined (implicitly) by the relation

$$\int_0^{\dot{R}_a} \frac{d\dot{R}_0}{\left[\dfrac{\delta^2(1-2\delta^2)}{3} + \dfrac{(1-8\delta^2)\dot{R}_0^2}{4} - \dfrac{9\dot{R}_0^4}{8}\right]^{1/2}} = X \quad , \tag{6.3.13}$$

with

$$\dot{B}_0^2 = \frac{1}{3}\left(1 - 4\delta^2 - 6\dot{R}_0^2\right) \tag{6.3.14}$$

and

$$\ddot{R}_0 = \frac{1}{\sqrt{3}}\tanh\left[\frac{X - X_0 + C_I}{2\sqrt{2}}\right] \quad \text{where} \quad C_I = 2\sqrt{2}\tanh^{-1}\left[\sqrt{\frac{1-4\delta^2}{2}}\right] \quad . \tag{6.3.15}$$

Near the transition point it follows that

$$\dot{R}_0 = \dot{a}_0 + \dot{a}_1\tilde{X} + \dot{a}_2\tilde{X}^2 + \dot{a}_3\tilde{X}^3 + \dot{a}_4\tilde{X}^4 + \dots \quad , \quad \tilde{X} \rightarrow 0+ \quad , \tag{6.3.16}$$

where $\tilde{X} = X - X_0$ and

$$\dot{a}_0 = \sqrt{\frac{1-4\delta^2}{6}} \quad , \quad \dot{a}_1 = \frac{(1+4\delta^2)}{4\sqrt{6}}$$

$$\dot{a}_2 = -\frac{\sqrt{1-4\delta^2}(1+4\delta^2)}{16\sqrt{6}} \quad , \quad \dot{a}_3 = \frac{(1+4\delta^2)(20\delta^2-7)}{192\sqrt{6}}$$

$$\dot{a}_4 = -\frac{\sqrt{1-4\delta^2}(1+4\delta^2)(1+28\delta^2)}{768\sqrt{6}}$$

(6.3.17)

and that

$$\ddot{R}_0 = \ddot{a}_0 + \ddot{a}_1\tilde{X} + \ddot{a}_2\tilde{X}^2 + \ddot{a}_3\tilde{X}^3 + \ddot{a}_4\tilde{X}^4 + \dots \quad , \quad \tilde{X} \to 0- \quad , \qquad (6.3.18)$$

where

$$\ddot{a}_0 = \sqrt{\frac{1-4\delta^2}{6}} \quad , \quad \ddot{a}_1 = \frac{(1+4\delta^2)}{4\sqrt{6}} \quad ,$$

$$\ddot{a}_2 = -\frac{\sqrt{1-4\delta^2}(1+4\delta^2)}{16\sqrt{6}} \quad , \quad \ddot{a}_3 = \frac{(1+4\delta^2)(1-12\delta^2)}{192\sqrt{6}}$$

$$\ddot{a}_4 = \frac{\sqrt{1-4\delta^2}(1+4\delta^2)(1+12\delta^2)}{768\sqrt{6}} \quad .$$

(6.3.19)

Also, near the wall, the solution for $\dot{R}_0$ has the form

$$\dot{R}_0 = \frac{1}{\sqrt{3}}\delta(1-2\delta^2)^{1/2}X + O(X^3) \quad , \quad X \to 0 \quad . \qquad (6.3.20)$$

6.4 Higher order terms in the outer regions

In order to obtain the higher order equations for $\dot{A}_1$, $\dot{A}_{20}$, $\dot{A}_2$ and $\dot{B}_1$, $\dot{B}_{20}$, $\dot{B}_2$ in region I, it is necessary to substitute the expressions (6.3.5) and (6.3.6) into (6.3.3) and (6.3.4) and compare orders of ϵ leading to:

179

$$\dot{A}_1 + \frac{4\partial^2 \dot{A}_1}{\partial X^2} - 3\dot{A}_0^2 \dot{A}_1^\star - 6|\dot{A}_0|^2 \dot{A}_1 - 12\dot{A}_0 \dot{B}_0 \dot{B}_1 - 6\dot{A}_1 \dot{B}_0^2 = 0 \quad , \qquad (6.4.1)$$

$$\dot{A}_{20} + \frac{4\partial^2 \dot{A}_{20}}{\partial X^2} - 3\dot{A}_0^2 \dot{A}_{20}^\star - 6|\dot{A}_0|^2 \dot{A}_{20} - 12\dot{A}_0 \dot{B}_0 \dot{B}_{20} - 6\dot{A}_{20} \dot{B}_0^2 = 0 \quad , \qquad (6.4.2)$$

$$\dot{A}_2 + \frac{4\partial^2 \dot{A}_2}{\partial X^2} - 3\dot{A}_0^2 \dot{A}_2^\star - 6|\dot{A}_0|^2 \dot{A}_2 - 12\dot{A}_0 \dot{B}_0 \dot{B}_2 - 6\dot{A}_2 \dot{B}_0^2 = \frac{4i\partial^3 \dot{A}_0}{\partial X^3} \qquad (6.4.3)$$

and

$$(1-4\delta^2)\dot{B}_1 - 9\dot{B}_0^2 \dot{B}_1 - 6\dot{B}_0 \dot{A}_0 \dot{A}_1^\star - 6\dot{B}_0 \dot{A}_1 \dot{A}_0^\star - 6\dot{B}_1 |\dot{A}_0|^2 = 0 \quad , \qquad (6.4.4)$$

$$(1-4\delta^2)\dot{B}_{20} - 9\dot{B}_0^2 \dot{B}_{20} - 6\dot{B}_0 \dot{A}_0 \dot{A}_{20}^\star - 6\dot{B}_0 \dot{A}_{20} \dot{A}_0^\star - 6\dot{B}_{20} |\dot{A}_0|^2 = 0 \quad , \qquad (6.4.5)$$

$$(1-4\delta^2)\dot{B}_2 - 9\dot{B}_0^2 \dot{B}_2 - 6\dot{B}_0 \dot{A}_0 \dot{A}_2^\star - 6\dot{B}_0 \dot{A}_2 \dot{A}_0^\star - 6\dot{B}_2 |\dot{A}_0|^2 = 4\delta^3 \dot{B}_0 - 4\delta \frac{\partial^2 \dot{B}_0}{\partial X^2} \quad . \qquad (6.4.6)$$

Similarly, the higher order equations for $\ddot{A}_1$, $\ddot{A}_{20}$, $\ddot{A}_2$ in region II are obtained by substituting

the expressions (6.3.7) and (6.3.8) into (6.3.3) and (6.3.4) and comparing orders of ϵ to give:

$$\ddot{A}_1 + 4\frac{\partial^2 \ddot{A}_1}{\partial X^2} - 3\ddot{A}_0^2 \ddot{A}_1^\star - 6|\ddot{A}_0|^2 \ddot{A}_1 = 0 \quad , \qquad (6.4.7)$$

$$\ddot{A}_{20} + 4\frac{\partial^2 \ddot{A}_{20}}{\partial X^2} - 3\ddot{A}_0^2 \ddot{A}_{20}^\star - 6|\ddot{A}_0|^2 \ddot{A}_{20} = 0 \quad , \qquad (6.4.8)$$

$$\ddot{A}_2 + 4\frac{\partial^2 \ddot{A}_2}{\partial X^2} - 3\ddot{A}_0^2 \ddot{A}_2^\star - 6|\ddot{A}_0|^2 \ddot{A}_2 = 4i\frac{\partial^3 \ddot{A}_0}{\partial X^3} \quad . \qquad (6.4.9)$$

In order to solve these equations it is convenient to set

$$\dot{A}_1 = \dot{R}_1 e^{iC} \quad , \quad \dot{A}_{20} = \dot{R}_{20} e^{iC} \quad , \quad \dot{A}_2 = \dot{R}_2 e^{iC} \qquad (6.4.10)$$

and

$$\ddot{A}_1 = \ddot{R}_1 e^{iC} \quad , \quad \ddot{A}_{20} = \ddot{R}_{20} e^{iC} \quad , \quad \ddot{A}_2 = \ddot{R}_2 e^{iC} \qquad (6.4.11)$$

and then the real and imaginary parts of the complementary solutions can be determined, together with the particular solutions for $\dot{R}_2$ and $\ddot{R}_2$.

The solutions for region I are found to be

$$\dot{R}_1 = \dot{R}_0' \left[\int_X^{X_0} \frac{\dot{C}_1}{\dot{R}_0'^2} dX + \dot{D}_1 \right] + i\dot{R}_0 \left[\int_X^{X_0} \frac{\dot{E}_1}{\dot{R}_0^2} dX + \dot{F}_1 \right] , \qquad (6.4.12)$$

$$\dot{R}_{20} = \dot{R}_0' \left[\int_X^{X_0} \frac{\dot{C}_{20}}{\dot{R}_0'^2} dX + \dot{D}_{20} \right] + i\dot{R}_0 \left[\int_X^{X_0} \frac{\dot{E}_{20}}{\dot{R}_0^2} dX + \dot{F}_{20} \right] , \qquad (6.4.13)$$

$$\dot{R}_2 = \dot{R}_0' \left[\int_X^{X_0} \frac{\dot{C}_2}{\dot{R}_0'^2} dX + \dot{D}_2 \right] + \dot{R}_0' \int_X^{X_0} \frac{\delta^3 \dot{R}_0^2}{\dot{R}_0'^2} dX$$

$$+ \dot{R}_0' \int_0^X \left[\frac{2\delta}{\dot{R}_0'^2} \int_0^X \frac{\dot{R}_0 \dot{R}_0' \dot{B}_0''}{\dot{B}_0} dX \right] dX + i\dot{R}_0 \left[\int_X^{X_0} \frac{\dot{E}_2}{\dot{R}_0^2} dX + \dot{F}_2 \right]$$

$$- i\dot{R}_0 \int_X^{X_0} \left[\frac{(1-8\delta^2)}{8} - \frac{27\dot{R}_0^2}{16} \right] dX , \qquad (6.4.14)$$

where $\dot{C}_i$, $\dot{D}_i$, $\dot{E}_i$, $\dot{F}_i$ and $\dot{C}_{20}$, $\dot{D}_{20}$, $\dot{E}_{20}$, $\dot{F}_{20}$ are real constants.

The solutions for region II are found to be

$$\ddot{R}_1 = \frac{1}{2\sqrt{6}}\mathrm{sech}^2\left[\frac{C'+X}{2\sqrt{2}}\right]\left\{6\ddot{C}_1\left[\frac{1}{2\sqrt{2}}\sinh\left[\frac{2(C'+X)}{\sqrt{2}}\right]+2\sqrt{2}\sinh\left[\frac{C'+X}{\sqrt{2}}\right]+\frac{3X}{2}\right]+\ddot{D}_1\right\}$$

$$+\frac{i}{\sqrt{3}}\tanh\left[\frac{C'+X}{2\sqrt{2}}\right]\left\{3\ddot{E}_1\left(X-2\sqrt{2}\coth\left[\frac{C'+X}{2\sqrt{2}}\right]\right)+\ddot{F}_1\right\}\quad ,$$

$$(6.4.15)$$

$$\ddot{R}_{20} = \frac{1}{2\sqrt{6}}\mathrm{sech}^2\left[\frac{C'+X}{2\sqrt{2}}\right]\left\{6\ddot{C}_{20}\left[\frac{1}{2\sqrt{2}}\sinh\left[\frac{2(C'+X)}{\sqrt{2}}\right]+2\sqrt{2}\sinh\left[\frac{C'+X}{\sqrt{2}}\right]+\frac{3X}{2}\right]+\ddot{D}_{20}\right\}$$

$$+\frac{i}{\sqrt{3}}\tanh\left[\frac{C'+X}{2\sqrt{2}}\right]\left\{3\ddot{E}_{20}\left(X-2\sqrt{2}\coth\left[\frac{C'+X}{2\sqrt{2}}\right]\right)+\ddot{F}_{20}\right\}\quad ,$$

$$(6.4.16)$$

$$\ddot{R}_2 = \frac{1}{2\sqrt{6}}\mathrm{sech}^2\left[\frac{C'+X}{2\sqrt{2}}\right]\left\{6\ddot{C}_2\left[\frac{1}{2\sqrt{2}}\sinh\left[\frac{2(C'+X)}{\sqrt{2}}\right]+2\sqrt{2}\sinh\left[\frac{C'+X}{\sqrt{2}}\right]+\frac{3X}{2}\right]+\ddot{D}_2\right\}$$

$$+\frac{i}{\sqrt{3}}\tanh\left[\frac{C'+X}{2\sqrt{2}}\right]\left\{3\ddot{E}_2\left(X-2\sqrt{2}\coth\left[\frac{C'+X}{2\sqrt{2}}\right]\right)+\ddot{F}_2+\frac{1}{16}\left(X-6\sqrt{2}\tanh\left[\frac{C'+X}{2\sqrt{2}}\right]\right)\right\}\quad ,$$

$$(6.4.17)$$

where

$$C' = C_\mathrm{I} - X_0 = 2\sqrt{2}\,\tanh^{-1}\left[\sqrt{\frac{1-4\delta^2}{2}}\right] - X_0 \qquad (6.4.18)$$

and $\ddot{C}_i$, $\ddot{D}_i$, $\ddot{E}_i$, $\ddot{F}_i$ and $\ddot{C}_{20}$, $\ddot{D}_{20}$, $\ddot{E}_{20}$, $\ddot{F}_{20}$ are real constants.

In order to determine the various constants in these solutions it is necessary to apply the relevant boundary conditions at $X=0$ and as $X\rightarrow\infty$, and the relevant bridging conditions at $X=X_0$. The solutions must remain bounded as $X\rightarrow\infty$, requiring that

$$\ddot{C}_1 = \ddot{C}_{20} = \ddot{C}_2 = 0 \quad , \qquad (6.4.19)$$

and the conditions at $X = X_0$ and $X = 0$ are determined by considering the transition zone centred on X_0 and the inner wall regions. These are considered in sections 6.5 and 6.6 respectively.

In order to determine the solution in the transition zone it is necessary to note the behaviour of the outer solution as $\bar{X} = X - X_0 \to 0\pm$. From (6.4.12) and (6.4.13) it follows that

$$\dot{R}_1 = \dot{b}_0 + \dot{b}_1\bar{X} + \dot{b}_2\bar{X}^2 + \dot{b}_3\bar{X}^3 + \dots \quad , \quad \bar{X} \to 0- \quad , \tag{6.4.20}$$

$$\dot{R}_{20} = \dot{c}_0 + \dot{c}_1\bar{X} + \dot{c}_2\bar{X}^2 + \dot{c}_3\bar{X}^3 + \dots \quad , \quad \bar{X} \to 0- \quad , \tag{6.4.21}$$

and from (6.4.14) that

$$\dot{R}_2 = \dot{d}_{00}\ln|\bar{X}| + \dot{d}_0 + \dot{d}_{10}\bar{X}\ln|\bar{X}| + \dot{d}_1\bar{X} + \dots \quad , \quad \bar{X} \to 0- \quad , \tag{6.4.22}$$

where

$$\dot{b}_0 = \dot{R}_1(X_0) = \dot{a}_1\dot{D}_1 + i\dot{a}_0\dot{F}_1$$

$$\dot{b}_1 = \dot{R}_1'(X_0) = (-\dot{a}_1^{-1}\dot{C}_1 + 2\dot{a}_2\dot{D}_1) + i(-\dot{a}_0^{-1}\dot{E}_1 + \dot{a}_1\dot{F}_1)$$

$$\dot{c}_0 = \dot{R}_{20}(X_0) = \dot{a}_1\dot{D}_{20} + i\dot{a}_0\dot{F}_{20}$$

$$\dot{c}_1 = \dot{R}_{20}'(X_0) = (-\dot{a}_1^{-1}\dot{C}_{20} + 2\dot{a}_2\dot{D}_{20}) + i(-\dot{a}_0^{-1}\dot{E}_{20} + \dot{a}_1\dot{F}_{20})$$

$$\dot{d}_{00} = \frac{1}{2}\dot{a}_0\delta$$

$$\dot{d}_0 = \dot{a}_1\dot{D}_2 + \dot{a}_1\hat{C} + i\dot{a}_0\dot{F}_2$$

$$\dot{d}_{10} = \dot{a}_0\dot{a}_2\dot{a}_1^{-1}\delta$$

$$\dot{d}_1 = (-\dot{a}_1^{-1}\dot{C}_2 + 2\dot{a}_2\dot{D}_2 - \delta^3\dot{a}_1^{-1}\dot{a}_0^2 + 2\dot{a}_2\hat{C} + \dot{a}_1\hat{D}) + i\left(-\dot{a}_0^{-1}\dot{E}_2 + \dot{a}_1\dot{F}_2 + \frac{(4\delta^2-5)\dot{a}_0}{32}\right)$$

$$\tag{6.4.23}$$

and $\hat{C}$ and $\hat{D}$ are constants associated with the finite part and linear term in $X - X_0$ of the expansion of the integral

$$\int_0^X \frac{2\delta}{\dot{R}_0'^2} \int_0^X \frac{\dot{R}_0\dot{R}_0'\dot{B}_0''}{\dot{B}_0} dX dX \tag{6.4.24}$$

183

as $X \to X_0$. Also, from (6.3.14)

$$\dot{B}_0 \sim \frac{(-\tilde{X})^{1/2}(1+4\delta^2)^{1/2}(1-4\delta^2)^{1/4}}{\sqrt{6}} \quad , \quad \tilde{X} \to 0- \quad , \tag{6.4.25}$$

indicating that the amplitude of the y-rolls falls to zero with a square root singularity as $X \to X_0-$ in the outer region.

From (6.4.15), (6.4.17) and (6.4.19) it follows that

$$\ddot{R}_1 = \ddot{b}_0 + \ddot{b}_1\tilde{X} + \ddot{b}_2\tilde{X}^2 + \ddot{b}_3\tilde{X}^3 + \dots \quad , \quad \tilde{X} \to 0+ \quad , \tag{6.4.26}$$

$$\ddot{R}_{20} = \ddot{c}_0 + \ddot{c}_1\tilde{X} + \ddot{c}_2\tilde{X}^2 + \ddot{c}_3\tilde{X}^3 + \dots \quad , \quad \tilde{X} \to 0+ \quad , \tag{6.4.27}$$

$$\ddot{R}_2 = \ddot{d}_0 + \ddot{d}_1\tilde{X} + \ddot{d}_2\tilde{X}^2 + \ddot{d}_3\tilde{X}^3 + \dots \quad , \quad \tilde{X} \to 0+ \quad . \tag{6.4.28}$$

where

$$\ddot{b}_0 = \ddot{R}_1(X_0) = \ddot{a}_1\ddot{D}_1 + i\ddot{a}_0\left(3\ddot{E}_1\left[X_0 - \frac{2\sqrt{2}}{\sqrt{3}}\ddot{a}_0^{-1}\right] + \ddot{F}_1\right)$$

$$\ddot{b}_1 = \ddot{R}_1{}'(X_0) = 2\ddot{a}_2\ddot{D}_1 + i\{3\ddot{E}_1(\ddot{a}_0 + \ddot{a}_1X_0) + \ddot{a}_1\ddot{F}_1\}$$

$$\ddot{c}_0 = \ddot{R}_{20}(X_0) = \ddot{a}_1\ddot{D}_{20} + i\ddot{a}_0\left(3\ddot{E}_{20}\left[X_0 - \frac{2\sqrt{2}}{\sqrt{3}}\ddot{a}_0^{-1}\right] + \ddot{F}_{20}\right)$$

$$\ddot{c}_1 = \ddot{R}_{20}{}'(X_0) = 2\ddot{a}_2\ddot{D}_{20} + i\{3\ddot{E}_{20}(\ddot{a}_0 + \ddot{a}_1X_0) + \ddot{a}_1\ddot{F}_{20}\}$$

$$\ddot{d}_0 = \ddot{R}_2(X_0) = \ddot{a}_1\ddot{D}_2 + i\ddot{a}_0\left(3\ddot{E}_2\left[X_0 - \frac{2\sqrt{2}}{\sqrt{3}}\ddot{a}_0^{-1}\right] + \ddot{F}_2 + \frac{1}{16}X_0 - \frac{3\sqrt{6}}{8}\ddot{a}_0\right)$$

$$\ddot{d}_1 = \ddot{R}_2{}'(X_0) = 2\ddot{a}_2\ddot{D}_2 + i\{3\ddot{E}_2(\ddot{a}_0 + \ddot{a}_1X_0) + \ddot{a}_1\ddot{F}_2\}$$

$$+ i\left\{\ddot{a}_0\left(\frac{1}{16} - \frac{3\sqrt{6}}{8}\ddot{a}_1\right) + \ddot{a}_1\left(\frac{X_0}{16} - \frac{3\sqrt{6}}{8}\ddot{a}_0\right)\right\}$$

$$\tag{6.4.29}$$

184

6.5 Transition region

The scalings for the solution in the transition region can now be obtained using (6.3.4). Assuming that $X-X_0 = \epsilon^\alpha \hat{X}$ and $\dot{B} = \epsilon^\beta \hat{B}$ with α and β to be determined and A approximated by $A_0(X_0) + \tilde{X} A_0'(X_0)$, substitution into (6.3.4) gives to leading order

$$4\delta\epsilon^{(1/2-2\alpha+\beta)}\frac{\partial^2 \hat{B}}{\partial \hat{X}^2} - 3\epsilon^{3\beta}\hat{B}^3 - \frac{\hat{B}\epsilon^{(\alpha+\beta)}\hat{X}(1+4\delta^2)\sqrt{1-4\delta^2}}{2} = 0 \quad , \tag{6.5.1}$$

and a full balance of terms requires

$$\alpha = \frac{1}{6} \quad , \quad \beta = \frac{1}{12} \quad . \tag{6.5.2}$$

Thus the transition zone is defined by the region $\hat{X} = O(1)$ where

$$X - X_0 = \epsilon^{1/6}\hat{X} \tag{6.5.3}$$

and expansions for A and $\dot{B}$ within the transition region are assumed in the form

$$A = \hat{A}_0(\hat{X}) + \epsilon^{1/6}\hat{A}_1(\hat{X}) + \epsilon^{1/3}\hat{A}_2(\hat{X}) + \epsilon^{1/2}\ln\epsilon \; \hat{A}_{30}(\hat{X}) + \epsilon^{1/2}\hat{A}_3(\hat{X})$$

$$+ \epsilon^{2/3}\ln\epsilon \; \hat{A}_{40}(\hat{X}) + \epsilon^{2/3}\hat{A}_4(\hat{X}) + \dots \quad , \tag{6.5.4}$$

$$\dot{B} = \epsilon^{1/12}\hat{B}_0(\hat{X}) + \epsilon^{1/4}\hat{B}_1(\hat{X}) + \epsilon^{5/12}\hat{B}_2(\hat{X}) + \dots \quad . \tag{6.5.5}$$

The expansions (6.5.4) and (6.5.5) are substituted into (6.3.3) and (6.3.4) using (6.5.3), and orders of ϵ compared to obtain in succession

$$\frac{4\partial^2 \hat{A}_0}{\partial \hat{X}^2} = 0 \quad , \tag{6.5.6}$$

$$\frac{4\partial^2 \hat{A}_1}{\partial \hat{X}^2} = 0 \quad , \tag{6.5.7}$$

$$\hat{A}_0 + 4\frac{\partial^2 \hat{A}_2}{\partial \hat{X}^2} - 4i\frac{\partial^3 \hat{A}_0}{\partial \hat{X}^3} - 3\hat{A}_0|\hat{A}_0|^2 = 0 \quad , \tag{6.5.8}$$

$$\frac{4\partial^2 \hat{A}_{30}}{\partial \hat{X}^2} = 0 \quad , \tag{6.5.9}$$

$$\hat{A}_1 + 4\frac{\partial^2 \hat{A}_3}{\partial \hat{X}^2} - 4i\frac{\partial^3 \hat{A}_1}{\partial \hat{X}^3} - 3\hat{A}_0^2\hat{A}_1^{\star} - 6|\hat{A}_0|^2\hat{A}_1 - 6\hat{A}_0\hat{B}_0^2 = 0 \quad , \tag{6.5.10}$$

$$\frac{4\partial^2 \hat{A}_{40}}{\partial \hat{X}^2} = 0 \quad , \tag{6.5.11}$$

$$\hat{A}_2 + 4\frac{\partial^2 \hat{A}_4}{\partial \hat{X}^2} - 4i\frac{\partial^3 \hat{A}_2}{\partial \hat{X}^3} - 3\hat{A}_0^2\hat{A}_2^{\star} - 6\hat{A}_0|\hat{A}_1|^2 - 6|\hat{A}_0|^2\hat{A}_2 -$$

$$3\hat{A}_1^2\hat{A}_0^{\star} - 12\hat{A}_0\hat{B}_0\hat{B}_1 - 6\hat{A}_1\hat{B}_0^2 = 0 \quad . \tag{6.5.12}$$

In order to determine the solutions for successive terms in the transition region, boundary conditions as $\hat{X} \to \pm \infty$ are required. Matching with the outer forms as $X \to X_0 \pm$ requires

$$\hat{A}_0 \to \dot{a}_0 e^{iC} \quad \text{as} \quad \hat{X} \to -\infty \quad , \quad \hat{A}_0 \to \ddot{a}_0 e^{iC} \quad \text{as} \quad \hat{X} \to \infty \quad , \tag{6.5.13}$$

$$\hat{A}_1 \sim \dot{a}_1 \hat{X} e^{iC} \quad \text{as} \quad \hat{X} \to -\infty \quad , \quad \hat{A}_1 \sim \ddot{a}_1 \hat{X} e^{iC} \quad \text{as} \quad \hat{X} \to \infty \quad , \tag{6.5.14}$$

$$\hat{A}_2 \sim (\dot{a}_2 \hat{X}^2 + \dot{b}_0)e^{iC} \quad \text{as} \quad \hat{X} \to -\infty \quad , \quad \hat{A}_2 \sim (\ddot{a}_2 \hat{X}^2 + \ddot{b}_0)e^{iC} \quad \text{as} \quad \hat{X} \to \infty \quad , \tag{6.5.15}$$

$$\hat{A}_{30} \to \left(\dot{c}_0 + \frac{1}{6}\dot{d}_{00}\right)e^{iC} \quad \text{as} \quad \hat{X} \to -\infty \quad , \quad \hat{A}_{30} \to \ddot{c}_0 e^{iC} \quad \text{as} \quad \hat{X} \to \infty \quad , \tag{6.5.16}$$

186

$$\hat{A}_3 \sim \left(\dot{a}_3\hat{X}^3 + \dot{b}_1\hat{X} + \dot{d}_{00}\ln|\hat{X}| + \dot{d}_0\right)e^{iC} \quad \text{as} \quad \hat{X} \to -\infty \ , \qquad (6.5.17)$$

$$\hat{A}_3 \sim \left(\ddot{a}_3\hat{X}^3 + \ddot{b}_1\hat{X} + \ddot{d}_0\right)e^{iC} \quad \text{as} \quad \hat{X} \to \infty \ , \qquad (6.5.18)$$

$$\hat{A}_{40} \sim \left(\dot{c}_1 + \frac{1}{6}\dot{d}_{10}\right)\hat{X}e^{iC} \quad \text{as} \quad \hat{X} \to -\infty \quad , \qquad \hat{A}_{40} \sim \ddot{c}_1\hat{X}e^{iC} \quad \text{as} \quad \hat{X} \to \infty \ ,$$

$$(6.5.19)$$

$$\hat{A}_4 \sim (\dot{a}_4\hat{X}^4 + \dot{b}_2\hat{X}^2 + \dot{d}_{10}\hat{X}\ln|\hat{X}| + \dot{d}_1\hat{X})e^{iC} \quad \text{as} \quad \hat{X} \to -\infty \ , \qquad (6.5.20)$$

$$\hat{A}_4 \sim (\ddot{a}_4\hat{X}^4 + \ddot{b}_2\hat{X}^2 + \ddot{d}_1\hat{X})e^{iC} \quad \text{as} \quad \hat{X} \to \infty \ . \qquad (6.5.21)$$

The solutions for $\hat{A}_0$, $\hat{A}_1$ and $\hat{A}_2$ can now be found as

$$\hat{A}_0 = \dot{a}_0 e^{iC} \ , \qquad (6.5.22)$$

$$\hat{A}_1 = \dot{a}_1\hat{X}e^{iC} \ , \qquad (6.5.23)$$

$$\hat{A}_2 = (\dot{a}_2\hat{X}^2 + \dot{b}_0)e^{iC} = \left(\frac{\dot{a}_0}{8}\left[3\dot{a}_0^2 - 1\right]\hat{X}^2 + \dot{b}_0\right)e^{iC} \ . \qquad (6.5.24)$$

These solutions are consistent with the assumptions that $\dot{a}_0 = \ddot{a}_0$ and $\dot{a}_1 = \ddot{a}_1$ already implicit in the leading order outer solutions, and in addition require that

$$\dot{b}_0 = \ddot{b}_0 \ . \qquad (6.5.25)$$

The expressions for $\dot{a}_0$ and $\dot{a}_1$ are given in (6.3.17). Also

$$\hat{A}_{30} = \left(\dot{c}_0 + \frac{1}{6}\dot{d}_{00}\right)e^{iC} \qquad (6.5.26)$$

and it is required that $\dot{c}_0$ and $\ddot{c}_0$ are related by

187

$$\dot{c}_0 + \frac{1}{6}\dot{d}_{00} = \ddot{c}_0 \quad . \tag{6.5.27}$$

The equation for $\hat{B}_0$ is now determined from (6.3.4) as

$$4\delta \frac{\partial^2 \hat{B}_0}{\partial \hat{X}^2} - 3\hat{B}_0^3 - \frac{\sqrt{1-4\delta^2}(1+4\delta^2)\hat{X}\hat{B}_0}{2} = 0 \quad . \tag{6.5.28}$$

From (6.4.25) the boundary conditions required to solve (6.5.28) are

$$\hat{B}_0 \sim a(-\hat{X})^{1/2} \quad , \quad \hat{X} \to -\infty \quad , \tag{6.5.29}$$

$$\hat{B}_0 \to 0 \quad , \quad \hat{X} \to \infty \quad , \tag{6.5.30}$$

where a is defined as

$$a = \left[\frac{(1+4\delta^2)\sqrt{1-4\delta^2}}{6} \right]^{1/2} \quad . \tag{6.5.31}$$

The asymptotic expansion of $\hat{B}$ as $\hat{X} \to -\infty$ can be determined by assuming a correction to (6.5.29) of the form $b(-\hat{X})^n$ and then finding b and n by substituting into (6.5.28) and balancing terms. This shows that

$$\hat{B}_0 \sim a(-\hat{X})^{1/2} + b(-\hat{X})^{-5/2} \quad , \quad \hat{X} \to -\infty \quad , \tag{6.5.32}$$

where b is defined as

$$b = \frac{-\delta}{\left[6(1+4\delta^2)\sqrt{1-4\delta^2} \right]^{1/2}} \quad . \tag{6.5.33}$$

The system (6.5.28)-(6.5.30) can be simplified by a scale transformation of $\hat{B}_0$ and $\hat{X}$ and the relevant solution has been discussed by Walton (1982). This provides a smooth adjustment in the amplitude of the y-rolls from the outer square-root form (6.5.29) to zero as $\hat{X} \to \infty$.

188

It is now possible to obtain the solution in the transition region for $\hat{A}_3$. Equation (6.5.10) can be integrated twice, giving

$$\hat{A}_3 = \left(\ddot{a}_3 \hat{X}^3 + \frac{3\dot{a}_0}{2} \int\limits_{\hat{X}}^{\infty} \int\limits_{\hat{X}}^{\infty} \hat{B}_0^2 d\hat{X} \; d\hat{X} + \alpha_3 \hat{X} + \beta_3 \right) e^{iC} \quad . \tag{6.5.34}$$

Since $\hat{B}_0$ is real it follows that

$$\hat{A}_3 \sim \left(\dot{a}_3 \hat{X}^3 + (\alpha_3 + \dot{a}_0 I) \hat{X} + \dot{d}_{00} \ln|\hat{X}| + (\beta_3 + \dot{a}_0 J) \right) e^{iC} \quad \text{as} \quad \hat{X} \to -\infty \quad , \tag{6.5.35}$$

where I and J are real constants depending on the integral properties of the solution for $\hat{B}_0$. Application of the boundary conditions (6.5.17) and (6.5.18) now requires

$$\dot{d}_0 - \dot{a}_0 J = \ddot{d}_0 \quad , \tag{6.5.36}$$

$$\dot{b}_1 - \dot{a}_0 I = \ddot{b}_1 \quad . \tag{6.5.37}$$

The solution for $\hat{A}_{40}$ can be found as

$$\hat{A}_{40} = \left(\dot{c}_1 + \frac{1}{6} \dot{d}_{10} \right) \hat{X} \quad , \tag{6.5.38}$$

where it is required that

$$\dot{c}_1 + \frac{1}{6} \dot{d}_{10} = \ddot{c}_1 \quad . \tag{6.5.39}$$

The equation for $\hat{B}_1$ is obtained from (6.3.4) as

$$4\delta \frac{\partial^2 \hat{B}_1}{\partial \hat{X}^2} - 9\hat{B}_0^2 \hat{B}_1 - \frac{\sqrt{1 - 4\delta^2}(1 + 4\delta^2)}{2} \hat{X}\hat{B}_1 = \frac{\partial^4 \hat{B}_0}{\partial \hat{X}^4} + 12\dot{a}_0 \dot{b}_0 \hat{B}_0 + \frac{\hat{X}^2 \hat{B}_0 (1 + 4\delta^2)(12\delta^2 - 1)}{16}$$

$$\tag{6.5.40}$$

and it can be shown that

189

$$\hat{B}_1 = c(-\hat{X})^{3/2} + O((-\hat{X})^{-1/2}) \quad , \quad \hat{X} \to -\infty \quad , \tag{6.5.41}$$

where

$$c = \frac{-\sqrt{1+4\delta^2}(12\delta^2-1)}{16\sqrt{6}(1-4\delta^2)^{1/4}} \quad , \tag{6.5.42}$$

and

$$\hat{B}_1 \to 0 \quad , \quad \hat{X} \to \infty \quad . \tag{6.5.43}$$

In principle $\hat{B}_1$ can now be found by solving (6.5.40) together with the boundary conditions (6.5.41) and (6.5.43).

Once $\hat{B}_1$ is known, it is possible to obtain the solution in the transition region for $\hat{A}_4$. Equation (6.5.12) can be integrated twice to obtain

$$\hat{A}_4 = \left(\ddot{a}_4 \hat{X}^4 + \ddot{b}_2 \hat{X}^2 + \frac{3\dot{a}_1}{2} \int\limits_{\hat{X}}^{\infty} (\int\limits_{\hat{X}}^{\infty} \hat{B}_0^2 \hat{X} d\hat{X}) d\hat{X} + 3\dot{a}_0 \int\limits_{\hat{X}}^{\infty} (\int\limits_{\hat{X}}^{\infty} \hat{B}_0 \hat{B}_1 d\hat{X}) d\hat{X} + \alpha_4 \hat{X} + \beta_4 \right) e^{iC} \quad . \tag{6.5.44}$$

Since $\hat{B}_0$ and $\hat{B}_1$ are real it follows that

$$\hat{A}_4 \sim \left(\dot{a}_4 \hat{X}^4 + \dot{b}_2 \hat{X}^2 + \dot{d}_{10} \hat{X} \ln|\hat{X}| + (\alpha_4 + \dot{a}_0 K + \dot{a}_1 L)\hat{X} \right) e^{iC} \quad \text{as} \quad \hat{X} \to -\infty \tag{6.5.45}$$

where K and L are real constants depending on the integral properties of the solutions for $\hat{B}_0$ and $\hat{B}_1$. Application of the conditions (6.5.20) and (6.5.21) now requires, in particular, that

$$\dot{d}_1 - \dot{a}_0 K - \dot{a}_1 L = \ddot{d}_1 \quad . \tag{6.5.46}$$

It should be noted that the jump conditions (6.5.25), (6.5.27), (6.5.36), (6.5.37), (6.5.39) and (6.5.46) generated by the presence of the transition zone all involve only the real parts of

190

the outer solutions for $\dot{R}_1$, $\ddot{R}_1$, $\dot{R}_{20}$, $\ddot{R}_{20}$, $\dot{R}_2$ and $\ddot{R}_2$ and that therefore the imaginary parts of these outer solutions and their first derivatives must be continuous at the transition point X_0. Phase-winding effects are associated with this imaginary part of the solution and so it is in fact unnecessary to calculate the various integrals I, J, K and L which arise in the preceding analysis in order to determine the phase-winding properties of the system.

6.6 Inner wall regions

There are two regions near the wall where the solution must adjust to the full boundary conditions (6.2.2). The outer wall region where $x \sim \epsilon^{-1/4}$ allows the amplitude of the y-rolls to decrease from the value $\bar{B} \sim [(1-4\delta^2)/3]^{1/2}$ attained as $X \to 0$ in region I. Locally,

$$\bar{B} = \bar{B}_0(\bar{X}) + \dots \quad , \tag{6.6.1}$$

$$A = \epsilon^{1/4} \bar{A}_0(\bar{X}) + \dots \quad , \tag{6.6.2}$$

where $x = \epsilon^{-1/4} \bar{X}$ and it is easily established that

$$\bar{A}_0 = \bar{X} \bar{A}_0'(0) \tag{6.6.3}$$

and that $\bar{B}_0$ is the solution of the system

$$\frac{\partial^4 \bar{B}_0}{\partial \bar{X}^4} - 4\delta \frac{\partial^2 \bar{B}_0}{\partial \bar{X}^2} - \bar{B}_0 + 3\bar{B}_0^3 + 4\delta^2 \bar{B}_0 = 0 \quad , \tag{6.6.4}$$

$$\bar{B}_0 \to \frac{1}{\sqrt{3}}(1-4\delta^2)^{1/2} \quad , \quad \bar{X} \to \infty \quad , \tag{6.6.5}$$

$$\bar{B}_0 = \frac{\partial \bar{B}_0}{\partial \bar{X}} = 0 \quad , \quad \bar{X} = 0 \quad . \tag{6.6.6}$$

Here the boundary conditions at $\bar{X} = 0$ are those discussed in section 2.2, first proposed by Brown and Stewartson (1977), and resulting from the behaviour of the solution in the inner

191

wall region where $x \sim 1$, to be discussed below. The system (6.6.4)-(6.6.6) would require a numerical solution and this is not attempted here, but it is noted that the adjustment represented by $\bar{B}_0$ will first affect the solution for A at order $\epsilon^{3/4}$ in the region where $\bar{X}=O(1)$. This is then expected to influence the outer solution for A in region I at order $\epsilon^{3/4}$ and the solution for ψ in the inner wall region to be discussed below at order $\epsilon^{3/2}$ but neither of these effects is large enough to be significant here.

In the inner wall region where $x \sim 1$ it is expected that

$$\psi = \epsilon \psi_0(x,y) + \ldots \quad , \quad \epsilon \to 0 \tag{6.6.7}$$

and substitution into the governing equation (6.2.1) shows that ψ_0 satisfies the linearised form

$$(\nabla^2 + 1)^2 \psi_0 = 0 \quad . \tag{6.6.8}$$

The relevant solution is

$$\psi_0 = \{(a_1 + b_1 x)e^{ix} + (a_2 + b_2 x + c_2 x^2 + d_2 x^3)e^{iy}\} + c.c \tag{6.6.9}$$

and matching with the outer wall region as $x \to \infty$ requires that

$$b_1 = \dot{A}_0'(0) \quad , \quad a_1 = \dot{A}_2(0) \tag{6.6.10}$$

and

$$d_2 = 0 \quad , \quad c_2 = \frac{1}{2}\dot{B}_0''(0) \quad . \tag{6.6.11}$$

Application of the boundary conditions $\psi = \partial \psi / \partial x = 0$ at $x=0$ also implies that

$$a_1 + a_1^\star = 0 \quad , \tag{6.6.12}$$

$$(a_1 - a_1^\star)i + b_1 + b_1^\star = 0 \quad , \tag{6.6.13}$$

192

$$a_2 = b_2 = 0 \quad . \tag{6.6.14}$$

From (6.6.10), (6.6.12) and (6.6.13) it follows that

$$\dot{A}_2(0) = iRe\, \{\dot{R}_0'(0)e^{iC}\} = i\dot{R}_0'(0)\cos C \tag{6.6.15}$$

and thus

$$\dot{R}_2(0) = \dot{R}_0'(0)\cos C\,(\sin C + i\cos C) \quad , \tag{6.6.16}$$

where, from (6.3.20),

$$\dot{R}_0'(0) = \frac{1}{\sqrt{3}}\delta(1-2\delta^2)^{1/2} \quad . \tag{6.6.17}$$

This result shows that the wall region generates a reaction in A of order $\epsilon^{1/2}$ in the outer regions and it will be shown in section 6.8 below that this creates a phase-winding effect in the primary roll pattern at large distances from the wall. It is also noted here that terms in A in the outer regions which are larger than order $\epsilon^{1/2}$ will have to vanish at $X=0$, so that $\dot{A}_1$ and $\dot{A}_{20}$ must satisfy

$$\dot{A}_1 = \dot{A}_{20} = 0 \quad \text{at} \quad X = 0 \quad . \tag{6.6.18}$$

6.7 Outer solutions

It is now possible to determine each of the remaining constants arising in the outer solutions for $\dot{A}_1$, $\ddot{A}_1$, $\dot{A}_{20}$, $\ddot{A}_{20}$, $\dot{A}_2$ and $\ddot{A}_2$.

For $\dot{R}_1$ and $\ddot{R}_1$, it is required from (6.5.25), (6.5.37) and (6.6.18) that

$$\dot{R}_1(0) = 0 \quad , \tag{6.7.1}$$

193

$$\ddot{R}_1(X_0) - \dot{R}_1(X_0) = 0 \quad , \tag{6.7.2}$$

$$\ddot{R}_1'(X_0) - \dot{R}_1'(X_0) = -I\dot{R}_0(X_0) \tag{6.7.3}$$

and it follows that

$$\dot{C}_1 = -\frac{\sqrt{1-4\delta^2}(1+4\delta^2)I}{24} \quad , \tag{6.7.4}$$

$$\dot{D}_1 = \ddot{D}_1 = -\int_0^{X_0} \frac{\dot{C}_1}{\dot{R}_0'^2} dX \quad , \tag{6.7.5}$$

$$\ddot{E}_1 = \dot{E}_1 = 0 \quad , \tag{6.7.6}$$

$$\dot{F}_1 = \ddot{F}_1 \quad . \tag{6.7.7}$$

The value of $\ddot{F}_1$ remains arbitrary but is just equivalent to a correction to the phase constant C and can therefore be taken as zero without loss of generality.

For $\dot{A}_{20}$ and $\ddot{A}_{20}$ it is required from (6.5.27), (6.5.39) and (6.6.18) that

$$\dot{R}_{20}(0) = 0 \quad , \tag{6.7.8}$$

$$\dot{R}_{20}(X_0) - \ddot{R}_{20}(X_0) = -\frac{\delta\sqrt{1-4\delta^2}}{12\sqrt{6}} \quad , \tag{6.7.9}$$

$$\dot{R}_{20}'(X_0) - \ddot{R}_{20}'(X_0) = \frac{(1-4\delta^2)\delta}{24\sqrt{6}} \quad . \tag{6.7.10}$$

It then follows that

$$\dot{C}_{20} = 0 \quad , \tag{6.7.11}$$

$$\dot{D}_{20} = 0 \quad , \tag{6.7.12}$$

$$\ddot{D}_{20} = \frac{\delta\sqrt{1-4\delta^2}}{3(1+4\delta^2)} \quad , \tag{6.7.13}$$

$$\ddot{E}_{20} = \dot{E}_{20} = 0 \quad , \tag{6.7.14}$$

$$\dot{F}_{20} = \ddot{F}_{20} \quad . \tag{6.7.15}$$

The constant $\ddot{F}_{20}$ remains arbitrary.

For $\dot{A}_2$ and $\ddot{A}_2$ it is required from (6.5.36), (6.5.46) and (6.6.16) that

$$\dot{R}_2(0) = \dot{R}_0^{/}(0)\cos C(\sin C + i\cos C) \quad , \tag{6.7.16}$$

$$\dot{a}_1\dot{D}_2 + \dot{a}_1\hat{C} - \dot{a}_0J + i\dot{a}_0\dot{F}_2 = \ddot{R}_2(X_0) \quad , \tag{6.7.17}$$

$$-\dot{a}_1^{-1}\dot{C}_2 + 2\dot{a}_2\dot{D}_2 - \delta^3\dot{a}_1^{-1}\dot{a}_0^2 + 2\dot{a}_2\hat{C} + \dot{a}_1\hat{D} - \dot{a}_0K - \dot{a}_1L$$
$$+ i\left\{-\dot{a}_0^{-1}\dot{E}_2 + \ddot{a}_1\dot{F}_2 + \frac{(4\delta^2-5)\dot{a}_0}{32}\right\} = \ddot{R}_2^{/}(X_0) \quad , \tag{6.7.18}$$

which leads to

$$\dot{C}_2 = \dot{a}_1^2\hat{D} + \dot{a}_1\dot{a}_2\hat{C} + \dot{a}_0\dot{a}_2J - \dot{a}_0\dot{a}_1K - \dot{a}_1^2L - \delta^3\dot{a}_0^2 \quad , \tag{6.7.19}$$

$$\dot{D}_2 = \frac{1}{2}\sin 2C - \int_0^{X_0}\frac{\dot{C}_2}{\dot{R}_0^{/2}}dX - \delta^3\int_0^{X_0}\frac{\dot{R}_0^2}{\dot{R}_0^{/2}}dX \quad , \tag{6.7.20}$$

$$\ddot{D}_2 = \dot{D}_2 + \hat{C} - \frac{4\sqrt{1-4\delta^2}J}{1+4\delta^2} \quad , \tag{6.7.21}$$

$$\ddot{E}_2 = \dot{R}_0^{\prime 2}(0)\cos^2 C \quad , \tag{6.7.22}$$

$$\dddot{E}_2 = -\dot{E}_2 - \frac{(1-4\delta^2)^2}{48} \quad , \tag{6.7.23}$$

$$\dot{F}_2 = \ddot{F}_2 + 3\ddot{E}_2\left(X_0 - \frac{4}{\sqrt{1-4\delta^2}}\right) + \frac{1}{16}\left(X_0 - 6\sqrt{1-4\delta^2}\right) \quad . \tag{6.7.24}$$

The constant $\ddot{F}_2$ remains arbitrary.

The determination of the constants in the solutions for $\dot{A}_2$ and $\ddot{A}_2$ is now completed and in particular the non-zero imaginary component of $\ddot{R}_2$ generated by the reaction with the lateral boundary produces a correction to the wavelength at large distances from the boundary. This can be seen by noting that

$$Im\{\ddot{R}_2\} \sim \frac{qX}{\sqrt{3}} \quad \text{as} \quad X \to \infty \quad , \tag{6.7.25}$$

where, from (6.7.22), (6.7.23) and (6.6.17),

$$q = \left(3\dddot{E}_2 + \frac{1}{16}\right) = -\frac{1}{2}\delta^2(1-2\delta^2)\cos 2C \quad . \tag{6.7.26}$$

This represents a correction to the overall wavelength of the primary roll pattern, because

$$A \sim \frac{1}{\sqrt{3}}e^{iC}\{1 + \epsilon^{1/2}iqX\} \quad , \quad X \to \infty \tag{6.7.27}$$

and so at large distances from the boundary

$$\psi \sim \frac{\epsilon^{1/2}}{\sqrt{3}}\exp\{i[1+\epsilon q]x + iC\} + c.c \quad . \tag{6.7.28}$$

From (6.7.26), the band of possible wavenumbers is restricted to the range

$$|q| < \frac{1}{2}\delta^2(1-2\delta^2) \quad . \tag{6.7.29}$$

196

It is interesting to note that this range is a maximum when δ^2 reaches the value 1/4 and that it reduces to zero when $\delta=0$. The case where δ tends to zero corresponds to the situation where the transition point X_0 moves away from the boundary and a new analysis is required to identify the phase-winding properties of the system in the case where both λ and δ are zero.

6.8 Discussion

In this chapter phase-winding effects have been considered for the combined x, y-roll pattern adjacent to a lateral wall $x=0$ with no forcing ($\lambda=0$). It has been shown that for y-roll patterns along the lateral wall within a waveband of order $\epsilon^{1/2}$ about the critical wavenumber, phase-winding solutions exist corresponding to adjustments of the wavenumber of the x-roll pattern within a band of order ϵ about the critical wavenumber. The precise range of available wavenumbers is given by the formula (6.7.29) and shrinks to zero as the value of the parameter δ, which defines the correction to the critical wavenumber in the y direction, tends to zero. As $\delta\to 0$, the transition line defining the extent of the y-rolls in the x direction moves away from the wall and a new analysis would be required to consider the special case where $\delta=0$. The implication of the present theory is that there will be a severe restriction on phase-winding of the x-roll pattern in this case, more severe than in the (unstable) case of pure x-rolls considered by Cross et al (1983). As argued in chapter 5, a solution with the minimum possible value of $|\delta|$ is needed to ensure stability, and so an analysis of the case where $\delta=0$ remains one of the most important aims of future work.

The analysis of the present chapter has focused on the case where $\lambda=0$ and $\mu=2$, but could be extended in a straightforward manner to general values of λ and μ, with a corresponding adjustment to the formula (6.7.29).

This thesis has considered aspects of pattern selection in Rayleigh-Bénard convection and

a related system, concentrating on the case where the pattern is formed in the region adjacent to an isolated lateral wall. Effects associated with the nonlinear interaction parameter μ, the lateral forcing parameter λ, the wavelength of the x-roll pattern (q) and the wavelength of the y-roll pattern (δ) have been analyzed using asymptotic and numerical methods. Generally speaking the results indicate that the existence of cross-rolls near the wall places a greater restriction on the band of wavenumbers of the main x-roll pattern than in the case where the cross-rolls are neglected. The present theory has not considered the effect of amplitude modulation of the x and y-roll patterns in the y direction, which can be expected to be significant where lateral walls also exist parallel to the x direction. In the future, it is hoped that relevant aspects of the present theory can be extended to obtain predictions of the structure and wavelength of roll patterns in finite rectangular planform containers, both for the simpler model and, eventually, for the full Rayleigh-Bénard system, allowing realistic comparisons to be made with experimental observations.
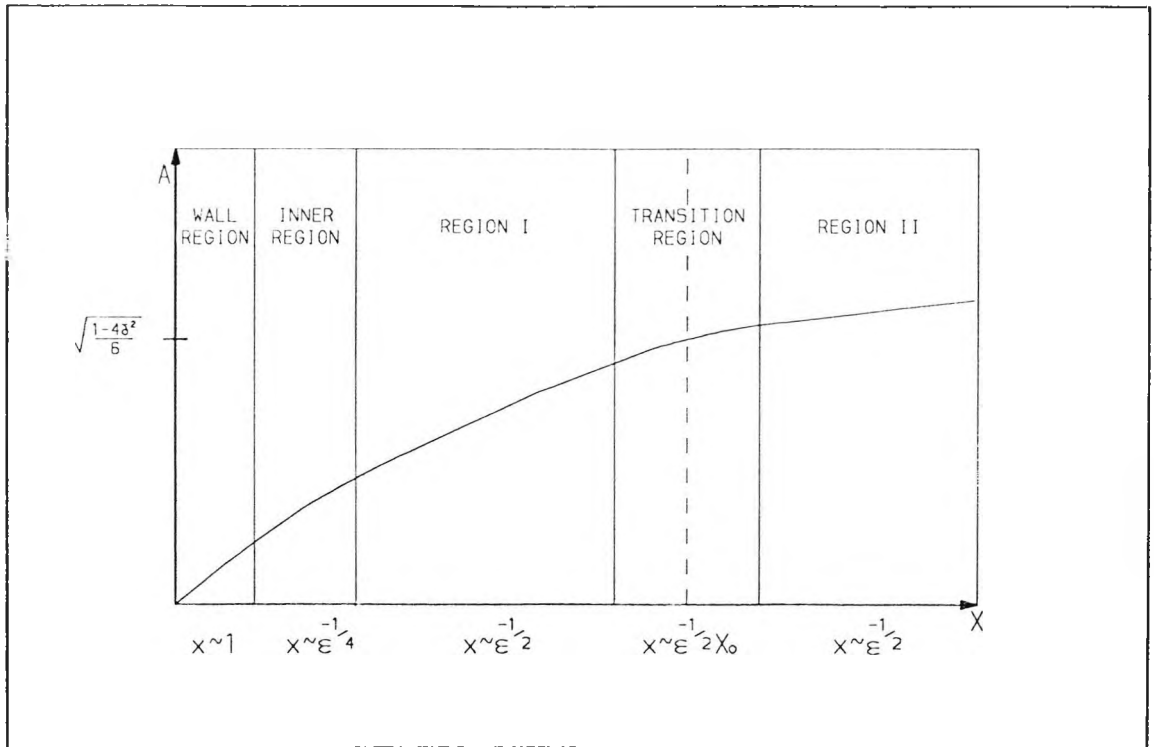
Fig. 6.1 : Schematic diagram showing the main flow regions

References

Brown, S. N. & Stewartson, K., 1977, On thermal convection in a large box. *Stud. in Appl. Math.* **57**, 187.

Brown, S. N. & Stewartson, K., 1978, On finite amplitude Bénard convection in a cylindrical container. *Proc. Roy. Soc.* **A360**, 455.

Brown, S. N. & Stewartson, K., 1979, On finite amplitude Bénard convection in a cylindrical container. Part II. *SIAM J. Appl. Math.* **36**, 573.

Bühler, K., Kirchartz, K. R. & Oertel, H., 1979, Steady convection in a horizontal fluid layer. *Acta Mechanica.* **31**, 155.

Chana, M. S. & Daniels, P. G., 1989, Onset of Rayleigh-Bénard convection in a rigid channel. *J. Fluid Mech.* **199**, 257.

Chandrasekhar, S., 1961, *Hydrodynamic and Hydromagnetic Stability.* Oxford, Clarendon Press.

Cross, M. C., 1980, Derivation of the amplitude equation at the Rayleigh-Bénard instability. *Phys. Fluids.* **23**, 1727.

Cross, M. C., 1982, Boundary conditions on the envelope function of convective rolls close to onset. *Phys. Fluids.* **25**, 936.

Cross, M. C., Daniels, P. G., Hohenberg, P. C. & Siggia, E. D., 1981, Effect of distant sidewalls on wave-number selection in Rayleigh-Bénard convection. *Phys. Rev. Lett.* **45**, 898.

Cross, M. C., Daniels, P. G., Hohenberg, P. C. & Siggia, E. D., 1983, Phase-winding solutions in a finite container above the convective threshold. *J. Fluid Mech.* **127**, 155.

Cross, M. C., Hohenberg, P. C. & Safran, S. A., 1982, Wave number selection in Rayleigh-Bénard convection: a numerical study. *Physica.* D**5**, 75.

Daniels, P. G., 1977, The effect of distant sidewalls on the transition to finite amplitude Bénard convection. *Proc. R. Soc. Lond.* A**358**, 173.

Daniels, P. G., 1978, The effect of distant sidewalls on the transition to finite amplitude Bénard convection II. *Mathematika.* **25**, 216.

Daniels, P. G., 1981, The effect of distant side-walls on the evolution and stability of finite-amplitude Rayleigh-Bénard convection. *Proc. R. Soc. Lond.* A**378**, 539.

Daniels, P. G., 1982, Effects of geometrical imperfection at the onset of convection in a shallow two-dimensional cavity. *Int. J. Heat Mass Transfer.* **25**, 337.

Daniels, P. G., 1982, The onset of Bénard convection in a shallow sloping container. *Q. Jl. Mech. Appl. Math.* **35**, 49.

Daniels, P. G., 1984, Roll-pattern evolution in finite-amplitude Rayleigh-Bénard convection in a two-dimensional fluid layer bounded by distant sidewalls. *J. Fluid Mech.* **143**, 125.

Daniels, P. G. & Chana, M. S., 1987, Multiple convective states in a long box heated from below. *Proc. ASME Winter Annual Meeting, Boston. HTD*, **94**, 49.

Daniels, P. G. & Golbabai, A., 1986, Phase-winding solutions for axisymmetric convection between rotating planes uniformly heated from below. *IMA J. of Appl. Maths.* **36**, 177.

Daniels, P. G. & Ong, C. F., 1990, Linear stability of convection in a rigid channel uniformly heated from below. *Int. J. Heat Mass Transfer.* **33**, 55.

Daniels, P. G. & Ong, C. F., 1990a, Nonlinear convection in a rigid channel uniformly heated from below. *J. Fluid Mech.* **215**, 503.

Daniels, P. G. & Weinstein, M., 1992, On finite-amplitude patterns of convection near a lateral boundary. *Q. Jl. Mech. Appl. Math.* **45**, 315.

Davies-Jones, R. P., 1970, Thermal convection in an infinite channel with no-slip sidewalls. *J. Fluid Mech.* **44**, 695.

Davis, S. H., 1967, Convection in a box: linear theory. *J. Fluid Mech.* **30**, 465.

Dubois, M. & Bergé, P., 1978, Experimental study of the velocity field in Rayleigh-Bénard convection. *J. Fluid Mech.* **85**, 641.

Dubois-Violette, E., Guazzelli, E. & Prost, J., 1983, Dislocation motion in layered structures. *Philosophical Magazine A.***48**, 727.

Greenside, H. S. & Coughran, W. M., 1984, Nonlinear pattern formation near the onset of Rayleigh-Bénard convection. *Phys. Rev. Lett.* A**30**, 398.

Guazzelli, E., Guyon, E. & Wesfreid, J. E., 1983, Dislocations in a roll hydrodynamic instability in nematics: static limit. *Philosophical Magazine A.***48**, 709.

Hall, P. & Walton, I. C., 1977, The smooth transition to the convective regime in a two-dimensional box. *Proc. R. Soc.* A**358**, 199.

Joseph, D. D., 1971, Stability of convection in containers of arbitrary shape. *J. Fluid Mech.* **47**, 257.

Kelly, R. E. & Pal, D., 1978, Thermal convection with spatially periodic boundary conditions: resonant wavelength excitation. *J. Fluid Mech.* **86**, 433.

Kessler, R., 1987, Nonlinear transition in three-dimensional convection. *J. Fluid Mech.* **174**, 357.

Kolodner, P., Walden, R. W., Passner, A. & Surko, C. M., 1986, Rayleigh-Bénard convection in an intermediate-aspect-ratio rectangular container. *J. Fluid Mech.* **163**, 195.

Koschmieder, E. L., 1993, *Bénard Cells and Taylor Vortices*. Cambridge University Press.

Langer, J. S., 1980, Instabilities and pattern formation in crystal growth. *Reviews of Modern Physics.* **52**, 1.

Luijkx, J. M. & Platten, J. K., 1981, On the onset of free convection in a rectangular channel. *J. Non- Equilib. Thermodyn.* **6**, 141.

Luijkx, J. M. & Platten, J. K. & Legros, J. Cl., 1982, Precise measurements of the wavelength at the onset of Rayleigh-Bénard convection in a long rectangular duct. *Int. J. Heat Mass Transfer.* **25**, 1252.

McKenzie, D. P. & Richter, F., 1976, Convection currents in the Earth's mantle. *Scientific American.* **235**, 72.

Newell, A. C. & Whitehead, J. A., 1969, Finite bandwidth, finite amplitude convection. *J. Fluid Mech.* **38**, 279.

Oertel, H., 1980, Three-dimensional convection within rectangular boxes. *In Natural Convection in Enclosures ASME HTD* (ed. K. E. Torrance & I. Catton), **8**, 11.

Pomeau, Y. & Manneville, P., 1980, Wavelength selection in cellular flows. *Phys. Lett.* A**75**, 296.

Pomeau, Y. & Manneville, P., 1981, Wavelength selection in axisymmetric cellular structures. *J. Physique.* **42**, 1067.

Pomeau, Y. & Zaleski. S., 1981, Wavelength selection in one-dimensional cellular structures. *J. Physique.* **42**, 515.

Rivier, N., Occelli, R., Pantaloni, J. & Lissowski, A., 1984, Structure of Bénard convection cells, phyllotaxis and crystallography in cylindrical symmetry. *J. Physique.* **45**, 49.

Ross, E. W., 1966, Transition solutions for axisymmetric shell vibrations. *J. Math. Phys.* **45**, 335.

Schlüter, A., Lortz, D. & Busse, F., 1965, On the stability of steady finite amplitude convection. *J. Fluid Mech.* **23**, 129.

Segel, L. A., 1969, Distant side-walls cause slow amplitude modulation of cellular convection. *J. Fluid Mech.* **48**, 203.

Stewartson, K. & Weinstein, M., 1979, Marginal convection in a large rigid box. *Phys. Fluids.* **22**, 1421.

Tesauro, G. & Cross, M. C., 1987, Grain boundaries in models of convective patterns. *Philosophical Magazine* A. **56**, 703.

Walton, I. C., 1982, On the onset of Rayleigh-Bénard convection in a fluid layer of slowly increasing depth. *Stud. in Appl. Math.* **67**, 199.

Walton, I. C., 1983, The onset of cellular convection in a shallow two-dimensional container of fluid heated non-uniformly from below. *J. Fluid Mech.* **131**, 455.

Wesfreid, J., Pomeau, Y., Dubois, M., Normand, C. & Berge, P., 1978, Critical effects in Rayleigh-Bénard convection. *J. Phys. Lett.* **39**, 725.

Zierep, J., 1958, Eine rotationssymmetrische zellularkonvektionsströmung. *Beitr. Phys. Atmos.* Bd. **30**, 215.